1985

Formation and reactivity of metal-ligand bonds: platinum(I) dimers and cobalt and chromium alkyls

Reed John Blau
Iowa State University

Blau, Reed John

FORMATION AND REACTIVITY OF METAL-LIGAND BONDS: PLATINUM (I) DIMERS AND COBALT AND CHROMIUM ALKYLS

Iowa State University Ph.D. 1985

Formation and reactivity of metal-ligand bonds: Platinum(I) dimers and cobalt and chromium alkyls

by

Reed John Blau

A Dissertation Submitted to the
Graduate Faculty in Partial Fulfillment of the
Requirements for the Degree of
DOCTOR OF PHILOSOPHY

Department: Chemistry
Major: Inorganic Chemistry

Approved:

Signature was redacted for privacy.

In Charge of Major Work

Signature was redacted for privacy.

For the Major Department

Signature was redacted for privacy.

For the Graduate College

Iowa State University
Ames, Iowa

1985

TABLE OF CONTENTS

LIST OF TABLES

LIST OF FIGURES

LIST OF SCHEMES

GENERAL INTRODUCTION

The subject of Part I is the characterization and conformational properties of $[Pt_2(\mu\text{-dppm})_2Cl(PPh_3)]^+$ and other related platinum(I) dimers. In addition, various mechanisms of ligand substitution forming $[Pt_2(\mu\text{-dppm})_2Cl(PPh_3)]^+$ are compared.

Part II describes the synthesis, characterization, and reactivity of $[\{Pt_2(\mu\text{-dppm})_2Cl\}_2(di\text{-}\eta^2\text{-}P_4)]^{2+}$, a complex where tetraphosphorus is bound to each of two platinum(I) dimers in an η^2 fashion.

Part III summarizes research on the formation and reactivity of metal-carbon bonds in cobalt and chromium alkyls.

PART I. SUBSTITUTION REACTIONS AND CONFORMATIONAL PROPERTIES OF PLATINUM(I) DIMERS

INTRODUCTION

History

Considerable research emphasis has recently been placed on the chemistry of dinuclear transition metal complexes. One goal of such research is to better understand reactions involving two or more metal centers. Such reactions are often invoked in heterogeneous catalysis or in homogeneous catalysis using dinuclear or cluster complex catalysts. There is a class of dinuclear complexes in which the metals are locked together by one or more bridging bidentate ligands. The role of these ligands is to prevent dissociation of dimer to monomer, to promote bridging by other groups, and to promote reactions of dinuclear complexes involving formation and cleavage of metal-metal bonds. This structural stabilization allows chemical species that would otherwise be only transient in existence, such as intermediates in catalytic processes, to become more amenable to study.

One of the most prominent of these bridging ligands is bis(diphenylphosphino)methane ($Ph_2PCH_2PPh_2$, also represented as dppm, and P-C-P). This readily available phosphine is stable under normal conditions. Like other phosphines, it binds strongly to many transition metals in low oxidation states and is often used to stabilize organometallic and hydride derivatives of the elements.[1]

Bis(diphenylphosphino)methane can act as a chelating agent but the four-membered ring so formed is strained,[2] and the ligand has a greater tendency to act either as a monodentate or bridging bidentate ligand. Many dinuclear complexes of platinum bridged by bidentate dppm have been reported. Oxidation states of the metal in these complexes range from (0) to (II).

The Pt(0) complexes are bridged[3] by three dppm ligands and are susceptible to oxidative addition reactions yielding products in oxidation states (I) or (II) depending on the particular reagents and conditions.[1] For example,[4] $[Pt_2(\mu\text{-dppm})_3]$ reacts with methyl iodide to form a Pt(I) dimer; under certain conditions this dimer reacts with further methyl iodide to form an iodo bridged Pt(II) dimer:

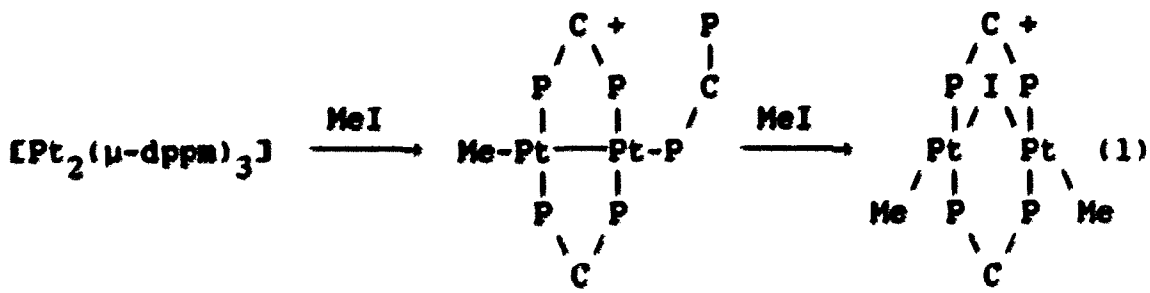

P-C-P = $Ph_2PCH_2PPh_2$

The Pt(I) dimers contain a single metal-metal bond, are normally bridged by two dppm ligands bound trans to each other. Additional ligands (L and L') are bound to each metal in a position trans to the metal-metal bond. They will be

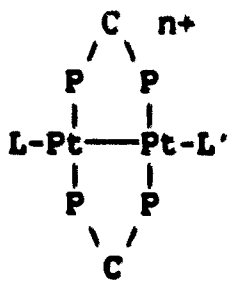

	n = 2	L = L' = PR_3, NR_3, py, CO
	n = 2	L = py; L' = CO
	n = 1	L = PR_3; L' = H^-, Me^-, X^-
	n = 1	L = CO; L' = H^-, Cl^-
	n = 0	L = L' = X^-

$[L{-}{-}L']^{n+}$ (P-C-P = $Ph_2PCH_2PPh_2$

defined subsequently as terminal ligands, and may be halides,[5] neutral ligands,[6] or a combination of both (i.e., L ≠ L' in $[L{-}{-}L']^{n+}$).[7] A notable exception[8] to the normal Pt(I) dimer structure is that of $[Pt_2(\eta^2\text{-dppm})_2(\mu\text{-dppm})]^{2+}$ which contains one bridging and two chelating dppm ligands (3-DPPM). It, like all the others shown, maintains a 16 electron count and an approximately local square planar geometry about each platinum.

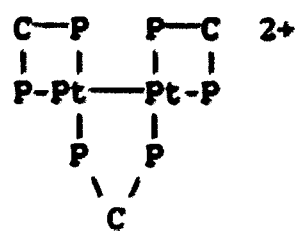

3-DPPM

The Pt(I) dimers bridged by two dppm ligands display high reactivity either by displacement of terminal ligands by anionic[9] or neutral ligands[6] or insertion of $SnCl_2$[10] into

metal-chloride bonds. However, the addition of small molecules to the metal-metal bond is of greatest interest (e.g., reactions of $[Pt_2(\mu\text{-dppm})_2Cl_2]$ in Scheme I-1). The often reversible insertions of small molecules such as H^+,[11] CO,[7] SO_2, CH_2 (from CH_2N_2), and S (from S_8)[12] have been reported. Of particular interest in these reactions is the formation of unique bonding types. For example, these constitute almost unique examples of CO and CH_2 bridging between two metal atoms in which there is no metal-metal bond.

Complexes with a bridging group other than the two dppm ligands (e.g., [Cl-Y-Cl] in Scheme I-1) have been termed "A-frame" complexes. These Pt(II) dimers may be derived from reactions of small molecules with Pt-Pt bonds as described above or from mononuclear Pt(II) complexes containing chelating dppm.[5] Other Pt(II) structural types have been reported but are of less importance.

The chemistry and structure types of palladium[13] and mixed palladium-platinum[14] dppm complexes are almost perfect mimics of the above described platinum complexes. There are also interesting parallels between dinuclear platinum chemistry and dinuclear rhodium and gold chemistry. For example, CO and H^+ insert into the Rh-Rh bond of $[Rh_2(\mu\text{-dppm})_2(CO)_2]$[15] and CH_2I_2 oxidatively adds to an Au(I) dimer bridged by two $[(CH_3)_2P(CH_2)_2]$ units to obtain an Au(III) "A-frame" containing two terminal iodides and a bridging methylene group.[16]

Scheme I-1. Typical Reactions of $[Pt_2(\mu\text{-dppm})_2Cl_2]$

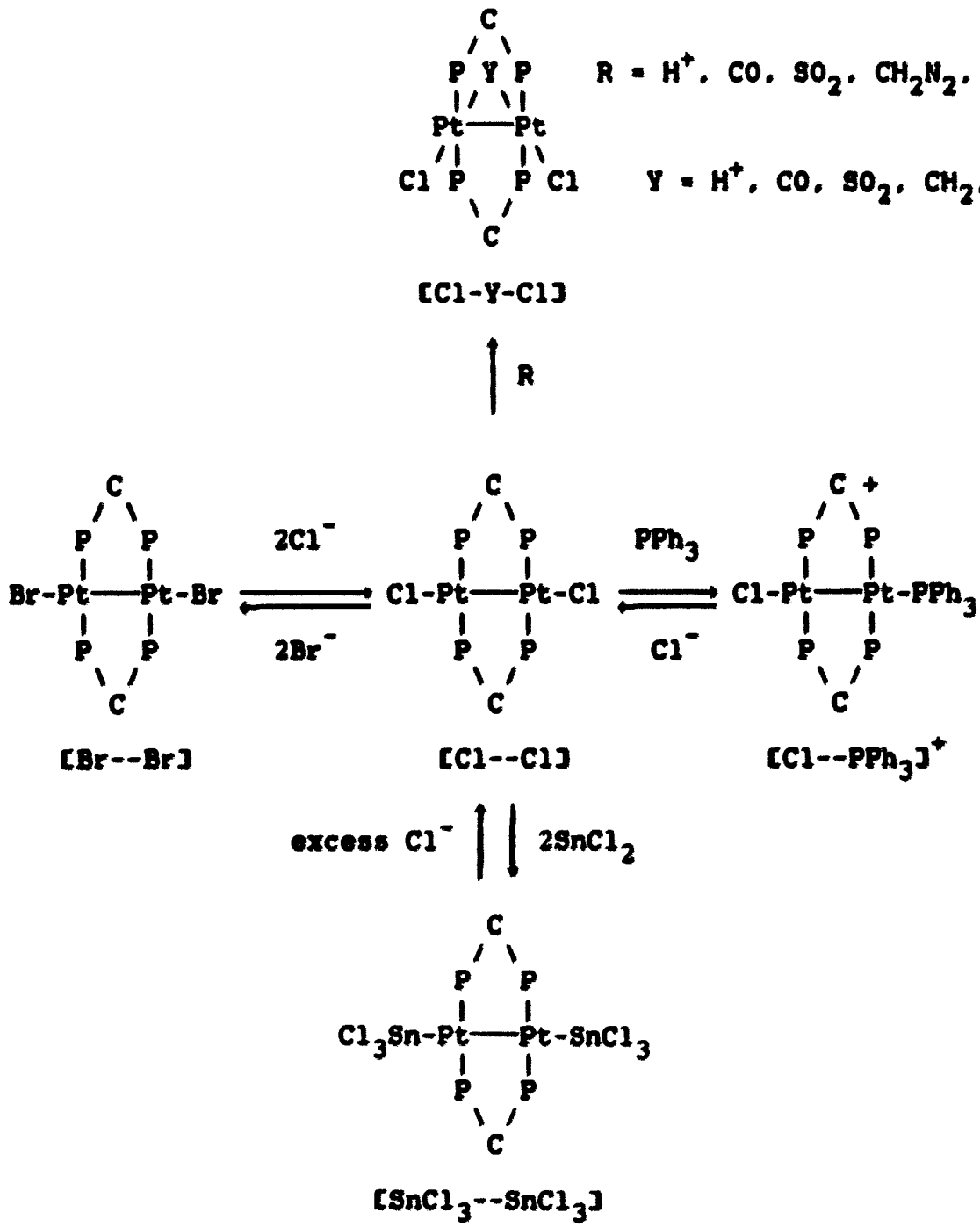

Statement of Problem

Although considerable research has been devoted to the synthesis and reactivity of Pt(I) dimers, only recently has research been devoted to the mechanisms by which they react.

A kinetic study of the reaction of $[Pt_2Br_2(\mu\text{-dppm})_2]$ with chloride ions in dichloromethane solvent[9] has shown that the rate of ligand substitution in Pt(I) complexes can be as much as 10^5 times faster than substitution in similar Pt(II) complexes. The kinetics of ligand substitution reactions of Pt(II) complexes have been studied extensively,[17,18] whereas, little is known about analogous reactions of Pt(I) complexes. Further research dealing with substitution reactions of Pt(I) complexes should yield interesting details regarding the similarities and differences between the substitution chemistry of Pt(I) and Pt(II) complexes.

$$[Br\text{--}Br] \underset{Br^-}{\overset{Cl^-}{\rightleftharpoons}} [Cl\text{--}Br] \underset{Br^-}{\overset{Cl^-}{\rightleftharpoons}} [Cl\text{--}Cl] \qquad (2)$$

Mechanistic details on insertions of small molecules into Pt-Pt bonds have recently been reported. Kinetic measurements suggest that reactions of diazomethane with most Pt(I) complexes occur by rate-limiting transfer of an electron pair from the metal-metal bond to the methylene group of

diazomethane (Scheme I-2), in other words, a bimolecular reaction. Some exceptions to this mechanism are the reactions [19]

Scheme I-2. "A-Frame" Formation from Selected Pt(I) Dimers

$$[L\text{--}L']^{n+} \xrightarrow{k_1[CH_2N_2]} [L\text{-}CH_2\text{-}L']^{n+}$$

n = 0; L = L' = Cl^-, Br^-, I^-

n = 1; L = CO; L' = Cl^-

n = 2; L = L' = py, CO, NH_3

of $[Pt_2(\mu\text{-dppm})_2(PPh_3)_2]^{2+}$ with diazomethane and other small molecules (Scheme I-3).[20] The reaction is found to be independent of both the identity and concentration of R at high [R]. This suggests that the rate-limiting step is a unimolecular reaction of $[PPh_3\text{--}PPh_3]^{2+}$, which was postulated although not unequivocally proven to occur via Pt_2P_2C ring opening forming INT.. It is not surprising, at least in this special case, that steric crowding could easily block a more efficient transformation, especially since there are seven phenyl groups about each platinum atom supplied by three phosphine donors.

It would be beneficial to determine if a mechanism(s) for terminal ligand substitution in Pt(I) complexes may also be dictated by the steric constraints of the complex involved, and if the two reactions occur by similar or completely independent transition states.

Scheme I-3. "A-Frame" Formation from $[Pt_2(\mu\text{-dppm})_2(PPh_3)_2]^{2+}$

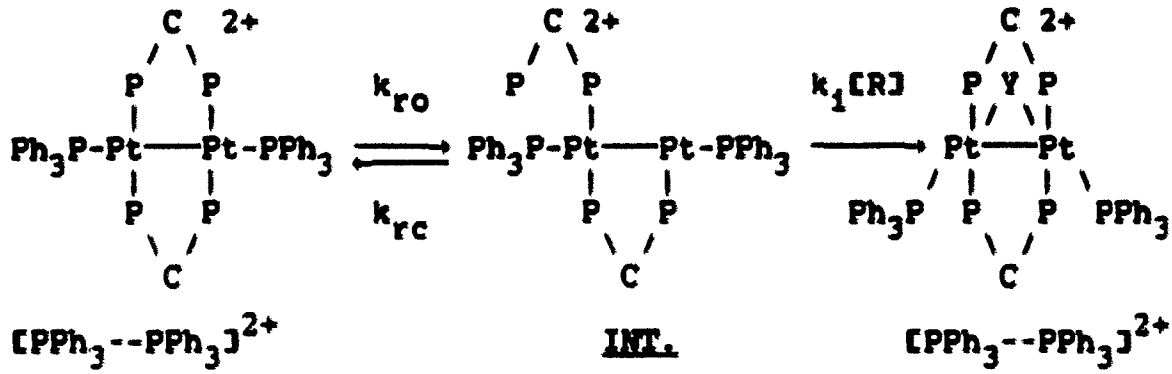

R = CO, SO_2, S_8, CH_2N_2

Y = CO, SO_2, S, CH_2

In summary, the major objectives of this research will be to obtain a better understanding of: (a) the mechanism(s) of ligand substitution in Pt(I) complexes, (b) the relationships between ligand substitution and small molecule addition to Pt-Pt bonds, and (c) general structural characteristics of Pt(I) complexes.

RESULTS AND DISCUSSION

Characterization of $[Pt_2(\mu\text{-dppm})_2Cl(PPh_3)]^+$

Phosphorus-31 NMR spectroscopy

Phosphorus-31 NMR spectroscopy is a very powerful method to study $Pt_2(\mu\text{-dppm})_2$ type complexes. High resolution of peaks which is not found in UV-VIS spectroscopy is possible because of the wide range of chemical shifts inherent in the ^{31}P NMR, the diamagnetic character of the complexes, broad band decoupling of the proton NMR, and the high magnetic field strength of the particular instrument used in this research (121.5 MHz).

Valuable information can be obtained not only from the chemical shifts, peak areas, and phosphorus-phosphorus coupling constants, but also from platinum-phosphorus coupling constants. The presence of ^{195}Pt in 33.7 % abundance with a nuclear spin I = 1/2 yields a source of information about the metal centers that is not available even in the closely related palladium complexes. For example, $[Pt_2(\mu\text{-dppm})_2Cl_2]$ ([Cl--Cl]) is present in three isotopomers each of which have completely different NMR spectra. The form containing no ^{195}Pt, pictured in Figure I-1 along with its $^{31}P\{^1H\}$ NMR spectrum, yields a single peak due to the four equivalent phosphorus nuclei. The other predominant form containing one ^{195}Pt has a spectrum which consists of two doublets with

coupling constants of 2936 Hz and -136 Hz for the $^{1}J(Pt,P)$ and cis-$^{2}J(Pt,P)$ respectively[5]. The spectrum for the third isotopomer (11.4 % natural abundance) containing two magnetically active isotopes is not normally resolved in ^{31}P NMR spectra of Pt(I) dimers.

General characterization The $^{31}P\{^{1}H\}$ NMR spectrum of $[Pt_2(\mu\text{-dppm})_2Cl(PPh_3)]^+$ ($[Cl\text{--}PPh_3]^+$) consists of three complex multiplets with accompanying ^{195}Pt satellites having approximate peak areas in a ratio of 1 : 2 : 2 (see Figure I-2). Such a spectrum is consistent with PPh_3 being bound to only one of the Pt centers resulting in two chemically distinct types of dppm phosphorus atoms. Phosphorus-phosphorus coupling and details on resonance assignments will be discussed in the atropisomerism section (page 63). The spectrum may be observed upon the addition of one equivalent of Cl^- to $[Pt_2(\mu\text{-dppm})_2(PPh_3)_2]^{2+}$ ($[PPh_3\text{--}PPh_3]^{2+}$) or upon the addition of one equivalent of PPh_3 to [Cl--Cl]:

$$[Cl\text{--}Cl] \xrightarrow[-Cl^-]{+PPh_3} [Cl\text{--}PPh_3]^+ \xleftarrow[-PPh_3]{+Cl^-} [PPh_3\text{--}PPh_3]^{2+} \qquad (3)$$

All of the above data for $[Cl\text{--}PPh_3]^+$ are consistent with a complex having asymmetry along the Pt-Pt axis and containing one chloride and one PPh_3 ligand.

The $^2J(PtPtP)$ coupling constants reveal even more about the structure and bonding of $[Cl--PPh_3]^+$.[21] Cis-$^2J(Pt,P)$ for bridging dppm are considerably smaller than the trans-$^2J(Pt,P)$ for terminal PR_3 in Pt(I) dimers bridged by two dppm ligands. This phenomenon is very evident in the $^{31}P\{^1H\}$ NMR spectrum of $[PPh_3--PPh_3]^{2+}$ found in Figure I-3, and provides evidence that PPh_3 is bound trans to the Pt-Pt bond in $[Cl--PPh_3]^+$. The $^2J(Pt,P)$ for the lowest intensity central resonance (P_T) of $[Cl--PPh_3]^+$ in Figure I-2 is very large (1232 Hz) and comparable to $^2J(Pt,P)$ for terminally bound PR_3 in other Pt(I) dimers ($^2J(Pt_A,P_T$ in Table I-3). The cis-$^2J(Pt,P)$ accompanying the phosphorus resonances assigned to dppm phosphorus adjacent to PPh_3 (P_A), and remote from PPh_3 (P_R) in $[Cl--PPh_3]^+$ are ±142 Hz and ±81 Hz respectively. The cis-$^2J(Pt,P)$ reported for other Pt(I) dimers are also consistently less than 150 Hz.[6] It is well-known that trans-$^2J(P,P)$ are much greater than cis-$^2J(P,P)$. For example, $^2J(P,P)$ is -19 Hz for cis-$[PtCl_2(PMe_3)_2]$ and 510 Hz for the trans isomer.[22] This disparity in the magnitude of cis and trans coupling constants is consistent with significant orbital overlap between ligands "trans" to each other and the absence of such overlap between ligands "cis" to each other. In the case of the Pt(I) complexes, significant orbital overlap between PR_3 and the trans platinum can only occur through a metal-metal bond. The $^3J(Pt,P)$ (P = PPh_3) of "A-frames" of the type

$[Pt_2(\mu\text{-}Y)(\mu\text{-dppm})_2(PPh_3)_2]^{2+}$ (Y = CH_2, CO, SO_2, and S) are less than 200 Hz[22] indicative of the absence of a Pt-Pt bond. In summary, the $^2J(Pt,P)$ for $[Cl\text{--}PPh_3]^+$ are consistent with dppm ligands being cis and the PR_3 ligand being trans to the Pt-Pt bond.

The magnitude of $^3J(PPtPtP)$ are also indicative of the presence of a strong Pt-Pt bond. In complexes containing the $Pt_2(\mu\text{-dppm})_2$ ring, Pt(I) complexes have large $^3J(P_A,P_A{}^*)$ (20-45 Hz), whereas the $^4J(P_A,P_A{}^*)$ of "A-frames" are normally less than 10 Hz.[23] $[Cl\text{--}PPh_3]^+$ has $^3J(P_A,P_A{}^*)$ in the range of 30-40 Hz which is further evidence for the presence of the Pt-Pt bond.

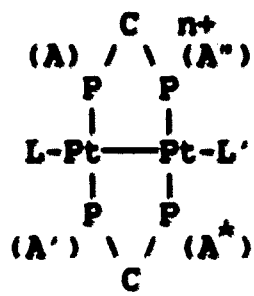

<u>Temperature dependence of NMR chemical shifts</u> The $^{31}P\{^1H\}$ NMR resonances of $[Cl\text{--}PPh_3]^+$ undergo temperature dependent shifts. The most striking observation about these dependencies is that the dppm resonances shift upfield whereas the PPh_3 resonance shifts downfield with increasing temperature. In $[Cl\text{--dppm}]^+$, all three resonances shift downfield (see Table I-1). In both complexes, the shifts with temperature for P_T are the greatest. Shifts similar to those in

Table I-1. Shifts in the $^{31}P\{^{1}H\}$ NMR resonances of $[Pt_2(\mu\text{-dppm})_2Cl(PPh_3)]^+$ with temperature

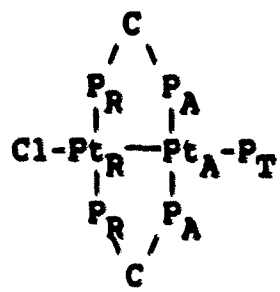

Complex	Temp. Range/K	NMR Shifts with Temp./10^2 ppm K^{-1}		
		P_T	P_A	P_0
$[Cl\text{--}PPh_3]$	253-293	1.71(8)	-0.59(2)	-0.34(1)
$[Cl\text{--}PPh_3]^a$	313-393	1.42(2)	-0.43(2)	-0.33(1)
$[I\text{--}PPh_3]$	253-293	0.95(2)	-0.84(2)	-0.03(2)
[Cl--dppm]	253-298	0.55(2)	0.02(4)	0.18(3)

[a]Solvent is $C_2D_2Cl_4$, normally it is CD_2Cl_2.

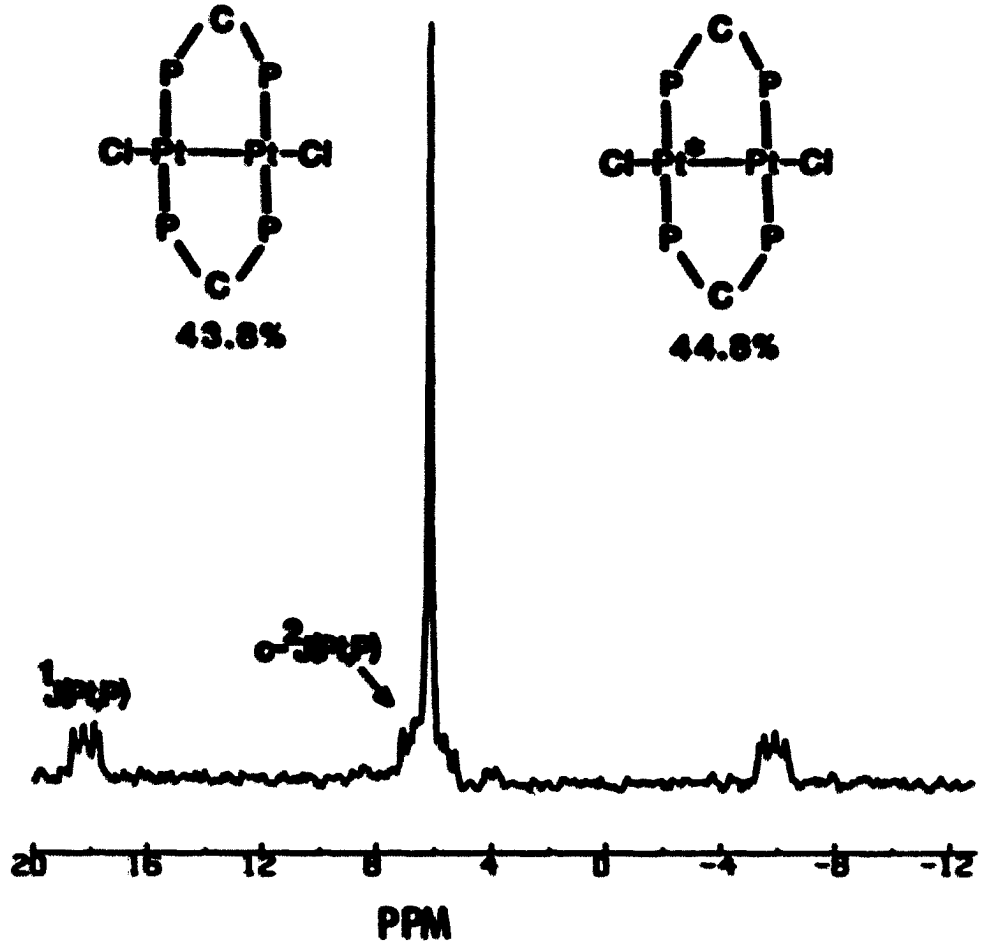

Figure I-1. The $^{31}P\{^{1}H\}$ NMR (121.5 MHz) spectrum of $[Pt_2(\mu\text{-dppm})_2Cl_2]$ in CD_2Cl_2 showing structural formulas and % natural abundance of the two major isotopes ($Pt^* = {}^{195}Pt$)

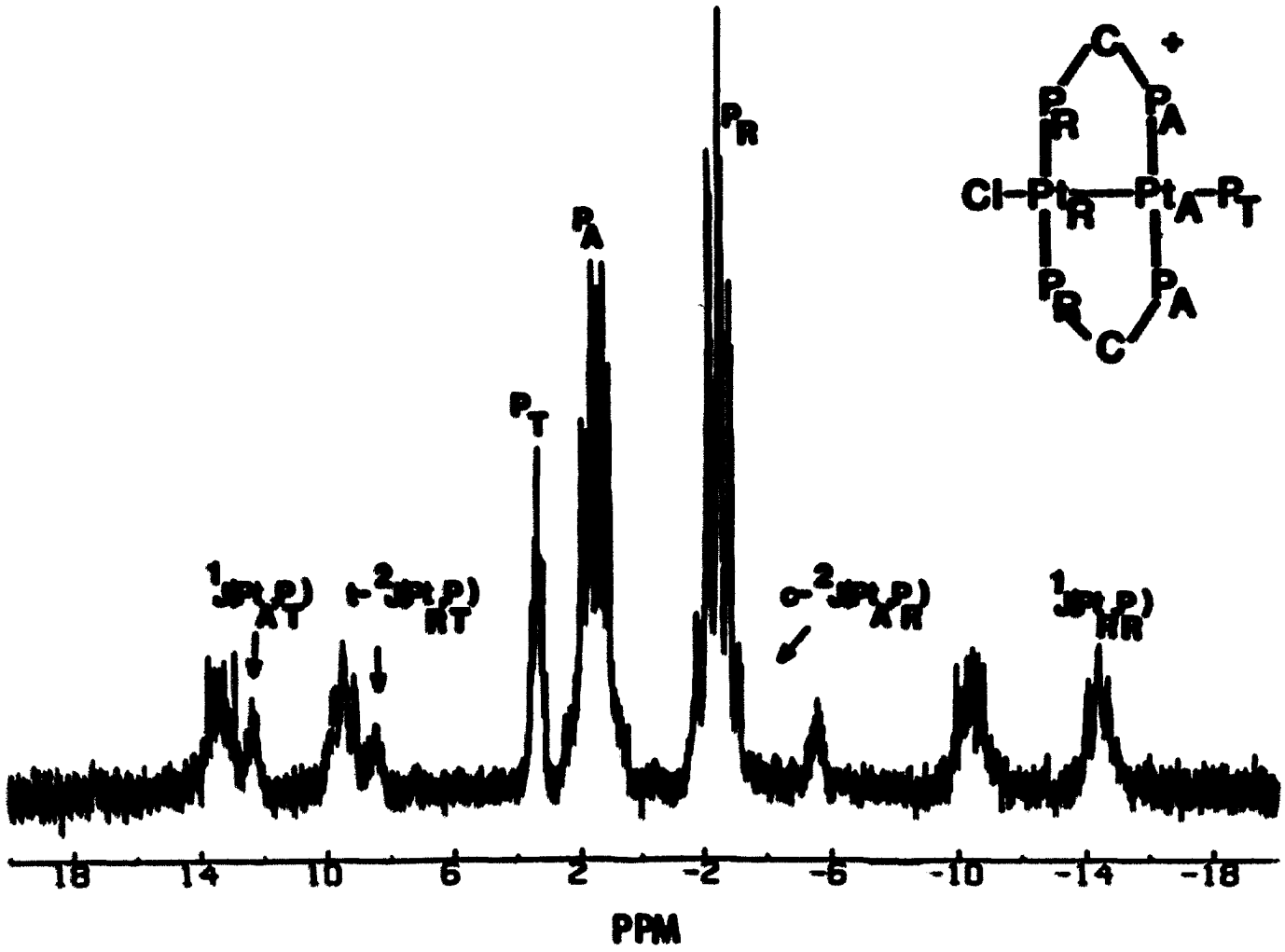

Figure I-2. The $^{31}P\{^{1}H\}$ NMR (121.5 MHz) spectrum of $[Pt_2(\mu\text{-dppm})_2Cl(PPh_3)]^+$ in CD_2Cl_2 (P_T = PPh_3)

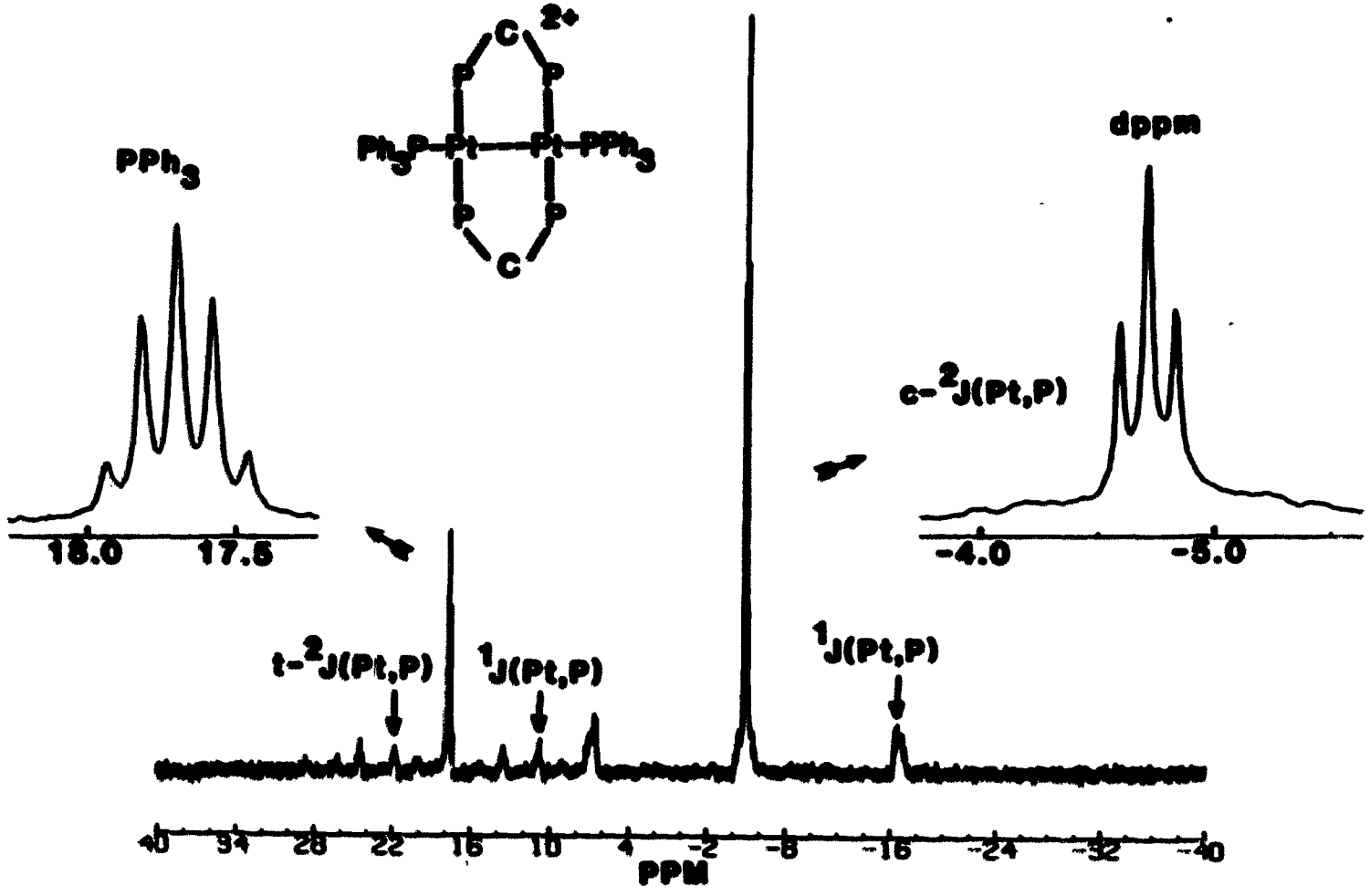

Figure I-3. The $^{31}P\{^{1}H\}$ NMR (121.5 MHz) spectrum of $[Pt_2(\mu\text{-dppm})_2(PPh_3)_2]^{2+}$ in CD_2Cl_2; the C-^{2}J(Pt,P) satellite is at the base of the central dppm resonance

$[Cl{-}{-}PPh_3]^+$ are also seen in $[I{-}{-}PPh_3]^+$. Because the total ^{31}P chemical shift is a delicate counterbalance of several parameters,[24] the exact cause(s) for these observations are not understood at this time. Temperature dependent shifts of ^{31}P NMR resonances of this magnitude are quite common.[25]

X-ray crystal structure

The X-ray crystal structure of $[Pt_2(\mu\text{-dppm})_2Cl(PPh_3)](PF_6) * C_6H_6$ (the refined structure is shown later in Figure I-6) was solved in collaboration with Sangsoo Kim and Dr. Robert A. Jacobson of Iowa State University. The general structural characteristics will be discussed in three parts:

1. bond lengths, Pt-P coupling constants, and the trans influence
2. distortion of square planar platinum
3. conformational geometry

Tables containing bond distances, bond angles, least squares planes, positional parameters, and thermal parameters are found in the appendix on page 172.

Bond lengths, coupling constants, and the trans influence

In this section, bond distances and platinum-phosphorus coupling constants of $[Cl{-}{-}PPh_3]^+$ will be compared with those of other related Pt(I) and Pt(II) complexes. Several interesting trends are found in these data. Some of these trends have previously been reported but are further illustrated with the addition of more recent data. They suggest:

1. The Pt-Pt bond has a trans influence similar to a hydride.
2. Because of the sensitivity of $^{1}J(Pt,P)$ to Pt-P bond length, a value for the Pt-PPh_3 bond length in $[PPh_3--PPh_3]^{2+}$ can be estimated.
3. Ligands with a large trans influence bound cis to Pt-P bonds tend to strengthen these Pt-P bonds.
4. Both cis- and trans-$^{2}J(Pt,P)$ are sensitive to the Pt-Pt bond strength.
5. Ligands with a large trans influence tend to weaken the Pt-Pt bond when they are bound trans to it.

Ligands can influence the ground state properties of groups to which they are bound in a trans position. This includes properties such as the trans metal-ligand bond distance, the vibrational frequency or force constant, the NMR coupling constant between the metal and the trans ligand donor atom, and a host of other parameters. This thermodynamic phenomenon is often called the trans influence. As the trans influence of a ligand increases, the $M-L_{trans}$ bond length increases. For example, X-ray crystallographic data suggest that, based on the ability of the ligands in the following series to lengthen the trans Pt-Cl bond, the trans influence order[26] is:

$$\sigma\text{-}R^- \approx H^- \geq PR_3 > CO \approx Cl^-$$

When the Pt-Cl bond length of 2.403 A in $[Cl{-}{-}PPh_3]^+$ is compared with other Pt-Cl bond distances (see Table I-2), it becomes apparent that the trans influence of a dppm-bridged Pt-Pt bond is intermediate between that of a hydride and a tertiary phosphine but resembling that of the former more than the latter.

It has been found that as a metal ligand bond distance increases, the $^1J(M,L_{trans})$ decreases.[24] $^1J(Pt_A,P_A)$ are fairly constant over the series of Pt(I) complexes found in Table I-3. The same can be said for $^1J(Pt_A,P_T)$, however the $^1J(Pt_A,P_T)$ are about 0.7 of $^1J(Pt_A,P_A)$. Using $^1J(Pt,P)$ and Pt-P bond distances for PR_3 in Pt(I) and Pt(II) complexes of the trans-$[Pt(P'R_3)_2(PR_3)(Y)]^{n+}$ type (see Table I-4), a trans influence order can be constructed:

$$H^- \approx L\text{-}Pt \gg Cl^- > F^-$$

As in the trans influence order generated from Pt-Cl bond distances, a Pt-Pt bond has a trans influence resembling that of H^-. Estimations on the trans influence of a Pt-Pt bond have been made elsewhere.[27,4]

The $^1J(Pt_A,P_T)$ in Table I-3 are relatively insensitive to the nature of the terminal ligand bound to Pt_B (L') except in the case of $[PR_3{-}{-}PR_3]^{2+}$ complexes, where steric influences could most likely cause an increase in the Pt-P bond length and a corresponding decrease in $^1J(Pt_A,P_T)$. In

$[PPh_3\text{--}PPh_3]^{2+}$, the $^1J(Pt_AP_T)$ of 1680 Hz is even smaller than the $^1J(Pt,P)$ observed for a phosphine trans to a methyl (e.g., 1719 Hz in c-$[PtMe(PEt_3)_2Cl]$[24]). A correlation between Pt-P bond length and $^1J(Pt,P)$ has been reported for Pt(II) complexes.[28] Using the data in Table I-4 and I-5, Pt-P bond lengths found in both Pt(I) and Pt(II) complexes were plotted versus $^1J(Pt,P)$ and fitted using a linear function (see Figure I-4). By extrapolation, the Pt-PPh_3 bond distance in $[PPh_3\text{--}PPh_3]^{2+}$ was estimated to be 2.37 ± 0.02 A which is significantly longer than the 2.333 A found in $[Cl\text{--}PPh_3]^+$. The weak Pt-PPh_3 bond found in $[PPh_3\text{--}PPh_3]^{2+}$ is the logical cause for the dissociative character inherent in its reactions.[20]

There is some variation in the magnitude of $^1J(Pt_R,P_R)$ with the terminal ligand bound to Pt_R and trans to Pt_A (L') in the Pt(I) complexes found in Table I-3. For example, values near 3500 Hz are found for L' = H^- compared to 2800 Hz for L' = PR_3. It is interesting to note that the Pt_R-P_R bond distance in $[H\text{--}dppm]^+$ (2.249 A) is considerably shorter than the corresponding distance in $[Cl\text{--}PPh_3]^+$ (2.277 A). The variation of Pt-P bond distances and $^1J(Pt,P)$ with cis ligands in Pt(I) and Pt(II) complexes is general in nature (see Table I-5). It appears that when phosphines are trans to each other, the two Pt-P bond distances are longest when two ligands with a weak trans influence are bound in a cis manner

Table I-2. Selected Pt-Cl bond lengths in trans-[Pt(Y)Cl(PR_3)$_2$]$^{n+}$

Complex	Y-	Pt-Cl/Å	ref
t-[PtH(PEt_3)$_2$Cl]	H-	2.422	-[a]
[Pt_2(μ-dppm)$_2$$Cl_2$]	Cl-Pt-	2.405	-[b]
[Pt_2(μ-dppm)$_2$Cl(PPh_3)]$^+$	Ph_3P-Pt-	2.403	-[c]
[Pt_2(μ-dppm)$_2$(CO)Cl]$^+$	OC-Pt-	2.384	-[d]
[Pt(PEt_3)$_3$Cl]$^+$	Et_3P-	2.366	-[e]
t-[Pt(PEt_3)$_2$$Cl_2$]	Cl-	2.249	24

[a] From Eisenberg and Ibers.[28]

[b] From Manojlović-Muir et al.[29]

[c] This work.

[d] From Manojlović-Muir et al.[30]

[e] From Russell et al.[31]

Table I-3. Platinum-phosphorus coupling constants (Hz) for $[Pt_2(\mu\text{-dppm})_2L(PR_3)]^{n+}$ complexes[a]

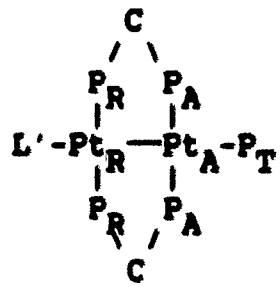

Complex	$^1J(Pt_A,P_A)$	$^1J(Pt_R,P_R)$	$^1J(Pt_A,P_T)$	$^2J(Pt_R,P_T)$	Ref
$[I\text{--}PPh_3]^+$	2881	2843	2200	1290	-[b]
$[Cl\text{--}dppm]^+$	2921	2872	2146	1270	-[b]
$[Cl\text{--}PPh_3]^+$	2876	2894	2186	1232	-[b]
$[PPh_3\text{--}PPh_3]^{2+}$	2800		1680	1008	6
$[PMePh_2\text{--}PMePh_2]^{2+}$	2870		1914	750	"
$[PMe_2Ph\text{--}PMe_2Ph]^{2+}$	2840		1938	650	"
$[H\text{--}dppm]^+$	2880	3510	2190	620	27
$[H\text{--}PPh_3]^+$	2894	3532	2181	596	"
$[H\text{--}PMePh_2]^+$	2850	3484	2162	592	"
$[H\text{--}PMe_2Ph]^+$	2884	3470	2188	576	"
$[Me\text{--}PPh_3]^+$	2976	3510	2040	490	4
$[Me\text{--}PMe_2Ph]^+$	2960	3510	2054	476	"
$[Me\text{--}dppm]^+$	2970	3550	2020	435	"

[a]Solvent was CD_2Cl_2 in all cases.

[b]This work.

Table I-4. Selected Pt-P bond lengths and $^{1}J(Pt,P)$ in trans-$[Pt(P'R_3)_2(PR_3)(Y)]^{n+}$

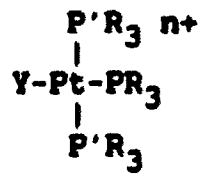

Complex	Y-	Pt-PR_3/A	$^{1}J(Pt,P_Y)$/Hz	ref
t-$[PtH(Pcy_3)_2(PPh_3)]^+$	H-	2.359		-[a]
$[H--dppm]^+$	H-Pt-	2.347	2190	-[b]
$[PtH(PEt_3)_3]^+$	H-	2.335	2037	31
$[Cl--PPh_3]^+$	Cl-Pt-	2.333	2146	-[c]
$[Pt(PEt_3)_3Cl]^+$	Cl-	2.251	3499	31
$[Pt(PEt_3)_3F]^+$	F-	2.224	3455	31

[a] From Clark and co-workers;[32] $Pcy_3 = P(C_6H_{11})_3$.

[b] From Manojlović-Muir and co-workers.[33] and ref 27.

[c] This work.

Table I-5. The "cis effect" of substituents on Pt-P bond lengths and $^{1}J(Pt,P)$ in trans-$[Pt(PR_3)_2(X)(Y)]^{n+}$

Complex	X-Pt-Y	Pt-P/A	$^{1}J(Pt,P)$/Hz	ref
$[Pt(PEt_3)_3Cl]^+$	P-Pt-Cl	2.354	2233	32
$[Pt(PEt_3)_3F]^+$	P-Pt-F	2.337	2382	32
$[CO--CO]^{2+}$	Pt-Pt-CO	2.320	2390	-[a]
t-$[Pt(PEt_3)_2Cl_2]$	Cl-Pt-Cl	2.314	2400	24
$[Cl--CO]^+$	Pt-Pt-CO	2.306	2591	-[b]
$[PtH(PEt_3)_3]^+$	H-Pt-P	2.301	2515	32
$[Cl--CO]^+$	Pt-Pt-Cl	2.295	2711	-[b]
$[Cl--PPh_3]^+$	Pt-Pt-P	2.278	2921	-[c]
$[H--dppm]^+$	Pt-Pt-P	2.277	2880	-[d]
$[Cl--PPh_3]^+$	Pt-Pt-Cl	2.277	2872	-[c]
t-$[PtH(PEt_3)_2Cl]$	H-Pt-Cl	2.268	2723	-[e]
$[Cl--Cl]$	Pt-Pt-Cl	2.268	2936	-[f]
$[H--dppm]^+$	H-Pt-Pt	2.249	3510	-[d]

[a] From Fisher and co-workers[34] and ref. 6.

[b] Ref. 7 and 30.

[c] This work.

[d] References 27 and 33.

[e] References 24 and 28.

[f] References 5 and 29.

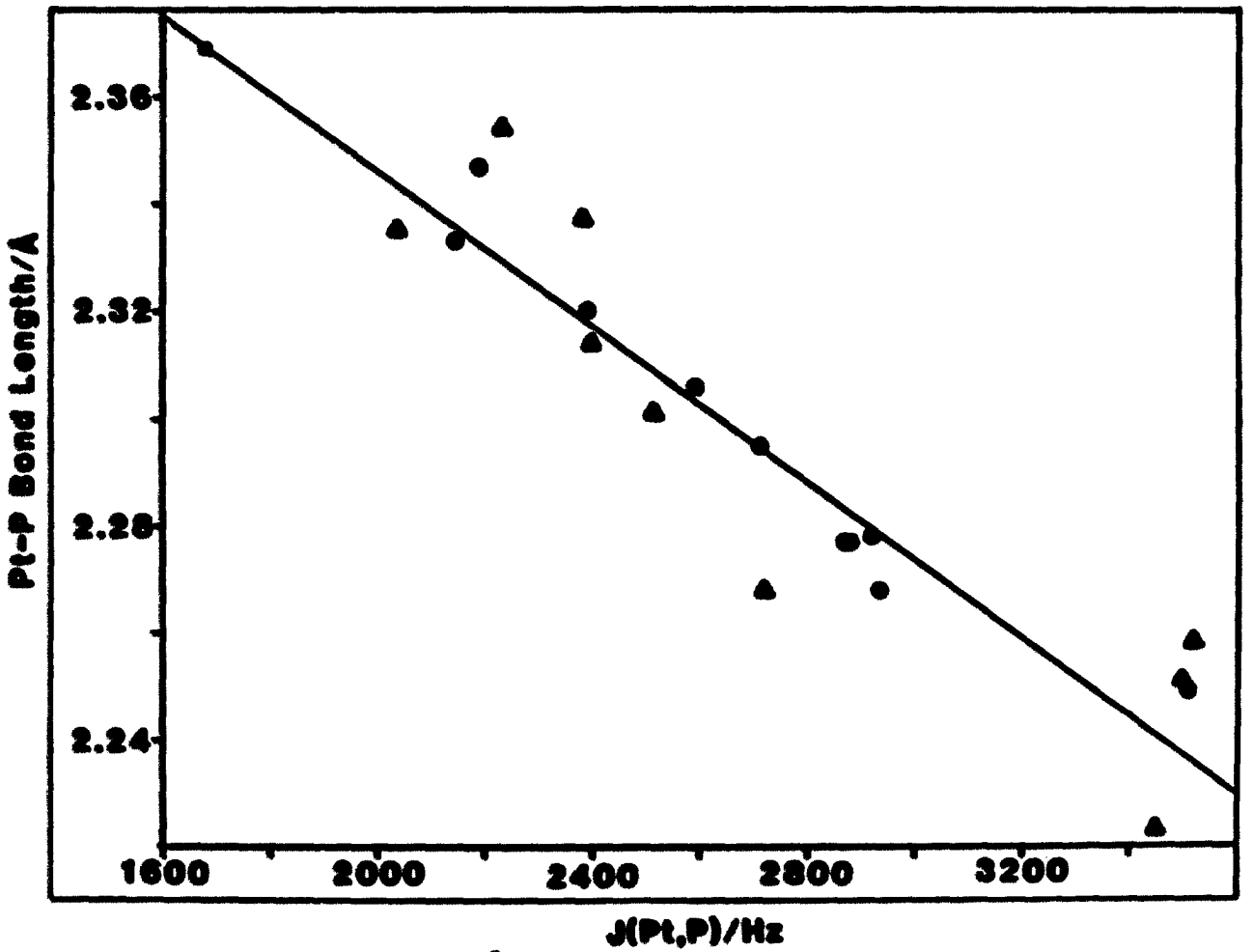

Figure I-4. Pt-P bond length vs. $^{1}J(Pt,P)$ for dppm bridged Pt(I) dimers (o) and Pt(II) complexes (Δ); least squares slope is extrapolated to $^{1}J(Pt_A,P_T)$ for $[Pt_2(\mu\text{-dppm})_2(PPh_3)_2]^{2+}$; (σ = 1680 Hz)

(2.31-2.35 A, $^{1}J(Pt,P)$ = 2200-2400 Hz). They become shorter when one of the two cis ligands have a strong trans influence (2.27-2.32 A, 2400-2900 Hz), and are shortest in the Pt_R-P_R bond distance of $[H{-}{-}dppm]^{+}$ (2.249 A, 3510 Hz) where two "ligands" with a strong trans influence (H^{-}- and Pt-) are cis to the pair of trans phosphines.

Despite the insensitivity of $^{1}J(Pt_A,P_T)$ to the ligand bound to Pt_R and trans to Pt_A (L'), trans-$^{2}J(Pt_R,P_T)$ are very sensitive to the nature (L') and follow the trans influence order (see Table I-3):

$$Me^{-} > H^{-} > PMe_2Ph > PMePh_2 > PPh_3 > X^{-}$$

The Pt_A-P_T bond distances in $[H{-}{-}dppm]^{+}$ and $[Cl{-}{-}PPh_3]^{+}$ are almost identical (2.347 and 2.333 A) and so $^{1}J(Pt_A,P_T)$ would be expected to vary little between the two complexes. Because the two corresponding Pt-Pt bond lengths vary considerably (2.769 and 2.665 A) and the $^{2}J(Pt_R,P_T)$ decrease dramatically with increasing Pt-Pt bond length (620 and 1232 Hz), the size of trans-$^{2}J(Pt_R,P_T)$ appears to be a good indicator of Pt-Pt bond strength. This correlation of trans-$^{2}J(Pt,P)$ with Pt-Pt bond distances in $[L'{-}{-}PR_3]^{n+}$ suggest that the Pt-Pt bond is weakened with increasing trans influence of L'. The Pt-Pt bond distances of other $[L'{-}{-}L]^{n+}$ complexes ($L \neq PR_3$) for which crystal structures have been solved also tend to support

this correlation (see Table I-6) but suggest that other factors may also effect the Pt-Pt bond length (trans influence of CO ≈ Cl^-).

A good correlation of Pt-Pt bond distance with not only trans- but also cis-^2J(Pt,P) is observed. It was proposed that the size of cis-^2J(Pt,P) in $[L--L']^{n+}$ should be a function of Pt-Pt bond strength in 1978 by Brown et al.[21] and was later substantiated in 1979 by Manojlovic-Muir et al.[30] Since then, the crystal structures of $[CO--CO]^{2+}$,[34] $[Cl--PPh_3]^+$, and $[H--dppm]^+$[33] (see Table I-6) have been solved. The cis-^2J(Pt,P) for $[CO--CO]^{2+}$ fits well in the trend of decreasing cis-^2J(Pt,P) with increasing Pt-Pt bond length as do the values for $[Cl--PPh_3]^+$ if one assumes the coupling constants have negative signs.

Cis and trans-^2J(Pt,P) tend to complement each other as a measure of Pt-Pt bond strength. Although the cis coupling constants should be observed in all Pt(I) dimers of this type, problems are often encountered in accurately determining their values: 1. It is often difficult to determine the sign of the coupling constant (e.g., in $[Cl--PPh_3]^+$). 2. The cis-satellites are not always well separated from the central resonance (e.g., in $[H--dppm]^+$). These problems are magnified in highly coupled systems such as complexes containing terminally bound phosphines, where correlation of trans-^2J(Pt,P)

Table I-6. Pt-Pt bond lengths and ^{31}P-^{195}Pt NMR coupling constants[a]

Complex	Pt-Pt/A	cis-^{2}J(Pt,P)/Hz	trans-^{2}J(Pt,P)/Hz	ref
[Cl--Cl]$^+$	2.620	-62, -92	na	-[b]
[CO--CO]$^{2+}$	2.642	-96	na	-[c]
[Cl--Cl]	2.651	-136	na	-[d]
[Cl--PPh_3]$^+$	2.665	±81, ±142	1232	-[e]
[H--dppm]$^+$	2.765	nr	620	-[f]

[a] na = not applicable, nr = not reported.

[b] Ref. 30.

[c] Ref. 6 and 34.

[d] Ref. 5 and 29.

[e] This work.

[f] Ref. 27 and 33.

with Pt-Pt bond length appears to be more useful because of its larger magnitude, and greater sensitivity. Therefore, although neither type of coupling constant is observed in all $[L--L']^{n+}$ due to the nature of L and L' (e.g., trans-$^2J(Pt,P)$) or experimental limitations (e.g., cis-$^2J(Pt,P)$) at least one of these constants are observed for practically all [L--L'].

Distortion of square planar platinum The square planar geometry around the platinum bound to PPh_3 (Pt1) is tetrahedrally distorted (see Figure I-5). The extent of this distortion is delineated by a comparison of bond angles (Table I-7) and least square planes (Table I-8) about each platinum. The cis bond angles around Pt1 diverge from 90^0 in a manner that will accommodate the steric requirements of the bulky PPh_3. The smaller than ideal P2-Pt1-P3 (160^0) and Pt_2-Pt1-P2 (165^0) angles relieve phenyl-phenyl repulsions of two PPh_3 phenyls (1B and 1C) and with the two adjacent equatorial phenyls (2B and 3A) respectively (see Figures I-5 and I-6). In fact, the Pt2-P1-P1-C11A torsional angle is much closer to 180^0 (-177^0) than the two angles just described. The extent and nature of distortions around Pt1 are also found around the Pt to which η^1-dppm is bound in $[H--dppm]^+$.[33]

It appears that steric repulsions in $[Cl--PPh_3]^+$ are relieved through distortions of the idealized square planar environment of Pt1 and not through elongation of the Pt-PPh_3 bond. The Pt-PPh_3 bond distance of 2.333 A is by no means

out of the ordinary considering the trans influence of the Pt-Pt bond. In $[PPh_3--PPh_3]^{2+}$, inward distortion of the $Pt(\mu\text{-dppm})_2$ ring from both directions may not be as favorable leaving Pt-P bond elongation as the only other alternative to relieve steric repulsions. This could be the reason for the very long $Pt-PPh_3$ bond length predicted above for $[PPh_3--PPh_3]^{2+}$.

Conformational geometry Conformations of the bridging dppm ligands enable the $Pt(\mu\text{-dppm})_2$ nucleus to adopt a twisted configuration (see Figures I-5 and I-7) in which the least squares coordination planes of the two metal atoms are rotated about the Pt-Pt bond to give a dihedral angle of 42^0 (individual $P_R\text{-}Pt_R\text{-}Pt_A\text{-}P_A$ torsional angles found in Table I-9 diverge on both sides of this intermediate figure). Similar interplanar angles of 33.5^0 and 39^0 have been reported in $[H--dppm]^{+}$[33] and $[Cl--Cl]$[29] respectively. Both $[Pt_2(\mu\text{-dppm})(\eta^2\text{-dppm})_2]^{2+}$ with one and $[Pt_2(CO)_2Cl_4]^{2-}$ with no bridging ligands have interplanar angles very near 60^0. The twisted configuration in Pt(I) dimers lowers considerably any antibonding interactions between filled d_π metal orbitals.

The twist in the coordination planes of the two metals causes different orientations of phenyls on the PPh_3 side of the cation than there are on the Cl^- side (see Figure I-7). The axial dppm phenyls adjacent to PPh_3 (see Rings 2A and 3B) are found on opposite sides of the idealized coordination

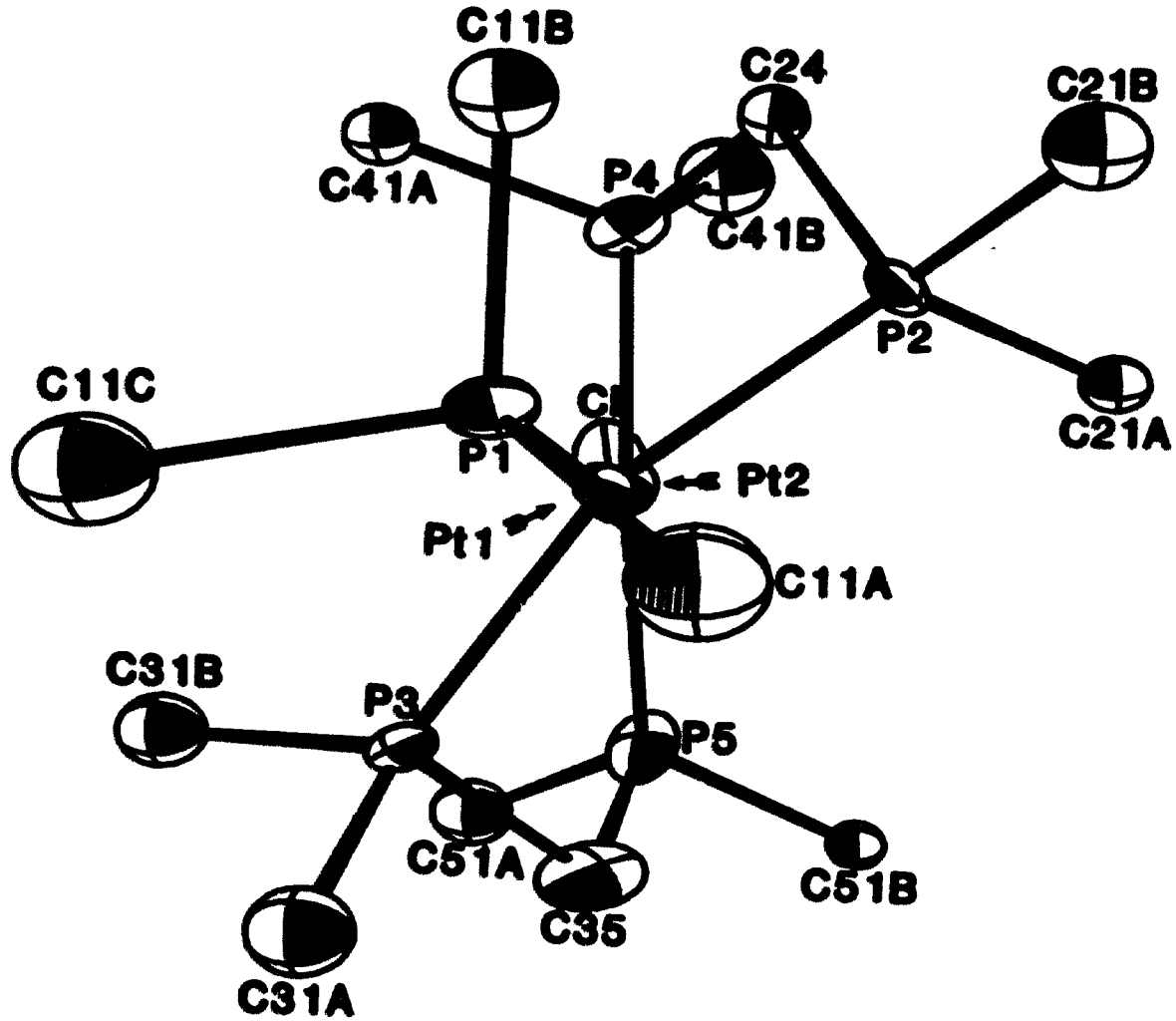

Figure I-5. Crystal structure of $[Pt_2(\mu\text{-dppm})_2Cl(PPh_3)]^+$ down the Pt-Pt bond axis; only α-carbons of the phenyl groups are included

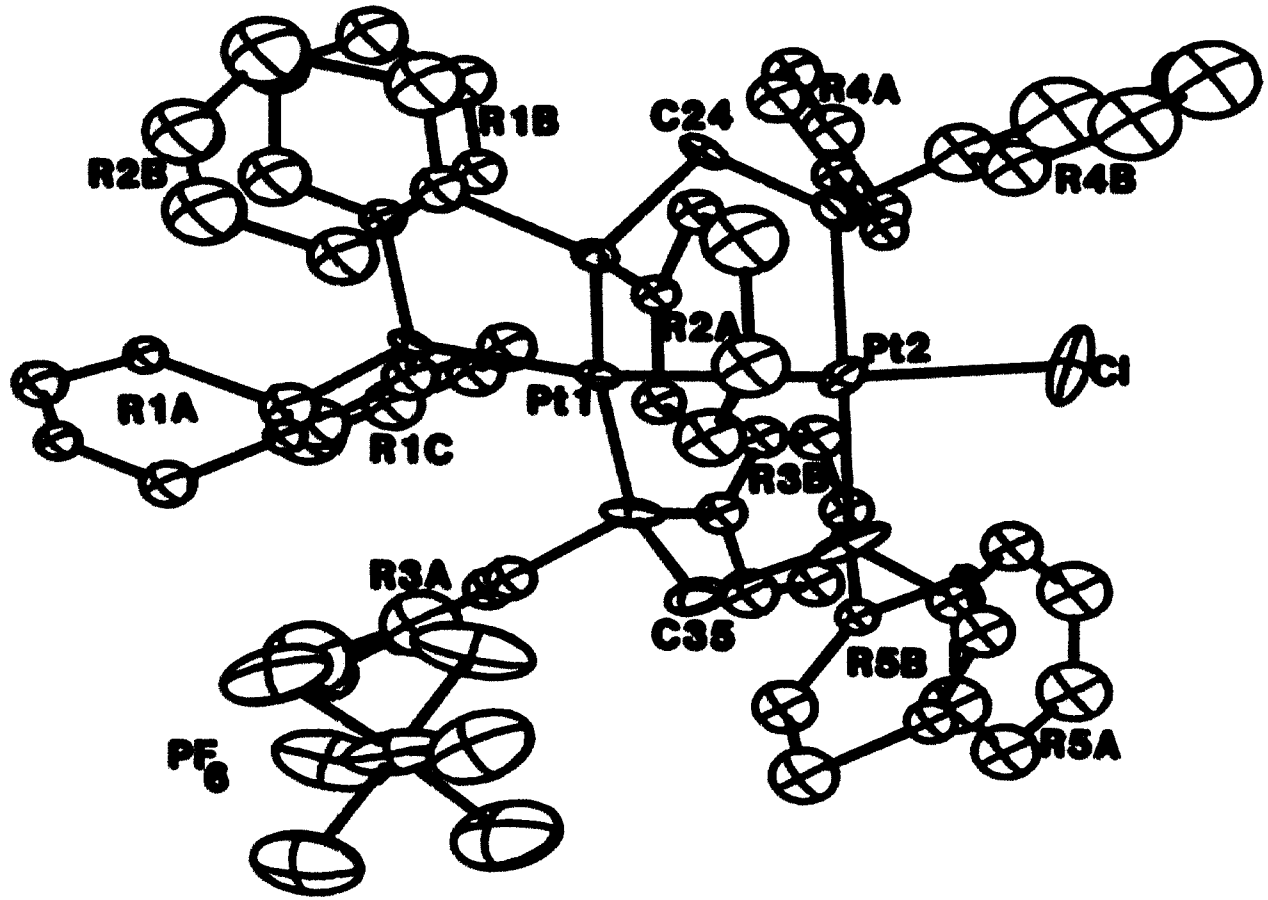

Figure I-6. Full ORTEP of $[Pt_2(\mu\text{-dppm})_2Cl(PPh_3)]^+$

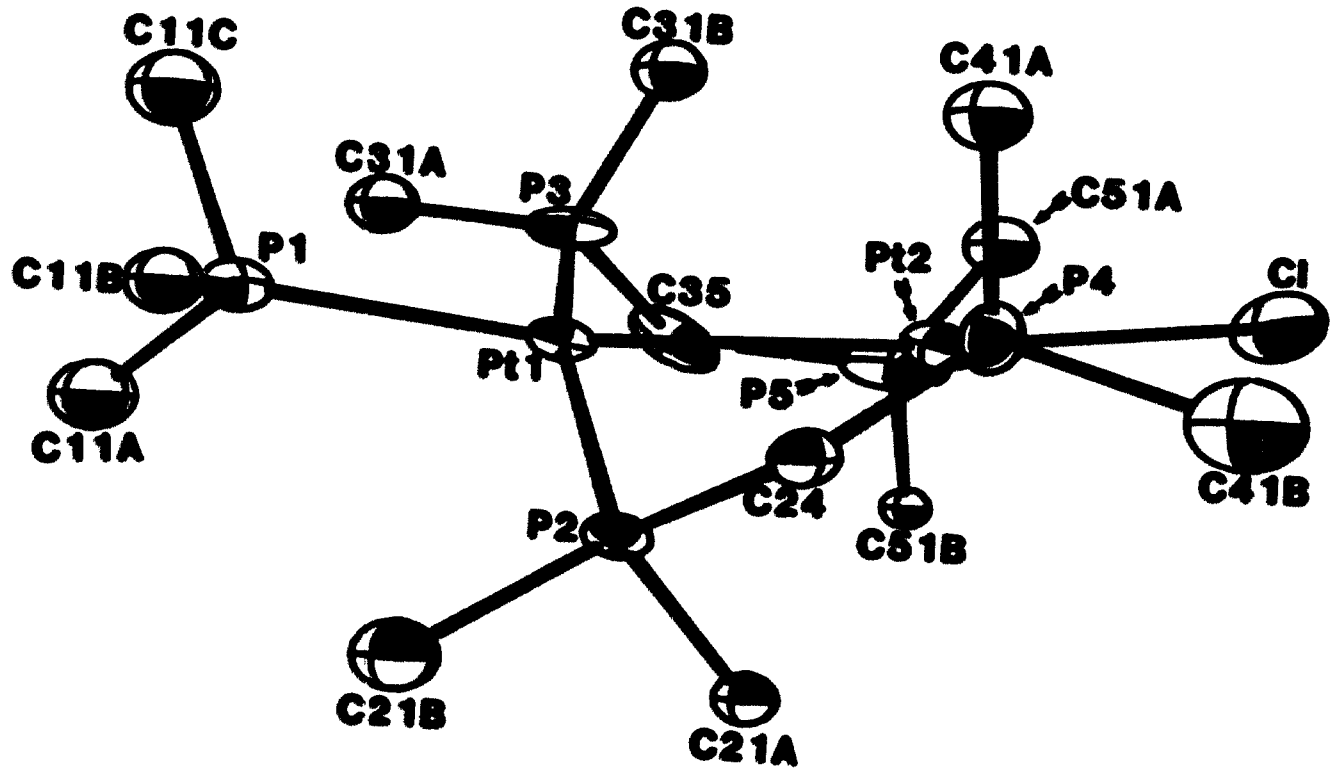

Figure I-7. Crystal structure of $[Pt_2(\mu\text{-dppm})_2Cl(PPh_3)]^+$ in a view perpendicular to the Pt-Pt bond axis; only the α-carbons of the phenyl groups are included

Table I-7. Bond angles around platinum atoms in $[Pt_2(\mu\text{-dppm})_2Cl(PPh_3)](PF_6)$

Pt bound to PPh_3		Pt bound to Cl-	
"90° angles"			
P2-Pt1-P1	97.3°	P4-Pt2-Cl	87.3°
P2-Pt1-Pt2	82.5°	P4-Pt2-Pt1	88.3°
P3-Pt1-P1	98.2°	P5-Pt2-Cl	92.7°
P3-Pt1-Pt2	85.9°	P5-Pt2-Pt1	92.0°
"180° Angles"			
P1-Pt1-Pt2	164.7°	Pt1-Pt2-Cl	173.3°
P2-Pt1-P3	160.0°	P4-Pt2-P5	176.9°

Table I-8. Least square planes and atomic deviations therefrom

Pt1 Plane
-0.49676X + 0.75125Y + 0.43457Z + -5.14011 = 0.0
Standard Deviation = 0.437

Atom[a]	Shift/A	Atom	Shift/A
Pt1*	-0.016	C1	0.915
Pt2*	0.325	P4	1.730
P1*	0.301	P5	-1.166
P2*	-0.312	C24	1.257
P3*	-0.297	C35	-1.674

Pt2 Plane
-0.06172X + 0.99546Y + -0.07249Z + -6.30433 = 0.0
Standard Deviation = 0.125

Atom	Shift/A	Atom	Shift/A
Pt1*	0.088	P1	0.584
Pt2*	-0.020	P2	-1.631
C1*	0.098	P3	1.317
P4*	-0.087	C24	-1.019
P5*	-0.079	C35	0.266

[a]Atoms used to calculate the plane are marked with an asterisk.

Table I-9. Selected torsional angles in $[Pt_2(\mu\text{-dppm})_2Cl(PPh_3)]^+$

Angle	degrees	Angle	degrees
P2-Pt1-Pt2-P4	-47.4	P3-Pt1-Pt2-P5	-34.3
P2-Pt1-Pt2-P5	129.4	P3-Pt1-Pt2-P4	148.8
Pt2-Pt1-P2-C24	59.0	Pt2-Pt1-P3-C35	58.8
Pt1-Pt2-P4-C24	38.1	Pt1-Pt2-P5-C35	9.7
Pt2-Pt1-P1-C11B	-48.3	Pt2-Pt1-P1-C11C	65.4
Pt2-Pt1-P1-C11A	-177.2		
Pt2-Pt1-P2-C21A	-59.7	Pt2-Pt1-P3-C31B	-62.9
Pt2-Pt1-P2-C21B	-178.6	Pt2-Pt1-P3-C31A	170.7
		Pt1-Pt2-P5-D51B	-118.2
Pt1-Pt2-P4-C41A	-84.6	Pt1-Pt2-P5-C51B	-98.3
Pt1-Pt2-P4-C41B	155.0	Pt1-Pt2-P5-C51A	126.2
Pt1-P2-C24-H1	76.8	Pt2-P4-C24-H1	-123.0
Pt1-P2-C24-H2	-163.6	Pt2-P4-C24-H2	117.2
Pt1-P3-C35-H3	58.7	Pt2-P5-C35-H3	-91.7
Pt1-P3-C35-H4	178.0	Pt2-P5-C35-H4	149.4

plane (see Figure I-6) with the equatorial phenyls being very nearly eclipsed (see Table I-9 for Pt2-Pt1-P-C torsional angles). On the Cl side of the structure, the phenyls are staggered with respect to each other with the equatorial phenyls (4B and 5A, see Pt1-Pt2-P-C torsional angles) very nearly bisecting the opposing phenyl-P-phenyl bond (see Figures I-5 and I-7).

The "extended" cyclohexyl type $Pt_2P_4C_2$ ring is found in a twisted chair conformation, the "twist" of which has just been described. The dppm methylene carbon C35 diverges 0.74 A from the plane defined by P3, P5, and the center of the Pt-Pt bond. The PCH_2P C24 appears to be closer to an envelope position since it diverges from the plane defined by P2, P4, and the center of the Pt-Pt bond by only 0.35 A. Pt-P-C-H torsional angles support the fact that C24 is closer to an equatorial position (see Table I-9).

Ultraviolet-visible spectral properties of Pt(I) dimers

The Pt(I) dimers of the type $[Pt_2(\mu\text{-dppm})_2X(PPh_3)]^+$ have two absorbtion maxima each that are not obscured by aromatic absorbtion bands (λ > 300 nm) (see Figure I-8a). Each of the corresponding $[Pt_2(\mu\text{-dppm})(\eta^2\text{-dppm})X(PPh_3)]^+$ which are the intermediates designated CHELATE in the section (page 106) on reactions of halides with $[PPh_3\text{--}PPh_3]^{2+}$ has at least one observable absorbtion maximum (see Figure I-8b). As X^- varies from Cl^- to Br^- to I^-, the charge transfer transitions tend to

Table I-10. Spectral properties of PPh_3 substituted Pt(I) dimers in the ultraviolet-visible region

Complex	Cl^-/nm	Br^-/nm	I^-/nm
$[X--PPh_3]^+$	308[a]	318	337
$[X--PPh_3]^+$	372[a]	376[a]	388
CHELATE	384	396	429

[a]Shoulder.

Figure I-8. Ultraviolet-visible absorbtion spectra of 0.02 mM a. $[Pt_2(\mu\text{-dppm})_2X(PPh_3)]^+$ and b. $[Pt_2(\mu\text{-dppm})(\eta^2\text{-dppm})X(PPh_3)]^+$ in CH_2Cl_2 where $\cdots\cdots$ = Cl^-, —— = Br^-, and ---- = I^-

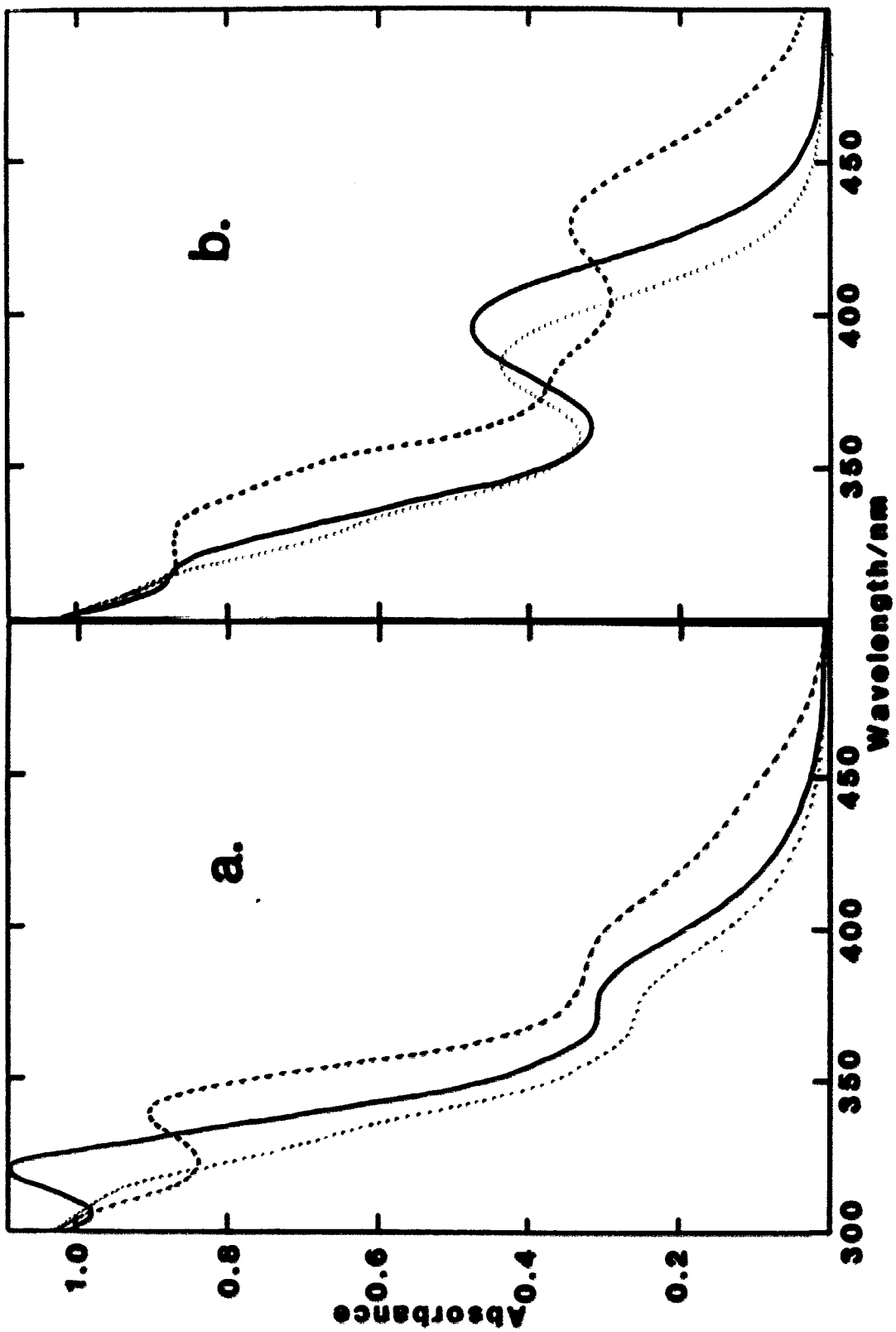
b.
a.
1.0
0.8
0.6
0.4
0.2
Absorbance
300
350
400
450
Wavelength/nm

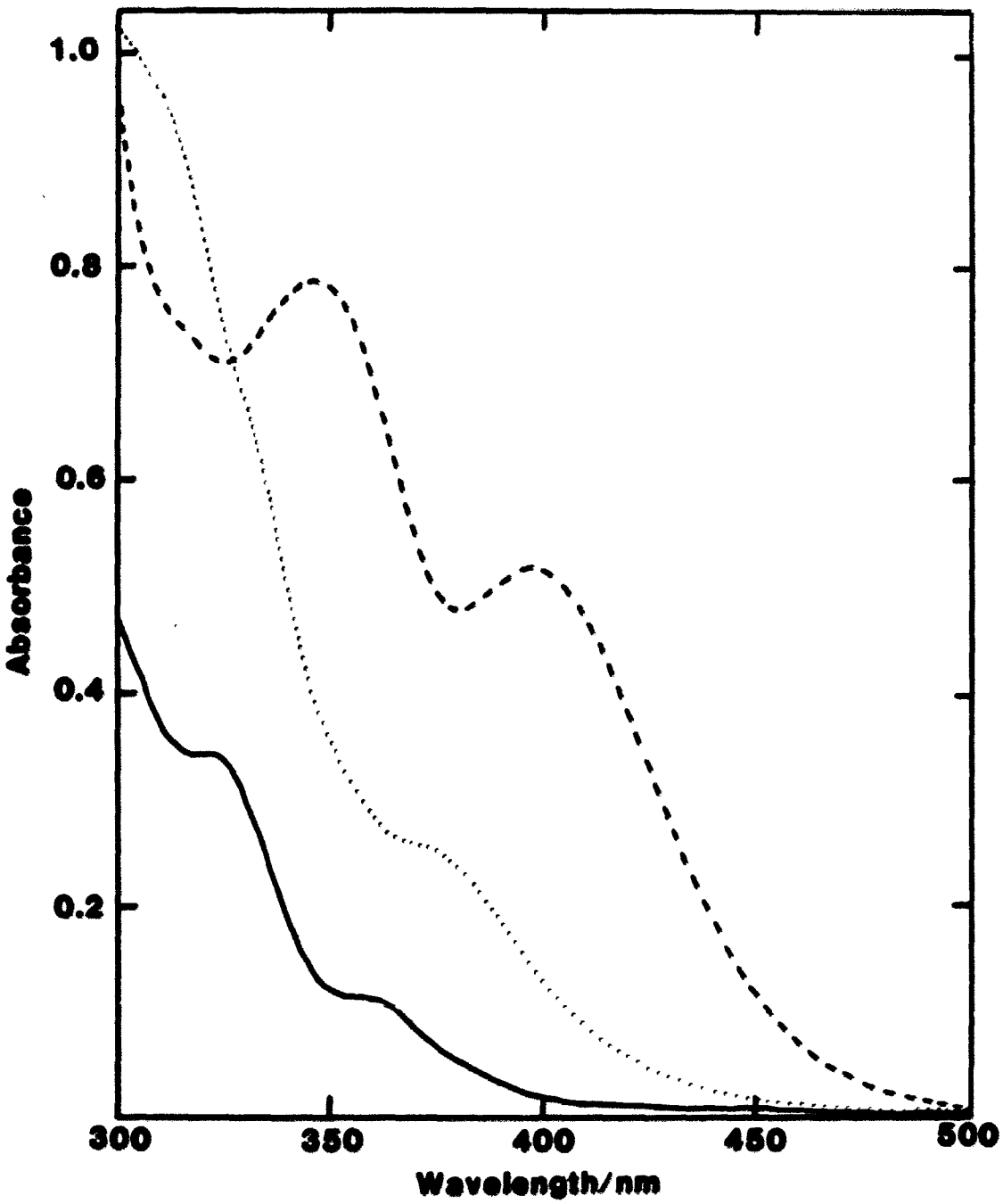

Figure I-9. Ultraviolet-visible absorbtion spectra of 0.02 mM $[Pt_2(\mu\text{-dppm})_2(PPh_3)_2]^{2+}$ (----), $[Pt_2(\mu\text{-dppm})_2Cl(PPh_3)]^{+}$ (····), and $[Pt_2(\mu\text{-dppm})_2Cl_2]$ (——) in CH_2Cl_2

lower energy (see Table I-10) as would be expected.

The absorbtion spectra for [Cl--Cl], [Cl--PPh_3]$^+$, and [PPh_3--PPh_3]$^{2+}$ vary considerably in spectral shape and molar absorbtivity at λ > 300 nm (Figure I-9). The molar absorbtivity increases upon replacement of terminal chlorides with PPh_3.

Conformational Properties of [$Pt_2(\mu\text{-dppm})_2Cl(PPh_3)$]$^+$

Conformational changes of the $Pt_2(\mu\text{-dppm})_2$ ring

Proton NMR of [$Pt_2(\mu\text{-dppm})_2Cl(PPh_3)$]$^+$ Proton NMR spectra of [Cl--PPh_3]$^+$ show the presence of complexes having two types of PCH_2P protons. There are two sets of PCH_2P resonances, one with a small (J < 20 Hz) and the other a large value (113 Hz) for ^3J(Pt,H). The chemical shift of the unresolved multiplet with J < 20 Hz is dependent on the counter-ion present and shifts upfield with increasing mole ratio of PF_6^- to Cl^- (see Figure I-10). The other resonance consists of three major peaks with area ratios 1 : 2.21 : 1, each of which is split into a doublet originating from geminal hydrogen coupling (^2J(H,H) = 13 Hz). The central doublet in this multiplet is due to the Pt isotopomer of [Cl--PPh_3]$^+$ containing no ^{195}Pt. The two satellites are due to the Pt isotopomer containing one ^{195}Pt (i.e., this isotopomer resonance is split into a doublet).[5]

This splitting pattern is characteristic of Pt

"A-frames"[12] where the presence of the bridging small molecule or atom causes inequivalence in the PCH_2P protons, but it stands in contrast to [Cl--Cl] (see Figure I-11), $[PPh_3--PPh_3]^{2+}$, and other known $Pt(I)(\mu\text{-dppm})_2$ complexes where two CH_2 protons are equivalent. Thus, $[Cl--PPh_3]^+$ is particularly remarkable in this respect, since this feature was quite unanticipated. We thus sought to understand the origin of this spectral feature, which appears to arise from conformational changes. As with the Pt "A-frames", the ^1H NMR data for $[Cl--PPh_3]^+$ suggest asymmetry along the axis perpendicular to the Pt_2P_4 "plane". This asymmetry may be caused by an interlocking of the phenyl rings of PPh_3 and dppm which forces the methylene group of each dppm to remain in a position above or below the Pt_2P_4 plane.

Molecular models suggest less steric repulsion between dppm and PPh_3 phenyls when the PCH_2P methylenes are in such out-of-plane configurations. When the complex is in a boat or chair form of the "extended" cyclohexyl type ring of $Pt_2P_4C_2$, rotation about the Pt-PPh_3 bond is hindered only by the two equatorial phenyls bound to the P_A of each bridging dppm (see Figure I-12a). The angle of rotation (ω_t) of the Pt-PPh_3 bond estimated from "ball and stick" models of the complex in a boat or chair form is about 60^0. As a PCH_2P carbon becomes planar, the angle of this Pt-PPh_3 bond rotation is further restricted ($\omega_t = 25^0$) due to intramolecular contact of the two

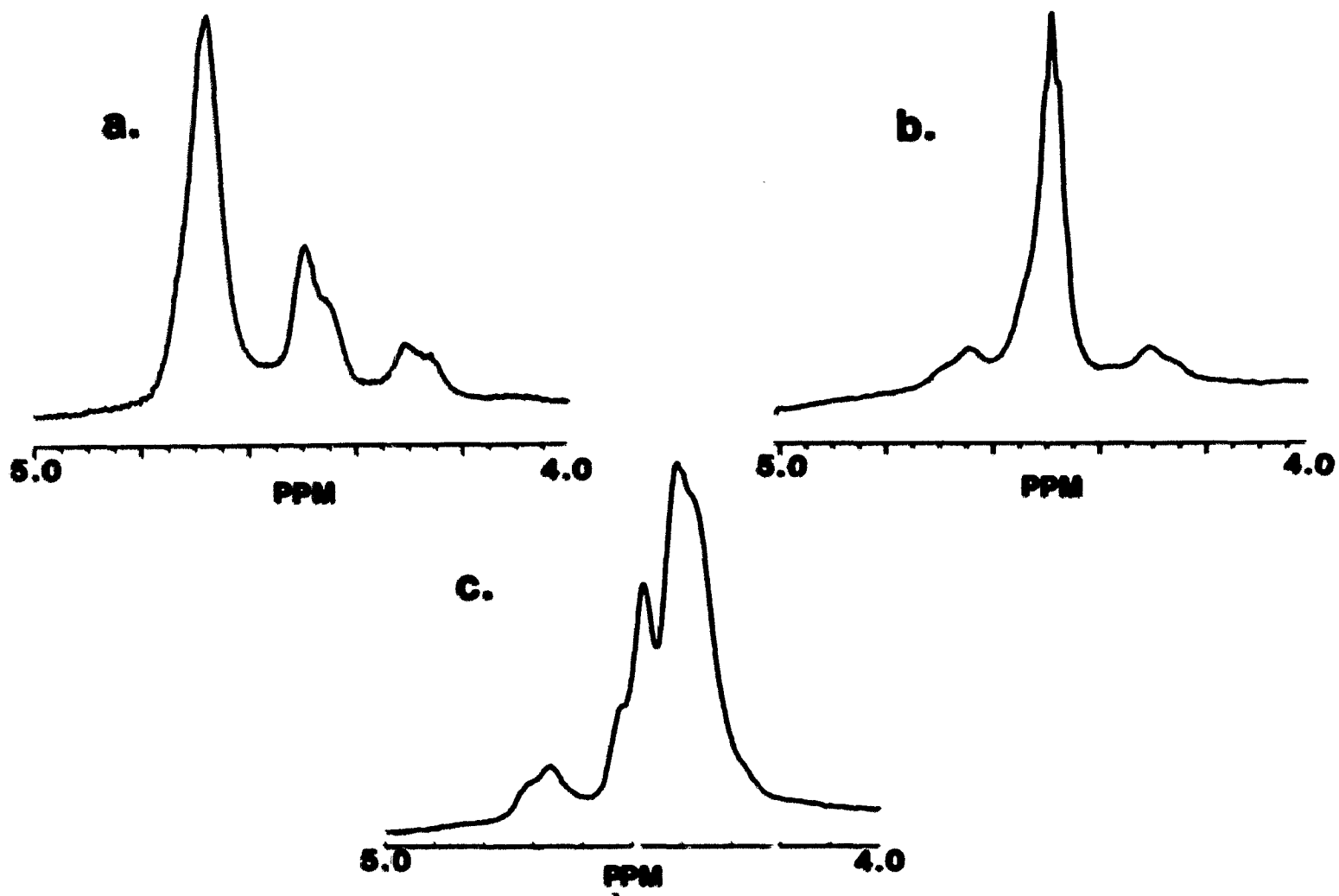

Figure I-10. The PCH_2P region of the ^1H NMR (300 MHz) of $[Pt_2(\mu\text{-dppm})_2Cl(PPh_3)]^+$ with: (a) only Cl^- present in CD_2Cl_2, (b) 1.2 Cl^- to 1 PF_6^- in CD_2Cl_2, and (c) only PF_6^- present in $C_2D_2Cl_4$

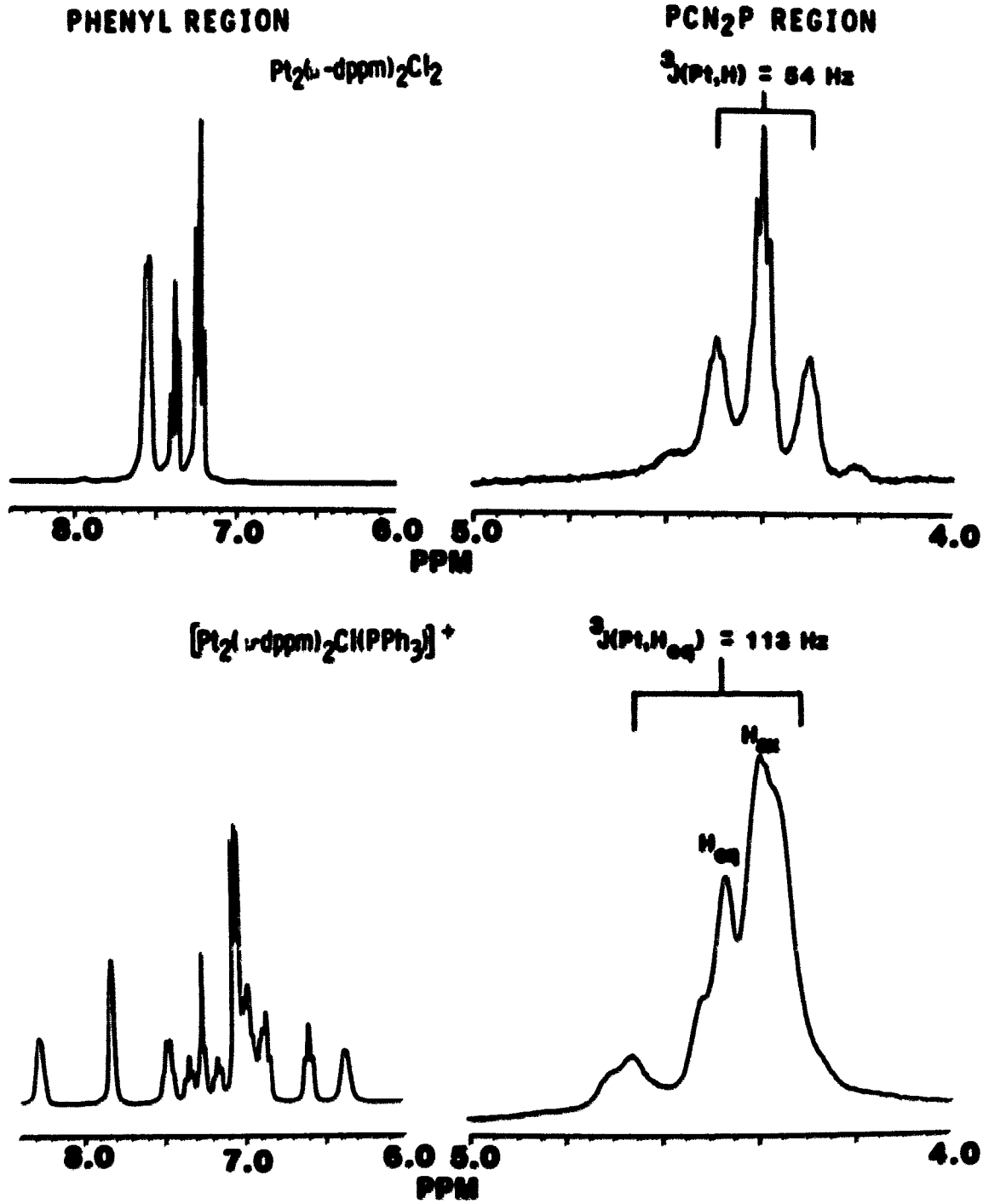

Figure I-11. The ^{1}H NMR (300 MHz) of $[Pt_2(\mu\text{-dppm})_2Cl_2]$ and $[Pt_2(\mu\text{-dppm})_2Cl(PPh_3)](PF_6)$ at ambient temperature

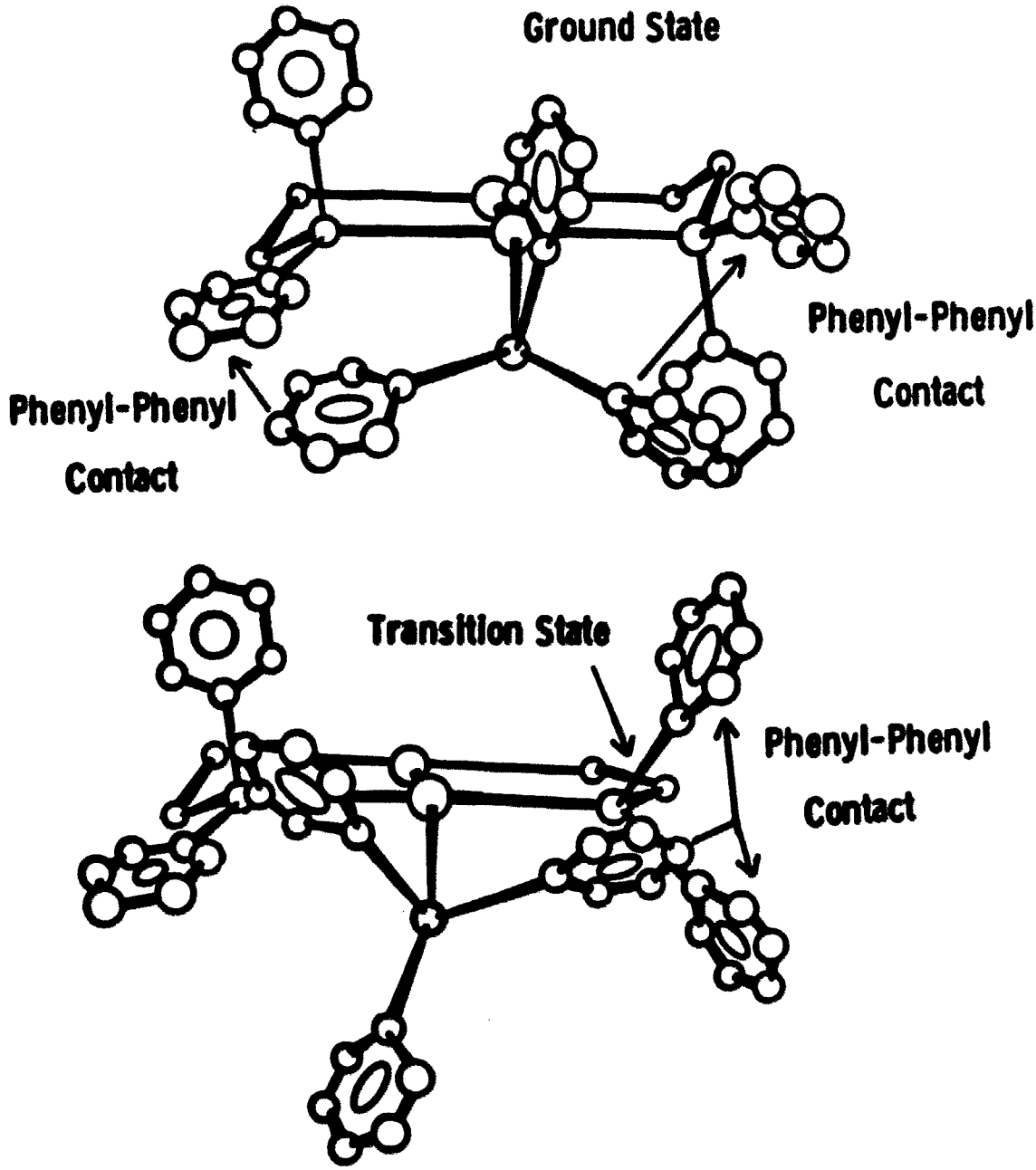

Figure I-12. Models for $[Pt_2(\mu\text{-dppm})_2Cl(PPh_3)]^+$ in a chair configuration (top) and a boat/chair transition (bottom); the arrows point from PPh_3 to those on dppm ligands that collide upon rotation of PPh_3 about the Pt-P bond

phenyls bound to the planar dppm with the PPh_3 phenyl that bisects the angle between them (see Figure I-12b). Because the constrained PPh_3 phenyl bisects the angle between the two dppm phenyls, ω_t increases from 25° to 55° when the the Pt-P bond is increased from 2.2 to 2.4 A. This suggests that the rate of boat/chair isomerization is very sensitive to the Pt-P bond distance.

Karplus[35] has found that the magnitude of the vicinal H-H coupling constants is a function of the dihedral angle (θ) between the two hydrogens. Coupling constants are at a maximum at $\theta = 0°$ and 180°, they are at a minimum at 90°. Such Karplus-type dependence in vicinal coupling constants has also been observed for other pairs of nuclei including coupling constants involving a metal center (e.g., $^3J(^{119}Sn,^{13}C)$[36]). Considering the dihedral angles between the Pt-P bond and the two types of C-H bonds ($\approx 70°$ axial, $\approx 180°$ equatorial), the equatorial protons should be assigned to the proton resonance with a 113 Hz Pt-H coupling constant. According to this assignment, the resonance due to axial protons is the one which undergoes counter-ion dependent shifts (e.g., Figure I-10). Since negatively charged counter-ions will most likely be associated with the Pt centers, their presence will cause greater perturbations in the chemical shift of axial protons while leaving the shift of equatorial protons largely unaffected.

Variable temperature ^{1}H NMR A feature of the ^{1}H NMR spectra of at least some "A-frame" complexes is that the PCH_2P resonances are better resolved at 80 ^oC than at 35 ^oC. This is thought to be due to insufficiently rapid interconversion of different conformations of the fused nonplanar five-membered Pt_2P_2C rings of the $Pt_2(\mu\text{-dppm})_2$ system[12] at the lower temperature. Variable temperature ^{1}H NMR was used to verify that $[Cl\text{--}PPh_3]^+$, although not an "A-frame", is subject to similar effects. The complications in its PCH_2P spectrum are caused by the "cog-like" steric interactions between the dppm and PPh_3 phenyl rings which slow the rate of exchange of the axial and equatorial positions for substituents on the "extended" cyclohexyl type $Pt_2P_4C_2$ ring. This exchange may occur by a boat to chair or a chair to chair transition. In the latter transition, the axial and equatorial positions of substituents on both Pt_2P_2C rings are exchanged simultaneously. The ^{1}H NMR spectra do not distinguish between these two processes.

The room temperature ^{1}H NMR spectrum of the PCH_2P region has already been described. As the temperature increases, the two PCH_2P resonances coalesce into one 1 : 2.21 : 1 triplet with a $^3J(Pt,H)$ of 57 Hz which is the average of the $^3J(Pt,H_{eq})$ and $^3J(Pt,H_{ax})$ found in the spectrum of $[Cl\text{--}PPh_3]^+$ at the slow exchange limit. The unsymmetrical formation of the high temperature triplet is due to the difference in the

coalescence temperatures of the low field (T_c = 360 ± 10 K) and high field (T_c = 333 ± 10 K) satellites (see Figure I-13). The majority of the phenyl resonances also broaden and coalesce, however, two phenyl multiplets remain essentially unchanged throughout the temperature increase (see Figure I-14). The computer integrated intensities of the two types of protons gave a broadened/nonbroadened ratio of 2.42 ± 0.13 at three selected temperatures. This suggests that the dppm phenyls are fluxional and those of PPh_3 are not (dppm/PPh_3 phenyl hydrogens = 2.67). The axial/equatorial exchange process causes interconversion of the environments of both the PCH_2P hydrogens and the dppm phenyl rings, whereas the PPh_3 phenyls are locked into one environment during such conformational changes.

Owing to the complexity of the spectrum, line shape analysis which is often used to obtain kinetic information from temperature dependent NMR spectra is very difficult. On the other hand, because of the complexity of the spectrum, a large number of different peaks coalesce over a fairly broad range of temperatures. Rate constants at the various coalescence temperatures were evaluated from the NMR data. A plot of ln (k/T) vs. 1/T proved to be linear and data obtained from the phenyl region lie on the same line as that obtained from the PCH_2P region (Figure I-15). This proves that the same process causes signal averaging of both the phenyl and PCH_2P

proton resonances and allows evaluation of the activation parameters for that process. The value of $\Delta S^{\ddagger}$ = -0.7 ± 3.4 eu is very reasonable for a conformational change. The value of $\Delta H^{\ddagger}$ is 16.5 ± 1.1 kcal/mol which is slightly higher than the upper limit for conformational changes of substituted cyclohexanes (e.g., for cis-1,2-di-t-butylcyclohexane $\Delta H^{\ddagger}$ = 15.4 ± 1.0 kcal/mol[37]), and is indicative of a highly strained transition state for this axial/equatorial exchange process in $[Cl{-}{-}PPh_3]^+$.

Proton NMR of related complexes Table I-11 contains $^3J(Pt,H)$ for PCH_2P hydrogens in a number of $Pt(\mu\text{-dppm})_2$ complexes. The $^3J(Pt,H)$ for Pt(I) complexes containing equivalent PCH_2P hydrogens are approximately the average value for the two $^3J(Pt,H)$ in Pt(I) complexes containing inequivalent hydrogens (e.g., Figure I-11). This must be the case, i.e., just as the 57 Hz coupling constant for the high temperature form of $[Cl{-}{-}PPh_3]^+$ is an average of two coupling constants, so also must the coupling constants reported for complexes containing equivalent hydrogens (on the NMR time scale) be an average of their respective axial and equatorial coupling constants.

Only in Pt(I) complexes which have potential for significant phenyl-phenyl repulsion during an axial/equatorial transition are nonequivalent hydrogens observed. With respect to the PCH_2P resonances, the following statement has been made

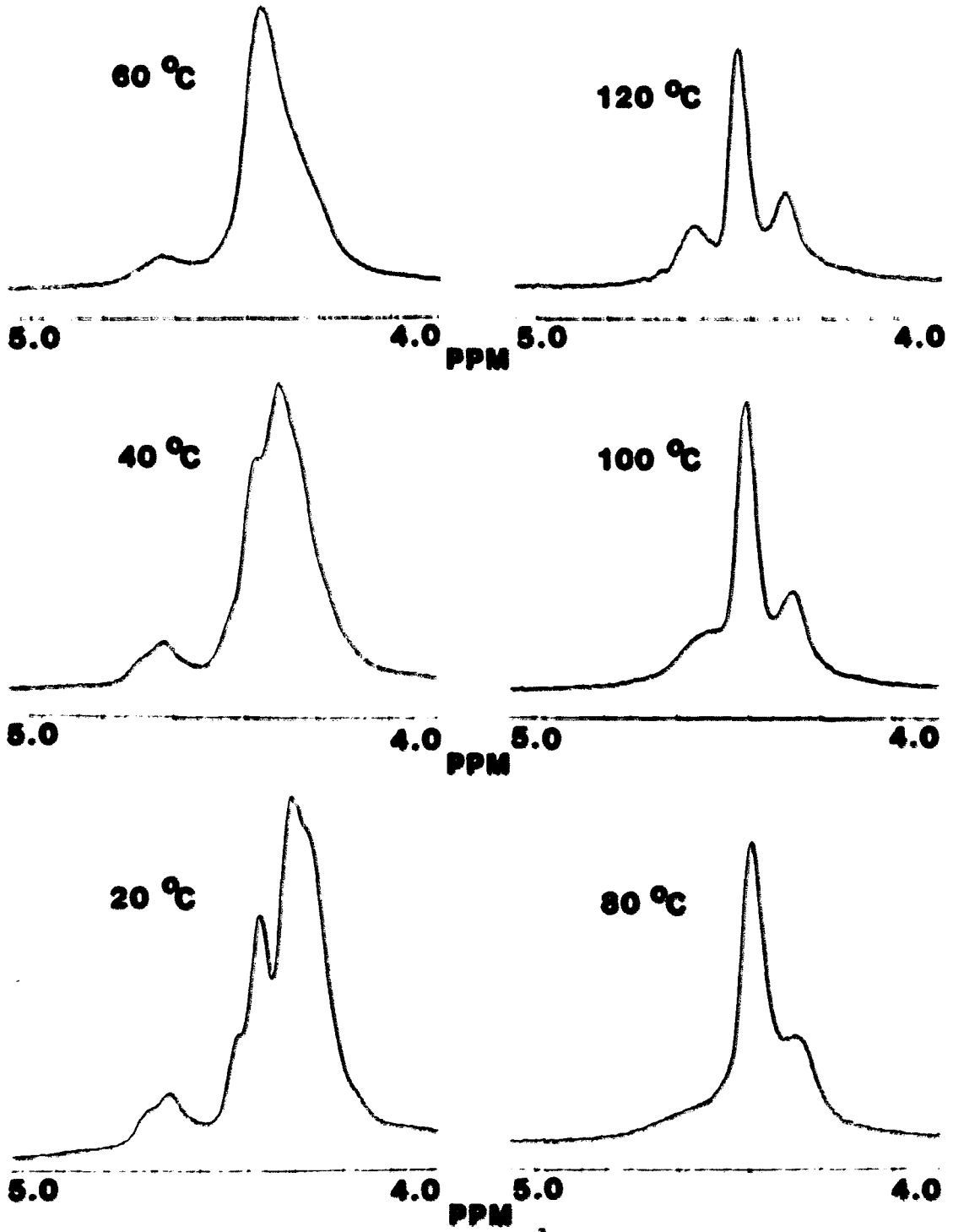

Figure I-13. PCH_2P region of the ^1H NMR (300 MHz) of $[Pt_2(\mu\text{-dppm})_2Cl(PPh_3)]^+$ in $C_2D_2Cl_4$ as a function of temperature

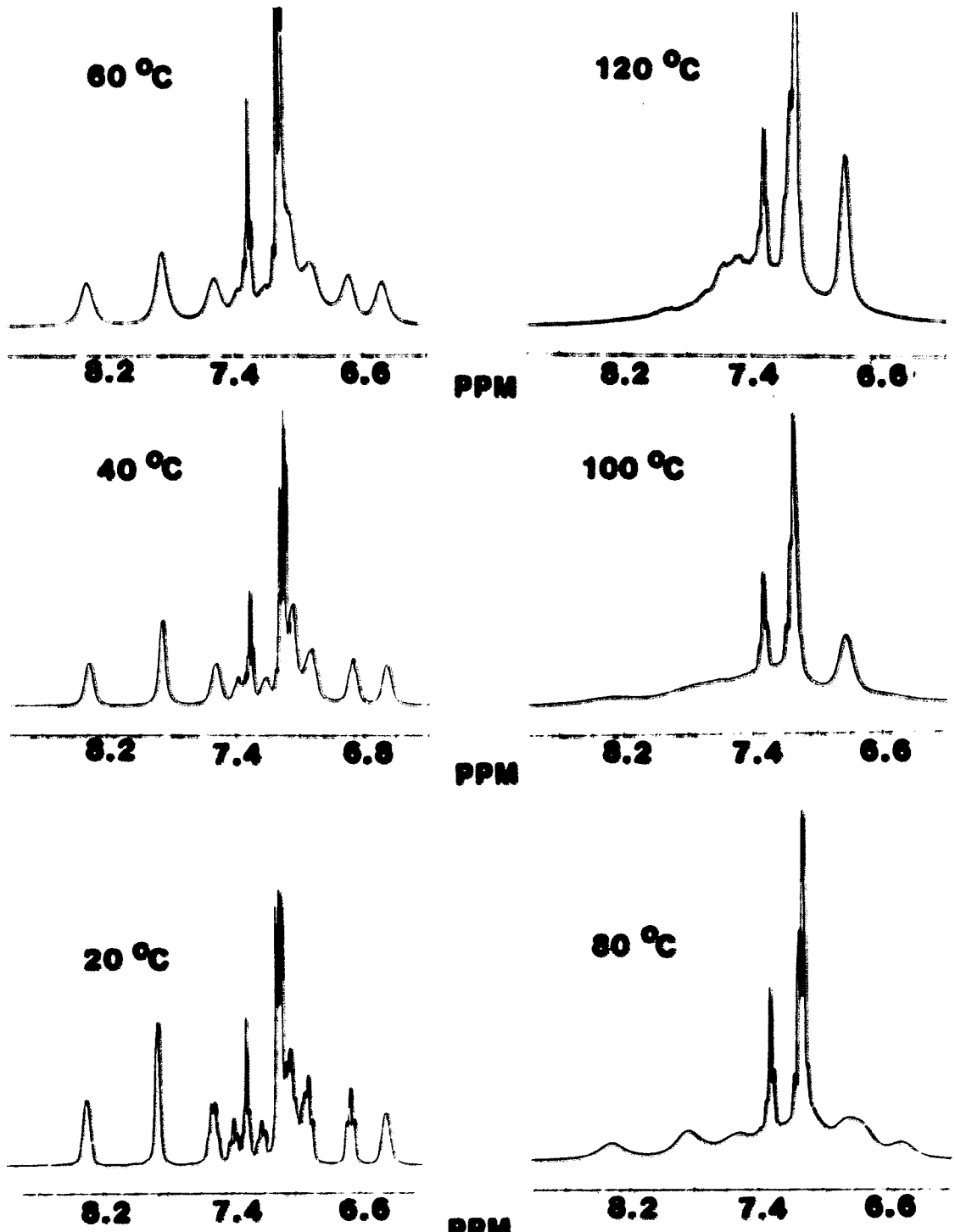

Figure I-14. Phenyl region of the ^{1}H NMR (300 MHz) of $[Pt_2(\mu\text{-dppm})_2Cl(PPh_3)]^+$ in $C_2D_2Cl_4$ as a function of temperature

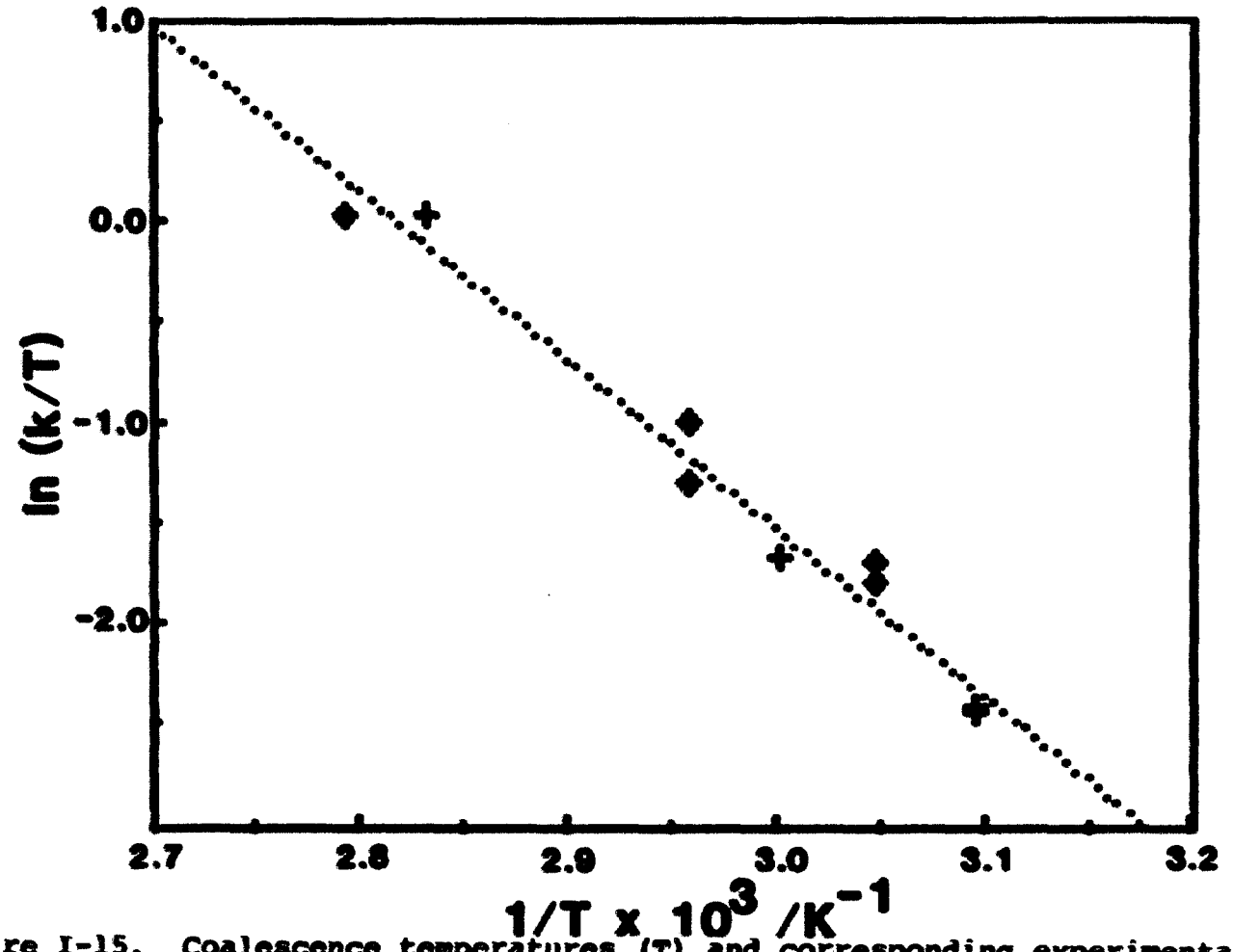

Figure I-15. Coalescence temperatures (T) and corresponding experimental rate constants for axial/equatorial exchange (k) from the phenyl (+) and PCH_2P (♦) regions of the ^1H NMR (300 MHz) of $[Pt_2(\mu\text{-dppm})_2Cl(PPh_3)]^+$ plotted as ln(k/T) vs. 10^3 $(1/T)/K^{-1}$

Table I-11. $^3J(Pt,H)$ (Hz) for PCH_2P hydrogens in selected $Pt_2(\mu\text{-dppm})_2$ complexes

Nonequivalent Hydrogens[a]			Equivalent Hydrogens[a]	
Complex	$^3J(Pt,H)_{ax}$	$^3J(Pt,H)_{eq}$	Complex	$^3J(Pt,H)$
$[Cl\text{--}PPh_3]^{+b}$	J < 10	113	$[Cl\text{--}PPh_3]^{+c}$	57
$[Cl\text{--}dppm]^{+}$	J < 10	124	$[H\text{--}PPh_3]^{+d}$	40,72
$[Cl\text{--}P_4\text{--}Cl]^{2+e}$	J < 10	110	$[H\text{--}PMe_2Ph]^{+d}$	38,68
$[Cl\text{-}CH_2\text{-}Cl]^{f}$	10	57	$[Cl\text{--}Cl]^{g}$	54
$[L\text{-}CH_2\text{-}L]^{2+h}$	12	48	$[L\text{--}L]^{2+i}$	56

[a]Unless specified, the NMR solvent is CD_2Cl_2.

[b]This spectrum was acquired at 20 °C in $C_2D_2Cl_4$.

[c]This spectrum was acquired at 120 °C in $C_2D_2Cl_4$.

[d]From ref. 27.

[e]$[\{Pt_2Cl(\mu\text{-dppm})_2\}_2(di\text{-}\eta^2\text{-}P_4)]^{2+}$, discussed in Part I-B.

[f]$[Pt_2(\mu\text{-dppm})_2(\mu\text{-}CH_2)Cl_2]$, from ref. 12.

[g]From ref. 5.

[h]$[Pt_2(\mu\text{-dppm})_2(\mu\text{-}CH_2)(PPh_3)_2]^{2+}$, from ref. 20.

[i]$[Pt_2(\mu\text{-dppm})_2(PPh_3)_2]^{2+}$, from ref. 6.

about [H--dppm]$^{+}$[27] and [Me--dppm]$^{+}$:[4] "complex, ill-resolved, temperature dependent peaks". Although not explicitly postulated by the authors of these two papers, axial/equatorial exchange in these complexes may also be slow. The ^{1}H NMR spectrum of [I--PPh_3]$^{+}$ is also indicative of nonequivalent PCH_2P hydrogens.[38]

One would predict that steric repulsions in [PPh_3--PPh_3]$^{2+}$ and [H--PPh_3]$^{+}$ cause slow axial/equatorial interchange. However, the PCH_2P protons in these complexes are equivalent, and in fact, remain so down to -80 °C in [PPh_3--PPh_3]$^{2+}$. Ligand dissociation cannot account for proton equivalence in [PPh_3--PPh_3]$^{2+}$ at ambient temperature since:

1. The sum of the rate constants estimated for PPh_3 dissociation (0.03 s^{-1}; discussed below) and Pt_2P_2C ring opening[20] (0.027 s^{-1}) in [PPh_3--PPh_3]$^{2+}$ are an order of magnitude slower than the estimated rate constant for the exchange process (0.83 s^{-1}) in [Cl--PPh_3]$^{+}$ at 25 °C.
2. The rate constant for axial/equatorial exchange in [PPh_3--PPh_3]$^{2+}$ must be <u>much faster</u> than 0.83 s^{-1} at 25 °C because the [Cl--PPh_3]$^{+}$ resonances are at the slow exchange limit whereas those of [PPh_3--PPh_3]$^{2+}$ are at the fast exchange limit at this temperature.

As discussed above, models suggest that the rate of axial-equatorial exchange should be very sensitive to the Pt-PPh_3 bond length. A long Pt-PPh_3 bond length in [PPh_3--PPh_3]$^{2+}$ has

already been predicted because of the dissociative nature of the complex's reactions, and its extraordinarily low value for $^{1}J(Pt,P_{T})$. Since H^{-} has a much larger trans influence than Cl^{-}, the Pt-PPh_3 bond of $[H\text{--}PPh_3]^{+}$ may be somewhat longer than that found in $[Cl\text{--}PPh_3]^{+}$ causing a much faster rate of exchange. It appears that the rate of axial/equatorial substituent interchange in Pt(I) complexes is not only dependent on the effective cone angle of the terminal ligands but also on Pt-L_T bond lengths.

It is interesting to note that two $^{3}J(Pt,H)$ coupling constants have been reported (see Table I-11) for the complexes $[H\text{--}PMe_2Ph]^{+}$ and $[H\text{--}PPh_3]^{+}$ whose resonances are at the fast exchange limit. This is caused by the inequivalence of the Pt atoms in these complexes. The same phenomenon is expected for other unsymmetrically substituted complexes including $[Cl\text{--}PPh_3]^{+}$, but in this case the $^{3}J(Pt,H)$ couplings are not resolved.

Atropisomerism

Atropisomers are structural isomers caused by "freezing" the internal rotation about a single bond. Evidence from the $^{31}P\{^{1}H\}$ NMR suggests the presence of structural isomers in $[Cl\text{--}PPh_3]^{+}$ in addition to the $Pt_2(\mu\text{-dppm})_2$ ring conformers already mentioned. We attribute these isomers to the atropisomers present because rotation about the Pt-P bond is hindered. The following section will discuss precedents for

atropisomerism in the literature and present evidence from experimental data and molecular models to support this assignment.

Literature precedents for atropisomerism Examples of atropisomerism in organic chemistry are numerous and have recently been reviewed.[39] Three such isomers that, to some extent, resemble the structure of $[Cl--PPh_3]^+$ are pictured below. Atropisomers can differ in reactivity by as much as

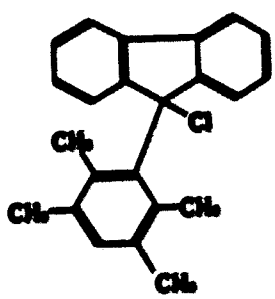

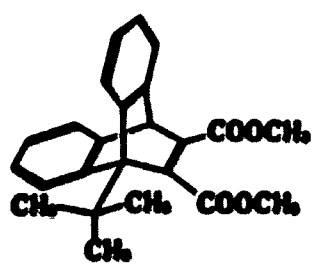

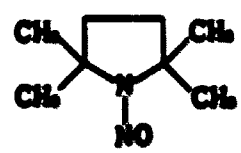

10,000 times.[40] Because of this difference in reactivity, the study of isolated atropisomers may yield valuable information on questions such as modes of attack in reactions and structural changes that will improve catalyst efficiency.

Although not so numerous, atropisomers in transition metal coordination chemistry have also been reported. The most widely known class of complexes exhibiting atropisomerism are those containing tetra-(ortho-substituted phenyl) porphyrins.[41] Phenyl rotation is hindered by steric repulsions

of the ortho substituent with the porphryin ring and often the different isomers can be distinguished by NMR techniques.[42]

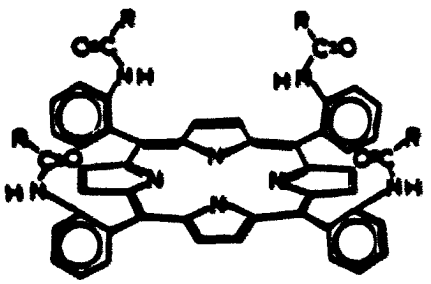

Another class of atropisomers in coordination chemistry are substitutionally inert Co(III) complexes made chiral by hindered rotation about one of the ligands.[43] As it happens, the bond about which rotation is hindered is never the metal-

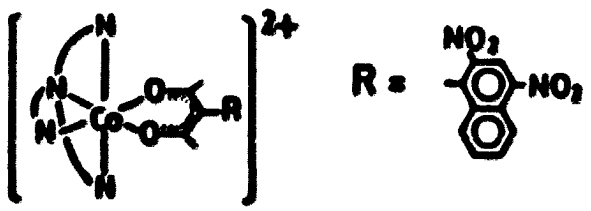

ligand bond and is often far removed from[44] it.

Cases of atropisomerism have been observed by ^{1}H NMR spectroscopy in transition metal carbenes where rotation around a carbon-heteroatom[45] or carbon-carbon[46] bond adjacent to the

metal-carbon bond is hindered. Finally, isomers derived from conformational preferences in the rotation around metal-phosphine bonds have been observed at low temperature by $^{31}P\{^{1}H\}$ NMR spectroscopy in a variety of metal complexes.[47] In general, the energy barriers to rotation about the M-P bond are low. Values of $\Delta G^{\ddagger}$ no greater than 10 kcal/mol have been reported.

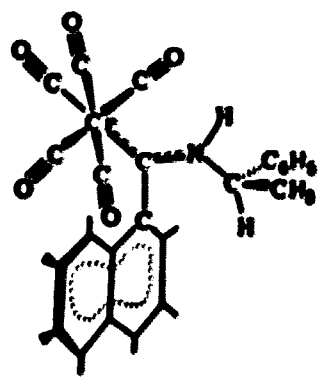

Two generalizations relevant to this work are found in the ubiquitous but spotty field of transition metal complex atropisomerism. No atropisomer capable of isolation ($\Delta G^{\ddagger}$ > 24 kcal/mol) has been reported where the isomers result from hindered rotation about the metal-ligand bond. Secondly, NMR spectroscopy is often very useful in distinguishing between two atropisomers, and in particular, $^{31}P\{^{1}H\}$ NMR is able to distinguish between isomers derived from rotation about a metal-phosphorus bond.

The possibility for atropisomerism has been alluded to for a Pt(I) dimer.[6] The ^1H NMR spectrum of $[Pt_2(\mu\text{-dppm})_2(PMe_2Ph)_2]^{2+}$ gave two distinct methyl resonances. This observation means that the two methyl groups of each PMe_2Ph ligand are nonequivalent and hence no plane containing both Pt-P bonds is a plane of symmetry in the molecule. A plane of symmetry would be expected if the Pt_2P_6 grouping were planar and if there was free rotation about the Pt-PMe_2Ph bonds. Asymmetry would be induced if: 1. there were a twist in the $Pt_2(\mu\text{-dppm})_2$ unit characteristic of Pt(I) dimer solid state structures and the twisted structure was rigid on the NMR time scale, or if: 2. there were atropisomers present caused by a high barrier to rotation about the Pt-PMe_2Ph bond thus locking the PMe_2Ph substituents in an asymmetric arrangement by steric interactions with the phenyl substituents of the μ-dppm groups. At 50 °C the NMR signals broadened but did not coalesce. This indicates a fairly high activation energy to any fluctional process, thus tending to support the second interpretation. This report is indicative of the types and magnitude of the activation energies for possible forms of atropisomerism in complexes related to $[Cl\text{--}PPh_3]^+$.

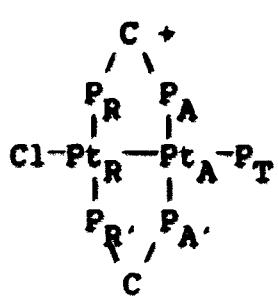

Phosphorus-phosphorus coupling constants The central resonances for P_T, P_A, and P_R consist of very complex splitting patterns (see Figure I-16). The following is an account of an attempt to interpret them. It is from these splitting patterns that evidence is derived for the existence of conformational isomers in $[Cl--PPh_3]^+$, the proposed identity of which is to some extent speculation, and based on indirect evidence. One assumption made in the interpretation is that P_R and $P_{R'}$ are symmetry related as are P_A and $P_{A'}$. A compilation of the exact coupling constants and chemical shifts is found in the experimental section (page 160).

The P_T resonance is the simplest of the three resonances to interpret and consists of a 20 Hz triplet split by a 9 Hz triplet (see Scheme I-4). The actual spectrum consists of seven peaks instead of the expected nine, however, the two peaks closest to the center are broader than the rest. According to Scheme I-4, each of these two peaks is the sum of two unresolved peaks (see Figure I-16 for the experimental and calculated spectrum).

Scheme I-4. Splitting Pattern for P_T Resonance

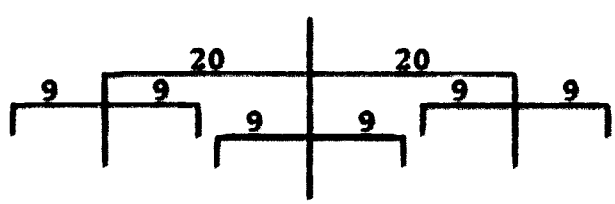

Relative Intensities	1	2	3B	4	3B	2	1

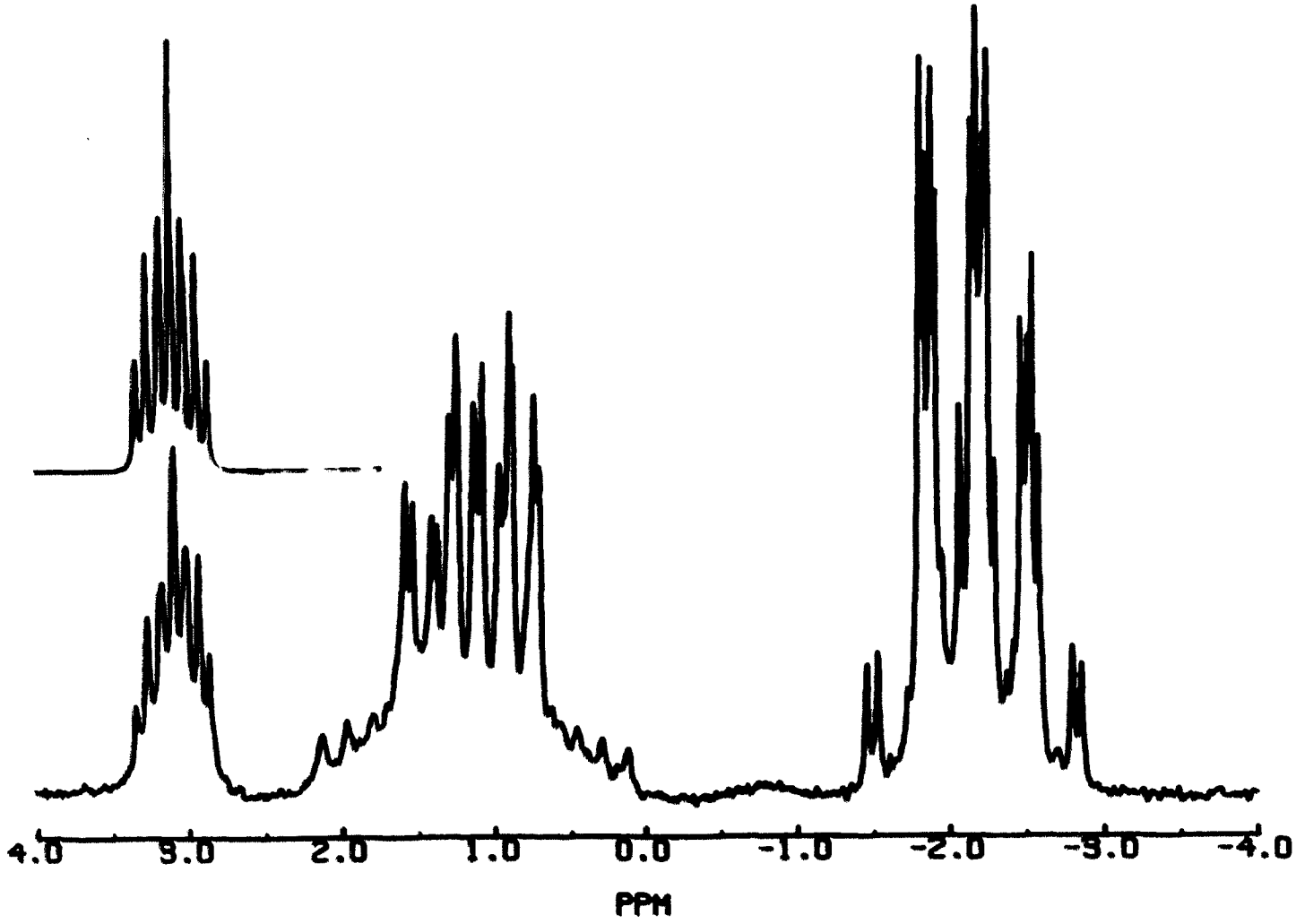

Figure I-16. Central resonances in the $^{31}P\{^{1}H\}$ NMR (121.5 MHz) of $[Pt_2(\mu\text{-dppm})_2Cl(PPh_3)]^+$ in CD_2Cl_2; Inset: Calculated P_T resonance

The identity of the two dppm resonances was established on the basis of the relative magnitudes of these two coupling constants. The 9 Hz coupling constant is assigned to $^{3}J(P_R,P_T)$. The fact that the value is measurable indicates the presence of a strong Pt-Pt bond. The 20 Hz coupling constant is assigned to $^{2}J(P_A,P_T)$ and is consistent with cis-$^{2}J(P,P)$ reported for Pt(II) complexes.[24]

The P_R resonance consists of the superposition of two splitting patterns, the centers of which are only about 4 Hz (0.03 ppm) apart. Portions of the $^{2}J(Pt_A,P_R)$ satellites lie beneath the central resonance and add to spectrum complexity. One splitting pattern consists of a 50 Hz doublet of 30 Hz doublets of 9 Hz doublets, whereas the other pattern consists of a 40 Hz doublet of 40 Hz doublets of 9 Hz doublets (see Scheme I-5). The superposition of these peaks yields a triplet-like structure with four peaks each in the outer two portions and six in the central portion of the triplet (see Figure I-17 for the experimental and calculated spectrum). The $^{2}J(P_A,P_R)$ and $^{3}J(P_A,P_{R'})$ are similar in magnitude to those of other $Pt(\mu\text{-dppm})_2$ complexes.

As with the P_R resonance, the P_A resonance is also a superposition of $^{2}J(Pt_R,P_A)$ satellites, and two splitting patterns (see Scheme I-6) the centers of which are separated by only 4 Hz. This multiplet is complex because all of the coupling constants are of comparable size (i.e., 40,40,20 and

Scheme I-5. Splitting Patterns for the P_R Resonance

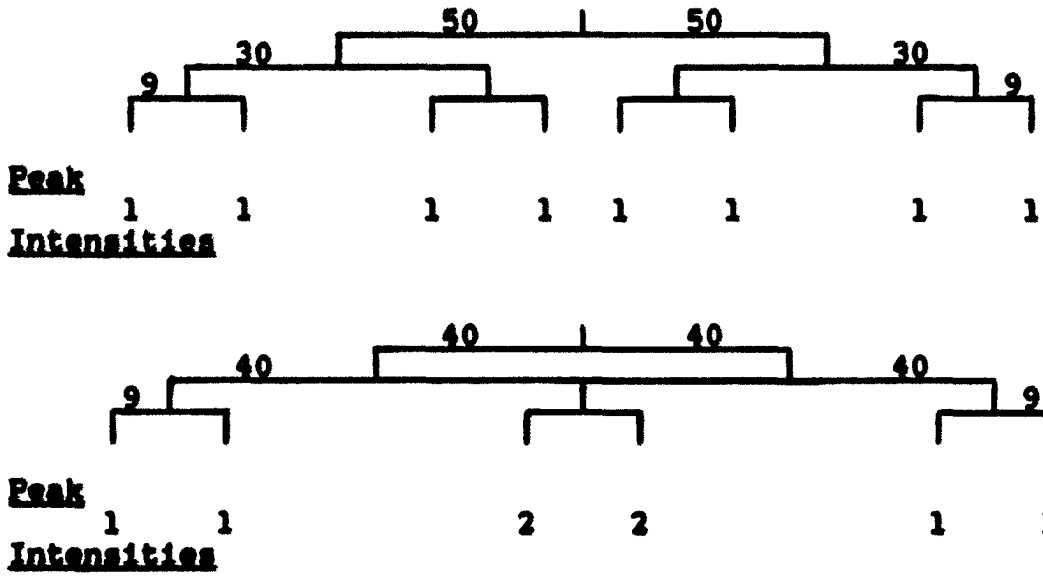

Scheme I-6. Splitting Patterns for the P_A Resonance

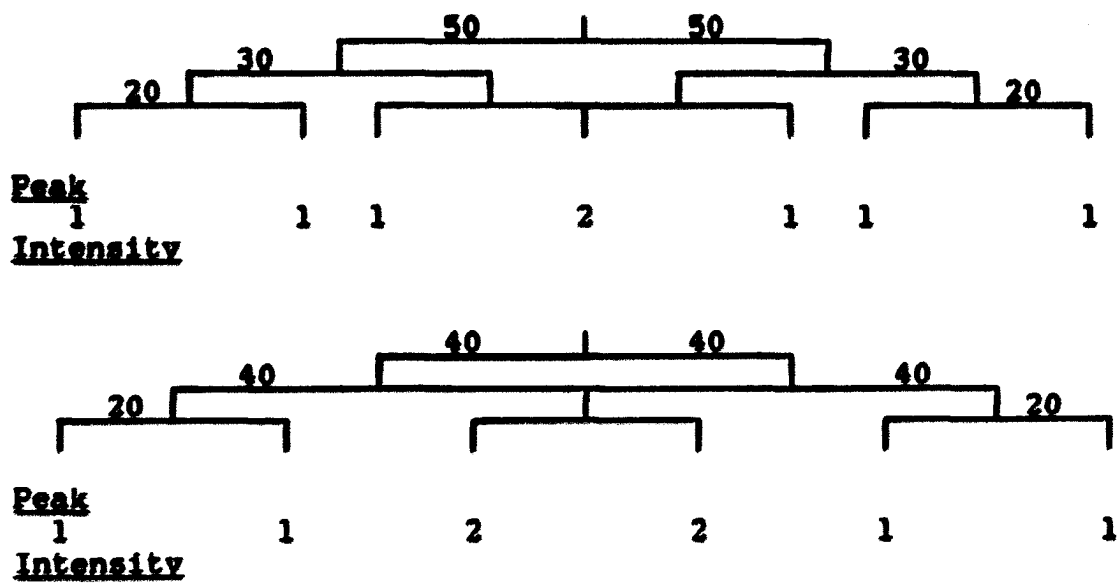

50,30,20 Hz doublets of doublets of doublets; see Figure I-18 for the experimental and calculated spectrum).

The splitting patterns for P_A and P_R are consistent with the presence of two isomeric forms of $[Cl--PPh_3]^+$ that vary more in the magnitude of their coupling constants than in their chemical shifts. Since $^2J(P_A,P_T)$ and $^2J(P_R,P_T)$ are practically identical in the two isomeric forms, evidence for two separate isomers is not seen in the P_T resonance because chemical shift differences of 4 Hz or less are often not resolved.

Two additional interpretations of the data will now be discussed: First, that the splitting patterns could be due to only one structural form of the complex. Second; that only one form of the complex exists with multiplets which arise from second-order effects.

Were the patterns only due to their being only one form of $[Cl--PPh_3]^+$, the presence of four individual $J(P_A,P_R)$ would require four inequivalent dppm phosphorus nuclei. We could then assign the coupling constants as follows: $^2J(P_A,P_R) = 50$ Hz, $^3J(P_A,P_{R'}) = 30$ Hz, $^2J(P_{A'},P_{R'}) = 40$ Hz, and $^3J(P_{A'},P_R) = 40$ Hz. Indeed, this would give a 50,30 pattern superimposed over a 40,40 pattern for resonance P_A, but it would also yield a 50,40 pattern superimposed over a 40,30 pattern for resonance P_R which is inconsistent with experimental fact. The converse is also true: If the assignments for coupling constants were made so that P_R has the correct pattern, P_A will have an incorrect pattern. The splitting

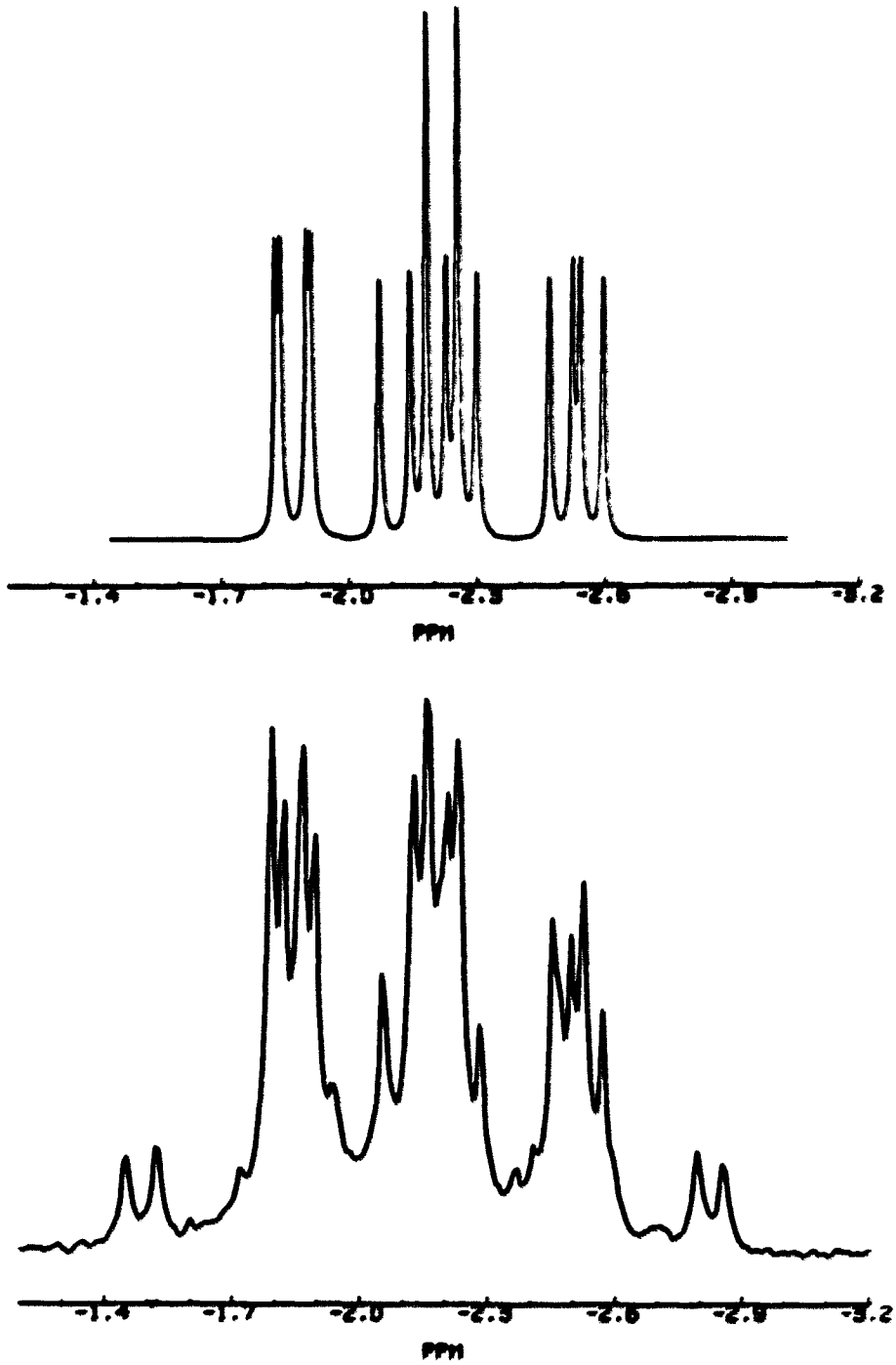

Figure I-17. The experimental (bottom) and calculated (top) P_R resonance of $[Pt_2(\mu\text{-dppm})_2Cl(PPh_3)]^+$

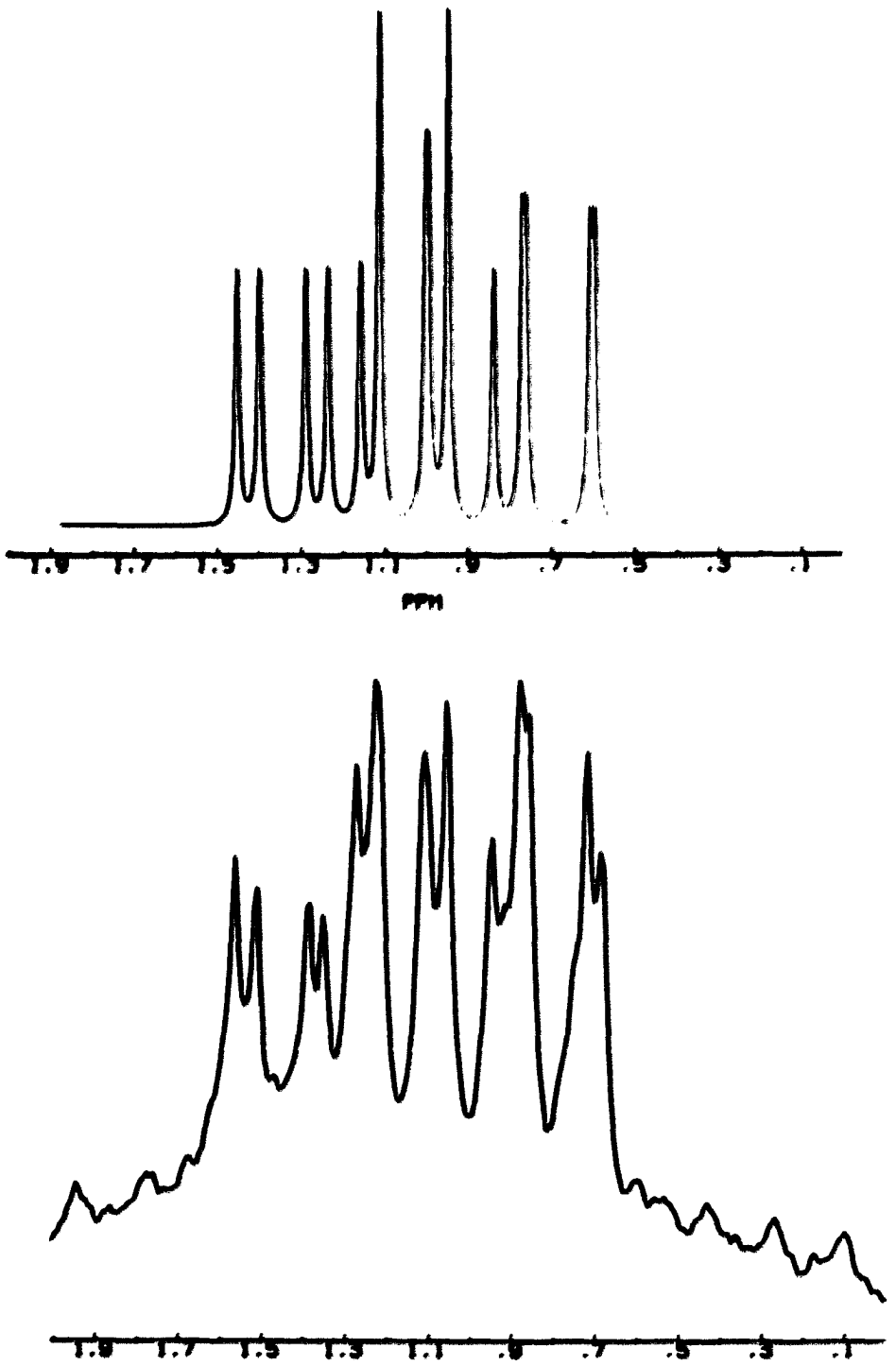

Figure I-18. The experimental (bottom) and calculated (top) P_A resonance of $[Pt_2(\mu\text{-dppm})_2Cl(PPh_3)]^+$

patterns are only consistent with two isomers having two pairs of inequivalent dppm phosphorus each.

The idealized splitting patterns described above would not be observed in a hypothetical complex containing five inequivalent phosphorus nuclei because, for example, the inequivalence of P_A and $P_{A'}$ would cause $^2J(P_A,P_{A'})$ to be larger than $\delta_A - \delta_{A'}$. These conditions cause a second order spectrum. P_A and $P_{A'}$ are symmetry related in $[Pt_2(\mu\text{-dppm})_2Cl(PPh_3)]^+$ if boat/chair isomerizations and twisting about the Pt-Pt bond are fast on the NMR time scale, and even if they are not, P_A and $P_{A'}$ are related by local symmetry (i.e., the symmetry of the complex when the positions of PPh_3 phenyls are disregarded). The chemical shift differences between the A and R type resonances are sufficiently large so that $\delta_A - \delta_R >> J(P_A,P_R)$. Because of this, an A_2X_2 instead of an AA'BB' spin system[48] is predicted. Second order effects need not be invoked nor are they necessary to explain the $^{31}P\{^1H\}$ NMR spectrum of $[Cl\text{--}PPh_3]^+$.

Other pertinent experimental observations The $^{31}P\{^1H\}$ NMR spectrum of $[Cl\text{--}PPh_3]^+$ was observed as a function of temperature from -20 to 120 ^0C. The purpose of this experiment was to confirm that the two isomers observed in the $^{31}P\{^1H\}$ NMR spectrum of $[Cl\text{--}PPh_3]^+$ were indeed boat/chair conformers. The distance between any two peaks in the spectrum that have the potential for mutual coalescence is about

10 Hz which is equivalent to an isomerization rate constant of about 50 s^{-1}. The estimated rate constant for boat/chair isomerization is 1583 s^{-1} at 120 ^{o}C. so we were expecting coalescence at much lower temperatures than 120 ^{o}C. To our surprise, no coalescence of peaks was observed; if anything, the spectrum resolution improved with increasing temperature. The isomers observed in the $^{31}P\{^{1}H\}$ NMR spectrum are definitely not boat/chair conformers, nor are they forms which are interconverted in concert with the chair/boat interconversion. In fact, the rate constants for PPh_3 dissociation and the process which leads to atropisomerization in $[Cl--PPh_3]^+$ must be less than 50 s^{-1} at 120 ^{o}C. This is not unreasonable since it predicts that the $\Delta G^{\ddagger}$ for isomerization is greater than 21 kcal/mol and still within a suitable range for phosphine dissociation, the ultimate method of atropisomerization.

The X-ray crystal data for $[Cl--PPh_3]^+$ have been reported and discussed in greater depth above (page 31). The pertinent factors are as follows: First, the complex crystallized in a "twisted-chair" conformation. Second, the bond angles around Pt_A are significantly distorted away from the idealized 90^{o} and 180^{o} to accommodate the bulky PPh_3. The fact that platinum-phosphorus orbital overlap is significant at nonidealized angles is very important in the discussion below.

Atropisomerism in $Pt_2(\mu\text{-dppm})_2Cl(PPh_3)]^+$ Data supporting the existence of atropisomers, and constraints which defend their identity in $[Cl\text{--}PPh_3]^+$ are summarized below:

1. One atropisomer must have the same structure (on the NMR time scale) as that found in the crystal structure.
2. The atropisomers cannot be easily interconvertible by axial to equatorial conformational changes of the $Pt_2(\mu\text{-dppm})_2$ ring.
3. P_A and $P_{A'}$ are symmetry related as are P_R and $P_{R'}$.
4. The barrier to atropisomerization must be high (> 21 kcal/mol).
5. Axial/equatorial substituent interchange must be possible, at least to some extent, in both atropisomers.
6. The environments about the dppm phosphorus nuclei in each atropisomer should be different.
7. Atropisomerism is not observed in $[PPh_3\text{--}PPh_3]^{2+}$; a fact which also should be explained.

Experimental data that allow some latitude in the determination of the atropisomer identity are:

1. Significant deviations from ideal bond angles around Pt_A are possible.
2. The ratio of the two atropisomers need not be 50:50.

The two plausible types of atropisomers in $[Cl\text{--}PPh_3]^+$ are those caused by the unlikely rotation around the $Pt\text{-}PPh_3$ bond or by hindered rotation about the Pt-Pt bond. Reasons why the

former is favored over the latter as the actual type of atropisomers are discussed below.

The two Pt-P type atropisomers are depicted in Figure I-19. The one form has the two symmetry related PPh_3 phenyls below all of the dppm phenyls (BELOW) whereas the second has the two symmetry related phenyls bisecting the dppm Ph-P-Ph angles (BISECT.). The twisted chair form of (BISECT.) is identical to the crystal structure of $[Cl--PPh_3]^+$. These two atropisomers cannot be interconverted through axial/equatorial exchange; indeed, if other conformational changes such as axial/equatorial exchange are fast on the NMR time scale, the two dppm phosphorus atoms remote from PPh_3 (P_R) are symmetry related as are the two adjacent ones (P_A) in both atropisomers.

Two possible methods of their atropisomerization are phosphine dissociation or an inter-ligand correlated rotation of phenyl rings. The former method has the necessary high activation energy (> 21 kcal/mol), and although little is known about the latter, an activation barrier of 21 kcal/mol does not seem unreasonable on the following grounds:

1. The activation barrier for correlated "intra-ligand" rotations of phenyls in ZAr_3 compounds (Z = N, HC, B, etc.) is often as high as 22 kcal/mol when Ar is a bulky phenyl,[49] and is even as high as 28.0 kcal/mol in tris(2,3,4,5,6-pentachlorophenyl)amine.[50]
2. Atropisomerization of "ball and stick" models of

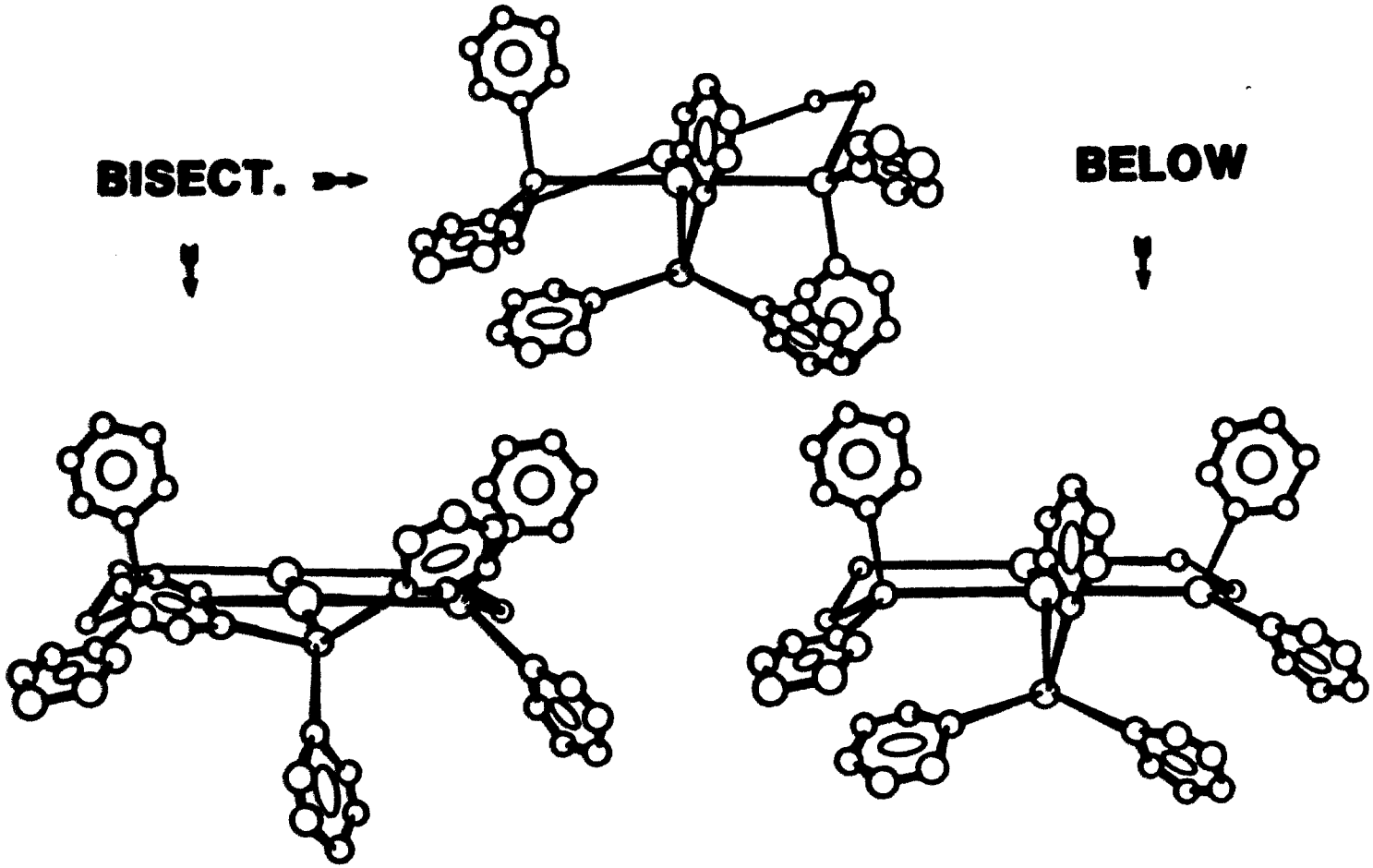

Figure I-19. Postulated Pt-P atropisomers in $[Pt_2(\mu\text{-dppm})_2Cl(PPh_3)]^+$: boat form of **BELOW** (bottom right); boat form of **BISECT.** (bottom left); twisted-chair form of **BISECT.** (top center)

$[Cl--PPh_3]^+$ was found to occur only upon considerable distortion of the Pt-P bonds away from the two phenyls intimately involved in the correlated rotation.

3. The probability of inter-ligand correlated rotation is really quite low since the two phenyls intimately involved need to be in close proximity of each other for this to occur, but, at the same time, they will tend to avoid each other as much as possible due to steric repulsions.

"Ball and stick" models suggest greater steric repulsions in BELOW than are found in BISECT and that BELOW should favor a boat conformation (see Figure I-19). In fact, boat/chair transformations in BELOW might not be possible if tetrahedral distortion about Pt_A was not possible. The somewhat slower and/or incomplete boat to chair transformation in BELOW and the possibility of greater distortion about its Pt_A may be a cause of the different average chemical environment around the otherwise similar dppm phosphorus nuclei in the two different atropisomers. In the even bulkier $[PPh_3--PPh_3]^{2+}$, the strain caused by the terminal phosphines being in BELOW-BELOW or BELOW-BISECT conformations may cause the formation of these atropisomers to be highly disfavored especially when the weaker Pt-P bonds predicted in $[PPh_3--PPh_3]^{2+}$ are considered. This may be the reason for the absence of atropisomers in this complex.

Possible atropisomers caused by hindered rotation around

the Pt-Pt bond are CHAIR A and the slightly more strained CHAIR B in Figure I-20. The greatest structural difference between the two is that two phenyls are colinear in CHAIR A whereas four are colinear in CHAIR B. This could cause differences in phosphorus chemical environment between them. Although these atropisomers have a few additional redeeming features, their properties do not fit very well within the constraints listed above. On the average, all of the dppm phosphorus nuclei are inequivalent unless local symmetry is invoked. "Ball and stick" models suggest that the barrier to this type of atropisomerization is not much higher than that for a boat/chair transformation at best. This theory's greatest downfall is the fact that the two chairs can be interconverted by a series of two boat/chair isomerizations either through BOAT A or the more strained BOAT B.

Because of the high barrier to isomerization of the two postulated atropisomers (BELOW and BISECT), it may be possible to separate them if appropriate chromatographic techniques are found. Unfortunately attempts to find these techniques have, at least to the present time, failed.

$[I\text{--}PPh_3]^+$ was also found to have two atropisomeric forms (J(P,P) are found on page 160 in the experimental section). The $^{31}P\{^1H\}$ NMR spectrum of [Cl--dppm] also suggests the presence of atropisomers (see Figure I-21) and in fact sufficient peaks are present so that more than two atropisomers could be

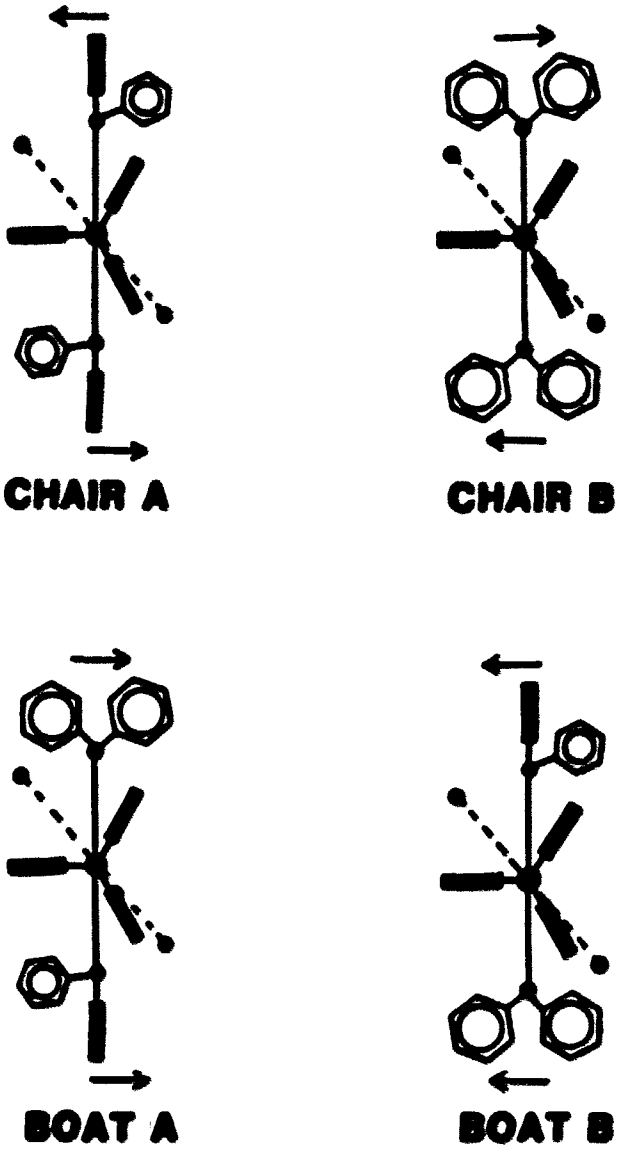

Figure I-20. Possible Pt-Pt atropisomers of $[Pt_2(\mu\text{-dppm})_2Cl(PPh_3)]^+$; the dashed lines represents the half of the complex remote from the terminal PPh_3; the solid rectangles are both dppm phenyls whose molecular planes are perpendicular to the plane of the paper and also all of the PPh_3 phenyls; the arrow signifies the direction dppm methylenes are pointing.

Figure I-21. The $^{31}P\{^{1}H\}$ NMR (300 MHz) of $[Pt(\mu\text{-dppm})_2Cl(\eta^1\text{-dppm})]^+$ in CD_2Cl_2 at -20 °C in CD_2Cl_2 obtained by the addition of 1.2 equivalents of dppm (singlet at -23.3 ppm) to $[Pt_2(\mu\text{-dppm})_2Cl_2]$ without further purification; Inset: enlarged spectrum showing the central resonances for P_A (left), and P_R (right), P_T (far right, partially obscured by P_R)

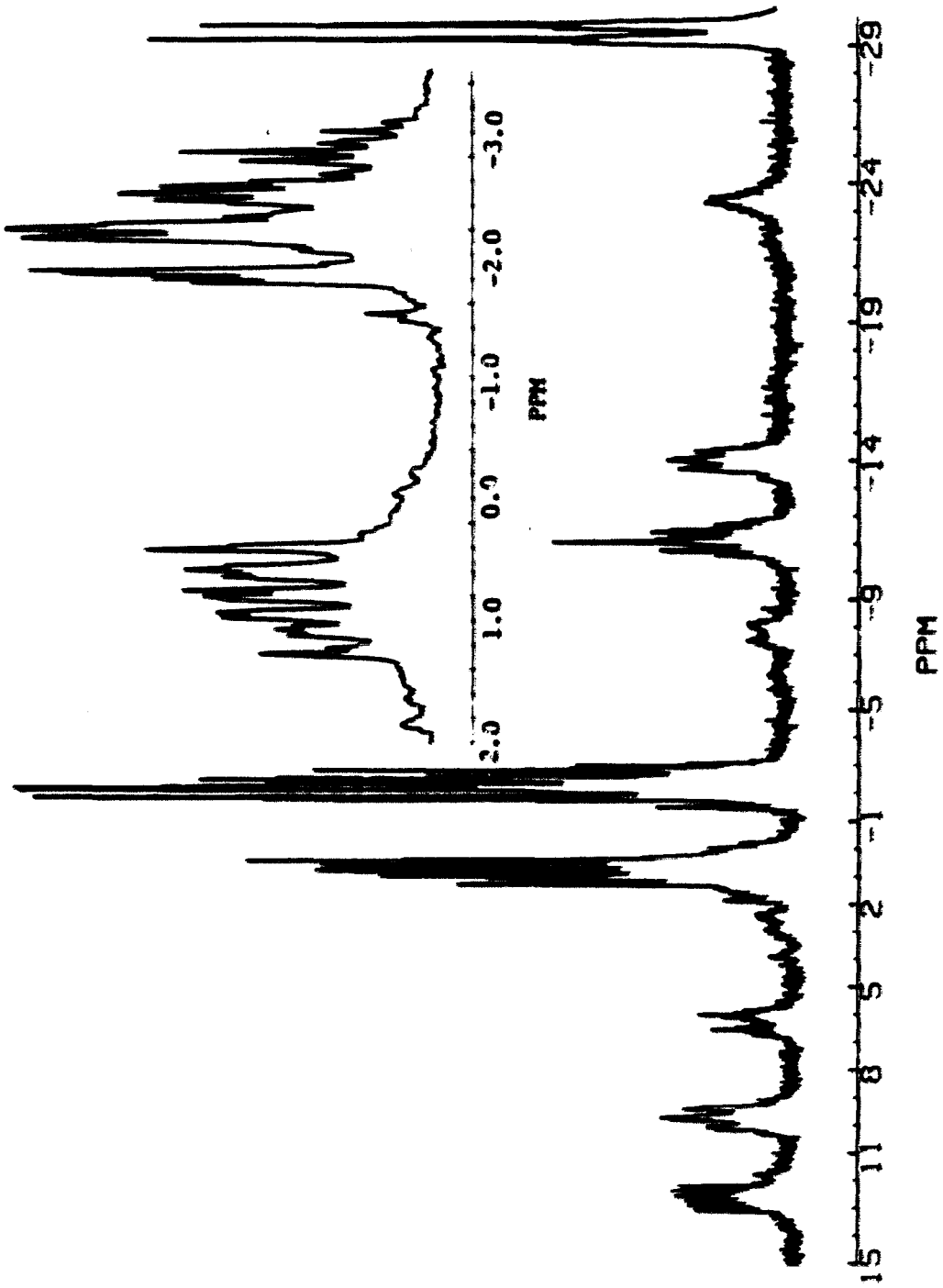
PPM
15
11
8
5
2
-1
-5
-9
-14
-19
-24
-29
PPM
2.0
1.0
0.0
-1.0
-2.0
-3.0

present. In order to obtain a better understanding of conformational changes in $[X\text{--}L]^+$ type complexes, syntheses of the unknown compounds $[Cl\text{--}P(o\text{-}Tol)_3]^+$ and $[Cl\text{--}AsPh_3]^+$ were attempted. Because the Pt-L bonds are so weak in these two, the equilibrium which otherwise greatly favors formation of $[Cl\text{--}L]^+$ over [Cl--Cl] in L = PPh_3 or dppm, greatly disfavors formation of the product when L = $P(o\text{-}Tol)_3$ or $AsPh_3$. Thus, the desired products did not form readily and the matter was not pursued further.

Mechanisms of Ligand Substitutions in Pt(I) Dimers

Ligand substitution in square planar complexes

In almost all of the substitution reactions studied with square planar complexes, the observed rate law has the form

$$-d[ML_3X]/dt = (k_s + k_Y[Y])[ML_3X] \qquad (4)$$

for the general reaction

$$ML_3X + Y \longrightarrow ML_3Y + X \qquad (5)$$

This rate law has been rationalized in terms of two parallel pathways, both involving an associative mechanism.[51] In the k_Y pathway the nucleophile Y attacks the metal complex and the reaction passes through a five coordinate transition state and

intermediate. The k_s pathway also involves the formation of a trigonal bipyramidal transition state, except that the solvent is the entering group in the rate determining step of the substitution of X by Y. The latter pathway should become less important in solvents of lower coordinating ability and k_s should approach zero.

In the substitution reactions of a sterically hindered complex of Pd(II) in aqueous solutions, the [Y]-independent pathway was assumed to be dissociative in nature.[52]

$$[Pd(Et_4dien)Cl]^+ + Br^- \longrightarrow [Pd(Et_4dien)Br]^+ + Cl^- \qquad (6)$$

However, negative activation volumes ($\Delta V^{\ddagger}$) found for [Y]-independent substitution reactions in aqueous solutions of other $[Pd(Et_4dien)X]^+$ type complexes support an associative interchange mechanism (I_a) for this complex as well. In other words, the negative values for $\Delta V^{\ddagger}$ are very close to the estimated volume of a water molecule in the second coordination sphere of a singly charged complex ion and support solvent association (k_s) and not ligand dissociation as the rate-determining step for this [Y]-independent substitution pathway. Similar results were found in other solvents containing an oxygen donor.[53]

Recently, substitution reactions of cis-$[Pt(Ph)_2(Me_2SO)_2]$ in $CDCl_3$ and benzene were reported[54] to occur by parallel

associative and dissociative pathways when L-L = 1,2-(diphenylphosphino)ethane:

$$cis\text{-}[Pt(Ph)_2(Me_2SO)_2] + L\text{-}L \longrightarrow [Pt(Ph)_2(L\text{-}L)] + 2Me_2SO \quad (7)$$

When weak nucleophiles such as L-L = 2,2'-bipyridine are used, only the dissociative pathway was observed. The authors propose that ligand dissociation instead of solvolysis (k_s) is the mechanism for the [L-L] independent pathway in reaction 7, stating that $CDCl_3$ and benzene are neither sufficiently nucleophilic to cause facile displacement of Me_2SO nor sufficiently coordinating to occupy a site in the coordination shell of Pt(II).

The k_s term for ligand substitution reactions of the square planar Pt(I) dimers should also be unimportant when conducted in CH_2Cl_2. And indeed, in the results described below and elsewhere[9], ligand substitution reactions of $[Pt_2(\mu\text{-dppm})_2X_2]$ ($X = Cl^-$, Br^-) occur almost totally by the k_Y pathway. The sterically encumbered $[Pt_2(\mu\text{-dppm})_2(PPh_3)_2]^{2+}$, however, undergoes substitution by a Y-independent pathway, which must surely occur by rate-limiting ligand dissociation as described below instead of by a solvent-assisted pathway.

Opening of a $Pt_2(\mu\text{-dppm})$ ring by Pt-P bond dissociation has been postulated as the rate-limiting step in the insertion of diazomethane and other small molecules into the Pt-Pt bond

of $[PPh_3--PPh_3]^{2+}$. Other dissociative processes are also consistent with the kinetic data and additional evidence supporting the one version of the proposed mechanism over another is indirect. The research reported in this section provides direct evidence that Pt-P bond dissociation is the rate determining step not only for ligand substitution but also insertion reactions of $[PPh_3--PPh_3]^{2+}$.

Reaction pathways to $[Pt_2(\mu\text{-dppm})_2Cl(PPh_3)]^+$

$[Pt_2(\mu\text{-dppm})_2Cl(PPh_3)]^+$ can be formed from both [Cl--Cl] and $[PPh_3--PPh_3]^{2+}$ (see Scheme I-7) with the reactions of the latter being effectively irreversible under the conditions employed in these studies.

$[Cl--PPh_3]^+$ is formed directly from [Cl--Cl] via a PPh_3-dependent pathway indicating an associative mechanism typical of square planar substitution reactions. Kinetic and other experimental data are consistent with sufficiently strong interactions of [Cl--Cl] with outer-sphere chloride to severely impede this nucleophilic attack of platinum by the bulky triphenylphosphine.

On the other hand, $[Cl--PPh_3]^+$ is formed from $[PPh_3--PPh_3]^{2+}$ via two parallel pathways which are dissociative in nature but whose rates are again very sensitive to the nature of the anions present in solution. One pathway is initiated by rate-limiting PPh_3 dissociation. The other, initiated by Pt_2P_2C ring opening via Pt-P bond scission,

yields $[Cl{-}{-}PPh_3]^+$ only after the formation of two observable intermediates, the latter of which (chloro-CHELATE) is stable for days at -10 °C and has been characterized by $^{31}P\{^1H\}$ NMR.

Scheme I-7. Formation Reactions of $[Pt_2(\mu\text{-dppm})_2Cl(PPh_3)]^+$

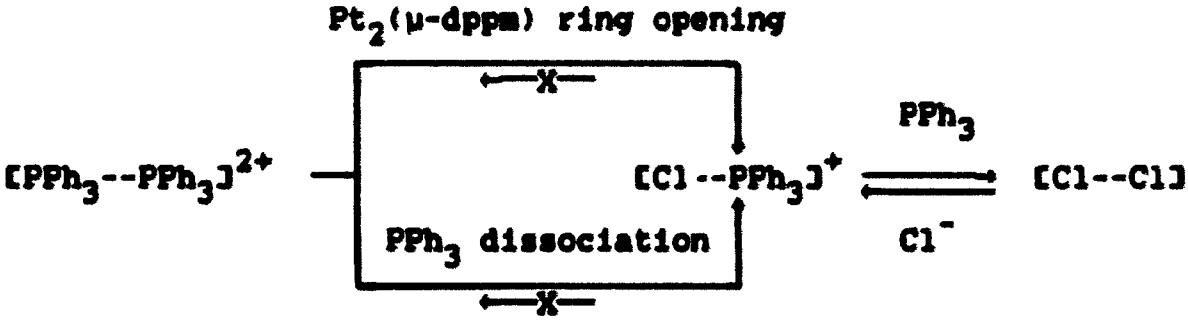

The NMR data for CHELATE are consistent with it being a Pt(I) dimer containing one bridging and one chelating dppm. A Pt(I) dimer containing one bridging and two chelating dppm (3-DPPM) has recently been prepared and fully characterized structurally.[8] Its existence lends further support for the structure of CHELATE. It follows from kinetic and the above-mentioned NMR data that the former and less stable intermediate, RING OPEN, should contain the "dangling" dppm that was bridging before Pt_2P_2C ring opening.

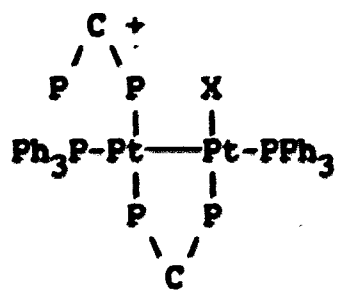

RING OPEN

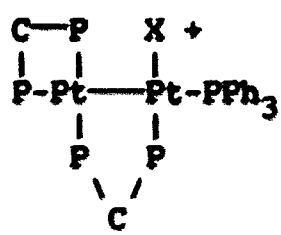

CHELATE

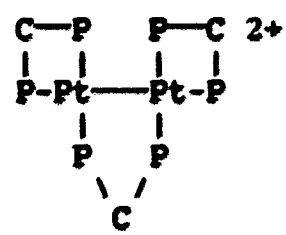

3-DPPM

Reaction of PPh_3 with $[Pt_2(\mu\text{-dppm})_2Cl_2]$

Outer sphere anion association with Pt(I) dimers Ion pairing constants between ions of 1+ and 1- charges in CH_2Cl_2[55] and 1,2-dichloroethane[56] are in the range of 10^3 -10^5 M^{-1}

$$\text{Cation}^+ + \text{Anion}^- \underset{}{\overset{K_{ip}}{\rightleftharpoons}} \text{Ion Pair} \qquad (8)$$

Observations pointing to strong ion pairing in $[Cl\text{--}PPh_3]^+$ are:

1. The chemical shift of the axial PCH_2P proton resonance varies markedly with the identity of the counter-ion (see Figure I-10 on page 46).
2. There are substantial differences in R_f values[57] depending on the added anion e.g., for $[Cl\text{--}PPh_3]^+\star(Cl^-)$ (R_f = 0.2) and $[Cl\text{--}PPh_3]^+\star(PF_6^-)$ (R_f = 0.95; 6.5 CH_2Cl_2 : 3.5 acetone on silica).

Experimental observations also indicate Cl^- coordination to $[Cl\text{--}Cl]$. For example, the $^{31}P\{^1H\}$ NMR resonance for $[Cl\text{--}Cl]$ shifts from 7.5 to 6.1 ppm occur upon addition of Cl^- to $[Cl\text{--}Cl]$ solutions in CD_2Cl_2. Changes in the UV-VIS spectrum also occur upon addition of Cl^-. The most dramatic evidence for this outer-sphere coordination of Cl^- to $[Cl\text{--}Cl]$ is observed in the kinetic measurements discussed below.

Reaction reversibility Many observations are consistent with the occurrence of an equilibrium between $[Cl\text{--}Cl]$

and $[Cl{-}{-}PPh_3]^+$ species in halocarbon solvents (see equation 9). Because the predominant forms of these Pt(I) dimers in solution depend on the nature and concentration of anions present and the total Pt(I) dimer concentration, the form of the applicable equilibrium expression and the value for K_{eq} will also vary. A seemingly simple equilibrium is complicated by very strong ion pairing in $[Cl{-}{-}PPh_3]^+$ and strong association of chloride ions with the neutral [Cl--Cl] discussed above.

$$PPh_3 + [Cl{-}{-}Cl]{\star}Ad \overset{K_{eq}}{\rightleftharpoons} [Cl{-}{-}PPh_3]^+{\star}Ad + Ad \qquad (9)$$

$$Ad = Cl^-,\ PF_6^-,\ ClO_4^-,\ \text{or solvent}$$

The products of the reaction between PPh_3 and [Cl--Cl] in CD_2Cl_2 at a 1 : 1 mole ratio were analyzed by $^{31}P\{^1H\}$ NMR. Substantial amounts of <u>both</u> PPh_3 and [Cl--Cl] were present, and in fact, a detectable amount of [Cl--Cl] is present even after the same reaction at a 3 : 1 ratio of PPh_3 to [Cl--Cl] (Figure I-22). K_{eq}' under these conditions ($[Cl{-}{-}Cl]_o$ = 33 mM, Ad' = Cl^-, Ad = Ad'' = solvent) is $5.7 \pm 0.8 \times 10^3\ M^{-1}$:

$$PPh_3 + [Cl{-}{-}Cl] \overset{K_{eq}'}{\rightleftharpoons} [Cl{-}{-}PPh_3]^+{\star}Cl^- \qquad (10)$$

As the mole ratio of PPh_3 to [Cl--Cl] is increased in $C_2H_4Cl_2$ solutions of 0.1 mM [Cl--Cl], the final absorbance sharply increases to a plateau (Figure I-23) because the molar absorptivities of $[Cl--PPh_3]^+$ are known to be higher than those of [Cl--Cl] at all wavelengths (see Figure I-9 on page 43). From these data, a "pseudo" equilibrium constant between PPh_3 and all Pt(I) species present is calculated to be (7.4 ± 0.7) x 10^3 M^{-1}. The actual value for K_{eq}' in equilibrium 10 will be lower since a significant concentration of $[Cl--PPh_3]^+_{tot}$ will not be ion paired and more $[Cl--PPh_3]^+*Cl^-$ must be formed to satisfy equilibrium 10 causing $[Cl--PPh_3]^+_{tot}$ to be higher than if $[Cl--PPh_3]^+*Cl^-$ was the only species of this type present. A similar phenomenon is observed when the equivalent of 20 mM $(n\text{-butyl})_4NClO_4$ is added to a 0.02 mM equilibrium mixture of [Cl--Cl] and $[Cl--PPh_3]^+$. A significant absorbance <u>increase</u> is observed. In this case, $[Cl--PPh_3]^+*ClO_4^-$ acts as the sink for $[Cl--PPh_3]^+$ species.

Addition of Cl^- to solutions containing $[Cl--PPh_3]^+$ partially reverses the overall reaction and causes the predicted absorbance decrease at all wavelengths. Equilibria of the type found in equation 9 are also observed for L = $P(o\text{-Tol})_3$, dppm, and $AsPh_3$; qualitative observations suggest that K_{eq} increases in the order:

$$L = AsPh_3 < P(tol)_3 < PPh_3 < \eta^1\text{-dppm}.$$

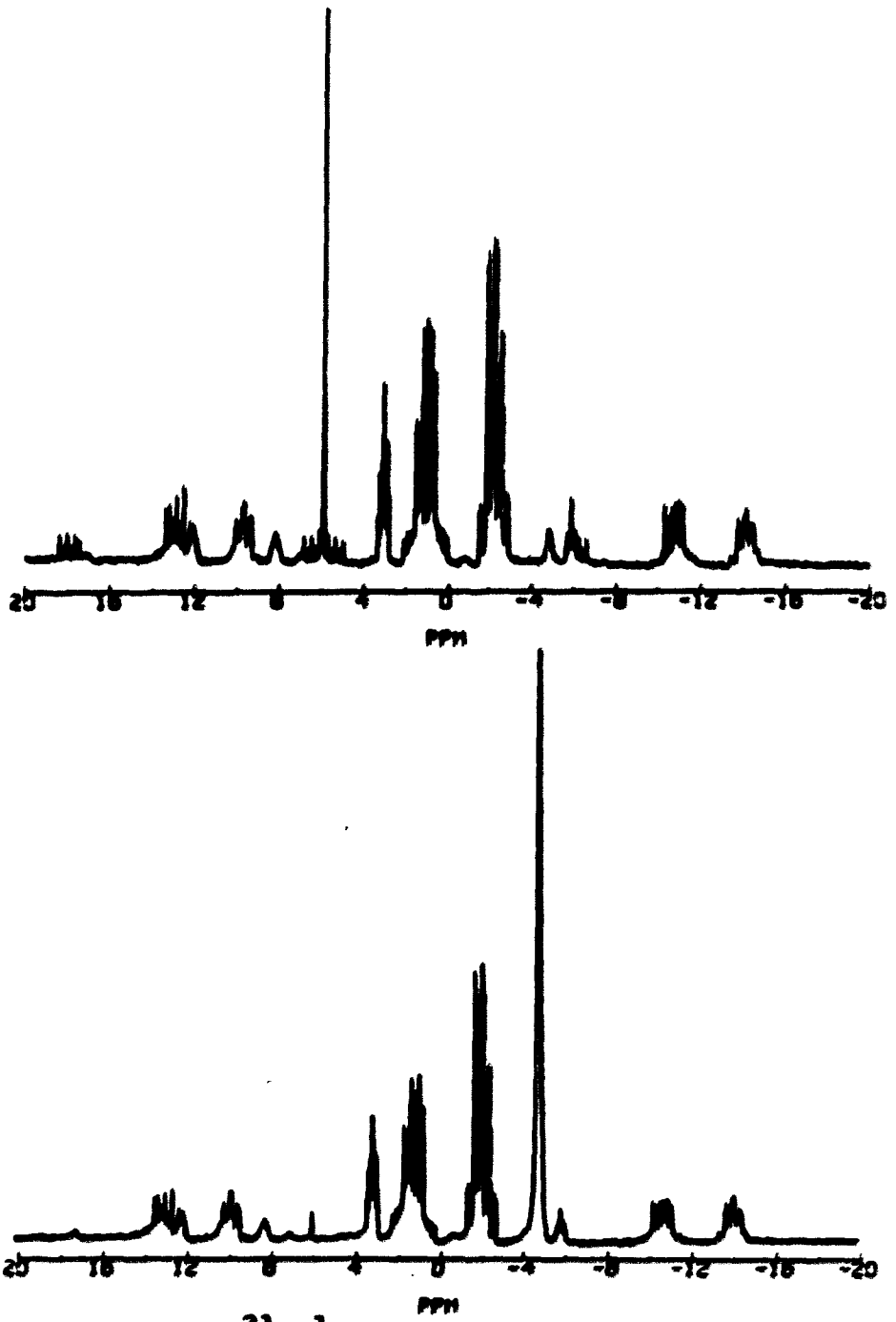

Figure I-22. The $^{31}P\{^{1}H\}$ NMR (121.5 MHz) after the reaction of 33 mM $[Pt_2(\mu\text{-dppm})_2Cl_2]$ (6.2 ppm) with 1 eq. (top) and 3 eq. (bottom) of PPh_3 (-4.5 ppm) in CD_2Cl_2

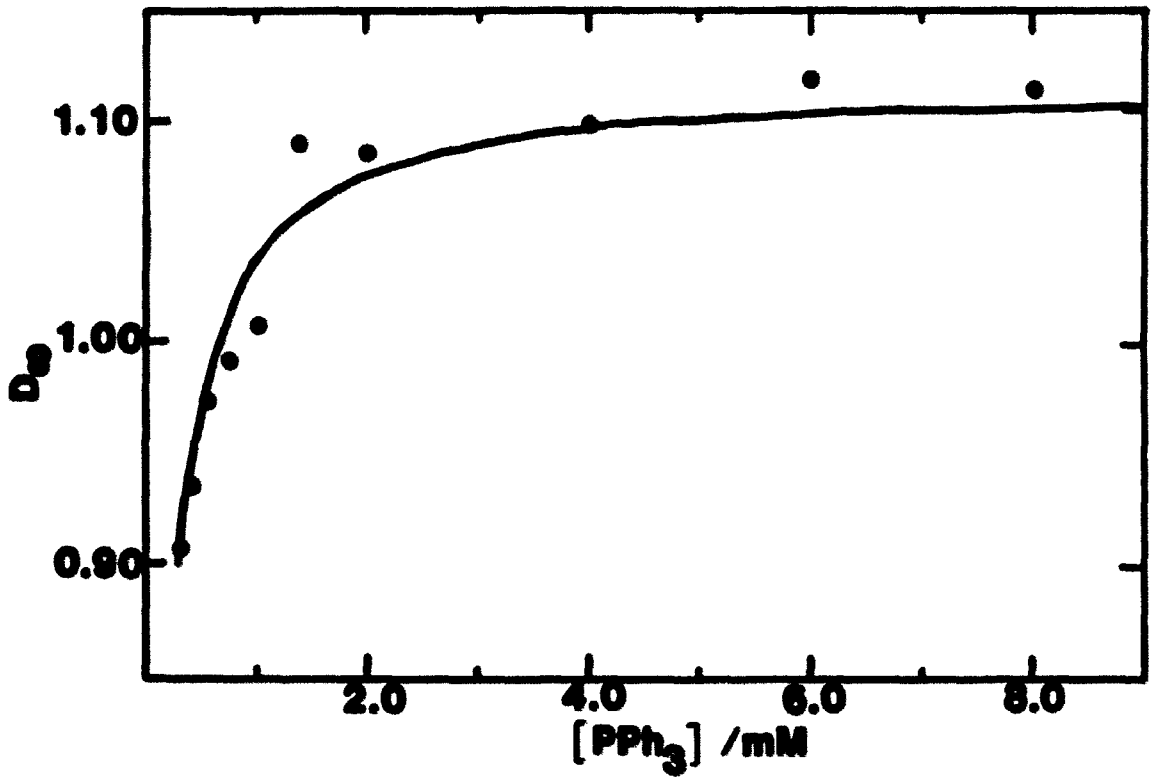

Figure I-23. Final absorbance (D_∞; 2 cm path length) at 372 nm of the reaction of PPh_3 with 0.1 mM $[Pt_2(\mu\text{-dppm})_2Cl_2]$ at 25 °C in 1,2-dichloroethane as a function of $[PPh_3]$; the solid line represents an equilibrium constant for the equilibrium between the reactants and $[Pt_2(\mu\text{-dppm})_2Cl(PPh_3)]^+$ of 7.4 ± 0.7 M^{-1}

Reaction kinetics Perhaps the most interesting observation about the reaction of PPh_3 with [Cl--Cl] is a comparison of reaction kinetics in the presence (0.5 mM) and absence of added Cl^-. For example, an approximate pseudo-first order rate constant for the reaction of 5 mM PPh_3 with 0.1 mM [Cl--Cl] at 25 °C is (roughly) 8.1 s^{-1}. In general, reactions in the absence of added Cl^- were not precisely first order and very sensitive to solvent impurities. With added Cl^-, however, the rates are much slower; for example, the rate constant for a 5.5 mM PPh_3 reaction is only 0.15 s^{-1} (see Figure I-24). Apparently there is outer sphere coordination of Cl^- to [Cl--Cl] which efficiently blocks attack of [Cl--Cl] by the incoming PPh_3 causing the decrease in the observed rate constant (see Scheme I-8). In the reactions with no added chloride, the chloride ion released during the reaction can associate with some of the unreacted [Cl--Cl] causing a lowering of the observed rate as the reaction progresses (i.e., the apparent first-order rate constant will decrease during the course of the run).

Scheme I-8. Important Equilibria in the Reaction of PPh_3 with $[Pt_2(\mu\text{-dppm})_2Cl_2]$ in CH_2Cl_2

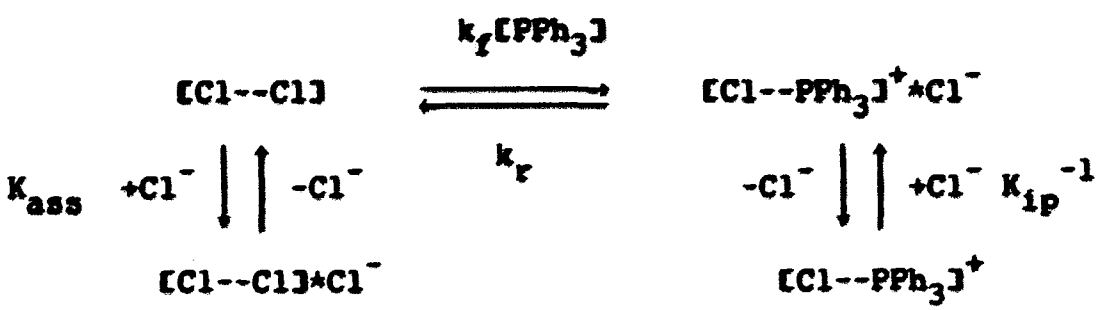

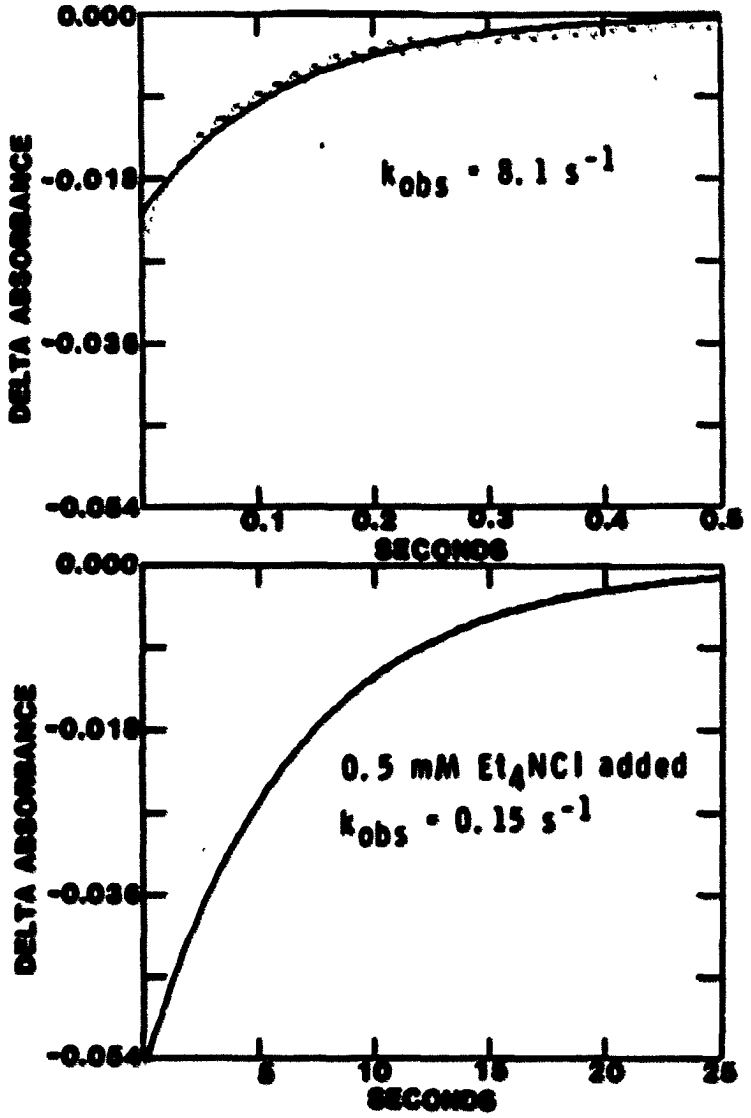

Figure I-24. Reactions of 5.0 mM (top) and 5.5 mM (bottom) PPh_3 with 0.1 mM $[Pt_2(\mu\text{-dppm})_2Cl_2]$ at 25 °C in CH_2Cl_2 in the absence and presence of 0.5 mM Et_4NCl respectively; the reactions were followed at 400 nm as a function of time using the stopped flow technique; the solid lines represent the best fit to first order kinetics

To determine the dependence of the reaction of [Cl--Cl] (0.1 mM) with PPh_3 upon $[PPh_3]$, reactions were conducted in the presence of high and constant $[Cl^-]$ (see Table I-12). A plot of k_{obsd} versus $[PPh_3]$ at constant $[Cl^-]$ (0.5 mM Et_4NCl) is linear (see Figure I-25) with a slope ($k_r/K_{ass}[Cl^-]$) of 15.2 ± 0.7 $M^{-1}s^{-1}$ and an intercept of 0.04 ± 0.02 s^{-1} at 25 °C. Absorbance changes for the reactions in Table I-12 remain relatively constant with increasing $[PPh_3]$ suggesting that the reaction is very near completion even at the lowest $[PPh_3]$.

The rate of [Cl--Cl] loss upon addition of PPh_3 in the reversible system in Scheme I-8 may be represented as follows:

$$-d[Cl\text{--}Cl]/dt = k_f[Cl\text{--}Cl][PPh_3] - k_r[[Cl\text{--}PPh_3]^+*(Cl)] \quad (11)$$

The pseudo-first order rate constant (k_{obsd}) can be written as:

$$k_{obsd} = \left(\frac{k_f[PPh_3]}{1 + K_{ass}[Cl^-]}\right) + k_r\left(\frac{K_{ip}[Cl^-]}{1 + K_{ip}[Cl^-]}\right) \quad (12)$$

At sufficiently high chloride, expression 12 simplifies to:

$$k_{obsd} = k_f[PPh_3]/K_{ass}[Cl^-] + k_r \quad (13)$$

If the intercept of Figure I-25 was due only to the reverse term of equation 12, only 28 % conversion of [Cl--Cl] to

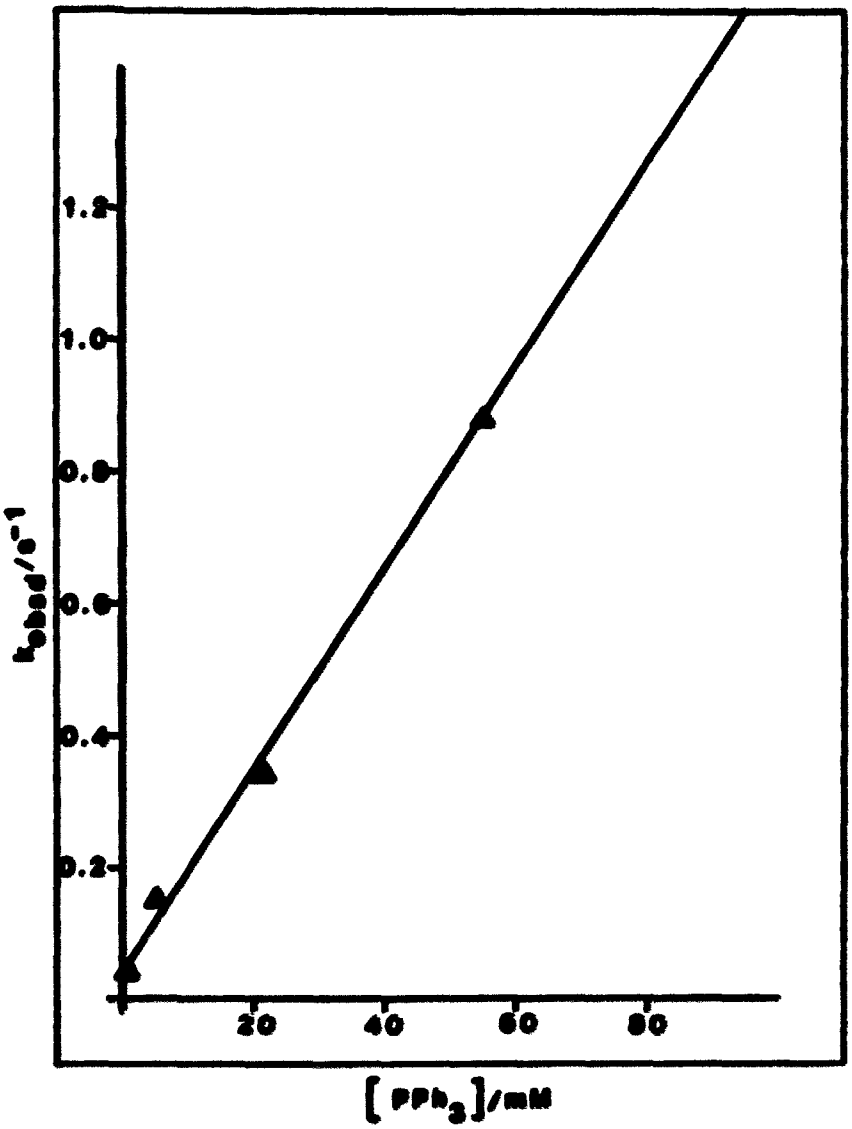

Figure I-25. Pseudo-first order rate constants (k_{obsd}) as a function of $[PPh_3]$ for reactions of PPh_3 with 0.1 mM $[Pt_2(\mu\text{-dppm})_2Cl_2]$ at 25 °C in CH_2Cl_2 with added Et_4NCl (0.5 mM); slope = 15.2 ± 0.7 $M^{-1}s^{-1}$; intercept = 0.04 ± 0.02 s^{-1}

Table I-12. Reaction of PPh_3 with $[Pt_2(\mu\text{-dppm})_2Cl_2]$ at 25 °C[a]

$[PPh_3]$/mM	k_{obsd}/s^{-1}	ΔAbs	# of runs
1.0	0.044 (1)	0.052 (1)	6
5.5	0.152 (3)	0.052 (3)	7
22.0	0.343 (6)	0.046 (5)	6
55.0	0.883(26)	0.040 (1)	5

[a]Reactions followed at 400 nm using stopped-flow techniques in the presence of 0.5 mM Cl^-; the numbers in parentheses are errors in the last digit.

$[Cl--PPh_3]^+$ would be expected at the lowest $[PPh_3]$ instead of the almost complete conversion that was observed. Because of this, the major portion of the intercept must be due to formation of $[Cl--PPh_3]^+$ by a $[PPh_3]$-independent pathway (e.g., rate-limiting ligand dissociation). Bear in mind that the pathway represented by this intercept is very minor when compared to the PPh_3 dependent pathway especially when the latter is not inhibited by added chloride. An associative pathway is by far the preferred method of ligand substitution in [Cl--Cl].

Reactions of halides with $[Pt_2(\mu\text{-dppm})_2(PPh_3)_2]^{2+}$

As briefly mentioned in the introduction to this section (page 83), the reactions of chloride with $[PPh_3--PPh_3]^{2+}$ are very anion dependent. The presence of noncoordinating anions such as ClO_4^- not only affects the rate of reaction but also the nature of the products (see Figure I-8 page 42). The mechanism proposed to account for the various reactions of chloride and other halides with $[PPh_3--PPh_3]^{2+}$ is summarized in Scheme I-9; the various pathways and the identity of different intermediates will be presented here.

The smoothest journey through this labyrinth of arrows from reactant to final product ($[X--PPh_3]^+$) may be accomplished by initially focusing on the reactions of $X = I^-$ with $[PPh_3--PPh_3]^{2+}$, the case in which the spectra of reactants, observable intermediates, and products exhibit the greatest

Scheme I-9. Formation of $[Cl{-}{-}PPh_3]^+$ from $[PPh_3{-}{-}PPh_3]^{2+}$

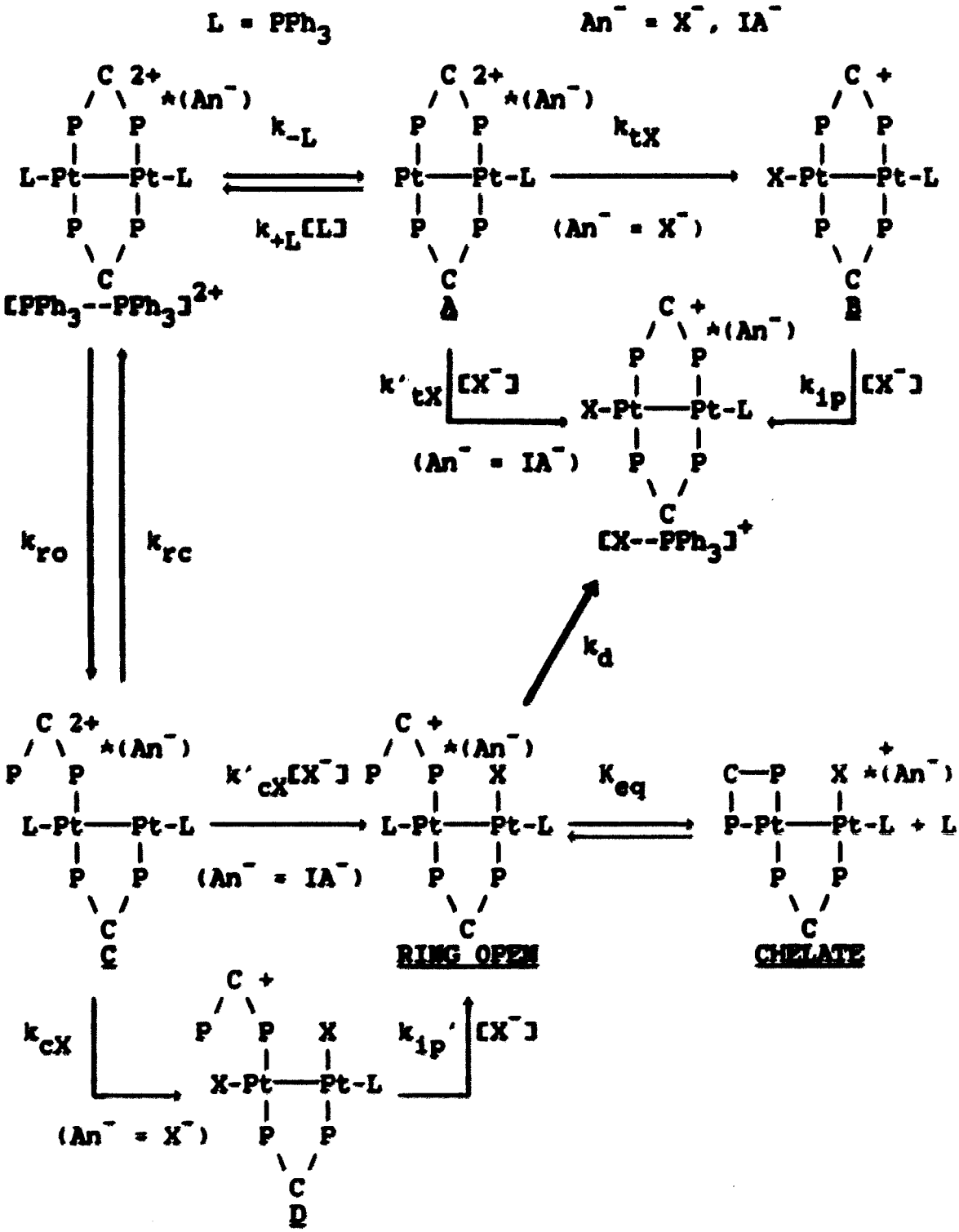

variation (Figure I-8). Consider, for example, the spectral changes during two specific reactions at 10 ^{0}C (see Figure I-26). Both reaction solutions contained identical initial concentrations of reactants $[PPh_3--PPh_3]^{2+}$ (0.02 mM) and $[(n\text{-butyl})_4NI]$ (0.2 mM) except, in addition, one solution contained 20 mM $[(n\text{-butyl})_4NClO_4]$.

In the presence of the "innocent" ClO_4^- ion (IA^- in general, since PF_6^- exhibits comparable behavior) the reaction (see Figure I-26a) occurred in only one stage, followed first order kinetics, and formed slowly, directly, and quantitatively final product, $[I--PPh_3]^+$ (compare Figure I-8a). This is interpreted as a pathway involving the dissociation of PPh_3.

With IA^- absent, on the other hand, there was an additional (and substantial) reaction pathway consisting of three distinct stages (Figure I-26b). The first stage, shown as $[PPh_3--PPh_3]^{2+}$ to RING OPEN in the general scheme, was complete within the first minute and was accompanied by absorbance increases at $\lambda > 410$ nm and decreases at $\lambda < 410$ nm. The second, RING OPEN to CHELATE, was finished within 15 minutes and occurred with absorbance decreases at $\lambda > 385$ nm and increases at $\lambda < 385$ nm. The final stage (CHELATE to $[I--PPh_3]^+$) occurred with spectral changes similar to those of the second stage but took hours to reach completion ($t_{1/2} \approx 1.5$ hours).

Figure I-26. Spectral scans (2 cm path length) of the reaction of 0.02 mM $[Pt_2(\mu\text{-dppm})_2(PPh_3)_2]^{2+}$ with 0.2 mM $[(n\text{-butyl})_4N]I$ in CH_2Cl_2 at 10 °C with (a) 20 mM $[(n\text{-butyl})_4N]ClO_4$ (scans every 2 min) and (b) no added perchlorate (scans every 2 min, then every 10 min; dashed spectrum is before I^- addition

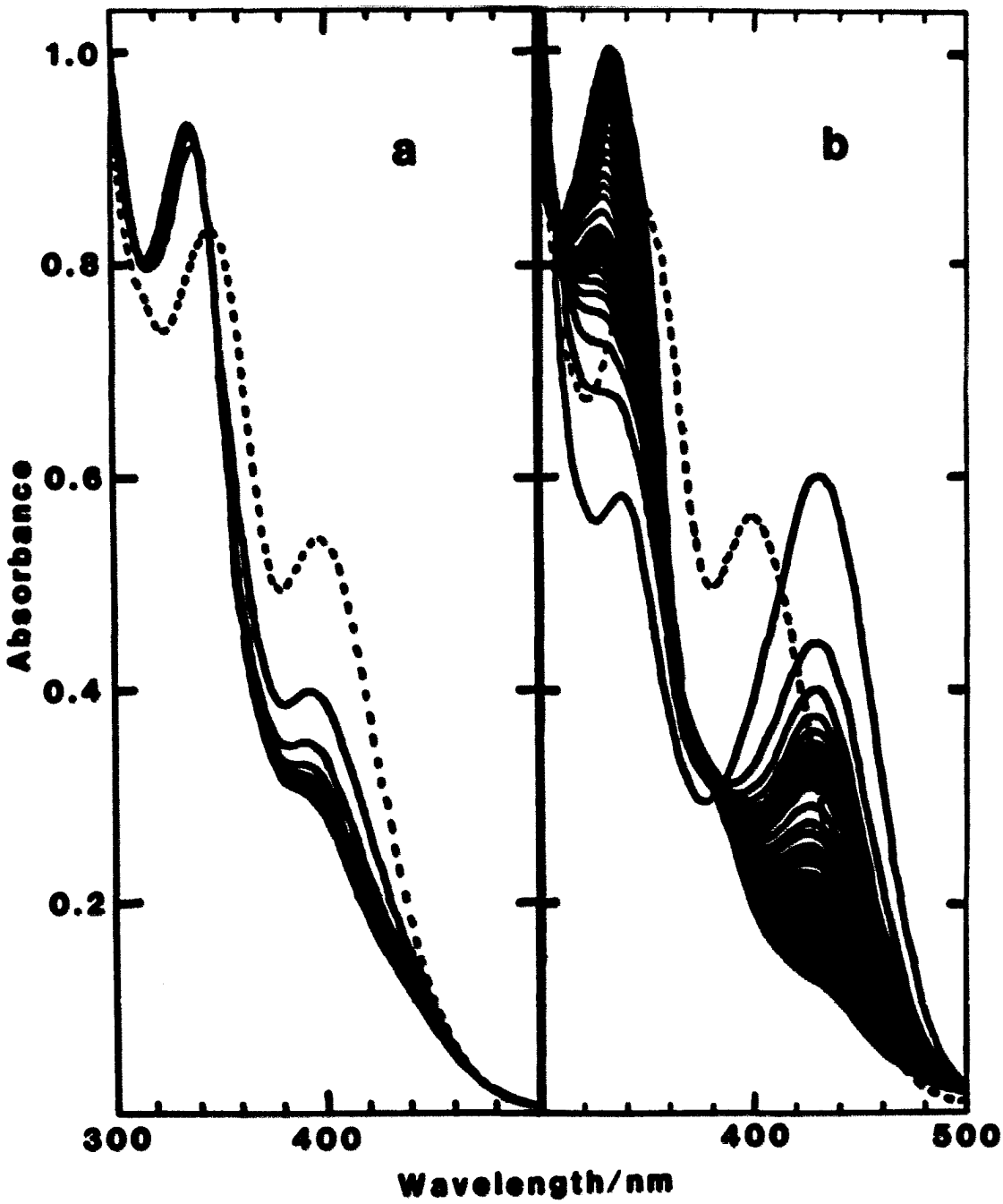
1.0
0.8
0.6
0.4
0.2
Absorbance
a
b
300
400
400
500
Wavelength/nm

Only after the latter stage of the ring opening pathway is $[I\text{--}PPh_3]^+$ produced essentially quantitatively. This is best illustrated by the $^{31}P\{^1H\}$ NMR of the products of the room temperature reaction of 16 mM $[PPh_3\text{--}PPh_3]^{2+}$ with 160 mM $[(n\text{-butyl})_4N]I$ in CD_2Cl_2 (Figure I-27a). The intensities of the five resonances attributed to iodo-CHELATE (discussed below) indicate that it was the major preliminary product. This CHELATE was stable for many hours at -20 °C but decomposed within 90 min at room temperature (80 mM PPh_3 was added after CHELATE formation; Figure I-27b). The spectrum of the final product is identical to that obtained for the product of the reaction of PPh_3 with [I--I] and was characterized as $[I\text{--}PPh_3]^+$ (see experimental page 158). Additional evidence for the formation of $[X\text{--}PPh_3]^+$ from CHELATE in the third stage is the fact that the ^{31}P NMR resonances of chloro-CHELATE were observed to disappear in concert with its 384 nm absorbtion maximum. This observation is important in connecting the UV-VIS spectrum and kinetics with the intermediate characterized by ^{31}P NMR.

To further illustrate the differences between the PPh_3 dissociation and $Pt_2(\mu\text{-dppm})$ ring opening pathways, consider kinetic traces at 347 nm for the reaction 0.02 mM $[PPh_3\text{--}PPh_3]^{2+}$ with 0.2 mM $[Et_4N]Br$ at 10 °C in CH_2Cl_2 (Figure I-28). Without ClO_4^-, the first stage of the reaction, $[PPh_3\text{--}PPh_3]^{2+}$ to RING OPEN in the $Pt_2(\mu\text{-dppm})$ ring opening

Figure I-27. The $^{31}P\{^{1}H\}$ NMR (121.5 MHz) spectra (signal accumulation at -20 ^{o}C; the peaks with the "x" are "folded over" peaks from the PF_6^- resonance at -150 ppm)
(a) of the products from the reaction of 16 mM $[Pt_2(\mu\text{-dppm})_2(PPh_3)_2]^{2+}$ with 160 mM $[(n\text{-butyl})_4N]I$ in CD_2Cl_2 at ambient temperature including $[Pt_2(\mu\text{-dppm})_2I(PPh_3)]^+$, $[Pt_2(\mu\text{-dppm})(\eta^2\text{-dppm})I(PPh_3)]^+$, and PPh_3;
(b) The $^{31}P\{^{1}H\}$ NMR of the solution in (a) after the addition of 80 mM PPh_3 and upon standing at ambient temperature for about 1.5 hr; PPh_3 and $[Pt_2(\mu\text{-dppm})_2I(PPh_3)]^+$ are the products

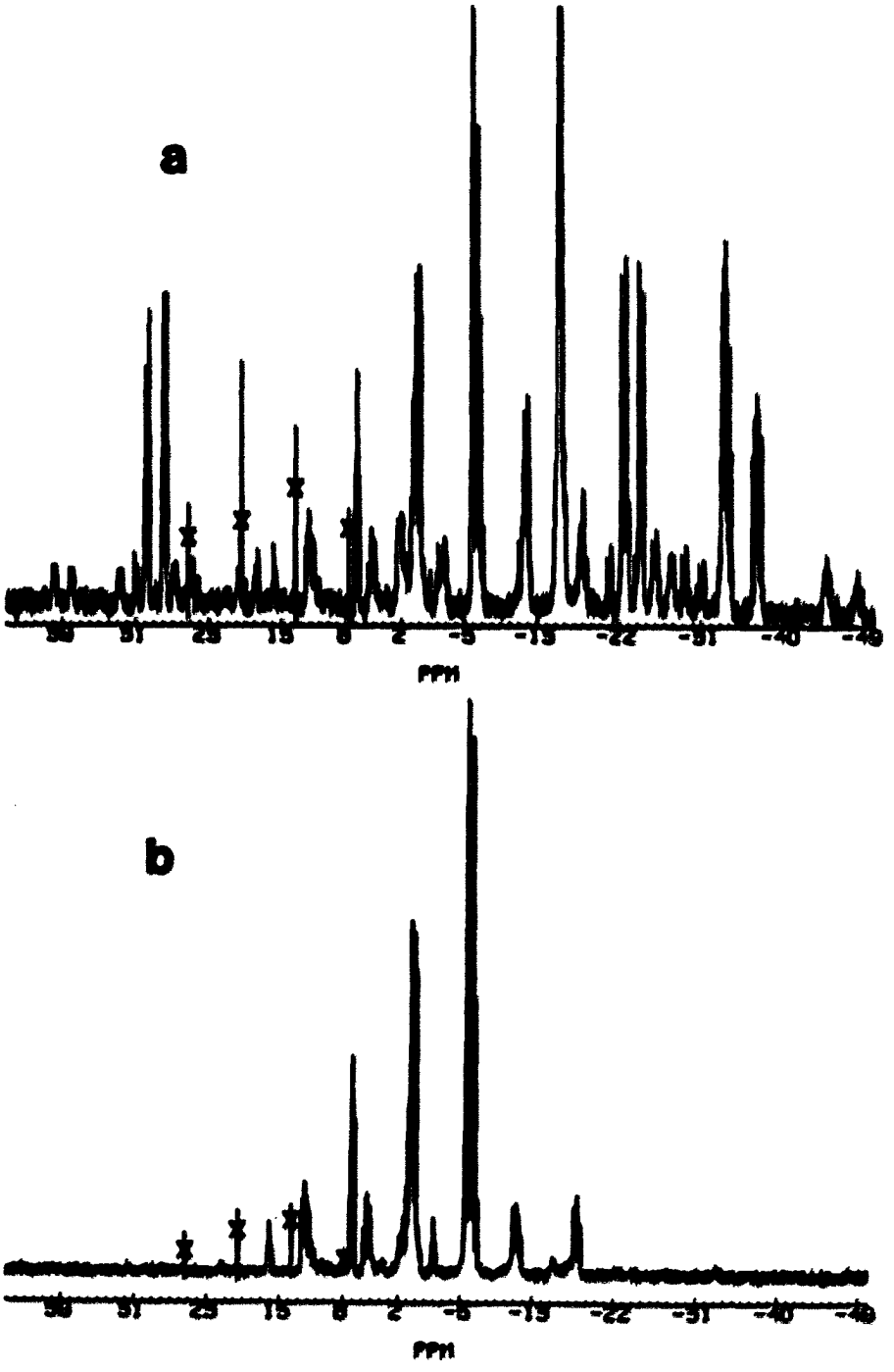
a
b
PPM
PPM

Figure I-28. Absorbance vs. time traces at 347 nm (2.0 cm) (370 nm (0.2 cm) for the inset) in the reaction of 0.02 mM $[Pt_2(\mu\text{-dppm})_2(PPh_3)_2]^{2+}$ with 0.2 mM $[Et_4N]Br$ at 10 °C in CH_2Cl_2; in the presence of $[(n\text{-butyl})_4N]ClO_4$ (20 mM, upper curve) the absorbance changes smoothly as $[Pt_2(\mu\text{-dppm})_2I(PPh_3)]^+$ is formed. In its absence (lower curve), there is an initial rapid change measureable by the stopped-flow method (inset), corresponding to formation of ring-opened intermediates; it is followed by a slower reaction forming $[Pt_2(\mu\text{-dppm})(\eta^2\text{-dppm})I(PPh_3)]^+$, which undergoes decomposition to $[Pt_2(\mu\text{-dppm})_2I(PPh_3)]^+$ over much longer times, and is not shown

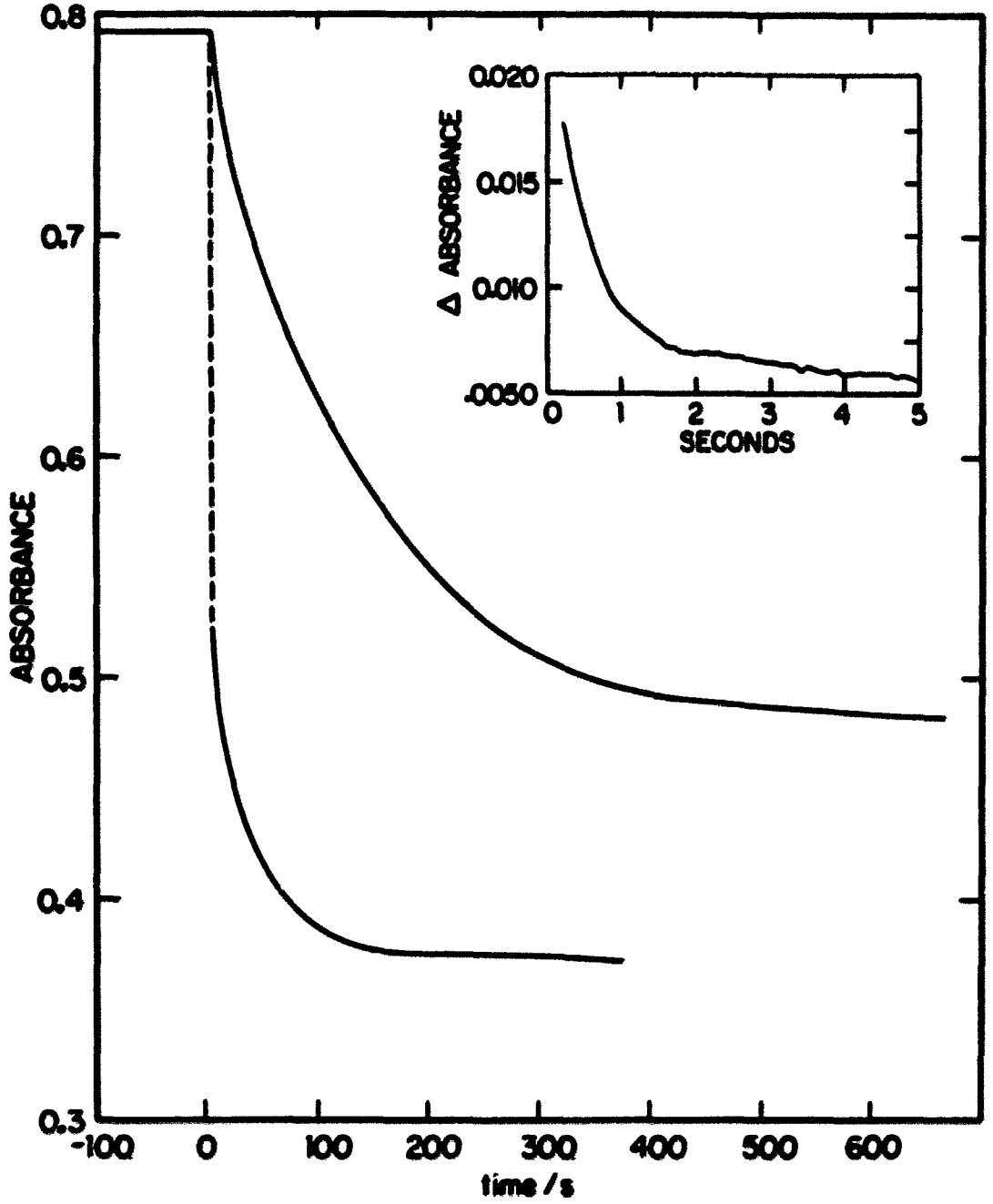
0.8
0.7
0.6
0.5
0.4
0.3
ABSORBANCE
-100
0
100
200
300
400
500
600
time / s
0.020
0.015
0.010
.0050
Δ ABSORBANCE
0
1
2
3
4
5
SECONDS

pathway of Scheme I-9, was too fast to be followed by normal spectrophotometric techniques ($t_{1/2}$ = 0.36 s) and could only be studied using a stopped-flow apparatus. The second stage (RING OPEN to CHELATE) was essentially complete in 5 min, but does not lead to a stable infinity absorbance (D_∞) because of the very slow reaction, CHELATE to $[Br{-}{-}PPh_3]^+$. The reaction of Br^- with $[PPh_3{-}{-}PPh_3]^{2+}$ in the presence of 20 mM $[(n\text{-butyl})_4N]ClO_4$; wherein $[Br{-}{-}PPh_3]^+$ forms by the PPh_3 dissociation pathway of Scheme I-9, was 280 times slower than the first stage of the reaction in the absence of ClO_4^-. It also followed first order kinetics (i.e., it had a stable D_∞).

With and without ClO_4^-, although the predominant pathway is different, in neither case does reaction correspond to 100 % of one pathway. That is, the halide reactions in the presence of ClO_4^- are predominated by the PPh_3 dissociation pathway at low $[X^-]$ but the ring opening pathway also becomes important with increasing $[X^-]$. In the absence of added IA^-, the reactions may occur by both ring opening and PPh_3 dissociation pathways. Under these conditions, $Pt_2(\mu\text{-dppm})$ ring opening appears to be more important, but because extinction coefficients for CHELATE and RING OPEN are comparable or much larger than those for $[X{-}{-}PPh_3]^+$ at all wavelengths (see Figure I-9), it is difficult to determine the precise quantity $[X{-}{-}PPh_3]^+$ actually present after the initial stages of the reaction. Under NMR conditions $[X{-}{-}PPh_3]^+$ (10 mM) is the major product for $X^- = Cl^-$, whereas CHELATE

predominates over $[X\text{--}PPh_3]^+$ when $X^- = I^-$. Furthermore, the product ratios vary from those observed in the NMR owing to the different extent of anion association when reactant concentrations are low.

Specific evidence supporting and further illustrating the mechanism for reactions of halides with $[PPh_3\text{--}PPh_3]^{2+}$ summarized in Scheme I-9 will now be presented as follows:

1. ^{31}P NMR evidence supporting $Pt_2(\mu\text{-dppm})$ ring opening
2. mechanistic evidence supporting $Pt_2(\mu\text{-dppm})$ ring opening
3. Pt-X bond formation by ion pair collapse
4. evidence for PPh_3 dissociation

^{31}P NMR Evidence for $Pt_2(\mu\text{-dppm})$ ring opening

Conditions were never found in which chloro-CHELATE predominated over $[Cl\text{--}PPh_3]^+$ in a NMR scale reaction; i.e., optimally, a 25 % relative yield of CHELATE was obtained. In fact, this reaction was repeated a number of times under different sets of conditions before the consistent presence of certain "impurity resonances" in the $^{31}P\{^1H\}$ NMR was finally acknowledged. CHELATE complexes are considerably more difficult to characterize than $[X\text{--}PPh_3]^+$ even when the two are at equal concentrations; there are four types of dppm phosphorus in the former compared to only two in $[X\text{--}PPh_3]^+$ causing the areas for the dppm resonances of the former to be half of those belonging to $[X\text{--}PPh_3]^+$. Additional phosphorus-phosphorus coupling also complicates the spectrum of the

former and further decreases its peak intensity relative to $[X\text{--}PPh_3]^+$ (e.g., Figure I-27a). Since iodo-CHELATE is the major product of the $[PPh_3\text{--}PPh_3]^{2+} + I^-$ reaction, it was readily characterized. Because the $^{31}P\{^1H\}$ NMR resonances and coupling patterns attributed to chloro-CHELATE are similar to those of iodo-CHELATE, a more certain identification of the chloro derivative is possible.

The $^{31}P\{^1H\}$ NMR resonances of iodo-CHELATE, as well as those belonging to chloro-CHELATE, are listed in Table I-13. It is both interesting and reassuring to note that within the pairs of bridging and chelating dppm phosphorus, similar chemical shifts are observed. The bridging phosphorus chemical shifts (-3 to -16 ppm; e.g., Figure I-29) are similar to those found in $[I\text{--}PPh_3]^+$ (1 and -6 ppm) and in $[PPh_3\text{--}PPh_3]^{2+}$ (-5.5 ppm), whereas those for chelating phosphorus (-22 to -36 ppm; e.g., Figure I-30) are similar to the chemical shifts of phosphorus in $[PtCl(Me)(\eta^2\text{-dppm})]$ and other Pt(II) complexes containing η^2-dppm (-36 to -40 ppm).[58] The PPh_3 resonances (28 to 32 ppm; e.g., Figure I-31) have chemical shifts similar to that of PPh_3 in $[Pt_2(\mu\text{-dppm})_2(\mu\text{-}CH_2)(PPh_3)_2]^{2+}$ (32.8 ppm).[20]

The magnitude of the respective platinum-phosphorus coupling constants found in iodo-CHELATE are in complete harmony with its structure as are those that could be determined for chloro-CHELATE (Table I-14). Only the

phosphorus nuclei trans to the Pt-Pt bond (P_1 and P_5) have $^2J(Pt,P)$ sufficiently large to be unobscured by the central resonances (e.g., Figure I-31). The $^2J(Pt_R,P_5)$ (723 Hz in iodo-CHELATE) is very similar to such coupling constants in $[PR_3--PR_3]^{2+}$ complexes (e.g., Table I-3), however the $^2J(Pt_A,P_1)$ (380 Hz), $^1J(Pt_R,P_1)$ (1607 Hz), and to some extent, the $^1J(Pt_R,P_2)$ (2706 Hz) of iodo-CHELATE are lower than the 650-1000 Hz, 2000-2200 Hz, and 2850-3000 Hz normally expected for dppm (i.e., η^1-bound or bridging) in $[L--L]^{n+}$ complexes. The strain in the four-membered chelate ring weakens these Pt-P bonds causing the lower than normal coupling constants. The $^1J(Pt_A,P_5)$ (2457 Hz) is 250 Hz larger than normal $^1J(Pt,P)$ for phosphines bound trans to the Pt-Pt bond in $[L--L]^{n+}$ complexes perhaps because the absence of a pair of dppm phenyls reduces steric repulsions and allows a shorter Pt-P distance. The $^1J(Pt_R,P_4)$ of 3045 Hz is normal as is the 4305 Hz $^1J(Pt_A,P_3)$; a phosphorus bound trans to a chloride normally has very large coupling constants (e.g., 3500 Hz in Table I-4), but when it is also bound cis to substituents with a large trans influence, the coupling constant should be even larger (e.g., 4179 Hz in cis-$[PtCl(Me)(PEt_3)_2]^{24}$) due to the "cis effect" illustrated in Table I-5.

Phosphorus-phosphorus coupling constants from Table I-14 provide further support for the CHELATE structure. The values of $^2J(P_1,P_2)$ and $^2J(P_3,P_4)$, 53.4 and 40.0 Hz, are very similar

Table I-13. $^{31}P\{^{1}H\}$ NMR chemical shifts in $[Pt_2(\eta^2\text{-dppm})(\mu\text{-dppm})X(PPh_3)]^+$

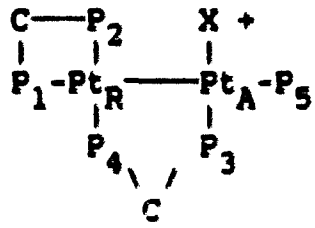

(P_5 = PPh_3)

CHELATE

	Chemical Shifts/ppm				
X^-	P_1	P_2	P_3	P_4	P_5
I^-	-23.5	-35.5	-15.6	-13.5	28.8
Cl^-	-22.7	-25.5	-11.3	-3.5	31.8

Figure I-29. The $^{31}P\{^{1}H\}$ NMR (121.5 MHz) spectrum (top) at -20 °C in CD_2Cl_2 of the central portions of the bridging dppm resonances (i.e., P_3 and P_4) of $[Pt_2(\mu\text{-dppm})(\eta^2\text{-dppm})I(PPh_3)]^+$; the spectrum was simulated (bottom) using coupling constants in Table I-14 excluding contributions from ^{195}Pt satellites; i.e., the cis-$^{2}J(Pt,P)$ satellites of these two resonances, and in addition, $^{1}J(Pt,P)$ satellites found between -11 and -11.5 ppm and at -15.8 and -16.2 ppm accompanying other central resonances not pictured here (see Figure I-27a for the total spectrum)

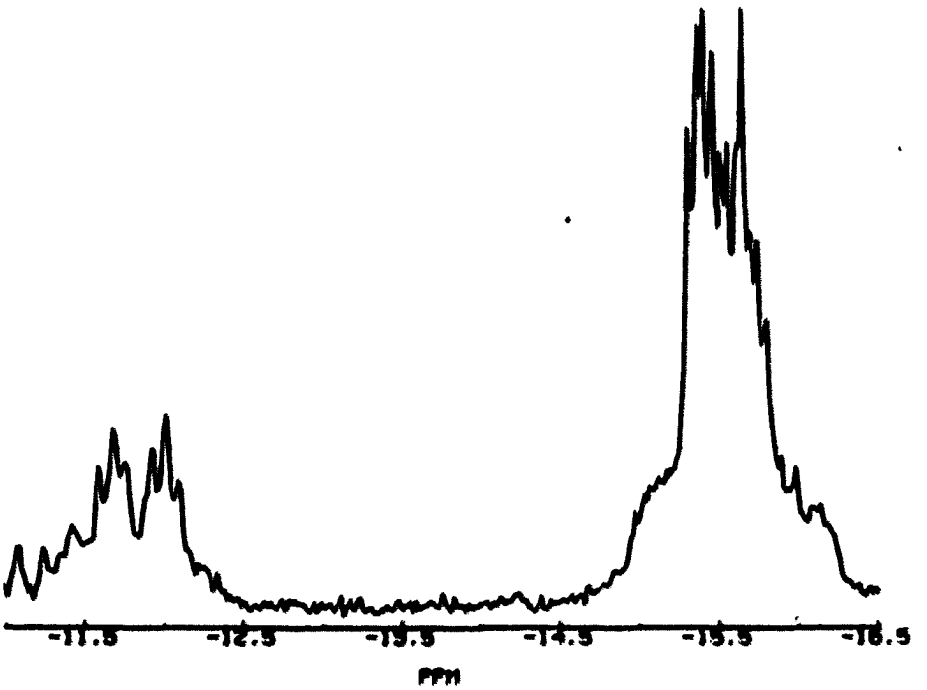
-11.5
-12.5
-13.5
-14.5
-15.5
-16.5
PPM

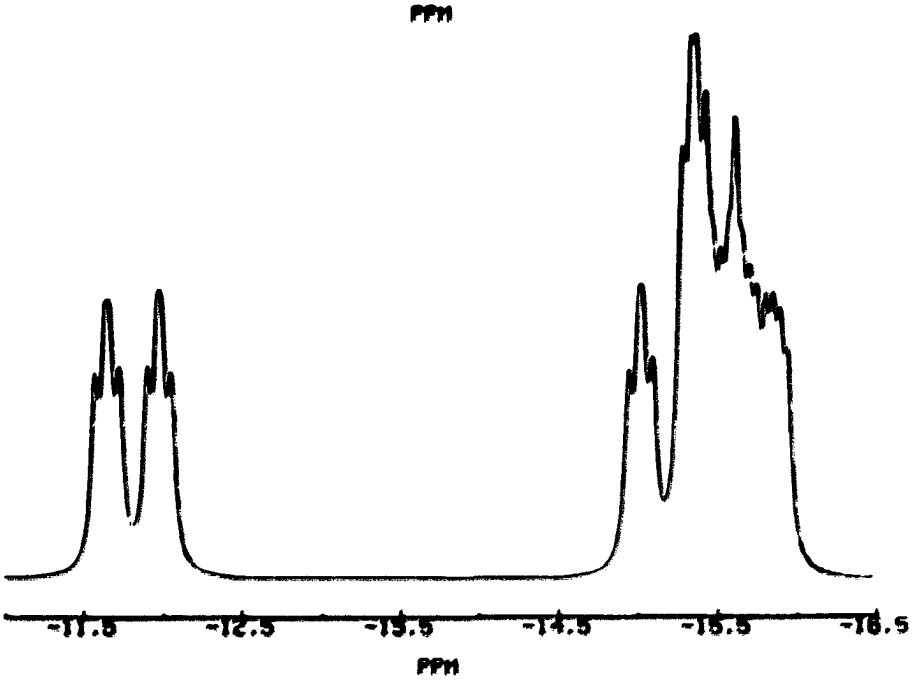
-11.5
-12.5
-13.5
-14.5
-15.5
-16.5
PPM

Figure I-30. The $^{31}P\{^{1}H\}$ NMR (121.5 MHz) spectrum at -20 ^{o}C in CD_2Cl_2 of the central portions of the chelating dppm resonances, P_1 (top) and P_2 (bottom) of $[Pt_2(\mu\text{-dppm})(\eta^2\text{-dppm})I(PPh_3)]^+$ including at least portions of their $^{2}J(Pt,P)$ satellites and the $^{1}J(Pt,P)$ satellites of P_2 (-22.9 ppm), P_4 (-24.3 ppm), and P_3 (-33.4 ppm)

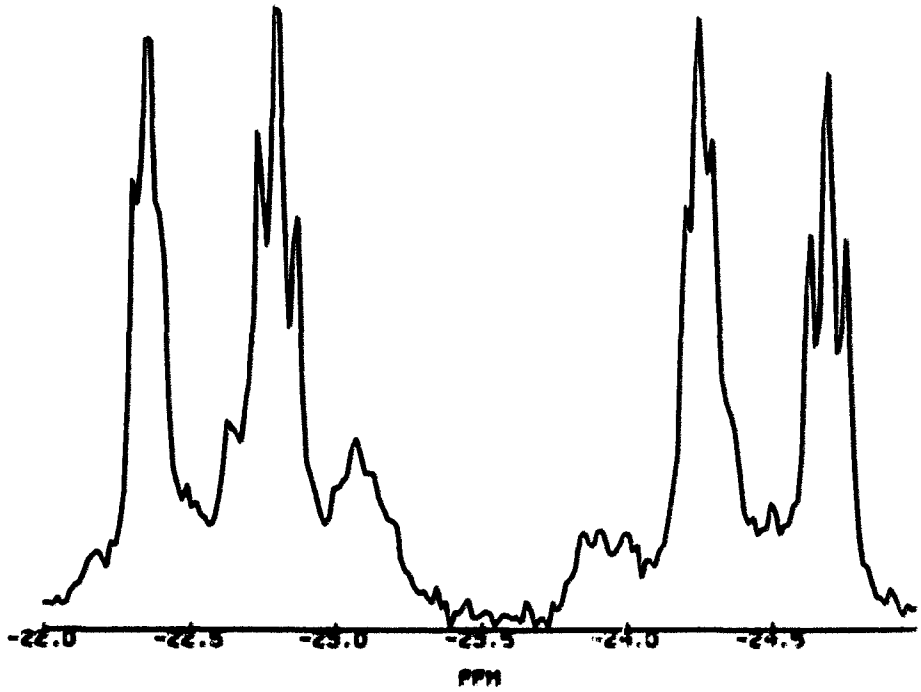
-22.0
-22.5
-23.0
-23.5
-24.0
-24.5
PPM

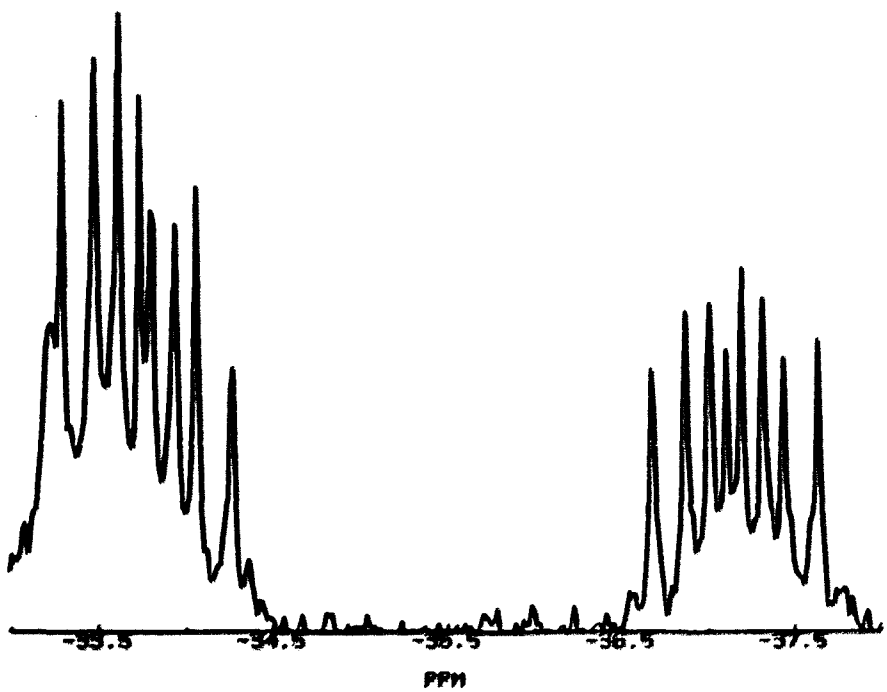
-35.5
-36.5
-37.5
PPM

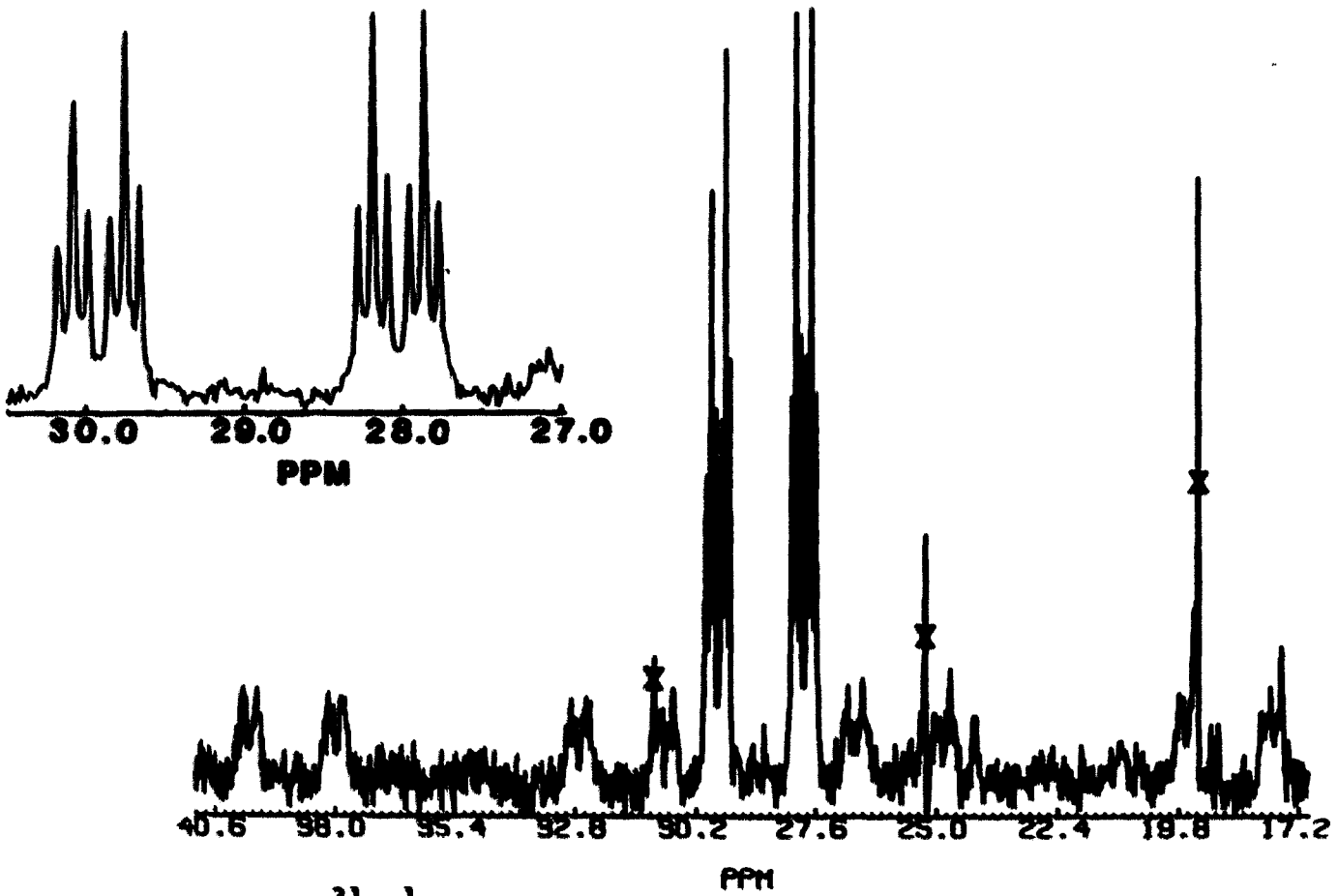

Figure I-31. The $^{31}P\{^{1}H\}$ NMR (121.5 MHz) spectrum at -20 °C in CD_2Cl_2 of the PPh_3 (P_5) resonance of $[Pt_2(\mu\text{-dppm})(\eta^2\text{-dppm})I(PPh_3)]^+$ including its ^{195}Pt satellites; the peaks with an "x" are due to the "folding over" of the PF_6^- resonance found at -150 ppm; the inset is an expanded view of the central resonance

Table I-14. Coupling constants in $[Pt_2(\eta^2\text{-dppm})(\mu\text{-dppm})X(PPh_3)]^+$

Constant[b]	Coupling Constants/Hz[a] I^-	Cl^-
$^1J(Pt_R,P_1)$	1607. (2.)	-
$^1J(Pt_R,P_2)$	2706. (10.)	2796. (15.)
$^1J(Pt_A,P_3)$	4305. (10.)	4215. (15.)
$^1J(Pt_R,P_4)$	3045. (10.)	3022. (15.)
$^1J(Pt_A,P_5)$	2457. (5.)	2213. (10.)
$^2J(Pt_A,P_1)$	380. (4.)	-
$^2J(Pt_R,P_5)$	723. (2.)	812. (10.)
$^2J(P_1,P_2)$	53.4 (0.6)	43.0 (1.1)
$^2J(P_1,P_4)$	7.5 (0.6)	9.3 (1.7)
$^2J(P_2,P_4)$	409.0 (0.8)	405. (4.)
$^2J(P_3,P_4)$	40.0 (0.8)	46.0 (0.7)
$^2J(P_3,P_5)$	11.2 (0.5)	8.5 (0.9)
$^3J(P_1,P_3)$	5.7 (0.7)	0. (3.)
$^3J(P_1,P_5)$	228. (3.)	239. (6.)
$^3J(P_2,P_3)$	23.3 (1.2)	14.2 (1.1)
$^3J(P_2,P_5)$	39.3 (0.2)	39.1 (1.0)
$^3J(P_4,P_5)$	11.2 (0.2)	8.5 (0.8)

[a]The numbers in parentheses are estimated errors in the coupling constants.

[b]The atoms are designated as shown in Table I-13.

to the corresponding two bond P-P couplings between phosphorus nuclei in the bridging dppm ligands found in $[Cl--PPh_3]^+$ (i.e., 40-50 Hz), whereas the $^2J(P_1,P_4)$ and $^2J(P_3,P_5)$ values, 7.5 and 11.2 Hz, are only half the cis-$^2J(P_APtP_T)$ value of (20 Hz) in $[Cl--PPh_3]^+$ but still in the range generally found for cis-$^2J(P,P)$.[24] The trans-$^2J(P_2,P_4)$ of 405 Hz fits nicely into the reported range of trans-$^2J(P,P)$ in Pt(II) complexes of 300 to 700 Hz,[24] the fact that it is observable shows that these two trans phosphorus nuclei are inequivalent; note that trans-$^2J(P,P)$ are not observed in $[L--L]^{n+}$ complexes.

Complexes containing two inequivalent phosphorus nuclei bound mutually trans to a Pt-Pt bond are rare. The $^3J(Pt_1,P_5)$ of 228 Hz is comparable to the 195 Hz value reported for $^3J(P_T,P_T)$ in $[PMe_2Ph--PMe_2Ph]^{2+}$.[6] This exceptionally large three bond P-P coupling constant is evidence for strong Pt-Pt bonding in CHELATE complexes, as is the fact that other $^3J(P,P)$ are even observed. The $^3J(P_1,P_4)$ and $^3J(P_4,P_5)$ of 5.7 and 11.2 Hz are predicted to be smaller than the $^3J(P_2,P_3)$ of 23.3 Hz from a Karplus correlation[35] since the dihedral angle between the former type of phosphorus should be about 90^0 compared to an angle between 120 and 180^0 for the latter. However, the surprisingly large $^3J(P_2,P_5)$ of 39.5 Hz does not fit into this correlation (dihedral angle $\neq 90^0$).

A logical precursor of CHELATE is RING OPEN whose $^{31}P\{^1H\}$ NMR spectrum should easily be recognized by the resonance due

to the uncoordinated phosphorus of η^1-dppm. In structurally-characterized Pt(I) dimers containing η^1-dppm, resonances for the uncoordinated phosphorus exhibit little or no coupling to Pt, they are shifted upfield from free dppm, and have very large ^2J(PCP) that are temperature dependent (see Table I-15). The temperature dependence of ^2J(PCP) has been attributed to the onset of a fluxional process involving exchange of coordinated and free ^{31}P centers of the η^1-dppm ligand.[4] Since no evidence for RING OPEN has been observed in the $^{31}P\{^1H\}$ NMR spectra of products of halide-$[PPh_3$--$PPh_3]^{2+}$ reactions, this precursor to CHELATE must lead a fleeting existence.

Precedents for chelated dppm are fairly numerous;[1] notable among these are the previously mentioned $[Pt_2(\mu\text{-dppm})(\eta^2\text{-dppm})_2]^{2+}$ (3-DPPM),[8] and the mononuclear Pt(II) complex, $[PtCl_2(\eta^2\text{-dppm})]$, from which [Cl--Cl] is synthesized.[5] Cursory UV-visible measurements on the reactivity of dppm with [Cl--Cl], $[Cl$--$PPh_3]^+$, and $[PPh_3$--$PPh_3]^{2+}$ suggested that substitution of terminal chloride and PPh_3 by dppm occurs readily. Thus, formation of CHELATE from RING OPEN seems reasonable.

Mechanistic evidence for $Pt_2(\mu$-dppm) ring opening. As has been mentioned, an intermediate formed prior to CHELATE is detected using ultraviolet-visible spectroscopy. The existence of this observable intermediate designated RING OPEN

Table I-15. $^{31}P\{^{1}H\}$ NMR data for the uncoordinated phosphorus in $[Pt_2(\mu\text{-dppm})_2(\eta^1\text{-dppm})Y]^+$ complexes

Y	Temp/^{o}C	Chemical Shift/ppm	^{2}J(PCP)/Hz	ref.
H	-80	-33.95	107	27
H	0	-32.10	85	27
H	30	-30.37	60	27
Me	-80	-31.9	94	4
Me	20	?	0	4
Cl^-	-20	-28.77	62	-[a]
Cl^-	25	-28.29	55	-[a]

[a] This work.

supports the structural assignment made by $^{31}P\{^{1}H\}$ NMR for CHELATE: Since the intermediate designated CHELATE contains the assigned η^2-dppm unit, then its formation must involve in some stage ring opening of $[PPh_3--PPh_3]^{2+}$. It is thus logical that an intermediate (C in Scheme I-9 on page 96) coming prior to both RING OPEN and CHELATE will be formed as a result of a Pt-dppm bridge opening process by dissociation of one end of μ-dppm. This ring opening will create a 14 electron center expected to react with incoming small nucleophiles (i.e., X^-) much more rapidly than dppm will displace PPh_3. Therefore, the logical formation of RING OPEN before CHELATE is substantiated by UV-VIS spectroscopy.

The apparent rate constants for CHELATE formation from RING OPEN (see Scheme I-9) should and were found to be independent of X^- concentration. Because RING OPEN complexes are separate and distinct, having different halides bound to one platinum in its inner coordination sphere, k_{-L}, should and does vary with the identity of X^- (see Table I-16).

In the very slow third stage of the reaction, there is no obvious route for a direct transformation between CHELATE and $[Cl--PPh_3]^+$, the final product. It is likely this entails more than a single step. Since the transformation of RING OPEN to CHELATE may be reversible, one possibility is that CHELATE acts as a dead end intermediate with RING OPEN being the species that eventually leads to $[Cl--PPh_3]^+$

Table I-16. Apparent rate constants for the formation of $[Pt_2(\eta^2\text{-dppm})(\mu\text{-dppm})X(PPh_3)]^+$ from $[Pt_2(\eta^1\text{-dppm})(\mu\text{-dppm})X(PPh_3)_2]^+$ at 10 °C[a]

Halide	[Halide]/mM	k_{app}/s^{-1}
Cl^-	0.2	0.026
Cl^-	2	0.028
Br^-	0.2	0.029[b]
Br^-	2	0.029
I^-	0.2	0.0056
I^-	2	0.0094

[a]Reaction of 2×10^{-5} M $[PPh_3\text{-}PPh_3]^{2+}$ in CH_2Cl_2 during the second stage of reaction followed at 347, 347, and 400 nm for Cl^-, Br^-, and I^- respectively.

[b]Average of three determinations, error = ±0.004.

formation. Some limited evidence presented below is supportive of such a scheme where the proposed ligand substitutions occur by Pt-P bond dissociation (Scheme I-10).

Scheme I-10. Mechanism for $[Cl{-}{-}PPh_3]^+$ Formation from RING OPEN

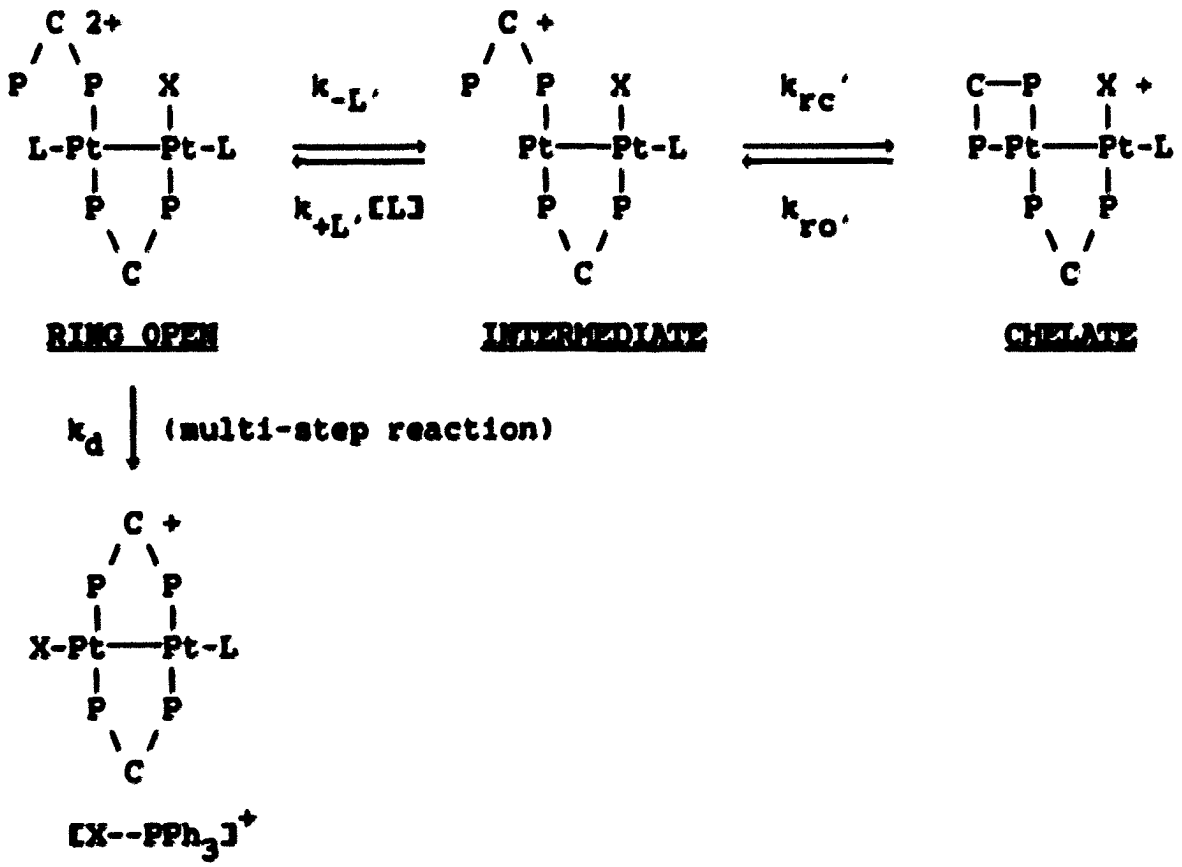

$[X{-}{-}PPh_3]^+$

Reactions of 0.02 mM $[PPh_3{-}{-}PPh_3]^{2+}$ with 0.2 mM $[(n\text{-butyl})_4N]I$ at 10 °C in CH_2Cl_2 were observed as a function of $[PPh_3]$ during the time range of the RING OPEN to CHELATE transformation ($t_{1/2}$ = 2 min). In the absence of added phosphine, CHELATE formation was the dominant reaction (see Figure

I-32a) since the spectrum at the pseudo-infinity of this second stage reaction is that of CHELATE. Further proof of this lies in the fact that a well-defined isosbestic point is observed at 388 nm indicative of a transformation between only two species. With added PPh_3, however, the situation is different. Even at the lowest $[PPh_3]$, the integrity of this isosbestic point was lost (Figure I-32b), signaling the onset of an additonal reaction in the time domain of $[I{-}{-}PPh_3]^+$ formation. As $[PPh_3]$ was increased, direct $[I{-}{-}PPh_3]^+$ formation became the major pathway, and conversely, formation of CHELATE became less and less important (see Figure I-32c and d). In fact, the observed rate constant for $[I{-}{-}PPh_3]^+$ formation increases 60 fold upon the addition of 2 mM PPh_3 (compare Figure I-32d with Figure I-26b). Inhibition of CHELATE formation with increasing $[PPh_3]$ may be caused by the increasing importance of the reaction represented by $k_{+L}[PPh_3]$ in Scheme I-10. It seems less likely that the rate acceleration by added PPh_3 is because of its enhancement of the direct reaction. Note that the reaction(s) represented by k_d (Scheme I-10) should not have a first order dependence in $[PPh_3]$ since $[I{-}{-}PPh_3]^+$ has one less PPh_3 than RING OPEN.

Spectral changes for chloride reactions were observed as a function of increasing $[PPh_3]$ under the same conditions as the iodide reactions. However, these observations were made on a slower time scale than the chloro-RING OPEN to CHELATE

Figure I-32. Spectral scans (every 2 min; solution in 2 cm cell) of the reaction of 0.2 mM $[(n\text{-butyl})_4N]I$ with 0.02 mM $[Pt_2(\mu\text{-dppm})_2(PPh_3)_2]^{2+}$ at 10 °C in CH_2Cl_2 in the presence of (a) no, (b) 0.2 mM, (c) 0.8 mM, and (d) 2.0 mM added PPh_3

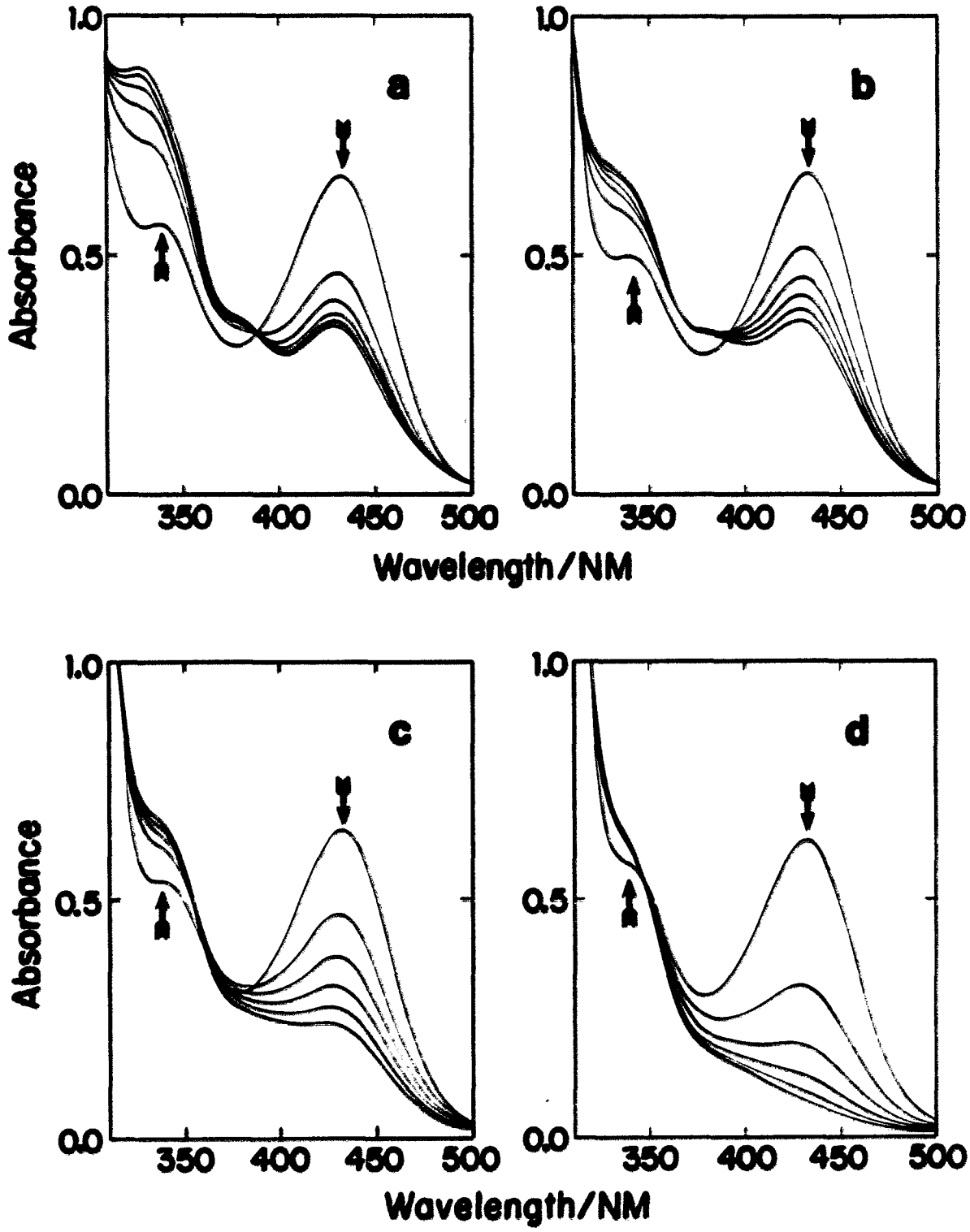
a
b
c
d
Absorbance
1.0
0.5
0.0
350
400
450
500
Wavelength/NM

transformation (Figure I-33). An obvious feature of these reactions is the decreasing initial absorbance at the CHELATE absorbance maximum (384 nm) with increasing [PPh_3]. This was not observed in the iodide reactions (i.e., at 428 nm in Figure I-32). In the absence of added phosphine, the half life of the second stage chloride reaction is 28 s (Table I-16) whereas the first spectral scan took 38 s; this reaction is more than 50 % complete by the end of the scan. On the other hand, because the iodo second stage is much slower ($t_{1/2}$ = 2 min), only a small percentage of it occurred during the first 38 second spectral scan. Thus, because the absorbance at 432 nm in the first scan of the iodide reaction does not vary with [PPh_3], one can assume that the yield of RING OPEN produced in its first stage is independent of added phosphine concentration. The [Cl--PPh_3]$^+$: RING OPEN absorbance ratios in the second scan (Figure I-33) of the chloride reaction (5 min into the reaction) should be fairly representative of their respective product ratios after the second stage reaction. The observed decrease in CHELATE yield with increasing [PPh_3] in the chloride reactions further illustrates the competition between formation of [X--PPh_3]$^+$ and CHELATE. The rate of CHELATE decomposition via Scheme I-10 is expected to increase with increasing [PPh_3] because added PPh_3 will increase the steady state concentration of the reactive RING OPEN; this predicted rate enhancement was indeed observed (Figure I-33).

Figure I-33. Spectral scans (every 5 min; solution in 2 cm cell) of the reaction of 0.2 mM $[Et_4N]Cl$ with 0.02 mM $[Pt_2(\mu\text{-dppm})_2(PPh_3)_2]^{2+}$ at 10 °C in CH_2Cl_2 in the presence of (a) no, (b) 0.2 mM, (c) 0.8 mM, and (d) 2.0 mM added PPh_3

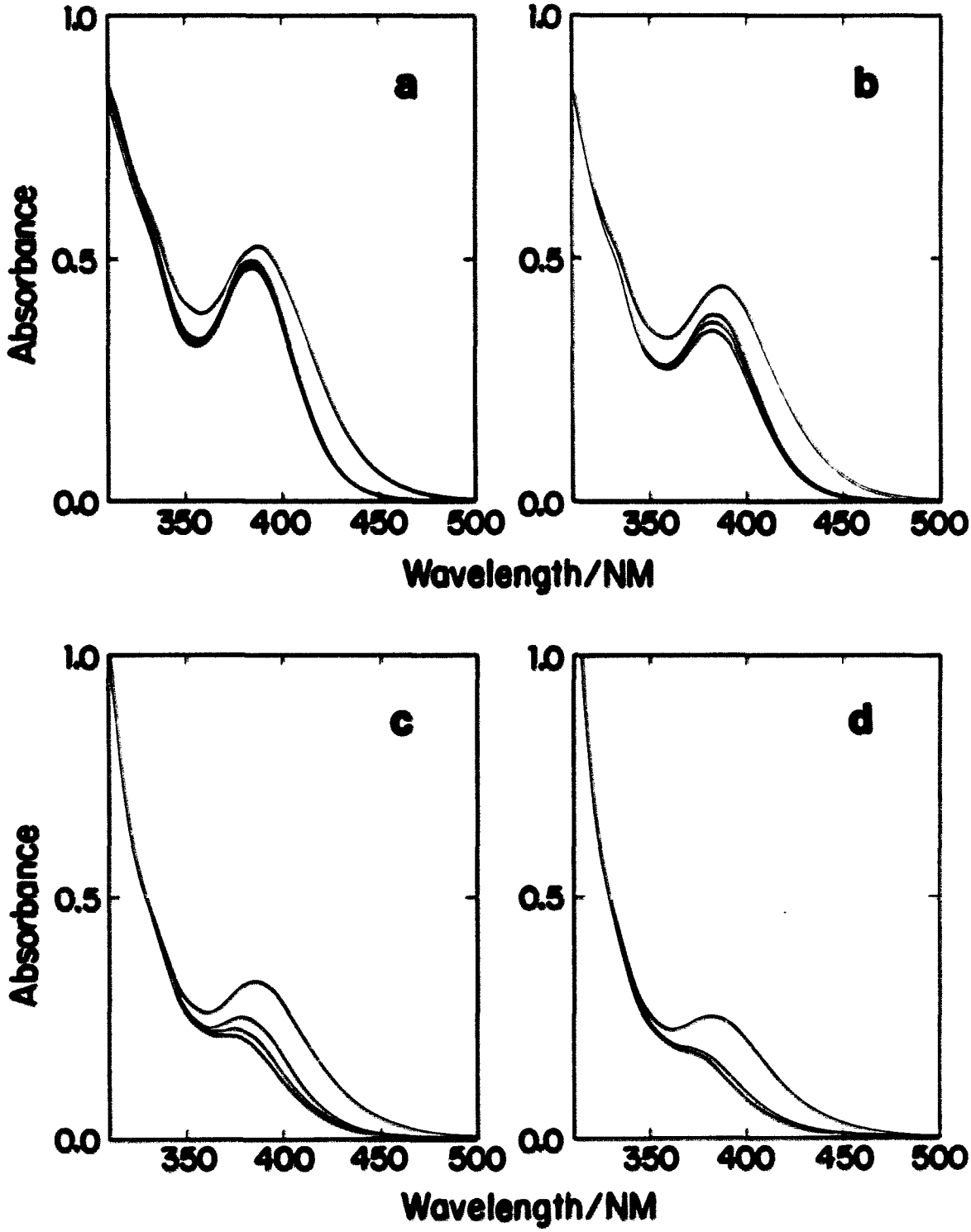
a
b
c
d
Absorbance
Wavelength/NM
1.0
0.5
0.0
350
400
450
500

When 2 mM PPh_3 is added to a 0.2 mM I^- reaction after formation of CHELATE, a small absorbance increase is followed by a very slow absorbance decrease at 428 nm (Figure I-34). These observations are consistent with a rapid but small increase in the steady state concentration of RING OPEN followed by the very slow $[I\text{--}PPh_3]^+$ formation. The latter is now limited by the rate of the Pt(η^2-dppm) ring opening reaction of CHELATE (k_{ro}, in Scheme I-10) instead of the rate of RING OPEN decomposition via the reaction(s) designated k_d in the case where 2 mM PPh_3 was added to the solution before the reaction of I^- (Figure I-32d).

No evidence for RING OPEN was seen in the $^{31}P\{^1H\}$ NMR spectrum after reaction of 16 mM $[PPh_3\text{--}PPh_3]^{2+}$ with a 10 fold excess of $[Et_4N]Cl$ even when a ten fold excess of 0.16 M PPh_3 was added. Furtermore, when 0.16 M PPh_3 was added to a CD_2Cl_2 solution containing about 10 mM iodo-CHELATE, no evidence for RING OPEN was observed in the $^{31}P\{^1H\}$ NMR. If the mechanism in Scheme I-10 is correct, the concentration of RING OPEN in solution must be fairly low once steady-state conditions are reached (i.e., after the second stage of reaction).

The nature of the reactions represented by k_d in Scheme I-10 have not been investigated. Perhaps $[PPh_3\text{--}PPh_3]^{2+}$ is reformed, in which case $[X\text{--}PPh_3]^+$ would eventually be formed by the PPh_3 dissociation pathway. $[X\text{--}PPh_3]^+$ could also be formed by direct substitution of the PPh_3 adjacent to X in

Figure I-34. Reaction of 0.2 mM [(n-butyl)$_4$N]I with 0.02 mM [$Pt_2(\mu\text{-dppm})_2(PPh_3)_2$]$^{2+}$ at 10 °C in CH_2Cl_2 (2 cm path length);

--- scans every 2 min immediately after addition of I^- (abs. decrease at 430 nm);

—— scans every minute starting 12 min after addition of I^- and immediately after addition of 2 mM PPh_3 (abs. increase at 430 nm);

··· scans 48 and 93 min after addition of the 2 mM PPh_3 (abs. decrease at 430 nm)

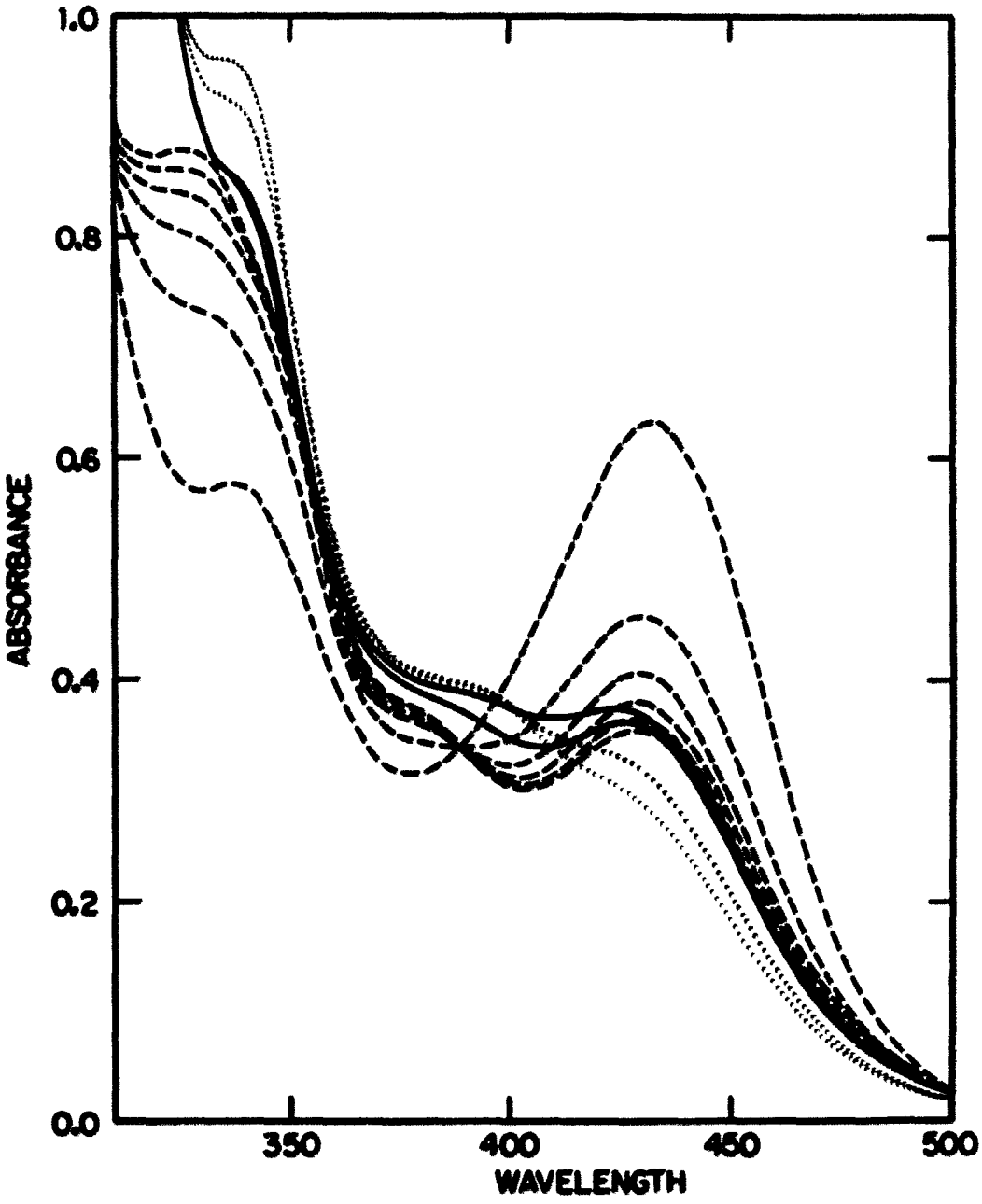
1.0
0.8
0.6
0.4
0.2
0.0
ABSORBANCE
350
400
450
500
WAVELENGTH

RING OPEN by a halide. This would need to be followed by subsequent reactions before $[X\text{--}PPh_3]^+$ could be formed.

The data presented in the preceding paragraphs provide definitive evidence from both UV-VIS and ^{31}P NMR spectroscopy that dppm bridge opening in $[PPh_3\text{--}PPh_3]^{2+}$ is a facile reaction. They reveal not only a mechanism by which $[Cl\text{--}PPh_3]^+$ is formed, but also, with the help of further data described below, provide a rare example of dissociative ligand substitution in four-coordinate, square planar complexes. This lends strong supporting evidence to the earlier contention that insertions of small molecules into the Pt-Pt bond of $[PPh_3\text{--}PPh_3]^{2+}$ occurs by prior and rate-limiting $Pt_2(\mu\text{-dppm})$ ring opening.

Pt-X bond formation by ion pair collapse With the identity of the product of the first stage of the $Pt_2(\mu\text{-dppm})$ ring opening pathway, RING OPEN, fairly well-substantiated, an in-depth discussion of the complexities in this stage is now appropriate. Important features of the first stage are its often rate-limiting unimolecular reactions and the marked sensitivity of its reactions to the anions present. Elementary reactions of importance in the proposed mechanism for this first stage are summarized in Scheme I-11.

The dramatic decrease in the rate of reaction of halides with $[PPh_3\text{--}PPh_3]^{2+}$ (e.g., Figure I-27) upon addition of innocent anions such as PF_6^- and ClO_4^- (IA^-) can be explained by

Scheme I-11 Reaction of $[Pt_2(\mu\text{-dppm})_2(PPh_3)_2]^{2+}$ with Halides

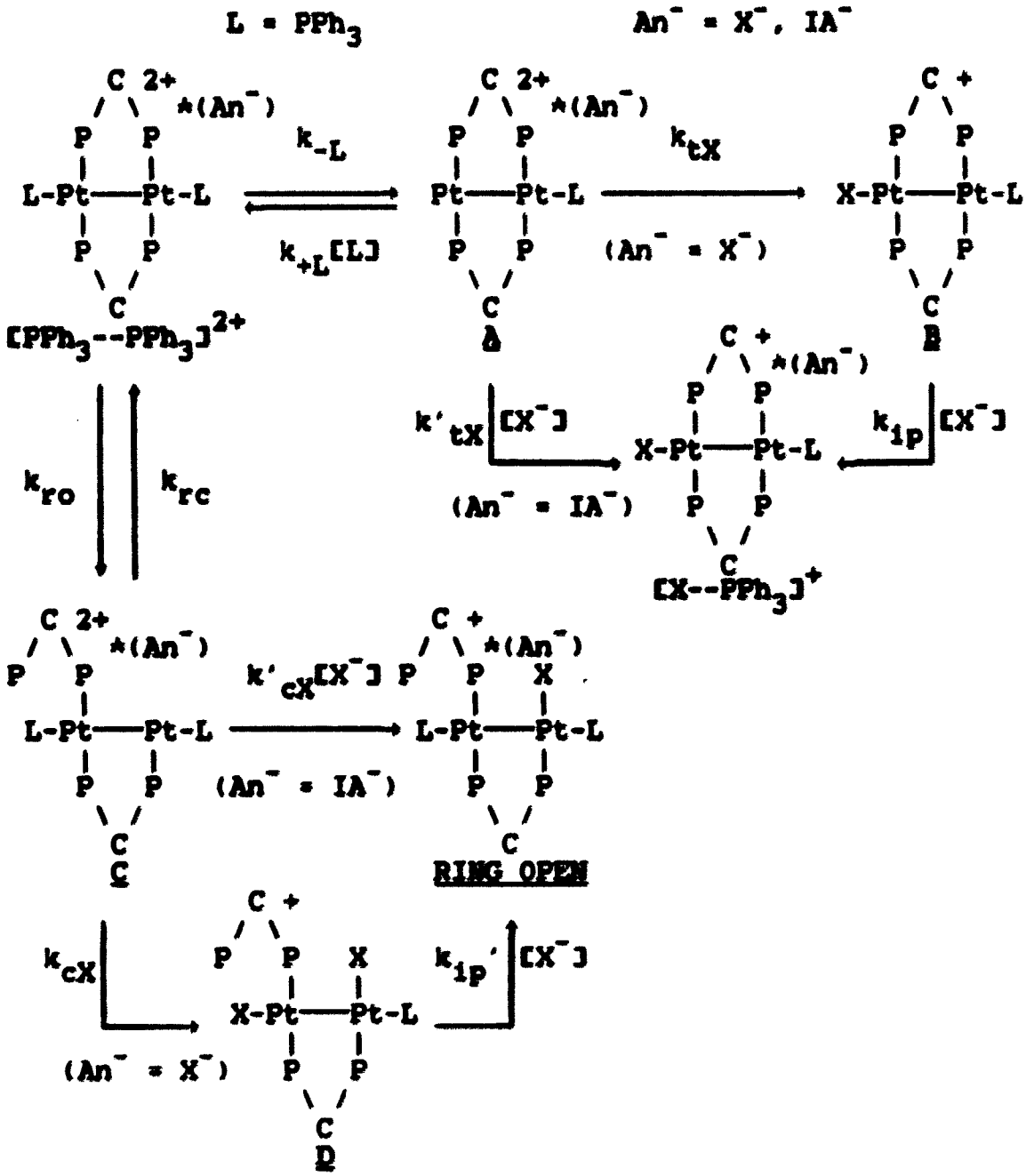

the mechanism in Scheme I-11. In the absence of IA^-, $[X\text{--}PPh_3]^+$ and RING OPEN are formed by the very rapid ion pair collapse of halides in the intermediates A and C into the inner coordination sphere vacancy created by Pt-P bond scission in $[PPh_3\text{--}PPh_3]^{2+}$. This ion pair collapse (i.e., k_{tX} and k_{cX} in Scheme I-11) yields the positively charged products, B and D, which are assumed to be in rapid equilibrium with their respective uncharged ion pairs, $[X\text{--}PPh_3]^+$ and RING OPEN. When the counter-ions of A and C are innocent anions, product formation can only occur by attack of halides from the bulk solvent (i.e., k'_{tX} and k'_{cX}). This, in and of itself, would be less probable relative to ion pair collapse but is even less favorable relative to the latter because: (a) the species attacked (e.g., A where $An^- = ClO_4^-$) has a smaller positive charge than is seen by the ion paired halide in A where $An^- = X^-$, and (b) the bulky IA^-, most certainly positioned near the positively charged Pt centers, will cause greater steric congestion at this site of halide attack.

The rate of $[PPh_3\text{--}PPh_3]^{2+}$ loss in the absence of IA^- can be represented as:

$$-d\left[[PPh_3\text{--}PPh_3]^{2+}\right]/dt = k_{tX}[A^*X] + k_{cX}[B^*X] \qquad (14)$$

If A and B are treated as steady state intermediates, and where needed, pseudo-first order excesses of X^- and PPh_3 are assumed, the apparent pseudo-first order rate constant k_{obs}

can be represented as:

$$k_{obs} = \frac{k_{-L}}{\left(\frac{k_{+L}[L]}{k_{tX}}\right) + 1} + \frac{k_{ro}}{\left(\frac{k_{rc}}{k_{cX}}\right) + 1} \qquad (15)$$

where L = PPh_3. The first and second terms in equation 15 represent respective PPh_3 dissociation and ring opening pathways. In all kinetic measurements, including those at very low $[X^-]$ (e.g., $[Br^-]$ = 0.02 mM in Table I-17), the observed rate constants were independent of halide concentration as predicted by this mechanism (see Table I-17; the concentration of innocent ion in solution (PF_6^-) is minimal when compared to that of X^-, i.e., $[IA^-] = 2[PPh_3\text{--}PPh_3]^{2+}]$). Kinetic measurements were not made as a function of $[PPh_3]$ in the absence of IA^-, however RING OPEN : $[Cl\text{--}PPh_3]^+$ product ratios do not vary significantly as a function of $[PPh_3]$ (e.g., Figure I-32) suggesting that PPh_3 dissociation is unimportant relative to ring opening under these conditions.

Although the reactions summarized in Table I-17 are independent of the concentration of halide added, they are not independent of the nature of the halide. The values of k_{obs} for Cl^- and Br^- are comparable, while the value for I^- is an order of magnitude smaller. It seems unlikely that this large discrepancy in k_{obs} is due to the fact that Cl^- and Br^- were added to the reaction as Et_4N^+ salts whereas I^- was added as $[(n\text{-butyl})_4N]I$; although this has not been explicitly

Table I-17. Reactions of X^- with $[Pt_2(\mu\text{-dppm})_2(PPh_3)_2]^{2+}$ in CH_2Cl_2 at 10 °C[a]

Halide(s)	$[X^-]$/mM		k_{obs}/s^{-1}[b]	#[c]
Br	0.2		1.95(5)	6
Br	0.5		1.90(5)	5
Br	10		2.1(1)	8
Br	50		1.76(9)	8
		Ave:	1.9(1)	
I	1		0.26(1)	8
I	2		0.25(2)	6
I	10		0.25(1)	8
		Ave:	0.25(2)	
Cl	0.2		1.43(7)	3
Cl	1		2.6(2)	3
Cl	4		1.3(2)	4
		Ave:	1.8(7)	
Cl,I	1.2,1.2		0.23(3)	5
Br,I	1.2,1.2		0.43(4)	8

[a] $[PPh_3\text{--}PPh_3]^{2+}$ = 0.02 mM, followed at 365 nm except for X^- = Br^- (370 nm) using the stopped flow technique; no ClO_4^- added.

[b] Number in parentheses is the error in the last digit.

[c] # = number of repetitions.

investigated, 0.2 mM bromide reactions in the presence of 20 mM $[Et_4N]PF_6$ are two fold slower than similar reactions in the presence of 20 mM $[(n\text{-butyl})_4N]ClO_4$ (see Table I-18 on page 145). Two additional possibilities exist: (a) If the values for k_{tX} and k_{cX} are sufficiently small so that the denominators in equation 15 are much larger than unity, the observed rate constant (k_{obs}) will vary with the identity of the halide and with their respective values for k_{tX} and k_{cX}. (b) Alternatively, the rate of Pt-P bond heterolysis may vary with the identity of the $[PPh_3\text{--}PPh_3]^{2+}\star(X^-)$ ion pair. The former seems less likely since ion pair collapse should be a very efficient process (i.e., the denominators in equation 15 should be close to unity).

The mixed halide reactions provide additional proof for the existence of the ion pair collapse mechanism: When comparable concentrations of Cl^- and I^- are allowed to react with $[PPh_3\text{--}PPh_3]^{2+}$, UV-VIS spectroscopy suggests I^- and not Cl^- reactions occur, contrary to their separate rates. Thus, the reaction products incorporate I^- not Cl^- (see Figure I-35), and do so with a k_{obs} ($0.23 \pm 0.03\ s^{-1}$) very close to the I^- value ($0.25 \pm 0.02\ s^{-1}$) but distinctly smaller than the Cl^- value ($1.8 \pm 0.7\ s^{-1}$). One would normally expect a predominance in chloride products and an observed rate constant near $1.8\ s^{-1}$, because the k_{obs} for Cl^- is 8-fold larger than that of I^-. Similarly, when equimolar concentrations of Br^- and I^-

are used, I^- products predominate again and the rate constant is 0.43 ± 0.04 s^{-1} which is still much smaller than the Br^- value of 1.9 ± 0.1 s-1 (see Figure I-36). Apparently, the $[PPh_3--PPh_3]^{2+}$-iodide ion pair formation constants are much larger than those involving Br^- and especially Cl^-; thus, $[PPh_3--PPh_3]^{2+}*(I^-)_n$ are the predominant reactant species in solution yielding, upon ion pair collapse, the observed results. The relative size of the respective ion pairing constants (K_{ip} in equation 8) may be estimated from these two experiments:

$$24K_{Cl} \leq 8K_{Br} = K_I$$

When $[PPh_3--PPh_3]^{2+}$ is ion paired with ClO_4^- (described in detail below), halide incorporation must occur by a method much less efficient than ion pair collapse. Rate constants for halide incorporation in the presence of ClO_4^- are much smaller (Figure I-37).

Competition between ring opening and PPh_3 dissociation

In the presence of IA^-, the observed rate constant takes a slightly different form than that found in equation 15:

$$k_{obs} = \frac{k_{-L}}{\left(\frac{k_{+L}[L]}{k'_{tx}[X^-]}\right) + 1} + \frac{k_{ro}}{\left(\frac{k_{rc}}{k'_{cx}[X^-]}\right) + 1} \qquad (16)$$

Again, the first and second terms represent respective PPh_3

Figure I-35. UV-VIS spectra (2 cm path length) of the initial products of the reactions of 0.02 mM $[Pt_2(\mu\text{-dppm})_2(PPh_3)_2]^{2+}$ at 10 °C in CH_2Cl_2 with:

--- 1.2 mM $[Et_4N]Cl$

··· 1.2 mM $[Et_4N]Cl$ and 1.2 mM $[(n\text{-butyl})_4N]I$ and

—— 1.2 mM $[(n\text{-butyl})_4N]I$; the spectra of the mixed halide experiment shows that I^- products predominate, in fact the shoulder at 385 nm due to Cl^- products is more than likely caused by the onset of secondary reactions which favor the formation of Cl^- products over those of I^-

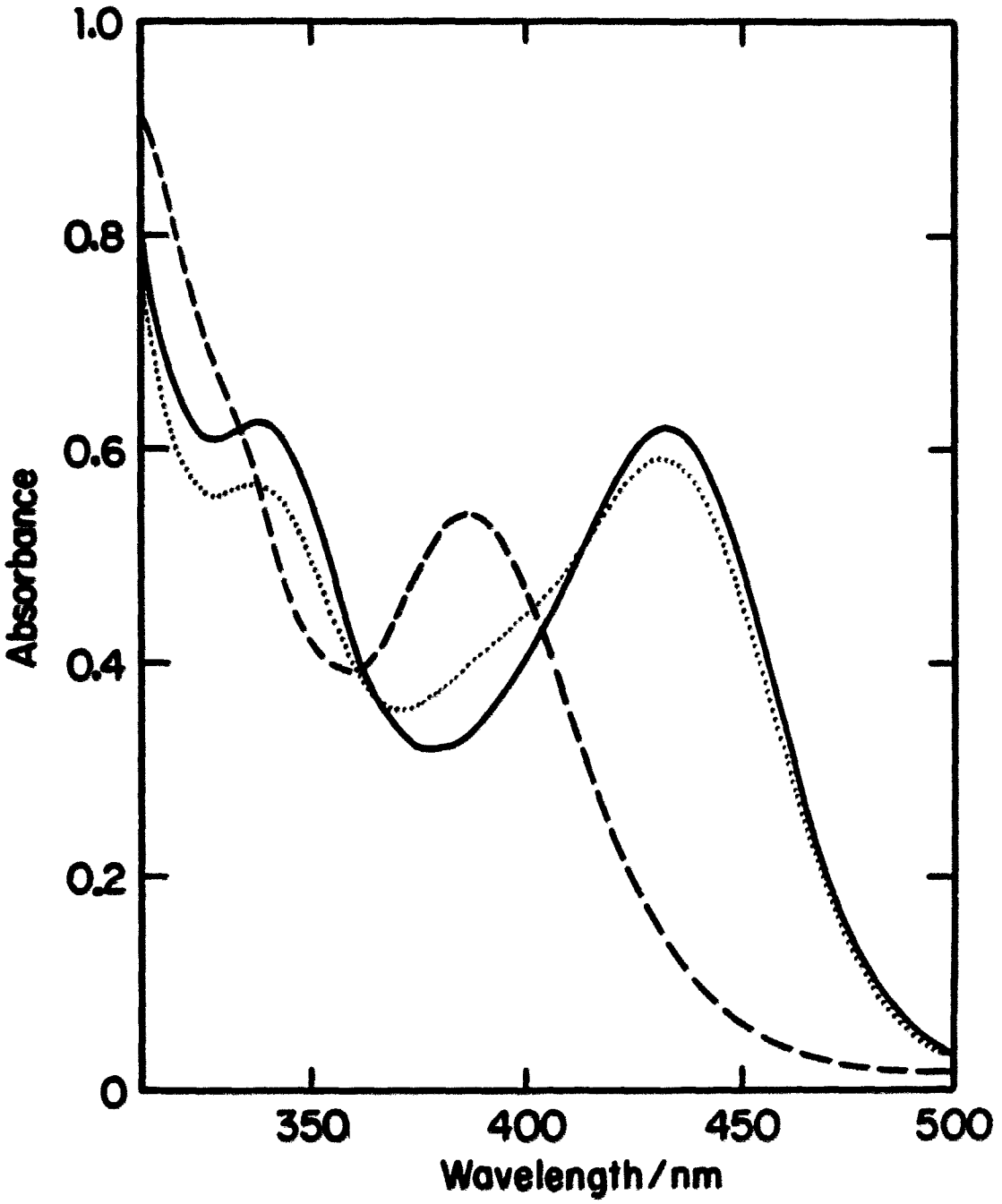
1.0
0.8
0.6
0.4
0.2
0
Absorbance
350
400
450
500
Wavelength / nm

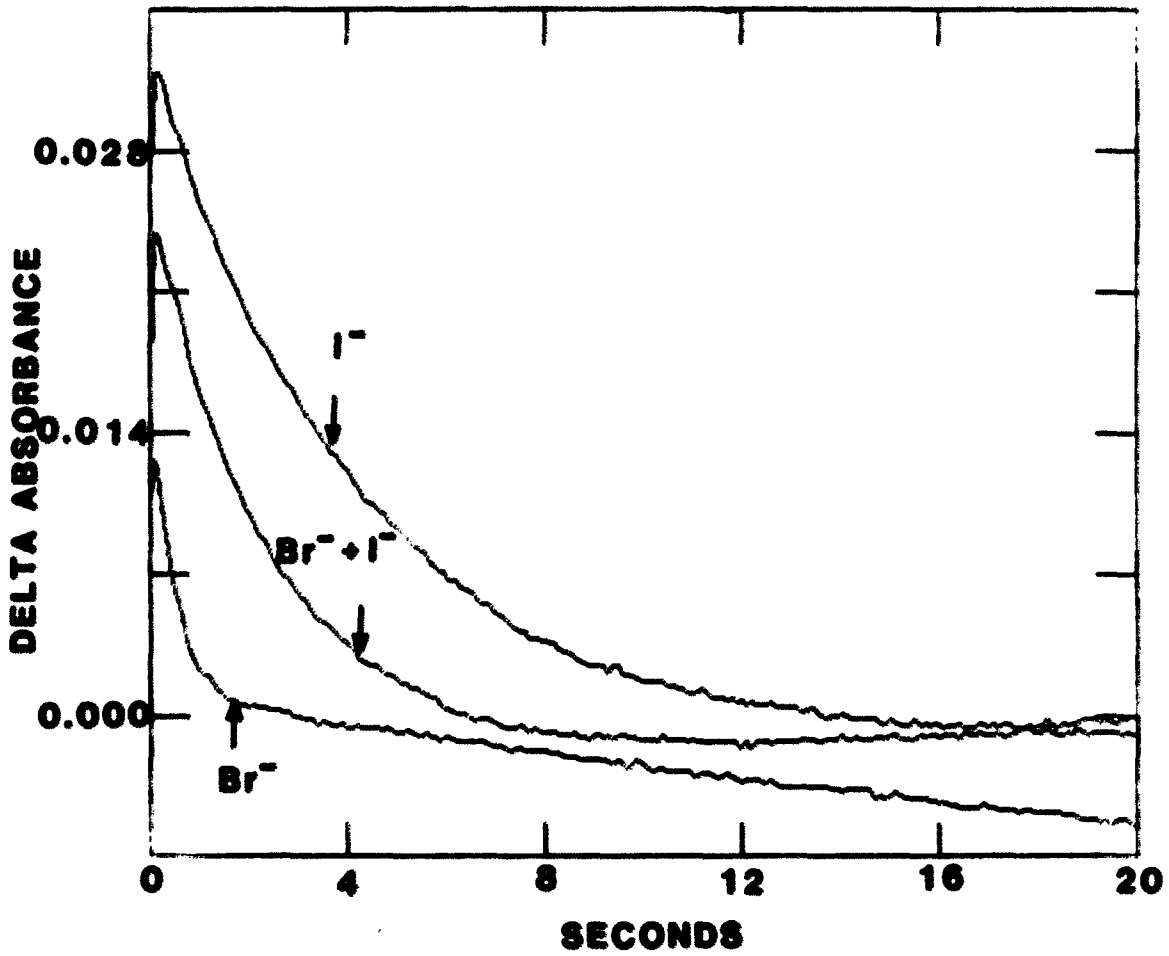

Figure I-36. Absorbance vs. time traces obtained by the stopped-flow technique for the reaction of 0.02 mM $[Pt_2(\mu\text{-dppm})_2(PPh_3)_2]^{2+}$ at 10 °C in CH_2Cl_2 with 1 mM $[(n\text{-butyl})_4N]I$ (followed at 365 nm; top trace), with 1.2 mM $[(n\text{-butyl})_4N]I$ and 1.2 mM $[Et_4N]Br$ (365 nm; middle trace), and 0.2 mM $[Et_4N]Br$ (370 nm; bottom trace)

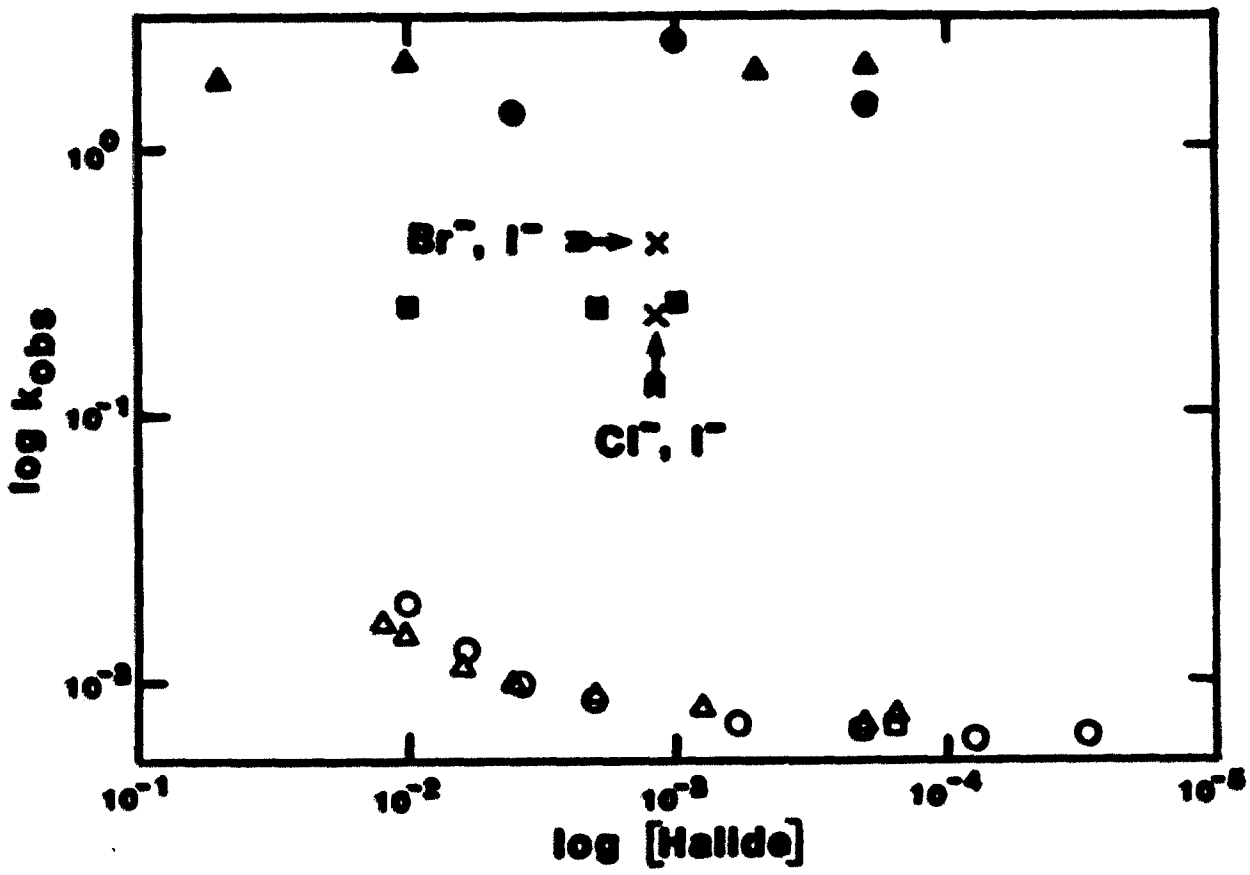

Figure I-37. Log k_{obs} vs. log $[X^-]$ for the reactions of 0.02 mM $[Pt_2(\mu\text{-dppm})_2(PPh_3)_2]^{2+}$ with halides at 10 °C in CH_2Cl_2: o = Cl^-, Δ = Br^-, □ = I^-; solid symbols = no added ClO_4^-; open symbols = 20 mM $[(n\text{-butyl})_4N]ClO_4$ added; X = 1.2 mM each of the respective halides added

dissociation and ring opening pathways. Under most conditions, the kinetic data fit one or another of the following simplified forms of this equation:

$$k_{obs} = k_{-L} + k_{ro} \tag{16a}$$

$$k_{obs} = k_{-L} + \frac{k_{ro}k'_{cx}[X^-]}{k_{rc}} \tag{16b}$$

$$k_{obs} = \frac{k_{-L}}{\left(\frac{k_{+L}[L]}{k'_{tx}[X^-]}\right) + 1} \tag{16c}$$

$$k_{obs} = \frac{k_{-L}}{\left(\frac{k_{+L}[L]}{k'_{tx}[X^-]}\right)} + \frac{k_{ro}}{\left(\frac{k_{rc}}{k'_{cx}[X^-]}\right)} \tag{16d}$$

Evidence for these limiting forms and the conditions under which a given form is observed will now be discussed.

The 16a limit: Under conditions where k'_{tx} and k'_{cx} are so large that the denominators of both terms of the general expression (equation 16) are nearly unity (i.e., high $[X^-]$ and low $[PPh_3]$), the apparent rate constant is simplified to

$$k_{obs} = k_{-L} + k_{ro} \tag{16a}$$

This limit was not reached even at $[X^-] = 10$ mM. At halide concentrations higher than this, sufficient concentrations of

the $[PPh_3\text{--}PPh_3]^{2+}\star X^-$ ion pair would be present ($[IA^-]$ = 20 mM) so that ion pair collapse would start to become important.

The 16b limit: Under conditions of low to moderate halide concentrations and in the absence of added $[PPh_3]$, equation 16 simplifies to:

$$k_{obs} = k_{-L} + \frac{k_{ro}k'_{cx}[X^-]}{k_{rc}} \qquad (16b)$$

The ring opening reaction shows a halide dependence whereas PPh_3 dissociation remains halide independent. This is nicely illustrated when k_{obs} is plotted versus $[X^-]$ (Figure I-38). The intercept is indeed halide-independent with k_{-L} =(6.36 ± 0.16) x 10^{-3} s^{-1} for $[PPh_3\text{--}PPh_3]^{2+}\star(ClO_4^-)$. Again k_{-L} depends on the identity of the counter ion. The reaction of 0.2 mM Br^- with 0.02 mM $[PPh_3\text{--}PPh_3]^{2+}$ in the presence of 20 mM PF_6^- yielded a k_{obs} of 3.7 x 10^{-3} s^{-1} (see Table I-18), a value that should be very close to $k_{-L}(PF_6^-)$. The slopes ($m = k_{ro}k'_{cX}/k_{rc}$) in Figure I-38 are of course dependent on the nature of the halide with m_{Cl} = 1.22 ± 0.06 $M^{-1}s^{-1}$, and m_{Br} = 0.85 ± 0.04 $M^{-1}s^{-1}$. This scheme predicts that as $[X^-]$ increases, there should be an increased yield of products from the $Pt_2(\mu\text{-dppm})$ ring opening pathway. This expectation can be verified directly by the increase in absorbance noted at the CHELATE absorbance maximum with increasing $[X^-]$ (see Table I-18).

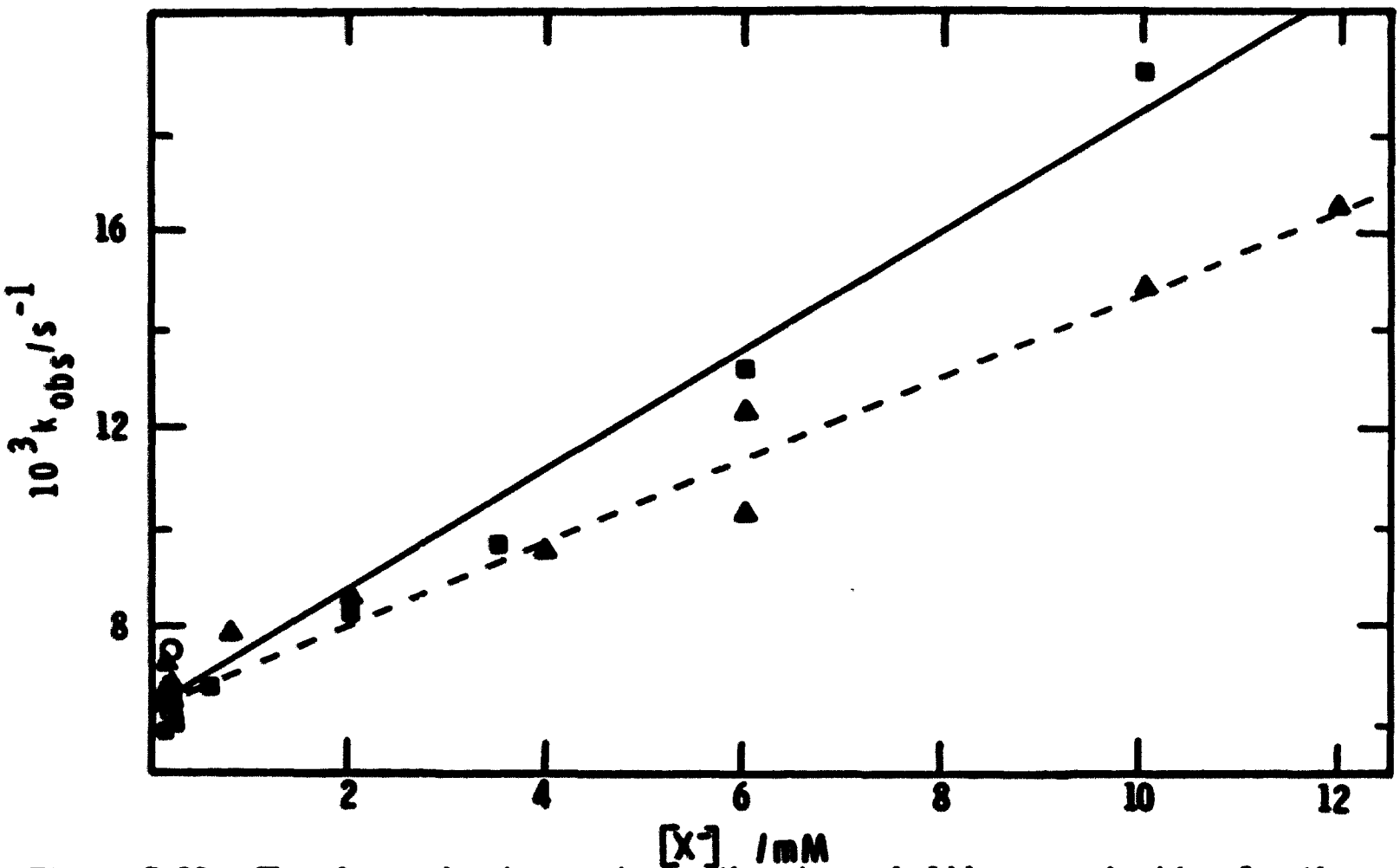

Figure I-38. The observed rate constants (k_{obs}) vs. halide concentration for the reactions of halides with $[Pt_2(\mu\text{-dppm})_2(PPh_3)_2]^{2+}$ in the presence of 20 mM $[(n\text{-butyl})_4N]ClO_4$ at 10 °C in CH_2Cl_2: ■ = Cl^-, ▲ = Br^-, and o = I^-

Table I-18. Reactions of $[PPh_3\text{--}PPh_3]^{2+}$ with halides at a 20 mM total salt concentration[a]

Halide	[Halide]/mM	$10^3 k_{obs}/s^{-1}$[b]	Abs_∞[c]
Cl^-	0.03	6.4	0.21
Cl^-	0.08	6.0	0.20
Cl^-	0.20	6.4(3)	0.22(1)
Cl^-	0.60	6.8	0.22
Cl^-	2.0	8.3	0.24
Cl^-	3.5	9.7	0.27
Cl^-	6.0	13.2	0.29
Cl^-	10.0	19.3	0.33
Cl^-[d]	0.2	1430.(70)	0.43
Br^-[e]	0.20	3.7	0.16
Br^-	0.15	7.3	0.18
Br^-	0.20	6.7(6)	0.17(2)
Br^-	0.80	7.9	0.21
Br^-	2.0	8.6	0.23
Br^-	4.0	9.5	0.24
Br^-	6.0	11.(1)	0.22(3)
Br^-	10.0	14.9	0.28
Br^-	12.0	16.6	0.31
Br^-[d]	0.20	1950.(50)	0.42(2)
I^-	0.15	6.4	0.15
I^-	0.20	6.9(9)	0.16(1)
I^-[d]	0.10	260.(10)	
I^-[d]	0.20		0.30(2)

[a]Reactions were run at 10 °C, 0.02 mM $[PPh_3\text{--}PPh_3]^{2+}$ and followed at 347 nm (Cl^- and Br^-) and 400 nm (I^-) using $(n\text{-butyl})_4N(ClO_4)$ to balance the total salt concentration.

[b]Numbers in parentheses are standard deviations of replicate measurements.

[c]Abs_∞ at 384 nm (Cl^-), 396 nm (Br^-), and 428 nm (I^-).

[d]Reactions in which ClO_4^- was not added.

[e]Et_4NPF_6 added instead of the perchlorate salt.

The above results suggest why yields of chloro-CHELATE were so low when the reaction of Cl^- with $[PPh_3--PPh_3]^{2+}$ was carried out in concentrated (10 mM) solutions solutions for NMR measurements: The extent of ion pairing in CD_2Cl_2 increases greatly with total salt concentration, and the ion pairing constant for PF_6^- with $[PPh_3--PPh_3]^{2+}$ could very well be higher than that for Cl^-. In other words, preferential ion pairing of PF_6^- over Cl^- at high total salt concentration inhibits halide incorporation by ion pair collapse, the reaction type which appears to favor $Pt_2(\mu\text{-dppm})$ ring opening products. Indeed, much higher yields of CHELATE (relative to $[X--PPh_3]^+$) result when $X = I^-$, a halide which has been shown to have an ion pair formation constant with $[PPh_3--PPh_3]^{2+}$ at least 25 times larger than that for Cl^- (e.g., Figure I-35).

The 16c limit: As shown in the 16b limit, the contribution of the ring opening term to k_{obs} is negligible at very low $[X^-]$ in the presence of 20 mM ClO_4^- (i.e., $[X^-] < 0.4$ mM). If PPh_3 is added to reaction solutions while keeping $[Cl^-]$ very low, equation 16 can be simplified as follows:

$$k_{obs} = \frac{k_{-L}}{\left(\frac{k_{+L}[L]}{k'_{tCl}[Cl^-]}\right) + 1} \qquad (16c)$$

The observed rate constant decreases with increasing $[PPh_3]$ such that k_{obs}^{-1} plotted versus $[PPh_3]/[Cl^-]$ is linear (see

Figure I-39) with a slope of $k_{+L}/k_{-L}k'_{tCl}$ and an intercept of k_{-L}^{-1}. The value of k_{-L} calculated from this plot (6.0 ± 1.6) x 10^{-3} s^{-1}) is within experimental error of its known value, $6.36 \pm 0.16 \times 10^{-3}$ s^{-1}. From the slope and the known value of k_{-L}, a value of $k_{+L}/k_{tCl} = 3.97 \pm 0.16 \times 10^{-2}$ is calculated. A compilation of these kinetic data is found in Table I-19.

The 16d limit: When $[PPh_3]$ becomes larger yet and $[Cl^-]$ is kept small and constant (ClO_4^- added), a final simplication of equation 16 can be observed:

$$k_{obs} = \frac{k_{-L}}{\left(\frac{k_{+L}[L]}{k'_{tX}[Cl^-]}\right)} + \frac{k_{ro}}{\left(\frac{k_{rc}}{k'_{cX}[Cl^-]}\right)} \qquad (16d)$$

A plot of k_{obs} against $[PPh_3]^{-1}$ ($[PPh_3]$ = 20 - 90 mM, $[Cl^-]$ = 0.2 mM) is linear (see Figure I-40). From the slope, a value for k_{+L}/k'_{tCl} is obtained (0.052 ± 0.002) which is barely within the limit of 3σ of that obtained in the 16c limit of 0.0397 ± 0.0016. The value of $k_{ro}k'_{cCl}/k_{rc} = 0.42 \pm 0.16$ $M^{-1}s^{-1}$ calculated from the intercept is three times smaller than the 1.22 ± 0.06 $M^{-1}s^{-1}$ calculated from the 16b limit. Perhaps insufficient data are present to calculate these values accurately or perhaps the $Pt_2(\mu\text{-dppm})$ ring opening term is also inversely dependent on $[PPh_3]$. No PPh_3 inhibition of k_{obs} was observed in the small molecule insertion reactions of $[PPh_3\text{--}PPh_3]^{2+}$.[20] The fact that data at high $[PPh_3]$ fit the

16c and 16d forms of equation 16 is very good evidence for PPh_3 dissociation in $[PPh_3\text{--}PPh_3]^{2+}$.

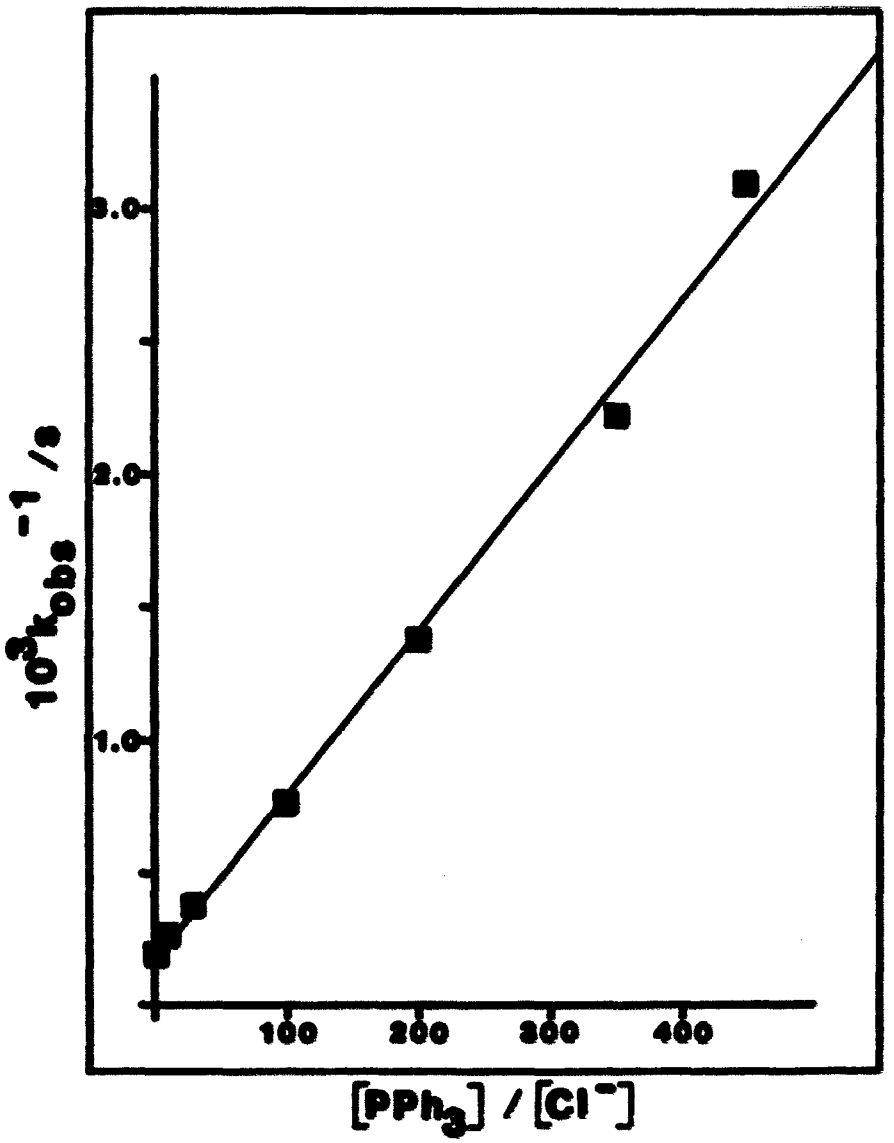

Figure I-39. Reactions of 0.02 mM $[Pt_2(\mu\text{-dppm})_2(PPh_3)_2]^{2+}$ with 0.2 mM $[Et_4N]Cl$ in the presence of 20 mM $[(n\text{-butyl})_4N]ClO_4$ and added PPh_3 at 10 °C in CH_2Cl_2 represented as k_{obs}^{-1} vs. $[PPh_3]/[Cl^-]$

Table I-19. Reaction of chloride with $[Pt_2(\mu\text{-dppm})_2(PPh_3)_2]^{2+}$ with added PPh_3 and constant $[Cl^-]$ and [Salt][a]

$[PPh_3]$/mM	$10^3 k_{obs}/s^{-1}$
0.20	5.32
2.0	3.81
6.0	2.67
20.	1.30
40.	0.73
70.	0.45
90.	0.32

[a]Reactions run at 10 °C with $[Cl^-]$ = 0.2 mM, $[PPh_3\text{--}PPh_3]^{2+}$ = 0.02 mM, and $[Salt]_{tot}$ = 20 mM using $[(n\text{-butyl})_4N]ClO_4$.

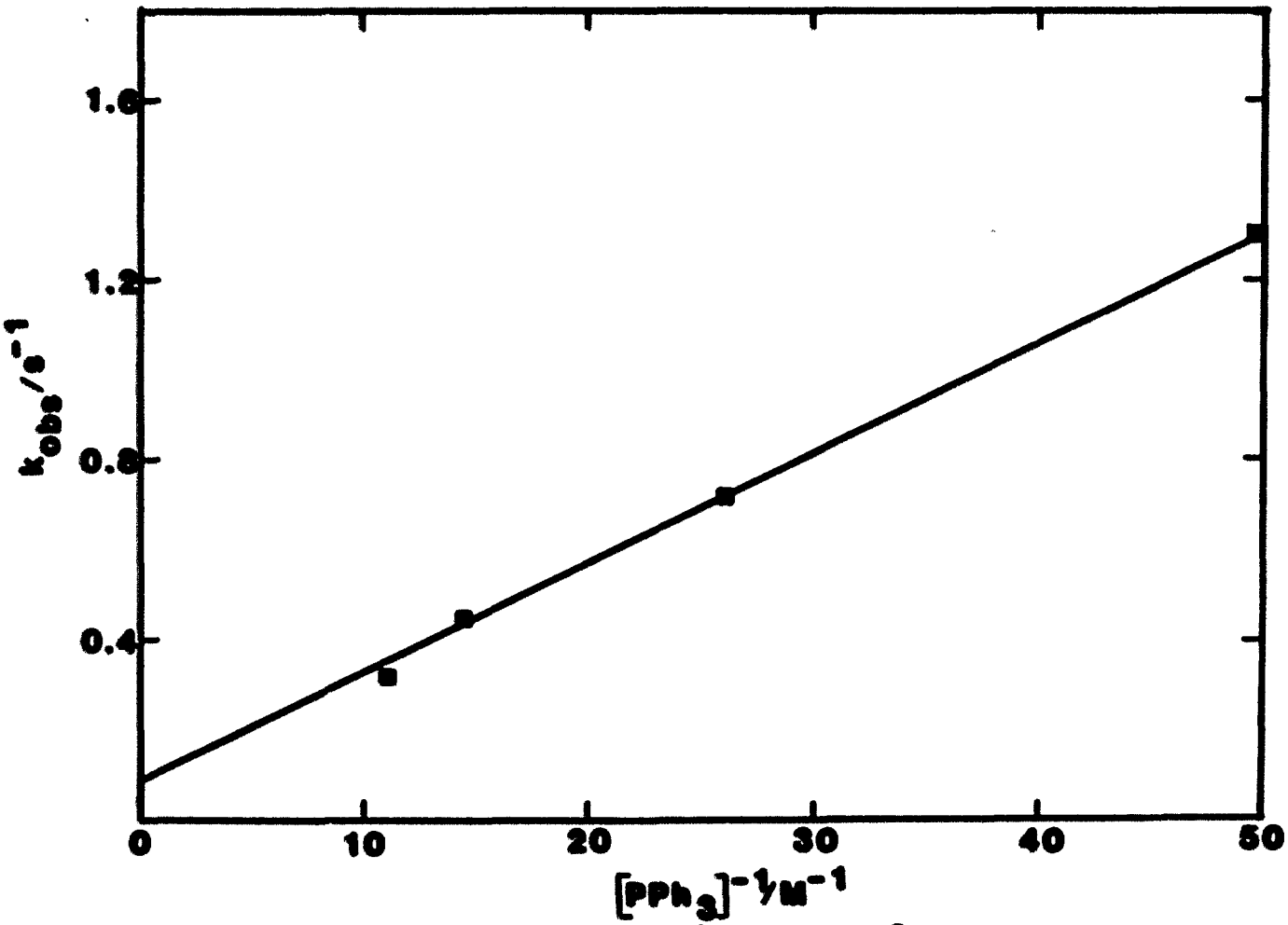

Figure I-40. Reactions of 0.02 mM $[Pt_2(\mu\text{-dppm})_2(PPh_3)_2]^{2+}$ with 0.2 mM $[Et_4N]Cl$ in the presence of 20 mM $[(n\text{-butyl})_4N]ClO_4$ and added PPh_3 (greater than 20 mM) at 10 °C in CH_2Cl_2 represented as k_{obs} vs. $[PPh_3]^{-1}$

CONCLUSIONS

The above mechanistic data dealing with ligand substitution parallel similar data from small molecule insertion reactions in Pt(I) dimers on two important points: 1. modes of reaction in Pt(I) dimers are often determined by steric factors, and 2. $Pt_2(\mu\text{-dppm})$ ring opening and the concurrent formation of a coordinatively unsaturated platinum center is an important reaction pathway in sterically encumbered complexes.

Although the small molecule insertion reactions of $[Cl\text{--}PPh_3]^+$ have not been studied, insertion is predicted to occur in an associative manner. The platinum bound to Cl^- is fairly accessible to reagent attack. Thus, dissociative processes are predicted to be much less important in $[Cl\text{--}PPh_3]^+$ than they are in $[PPh_3\text{--}PPh_3]^{2+}$.

It should be noted that the rates of small molecule insertion into $[PPh_3\text{--}PPh_3]^{2+}$ are <u>independent</u> of $[PPh_3]$ even at very high concentrations (i.e., they occur by rate limiting $Pt_2(\mu\text{-dppm})$ ring opening) whereas ligand substitution rates of the same complex are <u>retarded</u> by PPh_3 under conditions (i.e., in the presence of IA^- at low $[X^-]$) <u>where the triphenylphosphine dissociation pathway predominates.</u> These observations can be explained by one or both of the following hypotheses: 1. Small molecule insertion can occur only when ligand dissociation occurs cis to the Pt-Pt bond. 2. The first order

rate constant for $Pt_2(\mu\text{-dppm})$ ring opening (k_{ro}) is so much larger than that for PPh_3 dissociation (k_{-L}) that adding large concentrations of $[PPh_3]$ will have a minimal effect on k_{obs} in the absence of high concentrations of inert salts. Evidence suggests that at least the second effect is operative. Yields of $Pt_2(\mu\text{-dppm})$ ring opening products do not appear to vary significantly with $[PPh_3]$ in the reaction of iodide with $[PPh_3\text{--}PPh_3]^{2+}$ when no IA^- is added (see Figure I-32), i.e., the same conditions that small molecule insertions were studied as a function of $[PPh_3]$. If k_{-L} were an important component of these iodide reactions, the absorbance observed at 428 nm in the first spectral scan of each series of scans found in Figure I-32a-d should become higher with increasing $[PPh_3]$ due to increased yields of the higher absorbing RING OPEN relative to $[I\text{--}PPh_3]^+$. In addition, values for k_{-L} and k_{ro} support the insignificance of k_{-L} compared to k_{ro}. For example, k_{-L} for the perchlorate ion pair of $[PPh_3\text{--}PPh_3]^{2+}$ is 6.36×10^{-3} s^{-1} whereas k_{ro} is greater than 0.02 s^{-1} (see Table I-18). Why k_{ro} is so much greater than k_{-L} is not known, especially since the Pt-PPh_3 bonds are predicted to be so much weaker than the Pt-dppm bonds in $[PPh_3\text{--}PPh_3]^{2+}$ on grounds of the trans influence. One must always remember that the trans influence is a measure of bond strength and not necessarily ligand lability.

The reaction of Cl^- with $[PPh_3\text{--}PPh_3]^{2+}$ forming

$[Cl{-}{-}PPh_3]^+$ appears to be essentially irreversible in CH_2Cl_2. However, $[PPh_3{-}{-}PPh_3]^{2+}$ is formed from [Cl--Cl] and PPh_3 in methanol. Obviously, solvent polarity is one factor determining the relative stability of the three complexes. The relative platinum-ligand bond strengths are also a factor. The equilibrium between [Cl--Cl] and $[Cl{-}{-}PPh_3]^+$ in CH_2Cl_2 lies toward $[Cl{-}{-}PPh_3]^+$ presumably because Pt-P bonds are normally stronger than Pt-Cl bonds. On the other hand, the equilibrium between [Cl--Cl] and $[Cl{-}{-}P(o\text{-}Tol)_3]^+$ lies toward [Cl--Cl]. Apparently, this Pt-P_T bond is weaker than the Pt-PPh_3 bond due to steric repulsions, and although it may still be stronger than a Pt-Cl bond, it is unable to compensate for the propensity of molecules to be neutrally charged in nonpolar media. These adverse charge effects and weaker Pt-P bonds favor $[Cl{-}{-}PPh_3]^+$ over $[PPh_3{-}{-}PPh_3]^{2+}$. Pt-P bonds in $[PPh_3{-}{-}PPh_3]^{2+}$ are weakened not only by increased steric repulsions but also by the greater trans influence of PPh_3 compared to Cl^-.

One point brought out by this research is the importance outer-sphere coordination of anions plays in the chemistry of Pt(I) dimers in nonpolar solvents especially. Kinetic parameters can vary by more than a factor of ten depending on the nature of the anion. This is the case not only with charged species but even with the neutral [Cl--Cl]. Ion pairing effects on kinetic parameters have already been reported for Pt(I) dimers.[20] The first order rate constant $k_{ro}(ClO_4^-)$ at

25 ^{o}C (determined from insertion reactions of $[PPh_3--PPh_3]^{2+}$ $(ClO_4)^-$) is 0.06 s^{-1} whereas $k_{ro}(PF_6^-)$ is 0.027 s^{-1}. A similar trend in k_{-L} was found in this work ($k_{-L}(ClO_4^-)$ = 0.00636 s^{-1} and $k_{-L}(PF_6^-)$ = 0.0037 s^{-1} at 10 ^{o}C). An understanding of these ion pairing effects will allow fine-tuning of potential Pt(I) dimer based catalysts that otherwise may not be acheived. Ion pairing effects on transition metal carbonyl anions are well known.[59]

Our major research thrust represented in this thesis is in the area of reaction mechanisms. In addition, this thesis reports results in platinum coordination chemistry concerning molecular conformations and the use of Pt-P coupling constants as measures of metal-metal and metal-ligand bond strengths.

EXPERIMENTAL

Materials

Solvents

Most solvents (methylene chloride, methanol, benzene, chloroform, and acetone) were used as purchased. However, for use particularly in the kinetic studies of the reactions of $[PPh_3{-}{-}PPh_3]^{2+}$ with halides, five parts methylene chloride were treated with two parts sulfuric acid, washed twice with 5 % aqueous sodium carbonate, washed four times with water, and dried over $CaCl_2$ before use. Before using 1,2-dichloroethane as a solvent for kinetic measurements, it was stirred over sodium hydroxide pellets and then distilled over phosphorus pentoxide.

Methylene chloride-d_2 (99.5 % D) was used in obtaining NMR spectra at ambient and low temperatures. Tetrachloroethane-d_2 (98 % D; $C_2D_2Cl_2$) was used for the same purpose at high temperatures. Neither was further purified before use.

Reagents

The salts $[Et_4N]Cl$, $[Et_4N]Br$, $[Et_4N]PF_6$, were recrystallized from acetone-CH_2Cl_2-hexanes (2:2:1), methylene chloride-diethyl ether, and methylene chloride-hexanes, respectively. $[(n\text{-butyl})_4N]ClO_4$ was recrystallized from ethanol and purified $[(n\text{-butyl})_4N]I$ was donated by Dr. Makoto Shimura. NH_4PF_6 and dppm were used as purchased, whereas PPh_3 was either

recrystallized from ethanol or methylene chloride-hexanes.

$\underline{Pt_2(\mu\text{-dppm})_2L_2]^{n+}}$ $[Pt_2(\mu\text{-dppm})_2Cl_2]$ was synthesized from [Pt(cyclo-octadiene)Cl_2] in a series of three steps using the normal literature method.[5] It was characterized by $^{31}P\{^1H\}$ NMR (Figure I-1; page 16), ^1H NMR (Figure I-11; page 47), and UV-VIS (Figure I-9; page 43). $[Pt_2(\mu\text{-dppm})_2(PPh_3)_2](PF_6)_2$, synthesized from reaction of excess PPh_3 with [Cl--Cl] in methanol[6], was also characterized (e.g., $^{31}P\{^1H\}$ NMR spectrum in Figure I-3 on page 18 and UV-VIS spectrum in Figure I-9 on page 43).

$\underline{[Pt_2(\mu\text{-dppm})_2X(PR_3)]^+}$ $[Cl\text{--}PPh_3]^+$ was synthesized by the addition of 0.0448 g (0.170 mmol) of PPh_3 to a 5 ml CH_2Cl_2 solution containing 0.149 g (0.114 mmol) of [Cl--Cl]. After five minutes, 0.062 g (0.22 mmol) of $[Et_4N]PF_6$ were added and the resulting crude $[Pt_2(\mu\text{-dppm})_2Cl(PPh_3)](PF_6)$ was precipitated by the addition of pentanes. A column 7 mm in diameter containing approximately 4.5 g (dry weight) of Baker 60-200 mesh silica gel was prepared using CH_2Cl_2 as the solvent. A very concentrated solution of the crude product was then introduced on the column and eluted using CH_2Cl_2 until the resulting yellow band was 1/2 to 2/3 of the way down the column. A 9 acetone : 1 $CHCl_3$ mixture of solvents was then introduced in order to bring the band off the column in a concentrated form. The bright yellow solid obtained by addition of pentane to this solution contains no $[Et_4N]^+$ salts as

substantiated by ^{1}H NMR, and can be recrystallized yielding single crystals by slow evaporation of its CH_2Cl_2 : benzene solutions at 10 ^{o}C. This complex was characterized by $^{31}P\{^{1}H\}$ NMR (Figure I-2; page 17) as a nearly 1 to 1 mixture of two atropisomers (discussed on pages 58 to 80), the P-P coupling constants of which are found in Table I-20. $[Cl--PPh_3]^+$ was further characterized by its ^{1}H NMR (Figure I-11; page 47) and UV-VIS (Figure I-9; page 43) spectra and by X-ray crystallography (Figure I-6; page 34).

$[I--PPh_3]^+$ may be synthesized on a 10 to 40 mM scale by addition of excess PPh_3 to [I--I] in CH_2Cl_2, or by the addition of a ten fold excess of $[(n\text{-butyl})_4N]I$ to $[PPh_3--PPh_3]^{2+}$ in CH_2Cl_2 followed by allowing the resulting product solution to remain at room temperature for at least 2 hours. Attempts were not made to isolate this complex as a purified solid, but it should not be too difficult. Its ^{31}P NMR spectrum (Figure I-41) has resonances centered at 6.7 (P_T), 0.1 (P_A), and -6.6 (P_R) ppm, and also exists in two isomeric forms (see Table I-20 for P-P coupling constants).

$[Cl--dppm]^+$ was synthesized on a 10 to 40 mM scale by the addition of a slight excess of dppm to [Cl--Cl], was not isolated as a purified solid, but was characterized by ^{31}P NMR (Figure I-21; page 79) with resonances centered at -2.6 (P_T), 1.0 (P_A), -2.0 (P_R), and -29.5 (uncoordinated P) ppm. The spectrum suggests the presence of atropisomers although this

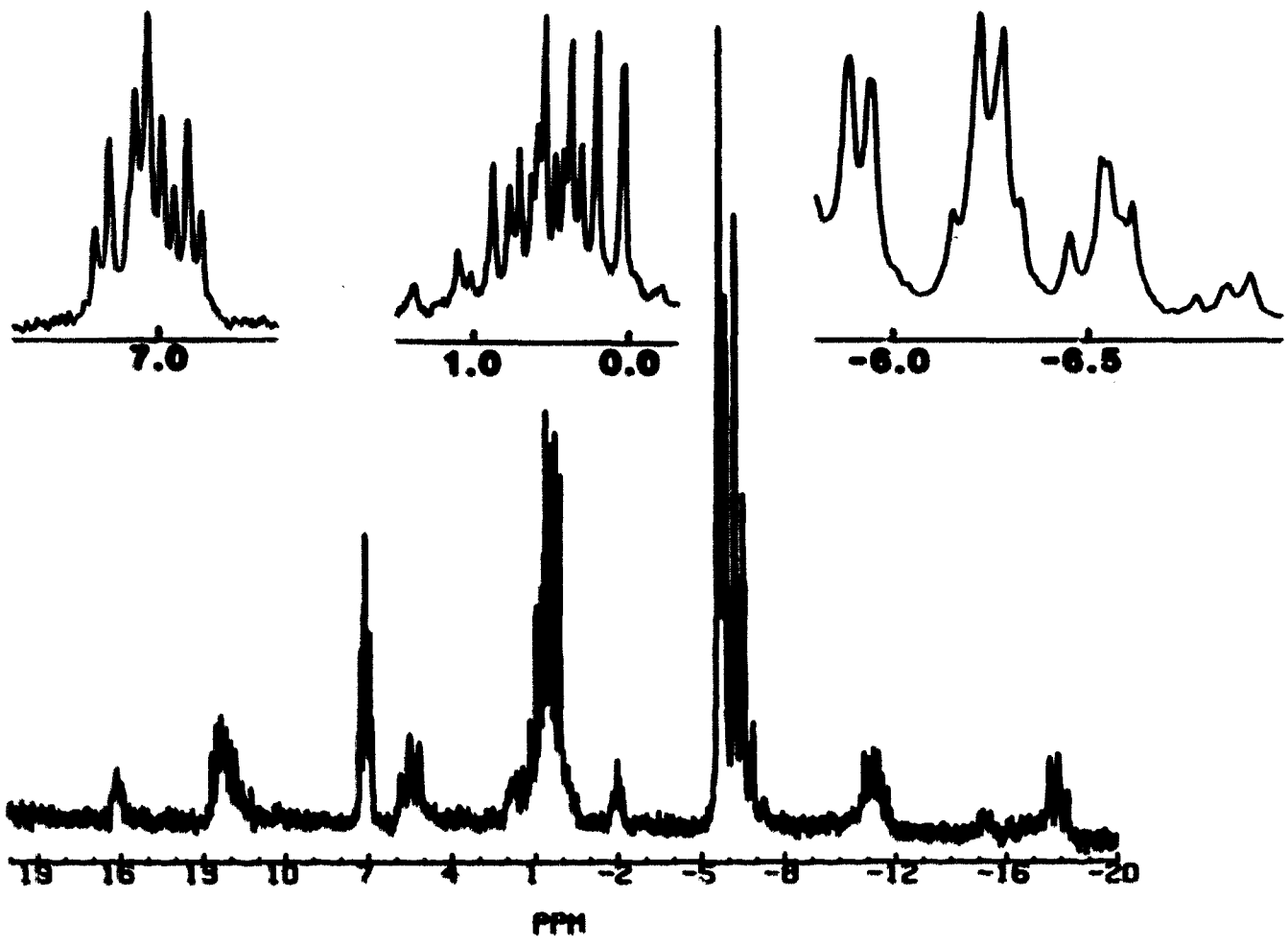

Figure I-41. The $^{31}P\{^{1}H\}$ NMR (121.5 MHz) of $[Pt_2(\mu\text{-dppm})_2I(PPh_3)]^+$ with insets showing the central resonances

Table I-20. ^{31}P NMR coupling constants in Hz for $[Pt_2(\mu\text{-dppm})_2X(PPh_3)]^+$ complexes[a] X = Cl^-, I^-

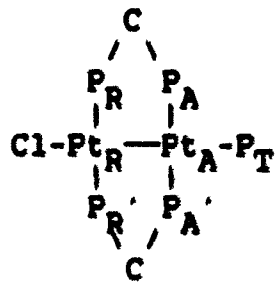

Coupling	$[Cl\text{--}PPh_3]^+$		$[I\text{--}PPh_3]^+$	
Constant	A	B	A	B
$^2J(P_A,P_R)$	48.7 (1.5)	41.8 (1.7)	39.6 (0.3)	40.4 (0.6)
$^3J(P_A,P_{R'})$	29.5 (1.2)	41.8 (1.7)	3I.4 (1.6)	40.4 (0.6)
$^2J(P_T,P_A)$	20.0 (0.7)	20.0 (0.7)	20.7 (0.3)	20.7 (0.3)
$^3J(P_T,P_R)$	8.8 (0.2)	8.8 (0.2)	7.3 (0.5)	7.3 (0.5)
$^1J(Pt_A,P_A)$	2876		2857	
$^1J(Pt_R,P_R)$	2894		2839	
$^1J(Pt_A,P_T)$	2186		2213	
$^2J(Pt_R,P_T)$	1232		1258	
$^2J(Pt_R,P_A)$	±142		--	
$^2J(Pt_A,P_R)$	±82		--	

[a]The J(P,P) for each atropisomer are found in the A and B columns; data for $[Cl\text{--}PPh_3]^+$ and $[I\text{--}PPh_3]^+$ are at 20 and -20 °C, respectively.

possibility was not pursued further.

$[Pt_2(\mu\text{-dppm})(\eta^2\text{-dppm})X(PPh_3)]^+$ Although not isolated, iodo-CHELATE was synthesized in solution in about 70 % yield by addition of a ten fold excess of $[(n\text{-butyl})_4N]I$ to a CH_2Cl_2 solution containing 16 mM $[PPh_3\text{--}PPh_3]^{2+}$. Chloro-CHELATE was synthesized under similar conditions with a yield no greater than 25 %. These thermally unstable complexes were characterized by $^{31}P\{^1H\}$ NMR (pages 106 to 117) and UV-VIS spectroscopy (Figure I-8b page 42).

Methods

Nuclear magnetic resonance spectroscopy

Routine ^1H NMR spectra were recorded using a Nicolet, NT-300 spectrometer in the FT mode, and variable temperature ^1H NMR measurements were obtained using the Bruker WM 300 spectrometer. All $^{31}P\{^1H\}$ NMR were recorded using the latter spectrometer operating at 121.5 MHz. Simulation of splitting patterns in $^{31}P\{^1H\}$ NMR spectra was accomplished using software (NIC-SIM) provided with the Nicolet NT-300 spectrometer.

Temperature control on the Bruker WM 300 spectrometer is self maintained above ambient temperature, in the temperature range between -20 and 20 ^oC it is maintained by a FTS Systems Inc. packaged air chiller, and below -20 ^oC, it is maintained by the controlled evaporation of liquid nitrogen.

Coalescence temperatures for peaks in ^1H NMR spectra of $[Cl\text{--}PPh_3]^+$ (Figures I-13 and I-14; pages 53 and 54) were

Table I-21. Parameters from the temperature dependent ^1H NMR (300 MHz) spectra of $[Pt_2(\mu\text{-dppm})_2X(PPh_3)]^+$

A/ppm[a]	B/ppm[a]	$\Delta\upsilon$/Hz[b]	k_{ex}/s^{-1}[c]	T_c/K
7.528	7.507	6.26	27.8	323
6.941	6.919	6.46	28.7	323
4.710	4.655	12.5	55.4	328
4.520	4.478	13.5	59.8	328
6.679	6.632	14.2	63.2	333
4.478	4.408	21.0	93.2	338
4.687	4.500	28.0	124.	338
6.929	6.655	81.8	364.	353
4.687	4.410	83.1	369.	358

[a]Positions of pairs of coalescing peaks at 20 °C.

[b]$\Delta\upsilon = \upsilon_A^0 - \upsilon_B^0$.

[c]Calculated using equation 17.

estimated via interpolation. Corresponding rate constants (k_{ex}) for the axial-equatorial positional exchange of substituents on the $Pt_2(\mu\text{-dppm})_2$ ring were calculated using:

$$k_{ex} = 2^{1/2}\pi(\upsilon_A^0 - \upsilon_B^0) \qquad (17)$$

where υ_A^0 and υ_B^0 are the frequencies in the slow exchange region of the two coalescing resonances. Assuming slow exchange at 20 °C (i.e., assigning υ_A^0 and υ_B^0 to peak positions in the ^1H NMR spectrum of $[Cl\text{--}PPh_3]^+$ at 20 °C) the data in Table I-21 were obtained and used to construct the plot of ln(k/T) vs. 1/T shown on page 55.

Ultraviolet-visible spectroscopy

UV-VIS spectra, single and multi-wavelength absorbance vs. time data were acquired using a Cary Model 219 recording spectrophotometer. Temperature control of ±0.1 °C was maintained using a Masterline Model 2800 refrigerated-heated bath and circulator (Forma Scientific) which was connected to a water-filled cell holder within the Cary 219 spectrophotometer. The fitting of data to linear and nonlinear equations was often accomplished with the assistance of an Apple II computer and appropriate software ("First Calc", a program in Pascal for analysis of first order kinetic data, and "NLLSQ" a more general program in BASIC for analysis of both linear and nonlinear equations).

Numerical data for kinetic analysis were collected by monitoring the absorbance at 347 nm versus time for the reactions of Cl^- and Br^- with $[PPh_3--PPh_3]^{2+}$, and at 400 nm for similar reactions of I^-. Determination of rate constants for chloride reactions in the presence of PPh_3 were hampered by the direct reaction of PPh_3 (or an impurity accompanying it) with $[PPh_3--PPh_3]^{2+}$. Rate constants for this minor reaction (normally 5 % of the total k_{obs}) were estimated using the method initial rates from abs. vs time data collected before addition of Cl^- to CH_2Cl_2 solutions already containing PPh_3 and $[PPh_3--PPh_3]^{2+}$. The rate constants for this minor reaction were then subtracted from the total k_{obs} before further analysis of the data.

Kinetics using the stopped-flow technique

Reactions too rapid for normal kinetic methods were often followed using a Canterbury Model SF-3A stopped-flow spectrometer interfaced with a OLIS 3820 Data System that was used for both data storage and analysis. Reactions of PPh_3 with [Cl--Cl] were monitored at 400 nm, and reactions of halides with $[PPh_3--PPh_3]^{2+}$ were monitored at either 365 or 370 nm. Analysis of kinetic data for the first stage of the halide reaction was hampered by the onset of the somewhat slower second stage. To avoid complications introduced by it, the first-stage constants were analyzed using the initial portion (3 to 5 half lives) and "floated" infinity absorbances.

X-ray crystallography

Single crystals containing $[Pt_2(\mu\text{-dppm})_2Cl(PPh_3)](PF_6)$ were formed by slow evaporation of benzene : CH_2Cl_2 solutions at 10 °C. These small crystals were then digested in a stoppered vial at ambient temperature over a period weeks until single crystals of a suitable size were formed. These crystals were found to readily lose solvent of crystallization and thus fracture within minutes on contact with air. In order to prevent this, a yellow crystal (approximate dimensions 1.0 x 0.1 x 0.2 mm) was wedged into a Lindeman glass capillary containing a small amount of mother liquor, after which the capillary was sealed.

The data collection and structure refinement were conducted by Sangsoo Kim under the direction of Dr. Robert A. Jacobson at Iowa State University. Experimental details of these procedures, although summarized here, are presented in detail in the appendix to this chapter (page 172).

Diffraction data was collected on a Syntex $P2_1$ diffractometer (Mo Kα, λ = 0.71069 A) at -20 °C. An asymmetric unit contained three molecules of benzene and included 101 non-hydrogen atoms: $[Pt_2ClP_5C_{68}H_{59}](PF_6) * 3(C_6H_6)$, corresponding to a formula weight of 1836.08 g/mol. The unit cell was found to be in the monoclinic $P2_1/n$ space group, having the following cell parameters: a = 21.604(6), b = 23.810(3), c = 15.304(3) A, β = 92.14(4)°, V = 7866(3) A^3, Z = 4, ρ_{calc} = 1.550 g/cm^3 μ = 39.54 cm^{-1}. Several phenyl rings, including

one of the benzene solvent molecules, were found to be disordered (see Figure I-42).

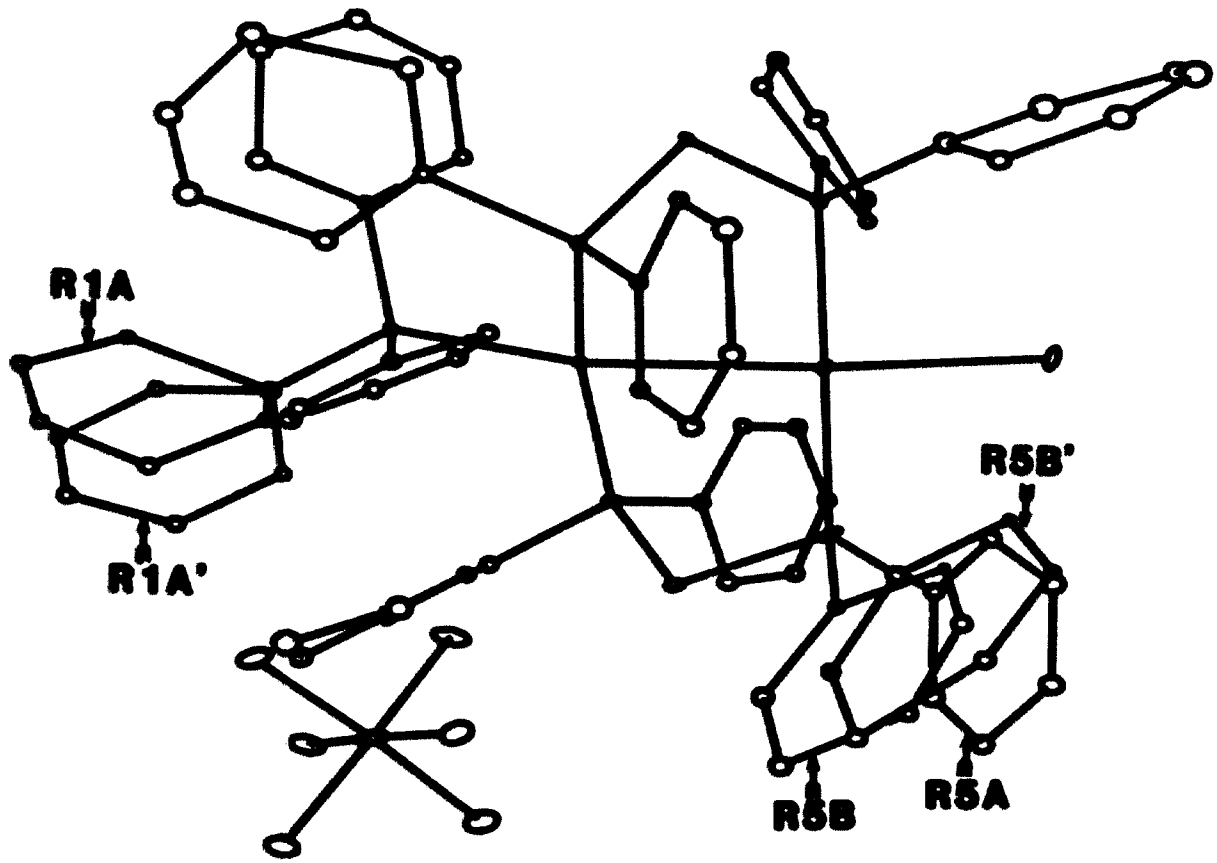

Figure I-42. ORTEP drawing of $[Pt_2(\mu\text{-dppm})_2Cl(PPh_3)](PF_6)$ showing the disordered phenyls

BIBLIOGRAPHY

1. Puddephatt, R. J. Chem. Soc. Rev. 1983, 12, 99.

2. Cowie, M.; Dwight, S. K. Inorg. Chem. 1979, 18, 1209.

3. Manojlovic-Muir, Lj.; Muir, K. W. J. Chem. Soc., Chem. Commun. 1982, 1155.

4. Azam, K. A.; Brown, M. P.; Hill, R. J.; Puddephatt, R. J.; Yavari, A. Organometallics 1984, 3, 697.

5. Brown, M. P.; Puddephatt, R. J.; Rashidi, M.; Seddon, K. R. J. Chem. Soc., Dalton Trans. 1977, 951.

6. Brown, M. P.; Franklin, S. J.; Puddephatt, R. J.; Thomson, M. A.; Seddon, K. R. J. Organomet. Chem. 1979, 178, 281.

7. Brown, M. P.; Puddephatt, R. J.; Rashidi, M.; Seddon, K. R. J. Chem. Soc., Trans. 1978, 1540.

8. Al-Resayes, S. I.; Mitchcock, P. B.; Nixon, J. F. J. Organomet. Chem. 1984, 267, C13.

9. Shimura, M.; Espenson, J. H. Inorg. Chem. 1984, 23, 4069.

10. Grossel, M. C.; Moulding, R. P.; Seddon, K. R. Inorg. Chim. Acta Lett. 1982, 64, L275.

11. Brown, M. P.; Puddephatt, R. J.; Rashidi, M.; Seddon, K. R. J. Chem. Soc., Dalton Trans. 1978, 516.

12. Brown, M. P.; Fisher, J. R.; Puddephatt, R. J.; Seddon, K. R. Inorg. Chem. 1979, 18, 2808.

13. Balch, A. L. Adv. Chem. Ser. 1982, 196, 243.

14. Pringle, P. G; Shaw, B. L. J. Chem. Soc., Dalton Trans. 1983, 889.

15. Kubiak, C. P.; Woodcock, C.; Eisenberg, R. Inorg. Chem. 1982, 21, 2119.

16. Jandik, P.; Schubert, U.; Schmidbaur, H. Angew. Chem. Int. Ed. Engl. 1982, 24, 74.

17. Basolo, F.; Pearson, R. G. "Mechanisms of Inorganic Reactions", 2nd ed.; Wiley: New York, 1967.

18. Wilkins, R. G. "The Study of Kinetics and Mechanism of Reactions of Transition Metal Complexes"; Allyn and Bacon: Boston, 1974.

19. Muralidharan, S.; Espenson, J. H. Inorg. Chem. 1983, 22, 2786.

20. Muralidharan, S.; Espenson, J. H. J. Amer. Chem. Soc. 1984, 106, 8104.

21. Brown, M. P.; Fisher, J. R.; Franklin, S. J.; Puddephatt, R. J.; Seddon, K. R. J. Organomet. Chem. 1978, 161, C46.

22. Goodfellow, R. J.; Taylor, B. F. J. Chem. Soc., Dalton Trans. 1974, 1676.

23. Muralidharan, S.; Espenson, J. H. Department of Chemistry, Iowa State University, Ames, unpublished results.

24. Pregosin, P. S.; Kunz, R. W. "NMR Basic Principles and Progress" Vol. 16; Springer-Verlag: New York, 1979.

25. Personal communication with Dr. J. G. Verkade, Chemistry Department, Iowa State University, Ames.

26. Purcell, K. F.; Kotz, J. C. "Inorganic Chemistry"; W. B. Saunders Company: Philadelphia, 1977; pp. 702-706.

27. Brown, M. P.; Fisher, J. R.; Hill, R. H.; Puddephatt, R. J.; Seddon, K. R. Inorg. Chem. 1981, 20, 3516.

28. Eisenberg, R.; Ibers, J. A. Inorg. Chem. 1965, 4, 773.

29. Manojlović-Muir; Lj; Muir, K. W.; Solomun, T. Acta Cryst. B 1979, 35, 1237.

30. Manojlović-Muir, Lj.; Muir, K. M.; Solomun, T. J. Organomet. Chem. 1979, 179, 479.

31. Russell, D. R.; Muhammed, M. A.; Tucker, P. A. J. Chem. Soc., Dalton Trans. 1980, 1737.

32. Clark, H. C.; Dymarski, M. J.; Oliver, J. D. J. Organomet. Chem. 1978, 154, C40.

33. Manojlović-Muir; Lj.; Muir, K. W. J. Organomet. Chem. 1981, 219 129.

34. Fisher, J. R.; Mills, A. J.; Sumner, S.; Brown, M. P.; Thomson, M. A.; Puddephatt, R. J.; Frew, A. A.; Manojlović-Muir, Lj.; Muir, K. W.; Organometallics 1982, 1, 1421.

35. Karplus, M. J. Amer. Chem. Soc. 1963, 85, 2870.

36. Doddrell, D.; Burfitt, I.; Kitching, W.; Bullpitt, M.; Lee, C.-H.; Mynott, R. J.; Considine, J. L.; Kuivila, H. G.; Sarma, R. H. J. Amer. Chem. Soc. 1974, 96, 1640 and references therein.

37. Kessler, H.; Gusowski, V.; Hancock, M. Tetrahedron Lett. 1968, 4665.

38. Blau, R. J.; Espenson J. H. Department of Chemistry, Iowa State University, Ames, unpublished results.

39. Oki, M. Topics in Stereochemistry 1983, 14, 1.

40. Oki, M. Acc. Chem. Res. 1984, 17, 154.

41. Freitag, R. A.; Mercer-Smith, J. A.; Whitten, D. G. J. Amer. Chem. Soc. 1981, 103, 1226 and references therein.

42. Walker, F. A.; Buchler, J.; West, J. T.; Hinds, J. L. J. Amer. Chem. Soc. 1983, 105, 6923.

43. Cabaret, D.; Maigrot, N.; Welvart, Z.; Duong, K. N. V.; Gaudemer, A. J. Amer. Chem. Soc. 1984, 106, 2870 and references therein.

44. Nakano, Y.; Yoshikawa, Y. J. Amer. Chem. Soc. 1984, 106, 429.

45. Schubert, U.; Ackermann, K.; Rustemeyer, P. J. Organomet. Chem. 1982, 231, 323.

46. Brunner, H.; Fischer, E. O.; Lappus, M. Angew. Chem. 1971, 83, 1022.

47. Bushweller, C. H.; Rithner, C. D.; Butcher, D. J. Inorg. Chem. 1984, 23, 1967 and references therein.

48. Hoffman, R. A.; Forsén, S.; Gestblom, B. "NMR Basic Principles and Progress" Vol. 5.; Springer-Verlag: New York, 1971.

49. Mislow, K. Acc. Chem. Res. 1976, 9, 26.

50. Hayes, K. S.; Nagumo, M.; Blount, J. F.; Mislow, K. J. Amer. Chem. Soc. 1980, 102, 2773.

51. Purcell, K. F.; Kotz, J. C. "Inorganic Chemistry"; W. B. Saunders Company: Philadelphia, 1977; pp. 696-710.

52. Blandemer, M. J.; Burgess, J.; Duce, P. R.; Hamshere, S. J.; Walker, J. J. J. Chem. Soc., Dalton Trans. 1980, 1809.

53. Coe, J. S. in "Mechanisms of Inorganic and Organometallic Reactions"; Twigg, M. V., ed.; Plenum Press: New York, 1983; vol. 1, chapter 4.

54. Lanza, S.; Minniti, D.; Romeo, R.; Moore, P.; Sachinidis, J.; Tobe, M. L. J. Chem. Soc., Chem. Commun. 1984, 542 and references therein.

55. Algra, G. P.; Balt, S. Inorg. Chem. 1981, 20, 1102.

56. Ito, K. Inorg. Chem. 1983, 22, 2872.

57. Pavia, D. L.; Lampman, G. M.; Kriz, G. S. "Introduction to Organic Laboratory Techniques"; W. B. Saunders Company: Philadelphia, 1976.

58. Cooper, S. J.; Brown, M. P.; Puddephatt, R. J. Inorg. Chem. 1981, 20, 1374.

59. Darensbourg, M. Y. submitted to Prog. Inorg. Chem.

APPENDIX. X-RAY CRYSTAL STRUCTURE DETERMINATION

Crystal Data

A yellow crystal of approximate dimensions 1.0 x 0.1 x 0.2 mm, was wedged into a Lindeman glass capillary and aligned on a Syntex $P2_1$ diffractometer. The approximate positions of 15 reflections selected from a rotation picture were used as input into an automatic indexing program. The resulting reduced cell and reduced cell scalars indicated a monoclinic crystal system, which was confirmed by the symmetry in the axial ω-oscillation photograph for each axis. Since those reflections were of low order for the $\vec{c}^*$ axis, the initial orientation matrix did not provide accurate settings for high-ordered reflections. From the axial photograph along $\vec{c}$, four reflections with large ℓ indices were selected, tuned, and included in the reflection array. The recalculated orientation matrix gave improved angle settings for those reflections. Reflections in $0k\ell$ and $0k\bar{\ell}$ octants were collected using ω-step scan technique to pick up stronger reflections with large ℓ indices. Three such reflections were finally chosen and tuned to recalculate a more accurate orientation matrix.

Accurate unit cell parameters were obtained by a least-squares fit to tuned 2θ values of 13 reflections ($20 < 2\theta < 35°$).

Collection and Reduction of X-ray Intensity Data

All data within a sphere of $2\theta \leq 45°$ (10987) in $hk\ell$ and $hk\bar{\ell}$ octants were measured by using an ω-step scan procedure with variable scan rates (min. 4.5°/min, max. 29.30°/min). As a general check on the electronic and crystal stability, the intensity of reflection $01\bar{8}$ were measured every 75 reflections. This standard reflection was not observed to vary significantly throughout the data collection period. The space group was uniquely identified as $P2_1/n$ by systematic absences occurring when $k = 2n+1$ for the 0k0 reflections and $h+\ell = 2n+1$ for the h0ℓ reflections. The intensity data were corrected for the Lorentz, polarization, and absorption effects, but not for the extinction. Symmetry-related reflections were averaged together, yielding 5611 independent observed ($I \geq 2\sigma_I$ and $F \geq 4\sigma_F$) reflections. The internal consistency factor ($R_I = \Sigma|I-\langle I\rangle|/\Sigma I$) was 0.057.

Structural Solution and Refinement

The positions of the Pt atoms were obtained from an analysis of a standard sharpened Patterson map. The positions of the remaining nonhydrogen atoms were determined by successive structure factor and difference electron density map calculations. It was difficult to locate the atomic positions of the several carbon atoms in phenyl rings because of large thermal motions and poor phasing. The PF_6 anion was not disordered, but several phenyl rings were (see Figure I-

42; page ---); including one of the benzene solvent molecules. Ring multipliers for the disordered groups were refined using isotropic temperature factors for individual atoms keeping positional parameters fixed. After optimization, these multipliers were fixed and the positional and anisotropic thermal parameters for Pt, C_α, P, F, and methylene carbons were refined by block-matrix least-squares procedure as were the isotropic thermal parameters for the rest of the atoms, minimizing the function $\Sigma\omega(|F_o|-|F_c|)^2$, where $\omega = 1/\sigma_F^2$. Some atoms did not behave well during the refinement cycles, characterized by the large shift in their parameters. Examination of $\langle\omega(|F_o|-|F_c|)^2\rangle$ with respect to $|F_o|$ and $\sin\theta/\lambda$, showed overweighting at large $|F_o|$ and small $\sin\theta/\lambda$. After the weights were adjusted to reduce the variation in $\langle\omega(|F_o|-|F_c|)^2\rangle$, these atoms were then better behaved.

The hydrogen positions were calculated assuming ideal geometries with the C-H bond distance set to 1.0A. The least-squares procedure converged to a conventional residual index of $R = \Sigma||F_o|-|F_c||/\Sigma|F_o| = 0.108$ and a weighted residual index of $R_\omega = [\Sigma\omega(|F_o|-|F_c|)^2/\Sigma\omega|F_c|^2]^{1/2} = 0.110$.

The final positional and thermal parameters are listed in Tables I-22 (atoms in $Pt_2(\mu\text{-dppm})_2$ ring), I-23 (phenyl carbons), and I-24 (hydrogen atoms), while bond lengths and angles for atoms other than phenyl carbons are listed in Tables I-25 and I-26, respectively. Bond distances, and

angles of carbons within the phenyl rings are found in Table I-27 accompanied with least squares planes of these rings.

Table I-22. Positional and anisotropic thermal parameters for the nonphenyl atoms in [Cl--PPh_3](PF_6)*3(C_6H_6)[a]

Atom	X	Y	Z	U(ave)
Pt1	1886.7(5)	2928.1(5)	2757.8(7)	39.
Pt2	2605.7(5)	2988.4(6)	4208.2(9)	52.
Cl	3174.(7)	3132.(5)	5570.(10)	131.
P1	1097.(4)	3044.(3)	1691.(5)	45.
P2	1445.(4)	2211.(3)	3497.(5)	40.
P3	2625.(4)	3459.(3)	2124.(7)	63.
P4	1721.(4)	2946.(5)	4976.(5)	60.
P5	3488.(4)	2979.(5)	3447.(10)	97.
P6	3478.(6)	1389.(4)	495.(13)	129.
F1	3289.(19)	1831.(10)	-176.(25)	174.
F2	2875.(13)	1022.(10)	351.(26)	153.
F3	3151.(18)	1761.(12)	1180.(26)	190.
F4	3708.(15)	946.(12)	1215.(27)	162.
F5	4111.(19)	1682.(17)	616.(37)	223.
F6	3796.(17)	1027.(11)	-243.(26)	169.
C24	1148.(15)	2501.(12)	4554.(17)	47.
C35	3318.(16)	3060.(18)	2241.(29)	93.

[a]Atom coordinates [x 10^4], temperature factors [A^2, x 10^3]; U(ave) is the average of U11, U22, and U33.

U11	U22	U33	U12	U13	U23
45.2(7)	31.4(6)	39.9(6)	-6.4(7)	17.9(5)	-3.5(6)
33.9(6)	44.7(7)	78.3(9)	2.4(7)	-6.5(6)	-12.5(8)
138.(11)	90.(8)	164.(12)	-13.(7)	****(10)	13.(8)
56.(5)	48.(5)	30.(4)	4.(4)	21.(3)	-7.(4)
52.(5)	31.(4)	37.(4)	-14.(3)	11.(4)	3.(3)
67.(6)	38.(5)	84.(7)	5.(4)	47.(5)	-8.(5)
68.(6)	80.(6)	31.(4)	19.(6)	4.(4)	-1.(5)
24.(4)	59.(6)	207.(13)	8.(5)	17.(6)	-12.(8)
86.(9)	38.(6)	264.(19)	-9.(6)	86.(11)	-24.(8)
246.(38)	63.(16)	214.(34)	13.(19)	130.(31)	25.(18)
112.(20)	70.(16)	276.(38)	-29.(15)	64.(23)	23.(21)
231.(37)	101.(20)	236.(37)	101.(23)	130.(31)	-8.(22)
129.(24)	88.(20)	268.(40)	-13.(17)	20.(25)	-8.(22)
156.(33)	165.(33)	348.(61)	-82.(27)	76.(37)	-87.(36)
190.(32)	78.(18)	239.(37)	5.(19)	94.(28)	-46.(21)
73.(22)	45.(18)	24.(15)	2.(16)	16.(15)	5.(14)
53.(22)	100.(32)	125.(33)	-41.(21)	29.(22)	-51.(28)

Table I-23. Positional and isotropic thermal parameters for phenyl atoms in [Cl--PPh_3](PF_6)*3(C_6H_6)[a]

Atom	X	Y	Z	U
C11A	1191.(20)	2626.(18)	774.(28)	91.(12)
C12A	1488.(23)	2111.(23)	854.(32)	42.(13)
C13A	1516.(33)	1672.(30)	156.(46)	72.(20)
C14A	989.(26)	1630.(24)	-302.(37)	49.(15)
C15A	904.(32)	1980.(31)	-372.(44)	74.(19)
C16A	507.(27)	2456.(24)	178.(37)	49.(15)
D12A	780.(34)	2761.(30)	-37.(47)	62.(20)
D13A	850.(29)	2426.(26)	-744.(41)	49.(16)
D14A	1313.(37)	2032.(39)	-703.(52)	82.(23)
D15A	1791.(34)	2007.(35)	-126.(47)	68.(20)
D16A	1759.(31)	2324.(28)	611.(43)	53.(17)
C11B	337.(14)	2972.(15)	2167.(19)	56.(8)
C12B	-137.(28)	2683.(25)	1782.(39)	138.(20)
C13B	-801.(26)	2797.(23)	2295.(35)	127.(18)
C14B	-770.(29)	3070.(27)	2994.(40)	144.(20)
C15B	-307.(23)	3339.(21)	3291.(32)	108.(15)
C16B	272.(19)	3299.(17)	2924.(27)	83.(12)
C11C	1065.(21)	3787.(19)	1237.(30)	98.(14)

[a]Atom coordinates [x 10^4] and isotropic temperature factor [A^2, x 10^3].

Table I-23 (continued)

Atom	X	Y	Z	U
C12C	1003.(25)	3877.(24)	304.(36)	124.(17)
C13C	883.(37)	4412.(33)	-70.(51)	181.(27)
C14C	900.(28)	4738.(25)	584.(39)	136.(19)
C15C	976.(25)	4808.(23)	1353.(36)	121.(17)
C16C	1101.(23)	4192.(21)	1920.(33)	111.(15)
C21A	1965.(14)	1653.(12)	3789.(19)	45.(8)
C22A	2500.(15)	1573.(14)	3358.(21)	56.(9)
C23A	2885.(20)	1105.(19)	3597.(28)	92.(13)
C24A	2745.(22)	736.(20)	4169.(30)	100.(14)
C25A	2167.(27)	823.(24)	4621.(38)	132.(18)
C26A	1796.(15)	1261.(14)	4428.(21)	55.(9)
C21B	801.(17)	1788.(15)	3022.(24)	71.(10)
C22B	947.(23)	1522.(21)	2259.(32)	106.(15)
C23B	470.(30)	1163.(28)	1814.(41)	147.(21)
C24B	38.(27)	1137.(26)	2048.(38)	136.(19)
C25B	-234.(34)	1405.(31)	2766.(48)	169.(25)
C26B	226.(29)	1808.(26)	3403.(41)	144.(21)
C31A	2592.(18)	3573.(17)	953.(26)	78.(11)
C32A	2642.(36)	3120.(32)	337.(50)	185.(27)
C33A	2490.(58)	3153.(54)	-608.(82)	256.(52)
C34A	2513.(30)	3723.(27)	-898.(41)	148.(21)
C35A	2464.(24)	4164.(22)	-299.(34)	114.(16)

Table I-23 (continued)

Atom	X	Y	Z	U
C36A	2493.(18)	4078.(16)	527.(25)	77.(11)
C31B	2794.(18)	4150.(16)	2499.(25)	75.(11)
C32B	2442.(18)	4401.(16)	3118.(25)	77.(11)
C33B	2536.(21)	4947.(20)	3373.(30)	99.(14)
C34B	3033.(21)	5256.(19)	3109.(29)	96.(13)
C35B	3406.(22)	5006.(20)	2535.(30)	101.(14)
C36B	3301.(23)	4490.(22)	2160.(33)	110.(15)
C41A	1346.(16)	3628.(14)	5109.(22)	61.(9)
C42A	721.(22)	3661.(20)	5139.(31)	100.(14)
C43A	454.(23)	4181.(21)	5337.(32)	106.(15)
C44A	792.(27)	4644.(24)	5246.(37)	129.(18)
C45A	1439.(21)	4650.(18)	5141.(29)	93.(13)
C46A	1704.(16)	4087.(14)	5078.(22)	62.(9)
C41B	1856.(25)	2687.(23)	5992.(35)	122.(17)
C42B	2196.(21)	2239.(19)	6210.(30)	100.(14)
C43B	2357.(34)	2012.(33)	7010.(47)	169.(25)
C44B	2287.(43)	2300.(38)	7626.(60)	206.(34)
C45B	2107.(27)	2837.(25)	7601.(36)	133.(18)
C46B	1880.(47)	2999.(44)	6722.(64)	235.(37)
C51A	4031.(20)	3562.(18)	3687.(27)	85.(12)

Table I-23 (continued)

Atom	X	Y	Z	U
C52A	3883.(21)	3964.(20)	4237.(30)	100.(14)
C53A	4291.(32)	4458.(30)	4333.(45)	158.(23)
C54A	4849.(33)	4410.(30)	3808.(45)	160.(23)
C55A	4980.(26)	4063.(24)	3129.(36)	125.(18)
C56A	4584.(27)	3560.(25)	3164.(37)	129.(18)
C51B	3924.(26)	2376.(23)	3296.(37)	39.(14)
C52B	4183.(40)	2165.(38)	2549.(55)	88.(25)
C53B	4563.(42)	1649.(37)	2528.(58)	91.(26)
C54B	4621.(27)	1450.(25)	3474.(38)	50.(15)
C55B	4341.(37)	1691.(33)	4071.(51)	74.(22)
C56B	4023.(19)	2170.(17)	4115.(26)	14.(10)
D51B	3923.(39)	2343.(35)	3788.(55)	82.(24)
D52B	4234.(28)	2080.(29)	3066.(38)	56.(16)
D53B	4610.(35)	1505.(32)	3088.(49)	74.(21)
D54B	4562.(34)	1355.(31)	4102.(48)	66.(20)
D55B	4324.(24)	1604.(21)	4761.(33)	35.(13)
D56B	3966.(20)	2032.(22)	4696.(28)	27.(11)
C111	5071.6(0)	3442.0(0)	825.6(0)	156.4(0)
C121	4745.5(0)	2985.3(0)	685.6(0)	142.7(0)
C131	5072.1(0)	2584.8(0)	1329.3(0)	198.2(0)

Table I-23 (continued)

Atom	X	Y	Z	U
C141	5625.7(0)	2875.7(0)	1781.4(0)	223.9(0)
C151	5700.4(0)	3443.5(0)	1614.5(0)	192.3(0)
C161	5240.8(0)	3890.3(0)	854.7(0)	187.8(0)
C112	8381.5(0)	9536.0(0)	2505.0(0)	147.3(0)
C122	8117.4(0)	9393.7(0)	1709.7(0)	137.8(0)
C132	8063.9(0)	9820.6(0)	1047.4(0)	188.5(0)
C142	8251.9(0)	10388.5(0)	1401.6(0)	132.1(0)
C152	8358.3(0)	10424.0(0)	2268.9(0)	148.8(0)
C162	8518.5(0)	10062.7(0)	2914.8(0)	203.6(0)
C113	8313.4(0)	4547.3(0)	1686.5(0)	271.5(0)
C143	9482.0(0)	4954.4(0)	2274.3(0)	171.9(0)
C123	8290.3(0)	4959.6(0)	2087.3(0)	98.0(0)
C133	8797.8(0)	5340.1(0)	2415.8(0)	201.3(0)
C153	9407.0(0)	4607.3(0)	2146.2(0)	67.9(0)
C163	8849.8(0)	4425.3(0)	1931.8(0)	113.3(0)
D123	8519.0(0)	5156.0(0)	2449.2(0)	159.6(0)
D133	9095.6(0)	5397.0(0)	2651.2(0)	207.5(0)
D153	9274.8(0)	4434.0(0)	1526.4(0)	139.3(0)
D163	8603.7(0)	4219.9(0)	1205.1(0)	113.4(0)

Table I-24. Estimated hydrogen atom coordinates and temperature factor in [Cl--PPh_3](PF_6)*(C_6H_6)[a]

Atom	X	Y	Z	U
H 1	748.2(0)	2715.1(0)	4437.7(0)	88.7(0)
H 2	1062.9(0)	2188.7(0)	4974.8(0)	88.7(0)
H 3	3267.6(0)	2680.7(0)	1951.5(0)	88.7(0)
H 4	3673.0(0)	3259.7(0)	1955.7(0)	88.7(0)
H 5	1706.4(0)	2032.7(0)	1424.4(0)	88.7(0)
H 6	1891.2(0)	1430.2(0)	65.2(0)	88.7(0)
H 7	945.2(0)	1277.8(0)	-662.5(0)	88.7(0)
H 8	152.2(0)	1909.3(0)	-811.0(0)	88.7(0)
H 9	131.7(0)	2687.4(0)	231.1(0)	88.7(0)
H 10	477.8(0)	3082.5(0)	-39.2(0)	88.7(0)
H 11	569.3(0)	2464.1(0)	-1272.4(0)	88.7(0)
H 12	1292.1(0)	1729.8(0)	-1173.2(0)	88.7(0)
H 13	2149.3(0)	1768.6(0)	-217.1(0)	88.7(0)
H 14	2126.0(0)	2345.1(0)	1032.0(0)	88.7(0)
H 15	-99.1(0)	2427.6(0)	1255.7(0)	88.7(0)
H 16	-1214.6(0)	2663.9(0)	2058.1(0)	88.7(0)
H 17	-1137.4(0)	3066.9(0)	3367.3(0)	88.7(0)

[a]Estimated Atom coordinates [x 10^4] and isotropic temperature factor [A^2, x 10^3].

Table I-24 (continued)

Atom	X	Y	Z	U
H 18	-356.0(0)	3598.7(0)	3808.7(0)	88.7(0)
H 19	640.2(0)	3499.2(0)	3194.0(0)	88.7(0)
H 20	1051.3(0)	3548.4(0)	-86.2(0)	88.7(0)
H 21	782.3(0)	4492.6(0)	-709.6(0)	88.7(0)
H 22	829.8(0)	5118.7(0)	309.9(0)	88.7(0)
H 23	969.4(0)	5192.9(0)	1635.3(0)	88.7(0)
H 24	1179.2(0)	4134.0(0)	2569.0(0)	88.7(0)
H 25	2614.2(0)	1835.8(0)	2883.6(0)	88.7(0)
H 26	3291.3(0)	1059.7(0)	3288.6(0)	88.7(0)
H 27	3022.0(0)	410.2(0)	4320.3(0)	88.7(0)
H 28	2045.3(0)	543.5(0)	5069.8(0)	88.7(0)
H 29	1402.1(0)	1310.3(0)	4741.9(0)	88.7(0)
H 30	1368.6(0)	1567.9(0)	2012.5(0)	88.7(0)
H 31	588.3(0)	927.7(0)	1309.1(0)	88.7(0)
H 32	-257.4(0)	904.8(0)	1679.3(0)	88.7(0)
H 33	-673.9(0)	1333.5(0)	2885.8(0)	88.7(0)
H 34	97.3(0)	2019.0(0)	3932.8(0)	88.7(0)
H 35	2689.0(0)	2727.0(0)	562.7(0)	88.7(0)
H 36	2642.3(0)	2844.9(0)	-931.6(0)	88.7(0)
H 37	2483.7(0)	3777.9(0)	-1541.9(0)	88.7(0)
H 38	2428.5(0)	4560.4(0)	-522.0(0)	88.7(0)

Table I-24 (continued)

Atom	X	Y	Z	U
H 39	2424.0(0)	4412.3(0)	910.8(0)	88.7(0)
H 40	2108.8(0)	4181.2(0)	3392.0(0)	88.7(0)
H 41	2235.9(0)	5125.4(0)	3775.2(0)	88.7(0)
H 42	3105.8(0)	5653.2(0)	3308.5(0)	88.7(0)
H 43	3792.7(0)	5212.1(0)	2380.6(0)	88.7(0)
H 44	3557.1(0)	4348.2(0)	1675.0(0)	88.7(0)
H 45	455.2(0)	3321.6(0)	5011.5(0)	88.7(0)
H 46	23.3(0)	4199.0(0)	5554.4(0)	88.7(0)
H 47	570.2(0)	5013.2(0)	5241.6(0)	88.7(0)
H 48	1688.1(0)	5001.2(0)	5106.0(0)	88.7(0)
H 49	2159.4(0)	4042.5(0)	5021.1(0)	88.7(0)
H 50	2382.9(0)	2032.5(0)	5699.9(0)	88.7(0)
H 51	2490.5(0)	1611.8(0)	7082.3(0)	88.7(0)
H 52	2390.8(0)	2145.5(0)	8198.5(0)	88.7(0)
H 53	2102.5(0)	3082.4(0)	8136.0(0)	88.7(0)
H 54	1788.3(0)	3430.4(0)	6646.5(0)	88.7(0)
H 55	3498.8(0)	3932.2(0)	4575.2(0)	88.7(0)
H 56	4192.0(0)	4789.3(0)	4725.4(0)	88.7(0)
H 57	5185.5(0)	4687.4(0)	3982.7(0)	88.7(0)
H 58	5294.2(0)	4138.9(0)	2694.9(0)	88.7(0)
H 59	4683.5(0)	3217.1(0)	2806.9(0)	88.7(0)

Table I-24 (continued)

Atom	X	Y	Z	U
H 60	4147.0(0)	2380.9(0)	1996.3(0)	88.7(0)
H 61	4738.3(0)	1468.2(0)	1966.6(0)	88.7(0)
H 62	4919.6(0)	1133.6(0)	3617.1(0)	88.7(0)
H 63	4334.0(0)	1413.8(0)	4617.8(0)	88.7(0)
H 64	3892.0(0)	2359.1(0)	4669.4(0)	88.7(0)
H 65	4195.9(0)	2278.3(0)	2499.6(0)	88.7(0)
H 66	4801.1(0)	1315.1(0)	2583.8(0)	88.7(0)
H 67	4802.6(0)	1015.2(0)	4239.9(0)	88.7(0)
H 68	4408.0(0)	1430.0(0)	5342.8(0)	88.7(0)

Table I-25. Selected intramolecular distances with Esd's for $[Pt_2(\mu\text{-dppm})_2Cl(PPh_3)3(PF_6)*3(C_6H_6)$

Around $Pt_2P_4C_2$ Ring Atoms	dist/Å	Atoms	P-C(Phenyl) dist/Å
Pt1-Pt	2.665 (2)	P1-C11A	1.74 (4)
Pt1-P1	2.333 (8)	P1-C11B	1.83 (3)
Pt1-P2	2.276 (7)	P1-C11C	1.90 (5)
Pt1-P3	2.280 (9)	P2-C21A	1.79 (3)
Pt2-P4	2.283 (9)	P2-C21B	1.85 (4)
Pt2-P5	2.271 (12)	P3-C31A	1.81 (4)
Pt2-C1	2.403 (14)	P3-C31B	1.78 (4)
P2-C24	1.89 (3)	P4-C41A	1.83 (3)
P4-C24	1.74 (3)	P4-C41B	1.69 (5)
P3-C35	1.78 (4)	P5-C51A	1.85 (4)
P5-C35	1.89 (4)	P5-C51B	1.74 (6)
		P5-D51B[a]	1.85 (8)

[a]Second P-C bond distance in the disordered phenyl ring 5B.

Table I-26. Selected interatomic angles (deg) with Esd's for $[Pt_2(\mu\text{-dppm})_2Cl(PPh_3)](PF_6)\cdot 3(C_6H_6)$

atoms	angle	atoms	angle
Pt2-Pt1-P1	164.7 (2)	Pt2-Pt1-P2	82.5 (2)
Pt2-Pt1-P3	85.9 (2)	Pt1-Pt2-C1	173.3 (3)
Pt1-Pt2-P4	87.3 (2)	Pt1-Pt2-P5	92.7 (3)
P1-Pt1-P2	97.3 (3)	P1-Pt1-P3	160.0 (3)
P2-Pt1-P3	160.0 (3)	C1-Pt2-P4	88.3 (4)
C1-Pt2-P5	92.7 (3)	P4-Pt2-P5	176.9 (4)
P2-C24-P4	106.3 (15)	P3-C35-P5	106.7 (20)
Pt1-P2-C24	108.3 (9)	Pt1-P3-C35	105.1 (14)
Pt2-P4-C24	115.8 (11)	Pt2-P5-C35	111.5 (14)
Pt1-P1-C11A	113.1 (15)	C11A-P1-C11B	113.7 (18)
Pt1-P1-C11B	110.8 (10)	C11A-P1-C11C	104.0 (20)
Pt1-P1-C11C	112.4 (14)	C11B-P1-C11C	102.3 (17)
Pt1-P2-C21A	114.3 (10)	Pt1-P2-21B	122.5 (12)
C24-P2-C21A	106.7 (13)	C24-P2-C21B	105.1 (15)
C21A-P2-C21B	98.7 (15)		
Pt1-P3-C31A	120.1 (13)	Pt1-P3-C31B	121.0 (13)
C35-P3-C31A	100.4 (19)	C35-P3-C31B	107.5 (19)
C31A-P3-C31B	100.5 (18)		
Pt2-P4-C41A	113.6 (11)	Pt2-P4-C41B	111.8 (19)
C24-P4-C41A	105.7 (15)	C24-P4-C41B	102.5 (21)
C41A-P4-C41B	106.4 (21)		
Pt2-P5-C51A	115.5 (14)	Pt2-P5-C51B	123.1 (19)
C35-P5-C51A	102.6 (19)	C35-P5-C51B	92.4 (23)
C51A-P5-C51B	107.7 (23)	C51A-P5-D51B	104.3 (29)
C51B-P5-D51B	24.2 (32)	C35-P5-D51B	116.1 (29)
Pt2-P5-D51B	106.9 (26)		

Table I-27. C-C bond distances, C-C-C bond angles, and least squares planes found for phenyl rings in the crystal structure for $[Pt_2(\mu\text{-dppm})_2Cl(PPh_3)](PF_6) * (C_6H_6)$

Ring 1A

$-0.48574x + -0.49229y + 0.722302z + 3.27729 = 0.0$[a]

Standard Deviation = 0.172[b]

Bond	Distances/A	Bond Angles/degrees		Atom	Shift[c]
C1-C2	1.38 (7)	C6-C1-C2	103. (4)	C1	-0.175
C2-C3	1.50 (9)	C1-C2-C3	126. (5)	C2	0.208
C3-C4	1.32 (9)	C2-C3-C4	112. (6)	C3	-0.097
C4-C5	1.34 (9)	C3-C4-C5	131. (6)	C4	-0.013
C5-C6	1.41 (9)	C4-C5-C6	118. (6)	C5	0.006
C6-C1	1.76 (7)	C5-C6-C1	119. (4)	C6	0.069
				P1	0.473

[a]Equation for the least squares plane.

[b]Standard Deviation of the least squares plane.

[c]Deviation (A) of atoms from the least squares plane.

Table I-27 (continued)

Ring 1A'

$0.55472x + 0.73448y + -0.39092z + -5.69046 = 0.0$[a]

Standard Deviation = 0.143[b]

Bond	Distances/A	Bond Angles/degrees		Atom	Shift/A[c]
C1-C2	1.53 (8)	C6-C1-C2	116. (5)	C1	-0.158
C2-C3	1.36 (9)	C1-C2-C3	116. (6)	C2	0.096
C3-C4	1.37(10)	C2-C3-C4	118. (6)	C3	0.039
C4-C5	1.36(11)	C3-C4-C5	127. (8)	C4	-0.120
C5-C6	1.36(10)	C4-C5-C6	118. (7)	C5	0.045
C6-C1	1.45 (8)	C5-C6-C1	119. (6)	C6	0.098
				P1	-0.117

Ring 1B

$-0.19787x + 0.80094y + -0.56510z + -3.67514 = 0.0$[a]

Standard Deviation = 0.039[b]

Bond	Distances/A	Bond Angles/degrees		Atom	Shift/A[c]
C1-C2	1.35 (7)	C6-C1-C2	123. (4)	C1	0.000
C2-C3	1.68 (8)	C1-C2-C3	111. (4)	C2	-0.020
C3-C4	1.25 (8)	C2-C3-C4	118. (5)	C3	0.043
C4-C5	1.26 (8)	C3-C4-C5	126. (6)	C4	-0.045
C5-C6	1.39 (6)	C4-C5-C6	122. (5)	C5	0.016
C6-C1	1.41 (5)	C5-C6-C1	119. (4)	C6	0.006
				P1	0.219

Table I-27 (continued)

Ring 1C

$0.99000x + 0.10828y + -0.09041z + -3.04979 = 0.0$[a]

Standard Deviation = 0.033[b]

Bond Distances/A		Bond Angles/degrees		Atom	Shift/A[c]
C1-C2	1.46 (7)	C6-C1-C2	129. (4)	C1	-0.036
C2-C3	1.42(10)	C1-C2-C3	123. (5)	C2	0.037
C3-C4	1.27(10)	C2-C3-C4	103. (6)	C3	-0.010
C4-C5	1.19 (8)	C3-C4-C5	150. (7)	C4	-0.017
C5-C6	1.72 (7)	C4-C5-C6	113. (5)	C5	0.014
C6-C1	1.42 (7)	C5-C6-C1	102. (4)	C6	0.012
				P1	-0.249

Ring 2A

$0.46090x + 0.54502y + 0.70037z + -8.05265 = 0.0$[a]

Standard Deviation = 0.012[b]

Bond Distances/A		Bond Angles/degrees		Atom	Shift/A[c]
C1-C2	1.36 (4)	C6-C1-C2	119. (3)	C1	0.008
C2-C3	1.43 (5)	C1-C2-C3	119. (3)	C2	-0.013
C3-C4	1.28 (6)	C2-C3-C4	124. (4)	C3	0.013
C4-C5	1.46 (7)	C3-C4-C5	117. (4)	C4	-0.008
C5-C6	1.34 (7)	C4-C5-C6	121. (5)	C5	0.002
C6-C1	1.41 (4)	C5-C6-C1	120. (4)	C6	-0.002
				P1	-0.091

Table I-27 (continued)

Ring 2B

$-0.24964x + 0.79008y + -0.55988z + -0.41555 = 0.0$[a]

Standard Deviation = 0.032[b]

Bond	Distances/A	Bond Angles/degrees		Atom	Shift/A[c]
C1-C2	1.38 (6)	C6-C1-C2	127. (4)	C1	-0.027
C2-C3	1.48 (8)	C1-C2-C3	119. (4)	C2	0.035
C3-C4	1.01 (9)	C2-C3-C4	120. (7)	C3	-0.009
C4-C5	1.42 (9)	C3-C4-C5	131. (7)	C4	-0.022
C5-C6	1.67(10)	C4-C5-C6	117. (6)	C5	0.025
C6-C1	1.39 (7)	C5-C6-C1	105. (5)	C6	-0.001
				P1	0.021

Ring 3A

$0.99499x + 0.09104y + -0.04132z + -6.23112 = 0.0$[a]

Standard Deviation = 0.103[b]

Bond	Distances/A	Bond Angles/degrees		Atom	Shift/A[c]
C1-C2	1.44 (9)	C6-C1-C2	111. (4)	C1	0.001
C2-C3	1.47(15)	C1-C2-C3	126. (7)	C2	0.085
C3-C4	1.43(14)	C2-C3-C4	110. (9)	C3	-0.122
C4-C5	1.40 (8)	C3-C4-C5	120. (7)	C4	0.085
C5-C6	1.28 (6)	C4-C5-C6	122. (5)	C5	0.004
C6-C1	1.38 (6)	C5-C6-C1	127. (4)	C6	-0.052
				P1	-0.094

Table I-27 (continued)

Ring 3B

0.56404x + -0.36643y + 0.74000z + -2.52655 = 0.0[a]

Standard Deviation = 0.049[b]

Bond	Distances/A	Bond Angles/degrees		Atom	Shift/A[c]
C1-C2	1.38 (5)	C6-C1-C2	116. (4)	C1	0.006
C2-C3	1.37 (6)	C1-C2-C3	122. (4)	C2	0.038
C3-C4	1.38 (6)	C2-C3-C4	122. (4)	C3	-0.044
C4-C5	1.35 (7)	C3-C4-C5	117. (4)	C4	0.002
C5-C6	1.37 (7)	C4-C5-C6	125. (4)	C5	0.044
C6-C1	1.47 (6)	C5-C6-C1	117. (4)	C6	-0.046
				P1	-0.011

Ring 4A

0.11788x + -0.05272y + 0.99163z + -7.56743 = 0.0[a]

Standard Deviation = 0.074[b]

Bond	Distances/A	Bond Angles/degrees		Atom	Shift/A[c]
C1-C2	1.36 (6)	C6-C1-C2	122. (3)	C1	0.034
C2-C3	1.41 (7)	C1-C2-C3	118. (4)	C2	-0.085
C3-C4	1.33 (7)	C2-C3-C4	118. (5)	C3	0.081
C4-C5	1.41 (7)	C3-C4-C5	125. (5)	C4	-0.028
C5-C6	1.46 (6)	C4-C5-C6	113. (4)	C5	-0.022
C6-C1	1.34 (5)	C5-C6-C1	121. (3)	C6	0.020
				P1	0.014

Table I-27 (continued)

Ring 4B

0.91234x + 0.37761y + -0.15828z + -4.40791 = 0.0[a]

Standard Deviation = 0.100[b]

Bond	Distances/A	Bond Angles/degrees		Atom	Shift/A[c]
C1-C2	1.33 (7)	C6-C1-C2	103. (6)	C1	-0.097
C2-C3	1.37 (9)	C1-C2-C3	131. (5)	C2	0.107
C3-C4	1.18(12)	C2-C3-C4	117. (7)	C3	-0.014
C4-C5	1.34(11)	C3-C4-C5	125. (9)	C4	-0.075
C5-C6	1.47(12)	C4-C5-C6	111. (7)	C5	0.060
C6-C1	1.34(11)	C5-C6-C1	128. (8)	C6	0.018
				P1	0.169

Ring 5A

0.51333x + -0.46940y + 0.71844z + -4.43147 = 0.0[a]

Standard Deviation = 0.088[b]

Bond	Distances/A	Bond Angles/degrees		Atom	Shift/A[c]
C1-C2	1.32 (6)	C6-C1-C2	125. (4)	C1	0.002
C2-C3	1.48 (8)	C1-C2-C3	119. (5)	C2	-0.025
C3-C4	1.48(10)	C2-C3-C4	112. (5)	C3	-0.022
C4-C5	1.37 (9)	C3-C4-C5	131. (6)	C4	0.090
C5-C6	1.47 (8)	C4-C5-C6	109. (5)	C5	-0.103
C6-C1	1.46 (7)	C5-C6-C1	120. (5)	C6	0.058
				P1	-0.206

Table I-27 (continued)

Ring 5B

0.81968x + 0.54728y + 0.16918z + -10.76806 = 0.0[a]

Standard Deviation = 0.057[b]

Bond	Distances/A	Bond Angles/degrees		Atom	Shift/A[c]
C1-C2	1.39(10)	C6-C1-C2	125. (6)	C1	-0.025
C2-C3	1.48(12)	C1-C2-C3	124. (7)	C2	0.001
C3-C4	1.53(11)	C2-C3-C4	105. (7)	C3	-0.003
C4-C5	1.21(10)	C3-C4-C5	125. (7)	C4	0.041
C5-C6	1.42 (9)	C4-C5-C6	130. (7)	C5	-0.068
C6-C1	1.36 (7)	C5-C6-C1	109. (5)	C6	0.055
				P1	0.021

Ring 5B'

0.81968x + 0.54728y + 0.16918z + -10.76806 = 0.0[a]

Standard Deviation = 0.057[b]

Bond	Distances/A	Bond Angles/degrees		Atom	Shift/A[c]
C1-C2	1.46(10)	C6-C1-C2	117. (6)	C1	-0.025
C2-C3	1.59(10)	C1-C2-C3	127. (6)	C2	0.001
C3-C4	1.60(10)	C2-C3-C4	99. (5)	C3	-0.003
C4-C5	1.29 (9)	C3-C4-C5	134. (6)	C4	0.041
C5-C6	1.78 (6)	C4-C5-C6	124. (5)	C5	-0.068
C6-C1	1.57(10)	C5-C6-C1	117. (5)	C6	0.055
				P1	0.021

Table I-27 (continued)

Benzene Ring 1

$-0.6379x + 0.24652y + 0.72956z + 3.98337 = 0.0$[a]

Standard Deviation = 0.041[b]

Bond	Distances/A	Bond Angles/degrees		Atom	Shift/A[c]
C1-C2	1.31	C6-C1-C2	164.	C1	-0.035
C2-C3	1.53	C1-C2-C3	100.	C2	-0.015
C3-C4	1.53	C2-C3-C4	110.	C3	0.042
C4-C5	1.39	C3-C4-C5	117.	C4	-0.030
C5-C6	1.84	C4-C5-C6	128.	C5	0.009
C6-C1	1.13	C5-C6-C1	69.	C6	0.029

Benzene Ring 2

$0.95775x + -0.11214y + -0.26485z + -13.57518 = 0.0$[a]

Standard Deviation = 0.098[b]

Bond	Distances/A	Bond Angles/degrees		Atom	Shift/A[c]
C1-C2	1.37	C6-C1-C2	133.	C1	0.070
C2-C3	1.44	C1-C2-C3	118.	C2	-0.074
C3-C4	1.51	C2-C3-C4	112.	C3	0.006
C4-C5	1.34	C3-C4-C5	117.	C4	0.081
C5-C6	1.35	C4-C5-C6	136.	C5	-0.107
C6-C1	1.43	C5-C6-C1	101.	C6	0.024

Table I-27 (continued)

Benzene Ring 3

$-0.17196x + -0.36379y + 0.91547z + 4.50579 = 0.0$[a]

Standard Deviation = 0.130[b]

Bond	Distances/A	Bond Angles/degrees		Atom	Shift/A[c]
C1-C2	1.16	C6-C1-C2	96.	C1	-0.144
C2-C3	1.50	C1-C2-C3	130.	C2	-0.107
C3-C4	1.76	C2-C3-C4	105.	C3	0.073
C4-C5	0.86	C3-C4-C5	132.	C4	0.018
C5-C6	1.31	C4-C5-C6	122.	C5	0.046
C6-C1	1.24	C5-C6-C1	127.	C6	0.109

Benzene Ring 3'

$-0.01968x + -0.62582y + 0.77972z + 5.16131 = 0.0$[a]

Standard Deviation = 0.092[b]

Bond	Distances/A	Bond Angles/degrees		Atom	Shift/A[c]
C1-C2	1.90	C6-C1-C2	- .	C1	0.045
C2-C3	0.87	C1-C2-C3	- .	C2	0.090
C3-C4	1.48	C2-C3-C4	98.	C3	0.040
C4-C5	1.73	C3-C4-C5	129.	C4	-0.103
C5-C6	1.60	C4-C5-C6	130.	C5	-0.018
C6-C1	1.27	C5-C6-C1	- .	C6	-0.054

PART II. $[\{Pt_2(\mu\text{-dppm})_2Cl\}_2(di\text{-}(\eta^2)\text{-}P_4)]^{2+}$, AN EXAMPLE OF $di\text{-}(\eta^2)\text{-}P_4$ COORDINATION

INTRODUCTION

The synthesis, characterization, and reactivity of $[[Pt_2(\mu\text{-dppm})_2Cl]_2\{di\text{-}(\eta^2)\text{-}P_4\}]^{2+}$ (also represented by $[Cl\text{--}P_4\text{--}Cl]^{2+}$) will now be reported. It consists of a dimer of Pt(I) dimers bridged in an η^2 fashion by molecular tetra-phosphorus. More cursory evidence for the existence of "monomeric" $[Pt_2(\mu\text{-dppm})_2Cl(\eta^2\text{-}P_4)]^+$ will also be reported.

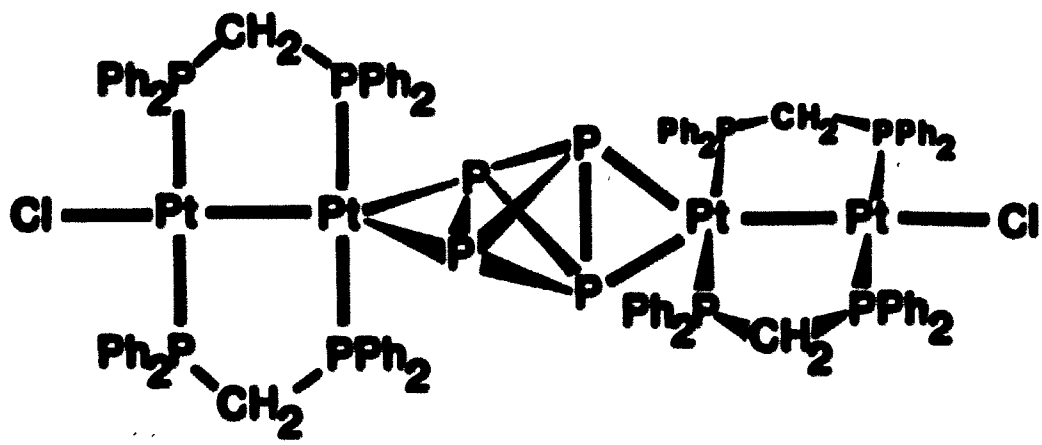

$[Cl\text{—}P_4\text{—}Cl]^{2+}$

Transition metal coordination complexes containing intact molecular tetra-phosphorus (P_4) are relatively rare. In 1971, Ginsberg et al.[1,2] reported the first P_4 containing complexes: $[M(P_4)(EAr_3)_2X]$ (M = Rh, E = P, Ar = Ph, m- or p-tolyl, X =Cl, Br, I; M = Rh, E = As, Ar =Ph, X = Cl; M = Ir, E = P, Ar = Ph, X = Cl). A complex representative of this series, $[Rh(P_4)(PPh_3)_2Cl]$ (also designated $Rh(\eta^2\text{-}P_4)$), has

recently been shown to contain η^2-P_4 by both ^{31}P NMR spectroscopy[3] and X-ray crystallography.[4] The metal-bonded P-P edge is perpendicular to the coordination plane of the rhodium, analogous to the η^2-alkenes which also bond perpendicularly in square-planar ML_3(alkene) complexes.

A further synthesis of a P_4-containing complex was reported in 1977 by Schmid and Kempny.[5] They were able to characterize the thermally unstable $[\{Fe(CO)_4\}_3P_4]$ obtained from the reaction of P_4 with $Fe_2(CO)_9$ (equation 18), but were unable to determine its mode of Fe-P_4 bonding. In the more recently characterized $[M\{N(CH_2CH_2PPh_2)_3\}P_4]$ (M = Ni, Pd) complexes (designated $M(\eta^1\text{-}P_4)$),[6] the P_4 tetrahedron is η^1- instead of η^2-coordinated to the metal.

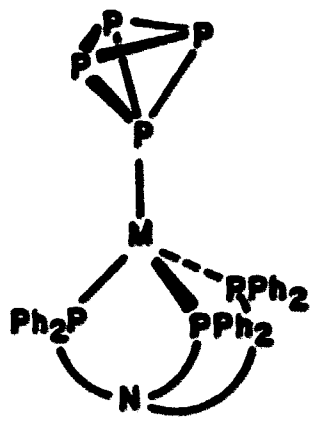

$M(\eta^1\text{-}P_4)$

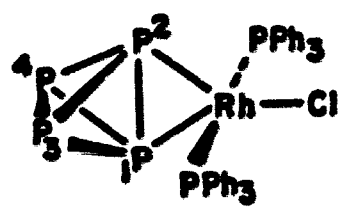

$Rh(\eta^2\text{-}P_4)$

The paucity of metal complexes containing an intact P_4

cage may be due, in part, to the propensity of several such complexes to induce fragmentation of molecular P_4. For example, $[\{Fe(CO)_4\}_3P_4]$ decomposes thermally to a polymer formulated as $[\{Fe(CO)_2\}P_2]_n$:[5]

$$[Fe_2(CO)_9] \xrightarrow{P_4} [\{Fe(CO)_4\}_3P_4] \xrightarrow{\Delta} [\{Fe(CO)_2\}P_2]_n \quad (1)$$

Also, a number of η^3-P_3-ML_3 and L_3M-(η^3-P_3)-ML_3 compounds have been synthesized by reaction of white phosphorus with a transition metal complex:[7]

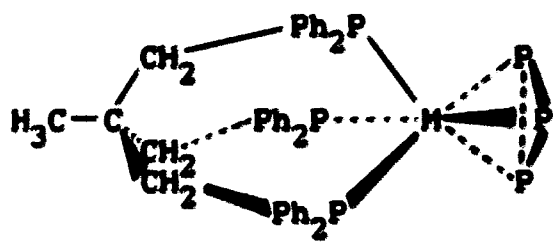

$[\eta^3\text{-}P_3\text{-}ML_3]$

where L_3 = $MeC(CH_2PPh_2)_3$

Another example of the ease of P_4 fragmentation is the reaction of $[Mo(\eta^5\text{-}C_5H_5)_2H_2]$ with P_4 at 90 °C, which yields a molybdenum complex of simple phosphene (H-P=P-H), $[Mo(\eta^5\text{-}C_5H_5)_2(\eta^2\text{-}P_2H_2)]$:[8]

(2)

Cp = η^5-C_5H_5

Finally, reaction of P_4 with $Co(BF_4)_2*6H_2O$ and dppm yields a very unique complex, $[Co(Ph_2PCH_2PPh_2\text{-}PPPP\text{-}Ph_2PCH_2PPh_2)]BF_4$, which contains an unusual zigzag-type tetra-phosphorus fragment. This complex apparently arises from a P_4 molecule which has been induced to rearrange to a linear P_4 chain by two dppm ligands:[9]

o = P from P_4 fragment; o = P from dppm

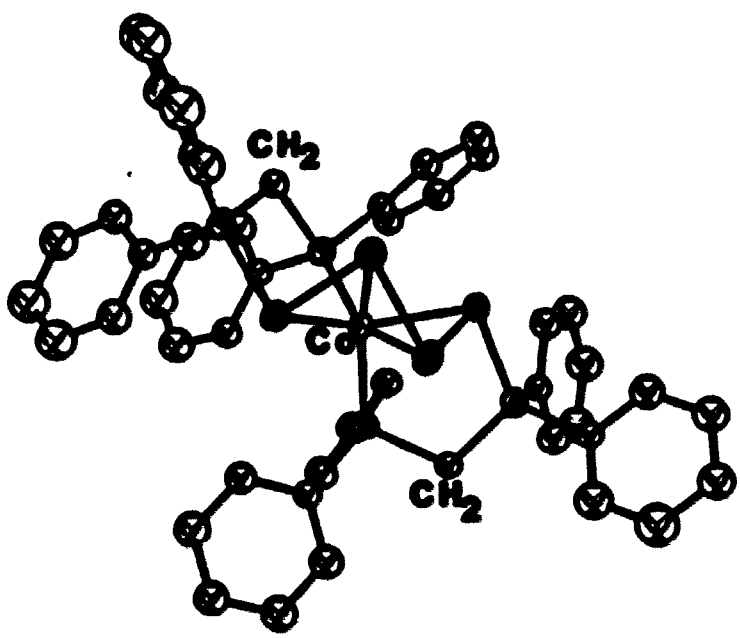

$[Co(Ph_2PCH_2PPh_2\text{-}PPPP\text{-}Ph_2PCH_2PPh_2)]^+$

Transition metal clusters formed by P_4 fragmentation can also be synthesized. For example, the first reported organometallic complex containing a naked phophorus atom as a ligand, $[Co(\eta^5\text{-}C_5H_5)P]_4$, was synthesized from P_4 and $Co(\eta^5\text{-}C_5H_5)(CO)_2$ in refluxing toluene:[10]

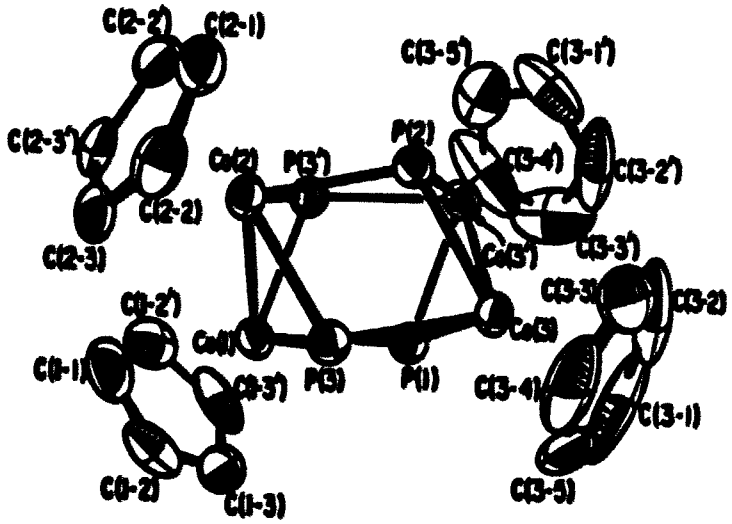

$[Co(\eta^4\text{-}C_5H_5)P]_4$

Very recently, a series of tetrahedral clusters, $P_n[Mo(CO)_2(\eta^5\text{-}C_5H_5)]_{4-n}$ (n = 2, 3), were synthesized from the reaction of $[(\eta^5\text{-}C_5H_5)(CO)_2Mo{\equiv}Mo(CO)_2(\eta^5\text{-}C_5H_5)]$ with P_4.[11] Another series of tetrahedral clusters, $P_n[Co(CO)_3]_{4-n}$ (n = 1, 2, 3), was synthesized from the reaction of P_4 with $Co_2(CO)_8$.[12] In the Mo and Co series of clusters, the metal and phosphorus atoms are situated at the corners of a somewhat distorted tetrahedron, thus resembling the structure of the parent molecular phosphorus.

Theoretical calculations on the relative stability of various modes of metal-P_4 bonding have been conducted.[13] In particular, EHMO calculations[14] on trans-$[Rh(P_4)(PH_3)_2Cl]$

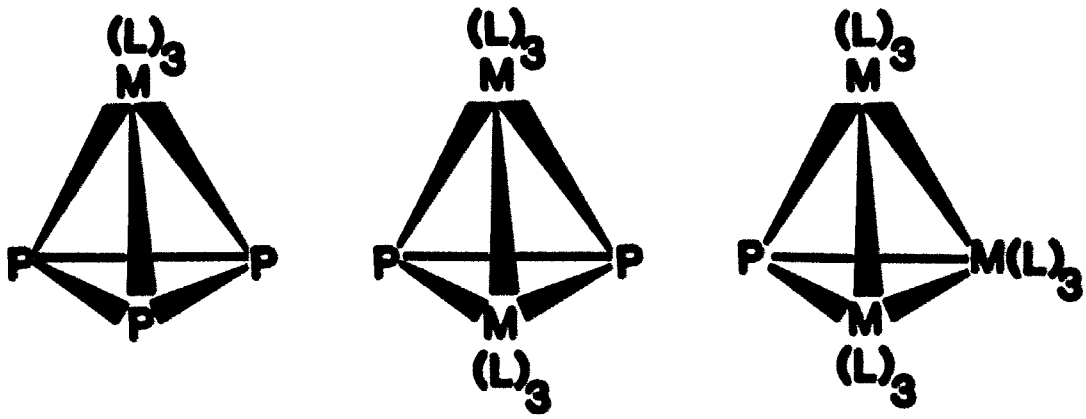

n=3 n=2 n=1

$$P_n[M(L)_3]_{4-n}$$

show that, with respect to the coordination plane of the Rh, the perpendicular conformation of the η^2-bonded P_4 ligand is favored with respect to the parallel conformation because of increased π bonding in the former. Furthermore, computed overlap populations for the η^2-perpendicular model successfully reproduce the observed weakening of the P-P bond adjacent to Rh that belongs to the (η^2-P_4) unit in trans-[Rh(η^2-P_4)(PPh_3)$_2$Cl] (P_1-P_2 in its structure on page 200). The authors[3] noted that since the opposite tetrahedral edge (P_3-P_4) is not substantially altered upon complex formation, complexes with di-(η^2)-P_4 ligands might be feasible. This prediction was realized in the synthesis and characterization

of $[\{Pt_2(\mu\text{-dppm})_2Cl\}_2\{di\text{-}\eta^2\text{-}P_4\}]^{2+}$ described below. The latter complex was synthesized from the reaction of $[Pt_2(\mu\text{-dppm})_2Cl_2]$ ([Cl--Cl]) with P_4 in methanol; other products containing P_4 or P_4 fragments are obtained from their reaction under different conditions. Although these have not been fully characterized, evidence for their existence will also be presented.

RESULTS AND DISCUSSION

Characterization of $[\{Pt_2(\mu\text{-dppm})_2Cl\}_2\{di\text{-}(\eta^2)\text{-}P_4\}]^{2+}$

Thermal decomposition

When $[Cl\text{--}P_4\text{--}Cl](PF_6)_2$ is heated, a slight change in its consistency occurs at 135 ± 5 °C along with the evolution of a P_4-like odor. At about 205 °C, the altered solid melts with apparent decomposition.

Variable temperature mass spectrometry confirmed the two-phase decomposition. At intermediate temperatures, peaks characteristic of P_4 were of importance (m/e {relative intensity} = 124 {1.00}, 93 {0.06}, 62 {0.09}). These two observations: (a) the molecular ion peak of P_4 (m/e = 124) is by far the most important P_4 related peak in intermediate temperature mass spectra, and (b) P_4 is evolved with only moderate heating; suggest that intact molecular P_4 is a component of the $[Cl\text{--}P_4\text{--}Cl]^{2+}$ complex. If the complex contained an η^3-P_3 group such as in $[\{Pt_2(\mu\text{-dppm})_2Cl\}_2(\eta^3\text{-}P_3)](PF_6)_2$, one might expect a larger yield of mass number 93 (equivalent to the molecular wieght of P_3).

At higher temperatures, peaks characteristic of dppm were evident. Notable among these are the molecular ion at 384 amu, and the peak corresponding to the molecular ion of PPh_3 (262 amu).

Molecular weight determination

Molecular weights for [Cl--Cl], $[PPh_3--PPh_3](PF_6)_2$, and $[Cl--P_4--Cl](PF_6)_2$ were determined in CH_2Cl_2 solutions using vapor pressure osmometry (Table II-2 in the experimental section). Experimentally determined molecular weights for the well-characterized [Cl--Cl] and $[PPh_3--PPh_3](PF_6)_2$ were relatively close to their theoretical values thus suggesting that credibile molecular weights for the structurally related $[Cl--P_4--Cl](PF_6)_2$ are possible using this technique. Values for ionic $[PPh_3--PPh_3](PF_6)_2$ deviated from the theoretical towards smaller molecular weights with decreasing concentration of complex. This is characteristic of either ligand and/or ion pair dissociation which become more important at lower concentrations and which lower the average molecular weight of particles in solution. A similar trend was also found in molecular weight readings for the ionic $[Cl--P_4--Cl](PF_6)_2$. Values for the three highest concentrations of $[Cl--P_4--Cl]^{2+}$ average to 2750 ± 31 g/mol; this is only 2 % below its actual molecular weight and is definitive evidence supporting the presence of two $Pt_2(\mu\text{-dppm})_2$ units in the complex.

Characterization by ^{31}P NMR spectroscopy

The ^{31}P NMR spectrum of $[Cl--P_4--Cl]^{2+}$ is indicative of the four P_4 phosphorus nuclei being symmetry related and bound in a di-η^2 fashion. It also suggests dppm ligands bridging

two symmetrically inequivalent platinums.

General Characterization The two dppm resonances found at 4.2 and -6.5 ppm respectively (Figure II-1), are indicative of asymmetrical substitution at the terminal positions of the two symmetrically equivalent platinum dimers in $[Cl--P_4--Cl]^{2+}$ (this complex basically has D_{2d} symmetry similar to Al_2Cl_6; the two $Pt_2(\mu\text{-dppm})_2$ planes are mutually perpendicular: see the drawing on page 199). The $^1J(Pt,P)$ coupling constants of 2600 to 2700 Hz are normal for $Pt_2(\mu\text{-dppm})_2$ complexes. The resonances are positioned such that one of the satellites from each resonance is buried underneath the central resonance of the other.

Each pair of equivalent dppm phosphorus nuclei is coupled to the other yielding the triplet structure (doublet of doublets) found for each resonance ($^2J(P_A,P_R) \approx {}^3J(P_A,P_{R'}) \approx$ 38 Hz; see page 62 for example of this notation). The peaks in the resonance centered at 4.2 ppm are broadened relative to those at -6.5 ppm by small coupling to the P_4 group in the former. On this basis, the downfield resonance (4.2 ppm) is assigned to the dppm phosphorus nuclei adjacent to P_4. In all $[X--PR_3]^+$ complexes studied to date, the dppm phosphorus nuclei adjacent to a terminal phosphorus donor have resonances downfield from those due to the dppm phosphorus adjacent to the terminal halide (e.g., Figures I-2, I-21, and I-41).

The resonance due to P_4 (Figure II-1) consists of a single

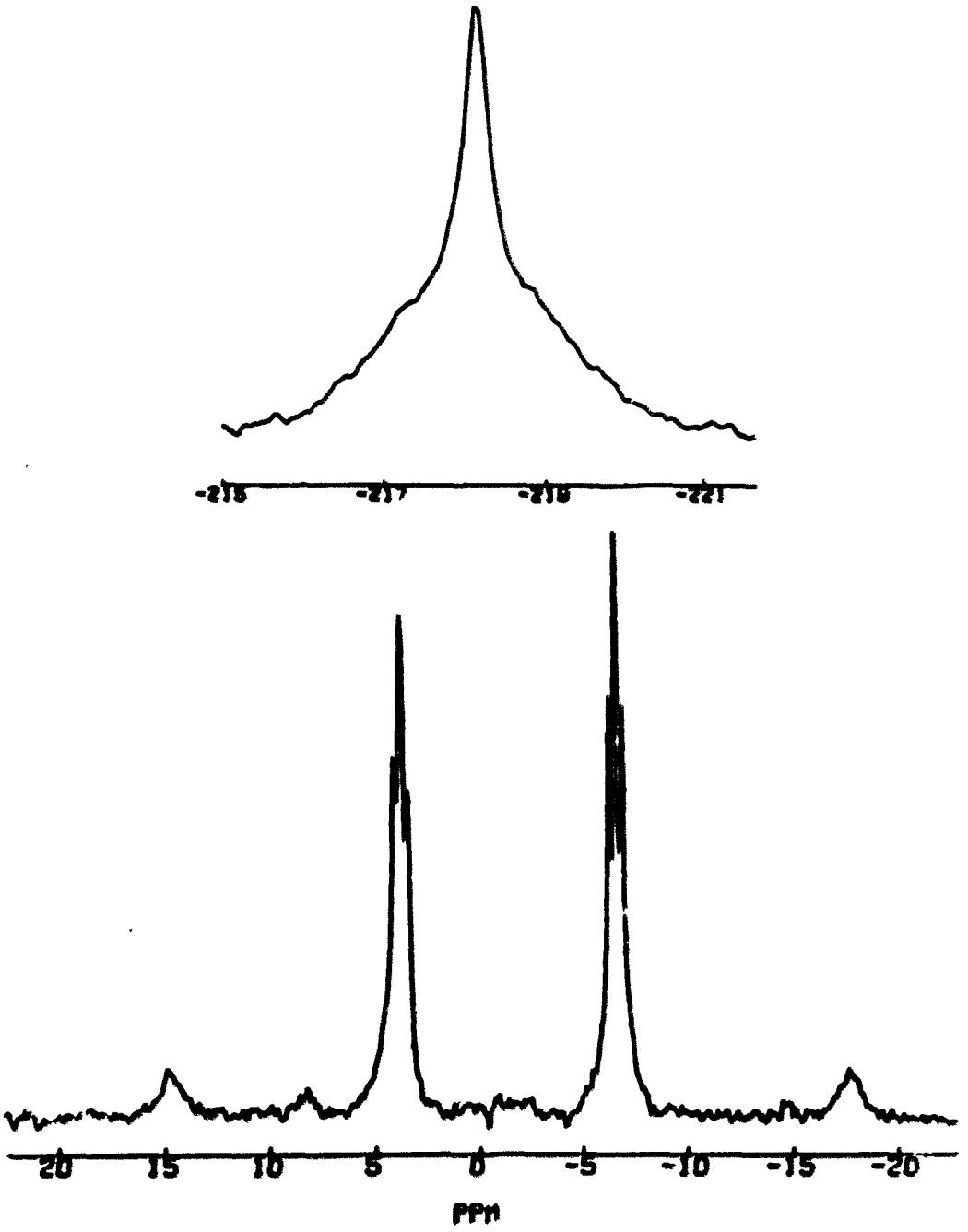

Figure II-1. The $^{31}P\{^{1}H\}$ NMR (121.5 MHz) spectrum in CD_2Cl_2 of $[\{Pt_2(\mu\text{-dppm})_2Cl\}_2(di\text{-}\eta^2\text{-}P_4)]^{2+}$; top: P_4 resonance; bottom: dppm resonances

peak with relatively broad, unresolved ^{195}Pt satellites at its base. It is interesting to note that the chemical shift for free P_4 in 4 CD_2Cl_2 : 1 benzene is -522 ppm compared to chemical shifts of -279.4 and -284.0 ppm for η^2-P_4 in $Rh(\eta 2\text{-}P_4)(CD_2Cl_2)$,[3] and -218 ppm for di-η^2-P_4 in $[Cl\text{--}P_4\text{--}Cl]^{2+}$. Increased coordination of P_4 to transition metals shifts its resonances to lower field.

The broadening of the latter resonance and its satellites is not due to fluxionality since no sharpening (or further broadening) of the resonance was observed even down to temperatures as low as -85 ^{o}C. This precludes a structure containing, for example, (di-η^1-P_4), $[\{Pt_2(\mu\text{-dppm})_2Cl\}_2$-(di-$\eta^1$-$P_4$)], with <u>two pair</u> of equivalent P_4 phosphorus (complexed and free) that are rapidly interchanging to yield one effective P_4 signal. As with the dppm resonance at 4.2 ppm, the P_4 resonance is broadened by small and thus unresolved coupling between P_A and P_4 type nuclei.

<u>Comparison of (di-η^2-P_4) and (η^3-P_3) models</u> The existence of ^{195}Pt satellites for the P_4 resonance is confirmed by the presence of shoulders symmetrically positioned about the central resonance (Figure II-2). Due to the close proximity of four platinum atoms to the P_4 cage, ten isotopomers of this complex are possible (Table II-3). Each isotopomer will have different coupling patterns for the P_4 resonance (Table II-5). Because none have a natural abundance

larger than 20 %, and all but one a natural abundance greater than 5 %; most of the isotopomers will make a significant contribution to the total spectrum. Using a computer program for curve analysis and peak deconvolution (NMRCAP), the best fit of the P_4 resonance was obtained using a model for $[Cl{-}{-}P_4{-}{-}Cl]^{2+}$ with $^2J(Pt_A,P_{R''})$ = 70 ± 10 Hz, $^2J(Pt_R,P_{A''})$ = 130 ± 15 Hz, and $^1J(Pt_A,P_{A''})$ = 180 ± 10 Hz. A fit using a model for the hypothetical $[\{Pt_2(\mu\text{-dppm})_2Cl\}_2(\eta^3\text{-}P_3)]^{2+}$ was less satisfactory (Figure II-2; see the experimental section for details).

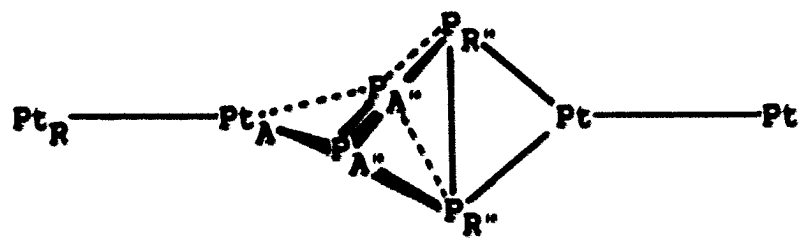

This η^3-P_3 model fits ^{31}P NMR data for other compounds quite nicely. For example, η^3-P_3 ^{31}P NMR resonances are found in the region around that of this P_4 resonance at -218 ppm (e.g., -217 ppm for $[(triphos)Pt(\eta^3\text{-}P_3)]^+$, -133 ppm for $[(triphos)Pd(\eta^3\text{-}P_3)]^+$, and -334 ppm for $[\{(triphos)Pd\}_2(\eta^3\text{-}P_3)]^+$;[6b] triphos = $\{Ph_2PCH_2\}_3CCH_3$) and coupling constants between platinum and η^3-P_3 are in the correct range (e.g., $^1J(Pt,P_3)$ = 171 Hz for $[(triphos)Pt(\eta^3\text{-}P_3)]^+$[6b] compared to $^1J(Pt_A,P_{A''})$ = 180 ± 10 Hz for $[Cl{-}{-}P_4{-}{-}Cl]^{2+}$). The three P_3 phosphorus in the proposed η^3-P_3 complex would also be

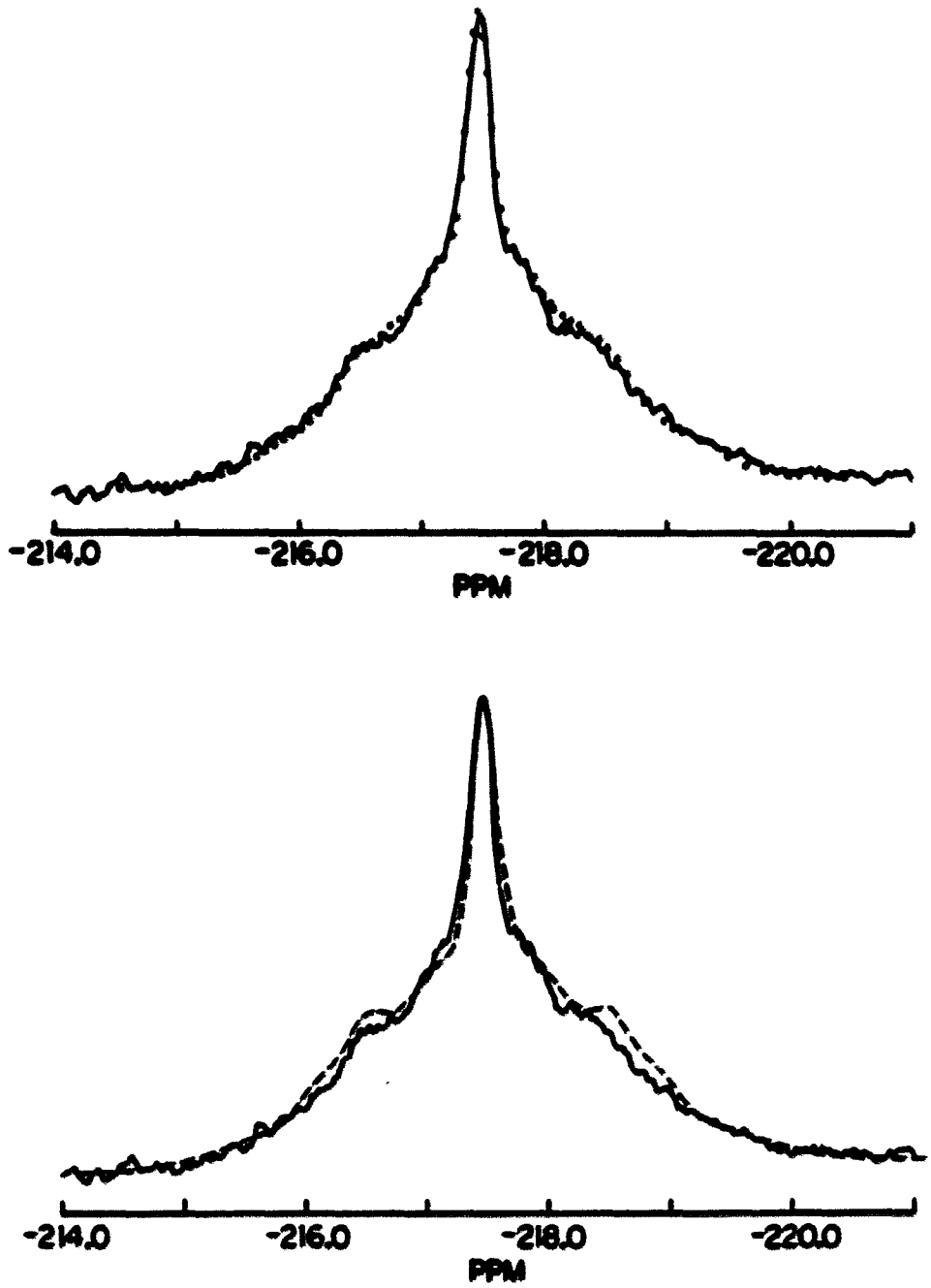

Figure II-2. Calculated and experimental curves for the P_4 resonance of $[\{Pt_2(\mu\text{-dppm})_2Cl\}_2(di\text{-}\eta^2\text{-}P_4)]^{2+}$; experimental (——); $di\text{-}\eta^2\text{-}P_4$ model (...); $\eta^3\text{-}P_4$ model (---)

symmetry-related, thus yielding the observed singlet central resonance. Unfortunately, vapor pressure osmometry data are insufficiently accurate to differentiate between η^3-P_3 and di-η^2-P_4 groups and attempts to grow single crystals, much less solve such a complicated structure (128 nonhydrogen atoms) have not, as of yet, reached fruition. However, besides the poorer fit of the -218 ppm resonance by the curve calculated for the η^3-P_3 model relative to that for the di-η^2-P_4 model (Figure II-2), other data support the latter over the former: (a) Mass spectral and thermal decomposition data suggest the presence of a P_4 unit in the complex. (b) Whereas the η^3-P_3 complexes of Pt and Pd are thermally stable in solution and can exist in weakly coordinating solvents (i.e., acetone)[6b], $[Cl{-}{-}P_4{-}{-}Cl]^{2+}$ is not, and very readily decomposes in acetone (discussed on page 226). Although the two proposed structures fit the data equally well on some counts, the di-η^2-P_4 model fits the data where the η^3-P_3 model falls short.

η^2 vs. η^1 bonding of P_4 The small values for the Pt-P_4 coupling constants support η^2 over η^1 bonding. For example, the $^1J(Pt_A,P_{A''})$ of 180 Hz and the $^2J(Pt_R,P_{A''})$ of 130 Hz in $[Cl{-}{-}P_4{-}{-}Cl]^{2+}$ are more than an order of magnitude smaller than $^nJ(M,P)$ for σ-bound phosphorus donors[15] (e.g., No. 1-6 in Table II-1 and $^2J(Pt_R,P_T)$ = 1232 Hz for $[Cl{-}{-}PPh_3]^+$). However, this $^1J(Pt_A,P_{A''})$ for $[Cl{-}{-}P_4{-}{-}Cl]^{2+}$ is in the same

Table II-1. Selected one-bond metal ligand coupling constants

No.	Complex	Ligand	$^1J(M,L)$/Hz
1	$[Cl{-}{-}P_4{-}{-}Cl]^{2+}$	$(di\text{-}\eta^2\text{-}P_4)$	180
2	$[Cl{-}{-}PPh_3]^{+}$	PPh_3	2186
3	$t\text{-}[RhL_2Cl(\eta^2\text{-}P_4)]$[a]	$(\eta^2\text{-}P_4)$	34
4	$[RhL_2Cl(PPh_3)]$[b]	PPh_3 trans to Cl^-	189
5	$[(triphos)Pt(\eta^3\text{-}P_3)]^{+}$[c]	$(\eta^3\text{-}P_3)$	138
	"	triphos	2476
6	$[(triphos)Rh(\eta^3\text{-}P_4)]$[c]	$(\eta^3\text{-}P_3)$	13
	"	triphos	171
7	$t\text{-}[PtL_2(CH_2{=}CH_2)Me]$[d]	$CH_2{=}CH_2$	50
	"	Me	615
8	$t\text{-}[PtL_2(CH{\equiv}CH)Me]$[d]	$CH{\equiv}CH$	18
	"	Me	632
9	$t\text{-}[PtL_2(CO)Me]$[e]	CO	1000
	"	Me	476
10	$t\text{-}[PtL_2\{C(OMe)Me\}Me]$[e]	$\{C(OMe)Me\}$	759
	"	Me	360

[a] L = PPh_3; see ref. 3.

[b] L = PPh_3; see ref. 15.

[c] See ref. 7b.

[d] L = PMe_2Ph; see ref. 16.

[e] L = $AsMe_3$; see ref. 17.

relative range as coupling constants between metals and π-bound phosphorus donors (see No. 1,3,5,6 in Table II-1). A large differential between $^{1}J(M,C)$ for π vs. σ bound carbon has also been noted, (No. 7-8[16] in Table II-1). Generally speaking, A-B coupling constants increase in magnitude with increasing "s" character in the corresponding A-B bonds. For example, in organoplatinum complexes,[17] as the hybridization of carbon bound to platinum changes from sp (-CO) through sp^2 ($-C(OCH_3)CH_3$) to sp^3 ($-CH_3$), $^{1}J(Pt,C)$ values decrease from 1000 Hz to 360 Hz (No. 9-10 in Table II-1). These correlations have been attributed to the contribution of the Fermi contact term to scalar spin-spin coupling.[18]

Bonding in the P_4 cage is basically achieved through a set of four sp hybridized orbitals pointing towards the center of the cage (radial orbitals), a set of 8 atomic p orbitals used in tangential bonding, and a set of 4 sp hybrid orbitals pointing away from the cage (lone pairs). Recent calculations for square planar $Rh(\eta^2\text{-}P_4)$ complexes suggest that P_4 molecular orbitals involved in $M(\eta^2\text{-}P_4)$ bonding are primarily of the tangential, and to a lesser extent, the lone pair type.[4,13] Other calculations suggest that the P_4 molecular orbitals cited[4,13] to be most intimately involved in this $M(\eta^2\text{-}P_4)$ bonding (in T_d symmetry: 5_{a1}, 6_{t2}, 2_e, and 2_{t1}^*), are predominantly "p" in character with an average of 7 % "s" character per molecular orbital (calculated for P_4 in an

unperturbed tetrahedral geometry).[19] Thus, little or no "s" character is found in P_4 molecular orbitals donating (or receiving) electron density to (or from) the metal. This is consistent with the very small Pt-P coupling constants observed for these types of complexes. A M(η^1-P_4) complex should have large ^1J(M,P) coupling constants because P_4 lone pairs are rich in "s" character. Unfortunately, ^{31}P NMR data have not been reported for known M(η^1-P_4) complexes reported thus far.[6]

Characterization by ^1H NMR spectroscopy

The ^1H NMR spectrum of $[Cl{-}{-}P_4{-}{-}Cl]^{2+}$ (Figure II-3) is very similar to that of $[Cl{-}{-}PPh_3]^+$ at ambient temperature (compare Figure I-11, page 47): a very broad range of phenyl resonances are observed, and the two respective axial and equatorial PCH_2P resonances are superimposed upon each other (compare Figure I-10b page 46). Apparently, axial-equatorial interchange of substituents on the two $Pt_2(\mu\text{-dppm})_2$ rings in $[Cl{-}{-}P_4{-}{-}Cl]^{2+}$ is slow on the NMR time scale at ambient temperature as it is for $[Cl{-}{-}PPh_3]^+$ (described on pages 44 to 58). This is not surprising since there are considerable phenyl-phenyl repulsions between the two sets of four dppm phenyls adjacent to the P_4 cage in the former complex (see model on page 199).

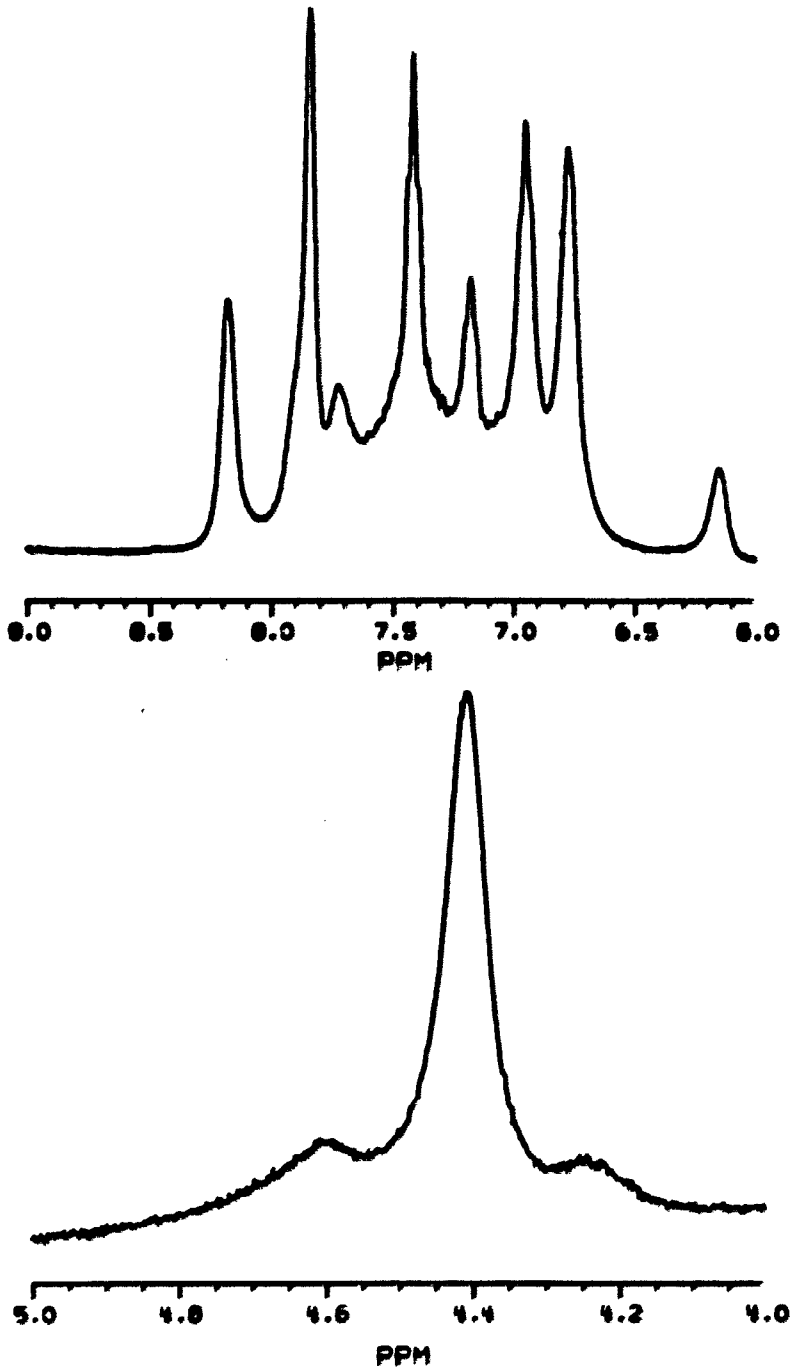

Figure II-3. The ^{1}H NMR spectrum (300 MHz) in CD_2Cl_2 of $[\{Pt_2(\mu\text{-dppm})_2Cl\}_2(di\text{-}\eta^2\text{-}P_4)]^{2+}$; top: the phenyl region; bottom: the PCH_2P region

Synthesis and Reactivity of Pt(I) Complexes of P_4

Comparisons of P_4 complexes with their PPh_3 models

Similarities between the reactions of PPh_3 and those of P_4 with [Cl--Cl] will now be discussed as will similarities in the reactivity of their respective products.

The products of the reaction of [Cl--Cl] with PPh_3 vary with the identity of the solvent; $[Cl--PPh_3]^+$ is formed in CH_2Cl_2, whereas $[PPh_3--PPh_3]^{2+}$ is the major product at high $[Pt_2]_{tot}$ concentrations in methanol. The products of the reaction of [Cl--Cl] with P_4 also vary with the identity of the solvent, and with the concentration of reagents present in solution: $[Cl--P_4--Cl]^{2+}$ is the major product at high $[Pt_2]_{tot}$ concentrations in methanol and, analogous to $[Cl--PPh_3]^+$ in the PPh_3 system, it is proposed that the monocationic $[Pt_2(\mu\text{-dppm})_2Cl(\eta^2\text{-}P_4)]^+$ ($[Cl--\eta^2\text{-}P_4]^+$) is the product of the reaction in CH_2Cl_2. Attempts to isolate the latter complex in a pure form have failed thus far because of its thermal instability. However, its ^{31}P NMR spectra, although of poor quality due to the presence of extraneous resonances, is consistent with this formulation (discussed on page 224).

When 0.75 eq of P_4 (2 to 8 mM) reacts with [Cl--Cl] in methanol, $[Cl--P_4--Cl]^{2+}$ is formed:

$$2[Cl--Cl] + P_4 \xrightarrow[\text{room temp.}]{\text{methanol}} [Cl--P_4--Cl]^{2+} + 2Cl^- \qquad (3)$$

It is readily characterized by a very sharp peak in its UV-VIS spectrum at 366 nm (ε = 4.7 x 10^4 $M^{-1}cm^{-1}$; see Figure II-4). If the product solution (6 mM) is diluted 600 fold by methanol (0.01 mM), the 366 nm peak disappears with a half life of two to three minutes yielding a featureless spectrum (Figure II-5). $[Cl{-}{-}P_4{-}{-}Cl]^{2+}$ could be in equilibrium with two or more smaller fragments (e.g., $[Cl{-}{-}\eta^2{-}P_4]^+$ and [Cl--Cl]):

$$[Cl{-}{-}P_4{-}{-}Cl]^{2+}\star(2Cl^-) \xrightleftharpoons{\text{methanol}} [Cl{-}{-}\eta^2{-}P_4]^+\star(Cl^-) + [Cl{-}{-}Cl] \quad (4)$$

At high concentrations, the proposed equilibrium favors $[Cl{-}{-}P_4{-}{-}Cl]^{2+}$ over its fragments, whereas, at lower concentrations, fragment formation is favored. The fragments are less absorbing than their parent and probably undergo further reaction.

A similar equilibrium involving $[PPh_3{-}{-}PPh_3]^{2+}$ in methanol is observed:

$$[PPh_3{-}{-}PPh_3]^{2+}\star(2Cl^-) \xrightleftharpoons{\text{methanol}} [Cl{-}{-}PPh_3]^+\star(Cl^-) + PPh_3 \quad (5)$$

Under conditions of $[PPh_3{-}{-}PPh_3]^{2+}$ synthesis (reaction of 0.012 mM [Cl--Cl] with 0.048 mM PPh_3), a mixture of $[PPh_3{-}{-}PPh_3]^{2+}$ and $[PPh_3{-}{-}Cl]^+$ appear to be present. However, upon dilution by methanol to 0.02 mM $[Pt_2]_{tot}$, absorbance generally decreases over a period of minutes ultimately

Figure II-4. UV-VIS spectra in CH_2Cl_2 (2 cm cell) of 0.02 mM $[(Pt_2(\mu\text{-dppm})_2Cl)_2(di\text{-}\eta^2\text{-}P_4)]^{2+}$ (upper) with $\varepsilon_{366} = 4.75 \times 10^4\ M^{-1}\ cm^{-1}$, and the products (lower) of its reaction with 0.03 mM $[NEt_4]Cl$

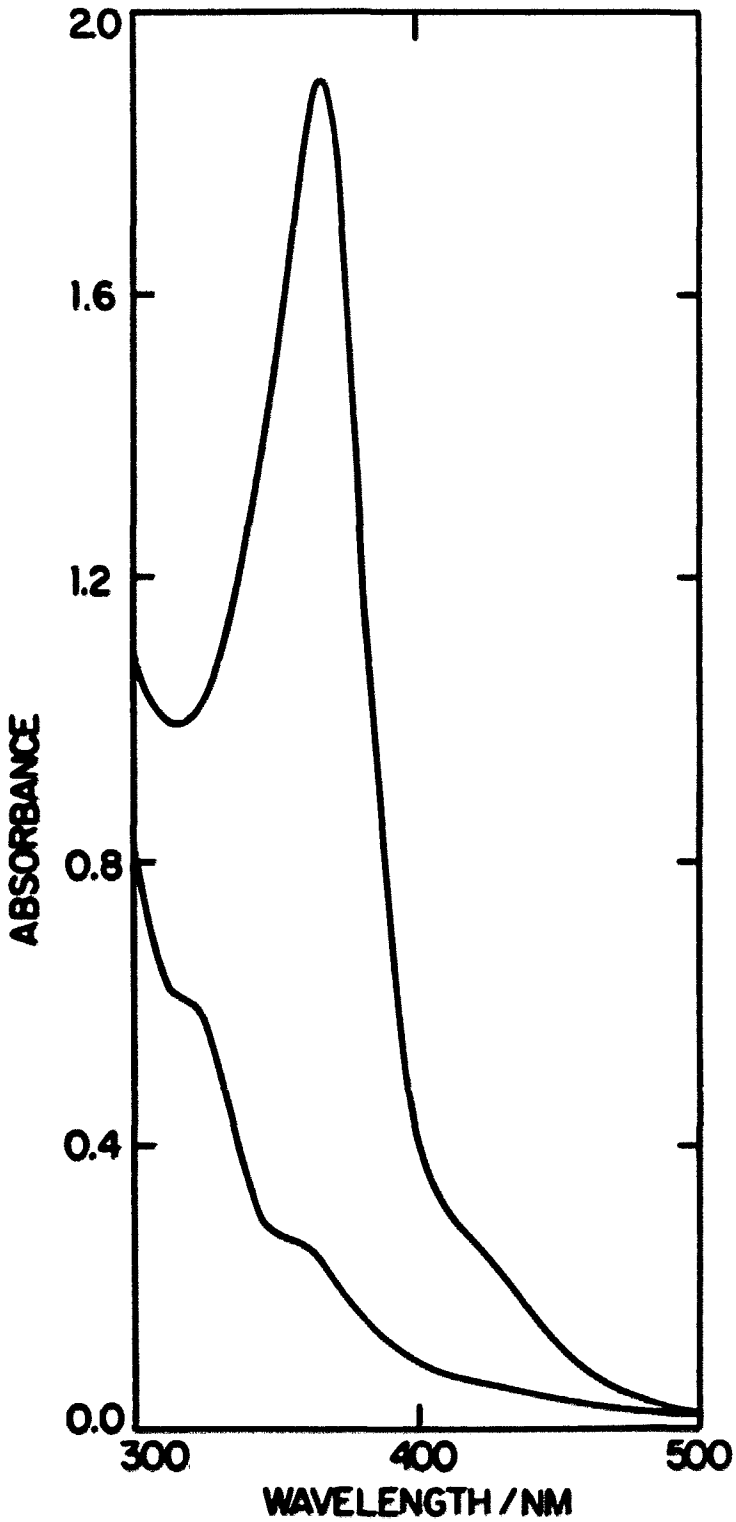
2.0
1.6
1.2
0.8
0.4
0.0
ABSORBANCE
300
400
500
WAVELENGTH / NM

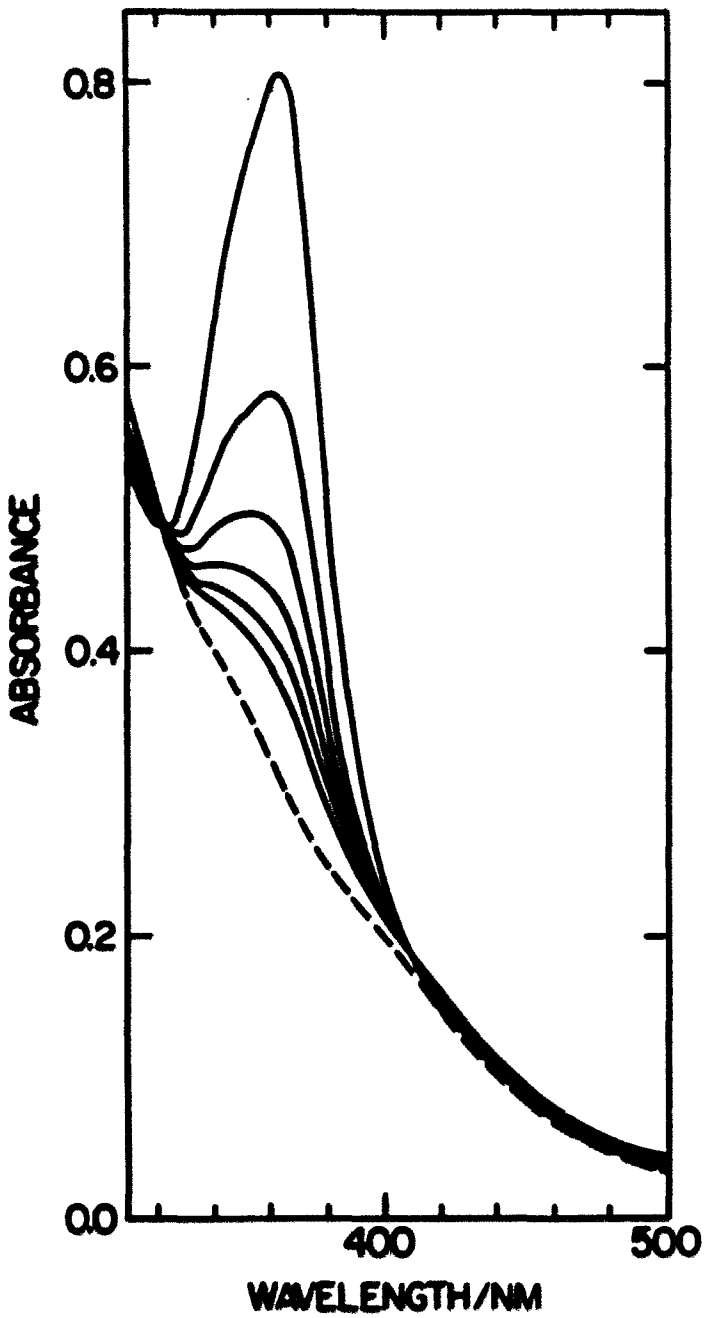

Figure II-5. UV-VIS spectral scans (every 2 min; 2 cm cell) of the mother liquor, diluted 600 fold by methanol, from the reaction (in methanol) of 0.75 eq. P_4 with 1 eq. $[Pt_2(\mu\text{-dppm})Cl_2]$ forming ~6 mM $[\{Pt_2(\mu\text{-dppm})_2Cl\}_2(di\text{-}\eta^2\text{-}P_4)]^{2+}$; the dashed spectrum is at $t = \infty$

forming the 372 nm shoulder characteristic of $[Cl{-}{-}PPh_3]^+$, which is then the only Pt(I) species present (Figure II-6).

There are also several parallels between the reactivity of $[PPh_3{-}{-}PPh_3]^{2+}$ and $[Cl{-}{-}P_4{-}{-}Cl]^{2+}$ in CH_2Cl_2. Both complexes are stable for hours in the absence of Cl^- even at very low concentrations (0.02 mM). However, as with $[PPh_3{-}{-}PPh_3]^{2+}$, $[Cl{-}{-}P_4{-}{-}Cl]^{2+}$ undergoes rapid and irreversible decomposition when chloride is added:

$$[PPh_3{-}{-}PPh_3]^{2+}\star(2PF_6^-) \underset{\text{x}}{\overset{Cl^-}{\rightleftharpoons}} [Cl{-}{-}PPh_3]^+\star(Cl^-) + PPh_3 \qquad (6)$$

$$[Cl{-}{-}P_4{-}{-}Cl]^{2+}\star(2PF_6^-) \underset{\text{x}}{\overset{Cl^-}{\rightleftharpoons}} [Cl{-}{-}\eta^2{-}P_4]^+\star(Cl^-) + [Cl{-}{-}Cl] \qquad (7)$$

The spectrum of the products of the reaction of <u>chloride</u> with 0.02 mM $[Cl{-}{-}P_4{-}{-}Cl]^{2+}$ has shoulders at 322 and 360 nm (Figure II-4), and is very similar to that obtained after reaction of 0.5 eq of <u>P_4</u> with $[Cl{-}{-}Cl]$ (0.04 mM) in CH_2Cl_2 (Figure II-7). It is very likely that mixtures of $[Cl{-}{-}Cl]$ and $[Cl{-}{-}\eta^2{-}P_4]^+$ are present in the two reaction solutions.

Observations point to an equilibrium between $[Cl{-}{-}\mu{-}P_4]^+(Cl^-)$ and $[Cl{-}{-}Cl]$ similar to that between $[Cl{-}{-}PPh_3]^+$ and $[Cl{-}{-}Cl]$:

$$[Cl{-}{-}Cl] + P_4 \overset{CH_2Cl_2}{\rightleftharpoons} [Cl{-}{-}\eta^2{-}P_4]^+\star(Cl^-) \qquad (8)$$

Figure II-6. (...) UV-VIS spectrum (0.01 cm cell) of the mother liquor, diluted 3.25 fold with methanol, from the reaction (in methanol) of 4 eq. PPh_3 with 1 eq. $[Pt_2(\mu\text{-dppm})_2Cl_2$ to form 12 mM $[Pt_2(\mu\text{-dppm})_2(PPh_3)_2]^{2+}$;
(——) spectral scans (2 min; 2 cm cell) of the same mother liquor but now after 600 fold dilution with methanol;
(---) spectrum at t = ∞ of the reaction after the 600 fold dilution

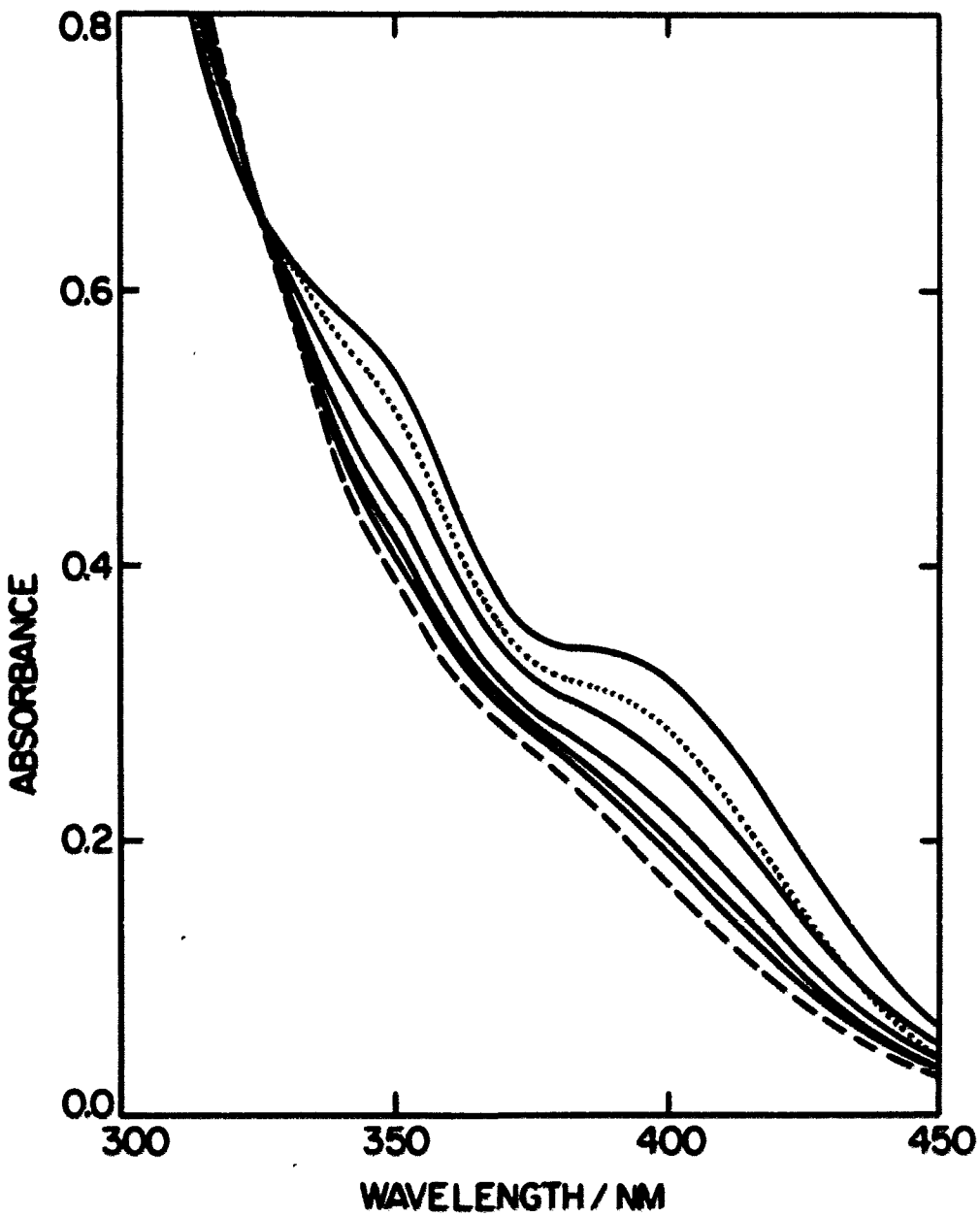
0.8
0.6
0.4
0.2
0.0
ABSORBANCE
300
350
400
450
WAVELENGTH / NM

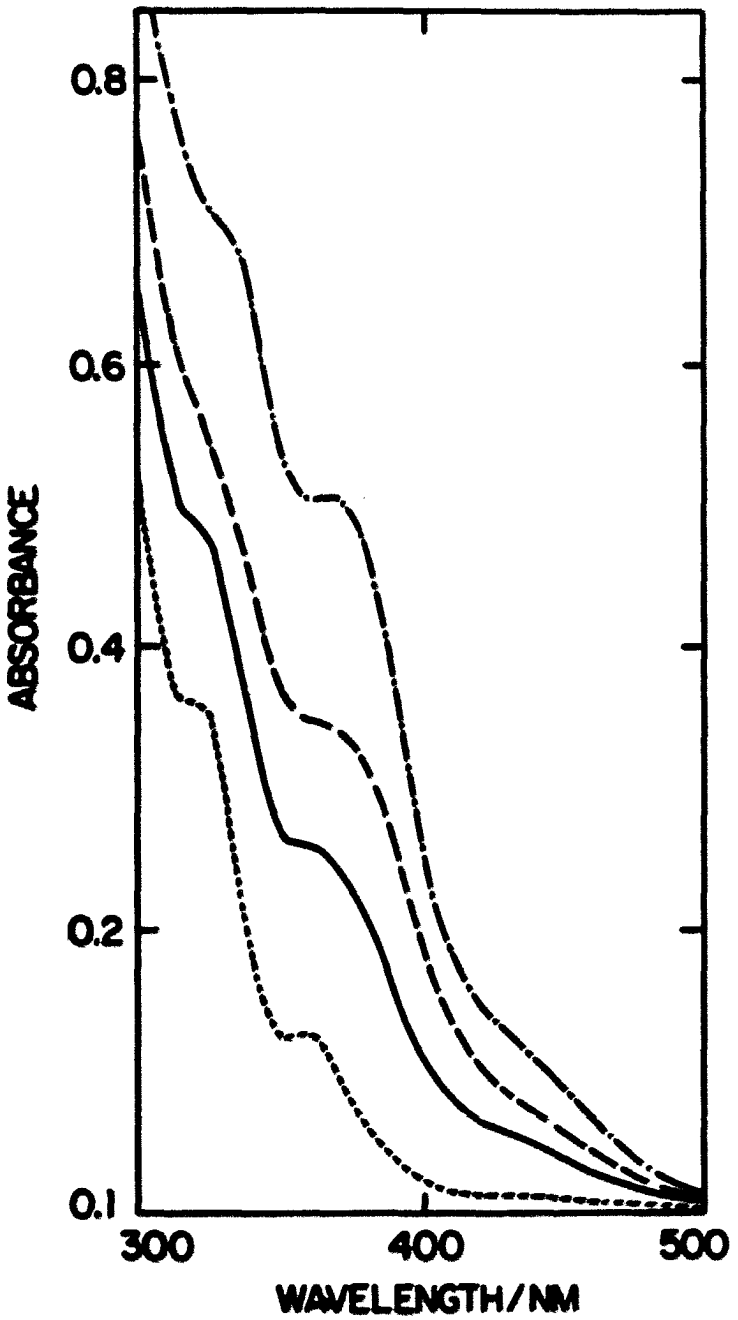

Figure II-7. UV-VIS spectrum (2 cm cell) of the reaction of 0.04 mM [$Pt_2(\mu\text{-dppm})_2Cl_2$] in CH_2Cl_2
(...) immediately after addition of 0.5 eq P_4;
(——) 22 min after addition of 0.5 eq P_4
(---) after addition of 1 eq P_4 (t = ∞);
(_._) after addition of 10 eq P_4 (t = ∞)

$$[Cl{-}{-}Cl] + PPh_3 \overset{CH_2Cl_2}{\rightleftharpoons} [Cl{-}{-}PPh_3]^+ \star (Cl^-) \qquad (9)$$

The reaction of 0.5 eq P_4 with 0.04 mM [Cl--Cl] in CH_2Cl_2 occurs with absorbance increases at all wavelengths. If additional P_4 is added, red shifts in the maxima and additional absorbance increases are observed ultimately yielding a spectrum (10 eq P_4) with a shoulder at 332 nm and a peak at 372 nm (Figure II-7). This final spectrum is almost identical to that of the reaction of only 0.75 eq of P_4 with a solution 100 fold more concentrated (4 mM) in [Cl--Cl] suggesting the presence of equilibrium 8.

By comparing the relative reactivity of monocationic-$[Cl{-}{-}PPh_3]^+$, and dicationic-$[PPh_3{-}{-}PPh_3]^{2+}$ in both methanol and CH_2Cl_2 with that of $[Cl{-}{-}P_4{-}{-}Cl]^{2+}$ and the proposed $[Cl{-}{-}\eta^2\text{-}P_4]^+$, it is evident that the latter complex behaves like the mono-cationic $[Cl{-}{-}PPh_3]^+$ and thus is very likely to have the (1+) charge that is consistent with its formulation. The $^{31}P\{^1H\}$ NMR of this product has two complex multiplets centered at 5 and -2 ppm which have $^1J(Pt,P)$ in the range of 2700 to 2900 Hz consistent with an asymmetrically substituted $Pt(I)(\mu\text{-dppm})_2$ complex. There is also another major multiplet at around -240 to -245 ppm that has a chemical shift similar to other (η^2-P_4) resonances: e.g., -218 ppm in $[Cl{-}{-}P_4{-}{-}Cl]^{2+}$, and -279.4 ppm ($P_1$ and P_2) and -284.0 ppm (P_3 and P_4) in

$[Rh(\eta^2\text{-}P_4)]$. Although not totally definitive, data suggest the existence of $[Pt_2(\mu\text{-dppm})_2Cl(\eta^2\text{-}P_4)]^+$.

General reactivity of $[\{Pt_2(\mu\text{-dppm})_2Cl\}_2(di\text{-}\eta^2\text{-}P_4)]^{2+}$

The PF_6^- salt of $[Cl\text{--}P_4\text{--}Cl]^{2+}$ is stable for weeks as a solid at temperatures below -10 °C. In CH_2Cl_2, it decomposes over a period of hours (-20 to 20 °C) to various products, most of which have not been characterized. Cursory ^{31}P NMR data suggest that, at least in highly concentrated solutions (> 2 mM), one of its major thermolysis products is $[Cl\text{--}\eta^2\text{-}P_4]^+$. Decomposition of both $[Cl\text{--}P_4\text{--}Cl]^{2+}$ and $[Cl\text{--}\eta^2\text{-}P_4]^+$ in CH_2Cl_2 produces other species having complex multiplets in the ^{31}P NMR region between -180 and -280 ppm indicative of P_4 or its fragments. Characterization of these products may provide information about P_4 cage fragmentation or possibly about other modes of P_4 coordination.

$[Cl\text{--}P_4\text{--}Cl]^{2+}$ decomposition in CH_2Cl_2 is not enhanced by the presence of oxygen but the complex is fairly light sensitive. Decomposition is almost complete after one minute of intense UV irradiation and is enhanced almost ten fold in the presence of ordinary room light. Products of this light induced decomposition have not been characterized but could possibly be different than those of thermolysis.

As was mentioned in the preceding section (page 212), $[Cl\text{--}P_4\text{--}Cl]^{2+}$ is not stable in polar solvents at low concentrations. Decomposition of the PF_6^- salt of $[Cl\text{--}P_4\text{--}Cl]^{2+}$ in

methanol occurs at approximately the same rate ($t_{1/2}$ = 2-3 min) as that of its chloride salt (Figure II-5), however the final product spectrum is slightly different. The rate of its decomposition increases with the coordinating ability of the solvent. For example, decomposition in acetone has a half life of 17 seconds, whereas decomposition in acetonitrile and dimethylformamide occurs upon mixing. Reaction with even small concentrations of PPh_3 also occurs upon mixing as does its previously mentioned reaction with Cl^- (equation 7). Because of the steric repulsions between phenyls of opposing Pt(I) dimers in $[Cl\text{--}P_4\text{--}Cl]^{2+}$, displacement of at least one of these dimers from the P_4 unit by even weak nucleophiles is facile.

CONCLUSIONS

$[\{Pt_2(\mu\text{-dppm})_2Cl\}_2(di\text{-}\eta^2\text{-}P_4)]^{2+}$, a dicationic $Pt_4P_{12}Cl_2$ cluster with D_{2d} symmetry immersed in an ellipsoid of hydrophobic phenyls, is the first reported example of molecular phosphorus bound to transition metals in a di-η^2 fashion. The P_4 center is stabilized with respect to reaction with oxygen, which is not surprising, since all potential sights for its attack are blocked. The complex, as a whole, however, is vulnerable to attack by the most innocent of nucleophiles, and only moderately stable towards thermal and photochemical degradation. Dissociation of a Pt-P_4 bond, promoted by considerable phenyl-phenyl repulsion, is most likely the intitial step in all of its reactions.

EXPERIMENTAL

Materials

The reagents and solvents used in research described in Part II are identical (with a few notable exceptions) to those in Part I. Because of this, most synthetic methods, procedures for purification, etc. pertaining to Part II have already been described in the experimental section of Part I and will not be repeated here.

White phosphorus

Sticks of white phosphorus (P_4) stored under water were donated by Dr. J. G. Verkade of Iowa State University. Solutions of P_4 were made by transferring a small portion of the element that had been freshly cut from the middle of a stick (and cautiously dried) to a preweighed volumetric flask in a glove bag flushed with nitrogen. The stoppered flask was then taken from the glove bag and weighed to obtain the weight of P_4 by difference. The flask was then filled to volume with deaerated solvent (preferably benzene). With vigorous stirring, benzene solutions 0.1 M in P_4 can be readily obtained. The ^{31}P NMR spectrum of such solutions (diluted 4-fold by CD_2Cl_2) consists of a single peak at -522 ppm. Literature values[20] for P_4 range between -450 (neat) and -490 ppm (in CS_2). No other resonance could be detected between 600 and -600 ppm.

$[\{Pt_2(\mu\text{-dppm})_2Cl\}_2(di\text{-}\eta^2\text{-}P_4)](PF_6)_2$

To a suspension of 150 mg of [Cl--Cl] (0.114 mmol) in deaerated methanol, 10.6 mg of P_4 (0.086 mmol) dissolved in 0.75 ml of benzene were added at a rate of 0.05 ml/min. The resulting yellowish-brown solution was then cooled using an ice bath. Next, 74 mg of NH_4PF_6 (0.46 mmol) dissolved in 1 ml of methanol were slowly added to the chilled solution causing the formation of a finely divided yellowish solid. The solid was collected using a "fine" glass frit, washed with water, then ether, and dried under vacuum for one hour. The synthesis yielded 143 mg (90 % yield) of a yellowish-brown powder. Its elemental analysis (observed: 41.65 % C, 3.44 % H; theory: 42.86 % C, 3.17 % H) suggests the presence of 4-5 eq of adventitious H_2O. The complex is readily characterized by its $^{31}P\{^1H\}$ NMR (Figure II-1) and UV-VIS spectrum (Figure II-4). Exposure of its solutions to light causes decomposition.

Methods

Most instrumentation and procedures relating to NMR and UV-VIS spectroscopy were described in the experimental section of Part I. Additional methods of analysis pertaining only to Part II will now be discussed.

General

Thermal decomposition of solid $[(Pt_2)_2P_4](PF_6)_2$ was monitored using a Fisher Model 355 digital melting point

analyzer. Mass spectra of its thermal decomposition products were collected on a Finnigan 4000 GC-MS-data system (a computer controlled low resolution GC-MS having a mass range of 2-1000 amu). The sample was heated in a vacuum to 350 ^{o}C over a period of seven minutes. The mass spectrum of volatile components was scanned every two seconds during that period. The data from each scan were stored for subsequent analysis.

Vapor pressure osmometry

Molecular weight determinations in CH_2Cl_2 were conducted on a Knauer vapor pressure osmometer equipped with a Universal thermistor probe at a cell temperature of 25.75 ± 0.25 ^{o}C and a head temperature of 23 ^{o}C. Temperature differences are measured between a solution and pure solvent placed on separate thermistors (in the osmometer cell) after sufficient time has elapsed for equilibration of evaporation and condensation processes. The cell head buffers the system against extraneous temperature changes. Readings were taken either 4 or 8 minutes after application of solvent, standard, or sample solution depending on the time needed for temperature equilibration. Baseline readings (solvent on both thermistors) were taken after no more than three standard or sample readings. Solutions of benzil, in the same concentration range as predicted for sample solutions (4-14 mM), were used to make a standard curve (ΔR vs. benzil molality in Figure II-8). Thermistor readings for sample solutions corrected for baseline

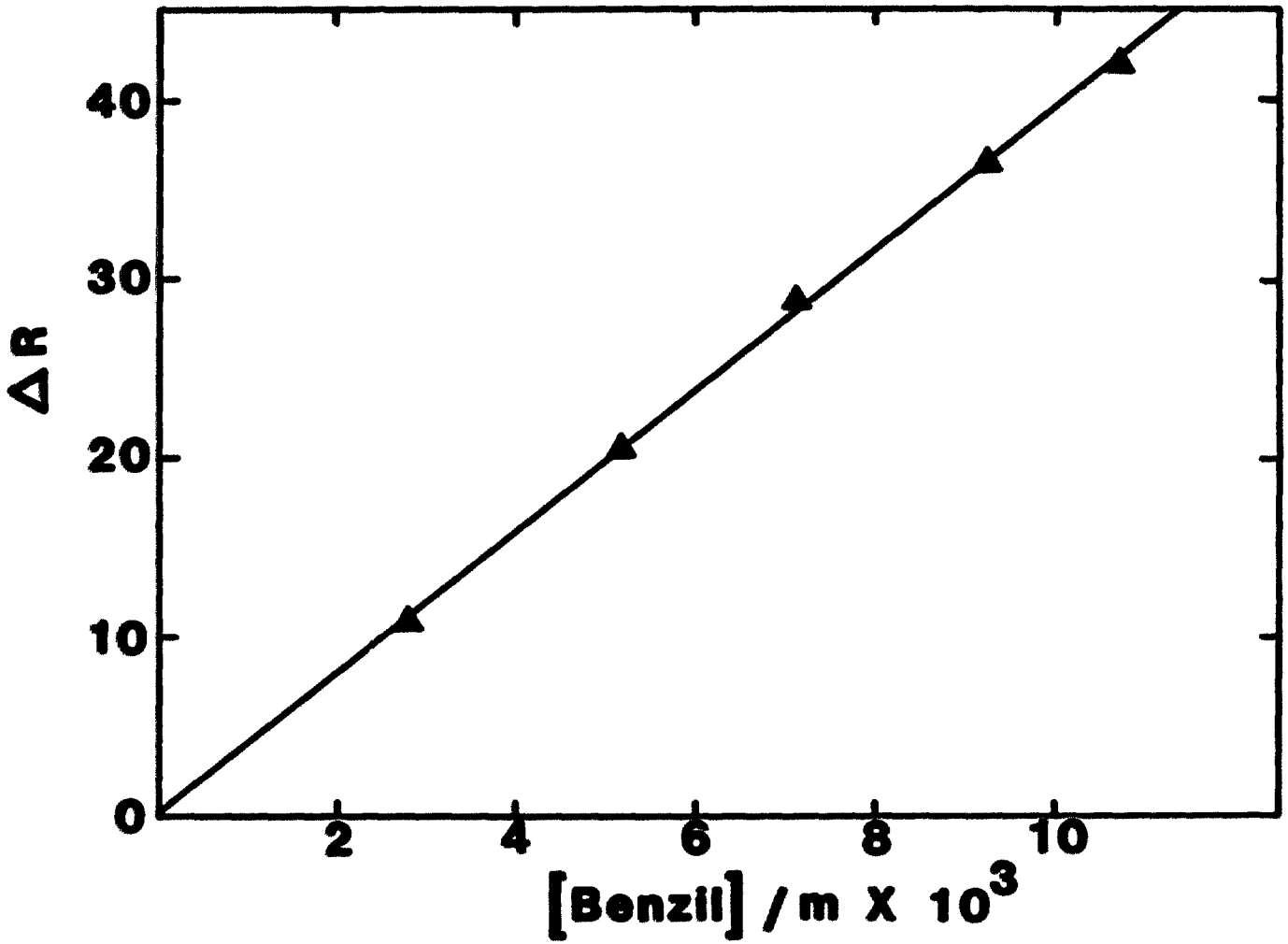

Figure II-8. Standard curve (slope = (3.95 ± 0.5) x 10^3 m^{-1}; intercept = 0.1 ± 0.3) for molecular weight determinations in CH_2Cl_2 using Benzil; obtained as described in the experimental section

(ΔR), the slope of the standard curve, and solute concentration were needed to calculate molecular weights (see Table II-2).

Spectral simulation of the P_4 resonance

Table II-3 lists the ten isotopomers of $[Cl--P_4--Cl]^{2+}$, their degeneracies, and relative abundance. Table II-4 assigns labels to the various various peaks in the theoretical spectrum, and in Table II-5, the contributions of each isotopomer to the peaks in Table II-4 for the $[Cl--P_4--Cl]^{2+}$ model are enumerated.

Curve analysis of the P_4 resonance of $[Cl--P_4--Cl]^{2+}$ was performed using software (NMRCAP) accompanying a Nicolet, NT-300 spectrometer. Satellite and central peaks were initially added to the total theoretical spectrum at their respective peak positions by varying peak height in proportion to the theoretical peak areas while holding the peak width constant. Computer calculated areas of such peaks were then obtained and held constant throughout the rest of the fitting procedure. In order to make adjustments in peak widths, corresponding adjustments in peak heights were also necessary in order to keep the computer calculated peak areas constant. Contraints were placed on peak width adjustments so that peaks with the same relative areas had somewhat similar widths. Satellite peaks of the C, D, and E type for the $[Cl--P_4--Cl]^{2+}$ model were combined as were areas for L, M, and N peaks (Table

Table II-2. Molecular weight determinations for dppm-bridged platinum(I) dimers[a]

Complex	conc.[b] (g/Kg)	ΔR	MN/gmol^{-1} (calc.)	MN/gmol^{-1} (theory)
[Cl--Cl][c]	4.60	13.9	1315	1314
	8.93	27.7	1276	
	13.16	41.5	1253	
$[PPh_3--PPh_3](PF_6)_2$	6.976	15.8	1752	1952
	12.829	27.5	1849	
	19.544	40.3	1918	
$[(Pt_2)_2P_4](PF_6)_2$	9.954	15.8	2501	2802
	10.284	16.1	2535	
	16.657	24.1	2738	
	22.217	32.8	2728	
	28.111	39.9	2786	

[a]Measurements made in CH_2Cl_2 with the vapor pressure osmometer cell at 25.75 ± 0.25 °C and head at 23 °C. Benzil was the standard.

[b]Concentration of solute in grams per Kg of solvent.

[c][Cl--Cl]*CH_2Cl_2 was the solid used in the measurements.

II-4). Satellite peaks O and Q were combined with the central resonance (0.64 % natural abundance each), and satellites R, S, U, and V were combined with T in the η^3-P_3 model. These "combined" peaks were broadened substantially relative to uncombined peaks of similar areas.

An analysis of the fit of theoretical curves to the experimental was conducted by eye. Error in the coupling constants was estimated by observing the effect small changes in individual coupling constants had on the theoretical spectrum. The major criterion used to determine the quality of a particular fit to the experimental curve was the ability of the calculated curve to simultaneously fit the central resonance and the outer satellites of the P_4 resonance. For example, (central resonance / total satellite) ratios are 0.78 for $[Cl\text{--}P_4\text{--}Cl]^{2+}$ with $^2J(Pt_A,P_R) = 0$, 0.41 for $[Cl\text{--}P_4\text{--}Cl]^{2+}$ with $^2J(Pt_A,P_R) \neq 0$, and 0.32 for $[\{Pt_2(\mu\text{-dppm})_2Cl\}_2(\eta^3\text{-}P_3)]^{2+}$. Relative intensities of the several peaks in each of the three models are given in Table II-5. The best fit is observed in the second model, the central resonance is much too large in the former model and too small in the latter relative to the outer satellites (see Figure II-2).

Table II-3. Relative abundance of the $[\{Pt_2(\mu\text{-dppm})_2Cl\}_2(di\text{-}\eta^2\text{-}P_4)]^{2+}$ isotopomers

Label[a]	Isotopomer[b]	Degeneracy	% Abundance[c]
0	Pt-Pt-P_2=P_2-Pt-Pt	1	19.2
1a	Pt*-Pt-P_2=P_2-Pt-Pt	2	19.6
1b	Pt-Pt*-P_2=P_2-Pt-Pt	2	19.6
2a	Pt*-Pt*-P_2=P_2-Pt-Pt	2	10.0
2b	Pt*-Pt-P_2=P_2-Pt*-Pt	2	10.0
2c	Pt*-Pt-P_2=P_2-Pt-Pt*	1	5.0
2d	Pt-Pt*-P_2=P_2-Pt*-Pt	1	5.0
3a	Pt*-Pt*-P_2=P_2-Pt-Pt*	2	5.1
3b	Pt*-Pt*-P_2=P_2-Pt*-Pt	2	5.1
4	Pt*-Pt*-P_2=P_2-Pt*-Pt*	1	1.3
Total	10	16	99.9

[a]Number in label corresponds to the number of ^{195}Pt nuclei in the respective isotopomer.

[b]Pt* = ^{195}Pt; where the degeneracy = 2, only one of the degenerate pair is shown, the other is obtained by switching labels on the two Pt dimers.

[c]% natural abundance of ^{195}Pt = 33.8 %.

Table II-4. Labeling of peaks in the theoretical models for the P_4 resonance[a]

Label	Peak	Label	Peak
A	central	L	$1/2(^1J + {}^2J - {}^2J')$
B	$1/2(^2J')$	M	$1/2(^1J + {}^2J)$
C	$1/2(^1J - {}^2J - {}^2J')$	N	$1/2(^1J + {}^2J + {}^2J')$
D	$1/2(^1J - {}^2J)$	O	$^2J - 1/2(^1J)$
E	$1/2(^1J - {}^2J + {}^2J')$	P	^2J
F	$1/2(^2J - {}^2J')$	Q	$^2J + 1/2(^1J)$
G	$1/2(^2J)$	R	$^1J - {}^2J$
H	$1/2(^2J + {}^2J')$	S	$^1J - 1/2(^2J)$
I	$1/2(^1J - {}^2J')$	T	^1J
J	$1/2(^1J)$	U	$^1J + 1/2(^2J)$
K	$1/2(^1J + {}^2J')$	V	$^1J + {}^2J$

[a] $^1J = {}^1J(Pt_A, P_{A''})$; $^2J = {}^2J(Pt_R, P_{A''})$; $^2J = {}^2J'(Pt_A, P_{R''})$; the positions of half of the satellite peaks relative to the central resonance are listed; the position of the remaining half are obtained by changing the sign of each peak.

Table II-5. Possible splitting patterns for the P_4 resonance[a]

Isotop. Labels	Peak Labels A	B	C	D	E	F	G	H
0	19.20	-	-	-	-	-	-	-
1a	9.80	-	-	-	-	-	-	-
1b	-	4.90	-	-	-	-	4.90	-
2a	-	2.50	-	1.25	-	-	-	-
2b	-	-	-	-	-	1.25	-	1.25
2c	-	-	-	-	-	-	2.50	-
2d	-	-	-	-	-	-	-	-
3a	-	-	-	0.64	-	0.64	-	0.64
3b	-	-	0.32	-	0.32	-	-	-
4	-	-	0.16	-	0.16	-	-	-
P_4[c]	29.00	7.40	0.48	1.89	0.48	1.89	7.40	1.89
P_4'[d]	43.8	-	-	2.85	-	-	11.18	-
P_3[e]	24.36	-	-	5.00	-	-	11.08	-

[a]Isotopomer and peak labels are from Tables II-3 and II-4.

[b]Total = A + 2[B + C + ··· X]

[c]The sum of isotopomer contributions to each peak for the $[Cl{-}{-}P_4{-}{-}Cl]^{2+}$ model where $^2J(Pt_A,P_{R''}) \neq 0$.

[d]Same as in footnote c, but where $^2J(Pt_A,P_{R''}) = 0$.

[e]Splitting pattern for the η^3-P_3 model where: W = (O + P + Q) and X = (R + S + T + U + V) from Table II-4.

Peak Labels								Total[b]
I	J	K	L	M	N	N	X	
-	-	-	-	-	-	-	-	19.20
-	-	-	-	-	-	-	-	19.60
-	4.90	-	-	-	-	-	-	19.60
-	-	-	-	1.25	-	-	-	10.00
-	2.50	-	-	-	-	-	-	10.00
-	-	-	-	-	-	-	-	5.00
1.25	-	1.25	-	-	-	-	-	5.00
-	-	-	-	0.64	-	-	-	5.12
0.64	-	0.64	0.32	-	0.32	-	-	5.12
-	-	-	0.16	-	0.16	-	-	1.28
1.89	7.40	1.89	0.48	1.89	0.48	-	-	99.92
-	11.18	-	-	2.85	-	-	-	99.92
-	11.08	-	-	5.0	-	2.69	2.85	99.75

BIBLIOGRAPHY

1. Ginsberg, A. P.; Lindsell, W. E. J. Amer. Chem. Soc. 1971, 93, 2082.

2. Ginsberg, A. P.; Lindsell, W. E.; Silverthorn, W. E. Trans. N. Y. Acad. Sci. 1971, 33, 303.

3. Lindsell, W. E. J. Chem Soc., Chem. Commun. 1982, 1422.

4. Lindsell, W. E.; McCullough, K. J.; Welch, A. J. J. Amer. Chem. Soc. 1983, 105, 4487.

5. Schmid, V. G.; Kempny, H.-P. Z. Anorg. Allg. Chem. 1977, 432, 160.

6. (a) Dapporto, P; Midollini, S.; Sacconi, L. Angew. Chem., Int. Ed. Engl. 1979, 18, 469. (b) Dapporto, P.; Sacconi, L.; Stoppioni, P.; Zanobini, F. Inorg. Chem. 1981, 20, 3834. (c) Di Vaira, M.; Sacconi, L. Angew. Chem., Int. Ed. Engl. 1982, 21, 330.

7. (a) Di Vaira, M.; Sacconi, L. Angew. Chem. Int. Ed. Engl. 1982, 94, 338 and references therein. (b) Di Vaira, M.; Sacconi, L.; Stoppioni, P. J. Organomet. Chem. 1983, 250, 183. (c) Di Vaira, M.; Peruzzini, M.; Stoppioni, P. Acta Cryst. C 1983, 39, 1210.

8. Green, J. C.; Green, M. L. H.; Morris, G. E. J. Chem. Soc., Chem. Commun. 1974, 212.

9. Cecconi, F.; Ghilardi, C. A.; Midollini, S.; Orlandini, A. J. Amer. Chem. Soc. 1984, 106, 3667.

10. Simon, G. L.; Dahl, L. F. J. Amer. Chem. Soc. 1973, 95, 2175.

11. Scherer, O. J.; Sitzmann, H.; Wolmershaeuser, G. J. Organomet. Chem. 1984, 268, C9.

12. Vizi-Orosz, A. J. Organomet. Chem. 1976, 111, 61.

13. Personal communication from Dr. T. A. Albright, Department of Chemistry, University of Houston, Houston, Texas 77004.

14. Howell, J.; Rossi, A.; Wallace, D.; Haraki, K.; Hoffmann, R. QPCE 1977, 10, 344.

15. Pregosin, P. S.; Kunz, R. W. "NMR Basic Principles and Progress" Vol. 16; Springer-Verlag: New York, 1979.

16. Chisholm, M. H.; Clark, H. C.; Manzer, L. E.; Stothers, J. B. J. Amer. Chem. Soc. 1972, 94, 5088.

17. Chisholm, M. H.; Clark, H. C.; Manzer, L. E.; Stothers, J. B. J. Chem. Soc., Chem. Commun. 1971, 1627.

18. Drago, R. S. "Physical Methods in Chemistry"; W. B. Saunders Company: Philadelphia, 1977; pp. 217-219, 294-296.

19. Osman, R.; Coffey, P.; Van Wazer, J. R. Inorg. Chem. 1976, 15, 287.

20. Emsley, J. W.; Feeney, J.; Sutcliffe, L. H. "High Resolution Nuclear Magnetic Resonance Spectroscopy" Vol. 2; Pergamon Press: New York, 1966.

PART III. FORMATION AND REACTIVITY OF METAL-CARBON BONDS IN ORGANOCOBALAMIN AND ORGANOCHROMIUM COMPLEXES

INTRODUCTION

Research on the formation and reactivity of metal-carbon bonds was conducted in three general areas:

1. Reactions of hydroxyl and other free radicals with organopentaaquochromium(2+) ions
2. Kinetic study of the reaction of aquochromium(II) ions with benzyl radicals in aqueous solutions: thermodynamics of the chromium-carbon bond
3. Homolysis and electron transfer reactions of benzylcobalamin

Only summaries of this research will be presented since full accounts have already been published or have been submitted for publication.

REACTIONS OF HYDROXYL AND OTHER FREE RADICALS WITH ORGANOPENTAAQUOCHROMIUM(2+) IONS[1]

Chain reactions (eqs. 1-6) can cause very rapid decomposition of $(H_2O)_5CrR^{2+}$ (R = CH_2OCH_3, $CH(CH_3)OC_2H_5$, $CH(CH_3)_2$, and $CH_2C_6H_5$) in the presence of H_2O_2. They can be intiated either by the direct addition of Cr^{2+} to solutions containing H_2O_2 and RCr^{2+} (eq. 2), or by other reactions producing the chain propagating intermediates ($R^\cdot$, Cr^{2+}, and $HO^\cdot$) such as the unimolecular homolysis of the R-Cr bond in RCr^{2+} (eq. 1). The homolysis fragments, $R^\cdot$ and Cr^{2+}, react readily with H_2O_2 yielding $HO^\cdot$ (eqs. 2 and 3), which, in turn, reacts with RCr^{2+} with accompanying cleavage of the chromium-carbon bond (eq. 4) to form $R^\cdot$ and Cr^{2+} again. The overall

$$CrR^{2+} \rightleftharpoons Cr^{2+} + R^\cdot \qquad (1)$$

$$Cr^{2+} + H_2O_2 \longrightarrow CrOH^{2+} + OH^\cdot \qquad (2)$$

$$R^\cdot + H_2O_2 \longrightarrow \text{"ROH"} + OH^\cdot \qquad (3)$$

$$CrR^{2+} + HO^\cdot \longrightarrow Cr^{2+} + (R\text{-}H) + H_2O \text{ (or ROH)} \qquad (4a)$$

$$CrR^{2+} + HO^\cdot \longrightarrow CrOH^{2+} + R^\cdot \qquad (4b)$$

$$OH^\cdot + H_2O_2 \longrightarrow HO_2^\cdot + H_2O \qquad (5)$$

$$2R^\cdot \longrightarrow R_2 \text{ (and } RH + (R\text{-}H)) \qquad (6)$$

chain length is not high because of efficient chain-terminating reactions: At very high H_2O_2 concentrations, reaction 5 predominates, whereas at very low H_2O_2 concentrations reaction 6 is important; maximum chain length is achieved at intermediate $[H_2O_2]$.

An estimate of ~1.6 x 10^9 $M^{-1}s^{-1}$ was made for the total rate constant (k_{4a} + k_{4b}) representing the reactions of HO. with CrR^{2+}. Experimental data supporting the above mechanism are presented in the article already published[1].

KINETIC STUDY OF THE REACTION OF AQUOCHROMIUM(II) IONS WITH BENZYL RADICALS IN AQUEOUS SOLUTIONS: THERMODYNAMICS OF THE CHROMIUM-CARBON BOND[2]

Flash-photolytic determinations based on both the photohomolysis of $CrCH_2Ph^{2+}$ (eq. 7) and on the photodecomposition of $(PhCH_2)_2CO$ (eqs. 8 and 9) in the presence of Cr^{2+} yielded a consistent value for k_{Cr}, the second-order rate constant for reaction 10: $k_{Cr} = (8.5 \pm 0.6) \times 10^7\ M^{-1}\ s^{-1}$ ($23 \pm 2\ ^{\circ}C$, 0-2 M CH_3CN in H_2O, 0.05 M $HClO_4$ at $\mu = 0.10$ M). The value of k_{Cr} is needed (a) to resolve the kinetics and thermodynamics of free radical reactions of $CrCH_2Ph^{2+}$,[3,4] (b) to complete the kinetic and thermodynamic characterization of benzylcobalamin,[5] and (c) to analyze reactions in which a benzyl group is transferred from one metal to another[6] (e.g., reaction 16 on page 250).

$$PhCH_2Cr^{2+} \xrightarrow{h\nu} PhCH_2^{\cdot} + Cr^{2+} \qquad (7)$$

$$(PhCH_2)_2CO \xrightarrow{h\nu} [(PhCH_2)_2CO]^{*} \longrightarrow PhCH_2^{\cdot} + PhCH_2CO \qquad (8)$$

$$PhCH_2CO \longrightarrow PhCH_2^{\cdot} + CO \qquad (9)$$

$$PhCH_2^{\cdot} \xrightarrow{k_{Cr}[Cr^{2+}]} PhCH_2Cr^{2+} \qquad (10)$$

$$PhCH_2^{\cdot} \xrightarrow{k_d[PhCH_2^{\cdot}]} PhCH_2CH_2Ph \qquad (11)$$

The value for k_{Cr}, evaluated by flash photolysis of

$CrCH_2Ph^{2+}$, was determined from product ratios of the competing pseudo-first and second order reactions, 10 and 11, as a function of Cr^{2+} concentration. The rate constant for radical dimerization (eq. 11) is known independently ($2k_d = 2.7 \times 10^9$ $M^{-1}s^{-1}$)[7], and thus the value of k_{Cr} can be obtained. The determination of k_{Cr} by flash photolysis of $(PhCH_2)_2CO$ was accomplished by monitoring the rate of $PhCH_2Cr^{2+}$ formation at 364 nm as a function of Cr^{2+} concentration and evaluating only that portion of the kinetic data (low $PhCH_2^{\cdot}$) where reaction 11 is negligible.

The value of k_{Cr}, together with literature values or estimates for other quantities, affords $\Delta G^0 = -59.9$ kJ mol^{-1} ($\Delta G_{Cr}^{\ddagger} = 27.8$, $\Delta G_{-10}^{\ddagger} = 87.7$), $\Delta H^0 = -123 \pm 10$ kJ mol^{-1} ($\Delta H_{-10}^{\ddagger}$ 133 ± 3), and $\Delta S^0 = -211 \pm 34$ J $mol^{-1}K^{-1}$ ($\Delta S_{Cr}^{\ddagger}$ -60 ± 35). Further details on the determination of k_{Cr} and subsequent thermodynamic values are presented in the paper already published[2].

HOMOLYSIS AND ELECTRON TRANSFER REACTIONS OF BENZYLCOBALAMIN[5]

The rate constants have been evaluated for decomposition of benzylcobalamin species (Figure III-1) present in acetate buffers ($PhCH_2$[Co]) and in dilute perchloric acid ($PhCH_2$[Co]$\cdot H^+$) in the presence of oxygen, 4-hydroxy-2,2,6,6-tetramethylpiperidinyloxy (4-HTMPO), and iron(III).

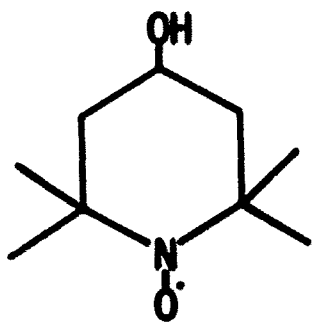

4-HTMPO

Homolysis

Many of these reactions are governed by initial and rate-limiting homolytic cleavage of the cobalt-carbon bond. In the case of 4-HTMPO (eqs. 12-14), the kinetic inhibition of benzylcobalamin decomposition by Vitamin B_{12r} ([Co(II)]; Figure III-2) can be observed because reaction 14, which produces Vitamin B_{12a} ([Co(III)]; Figure III-2), is

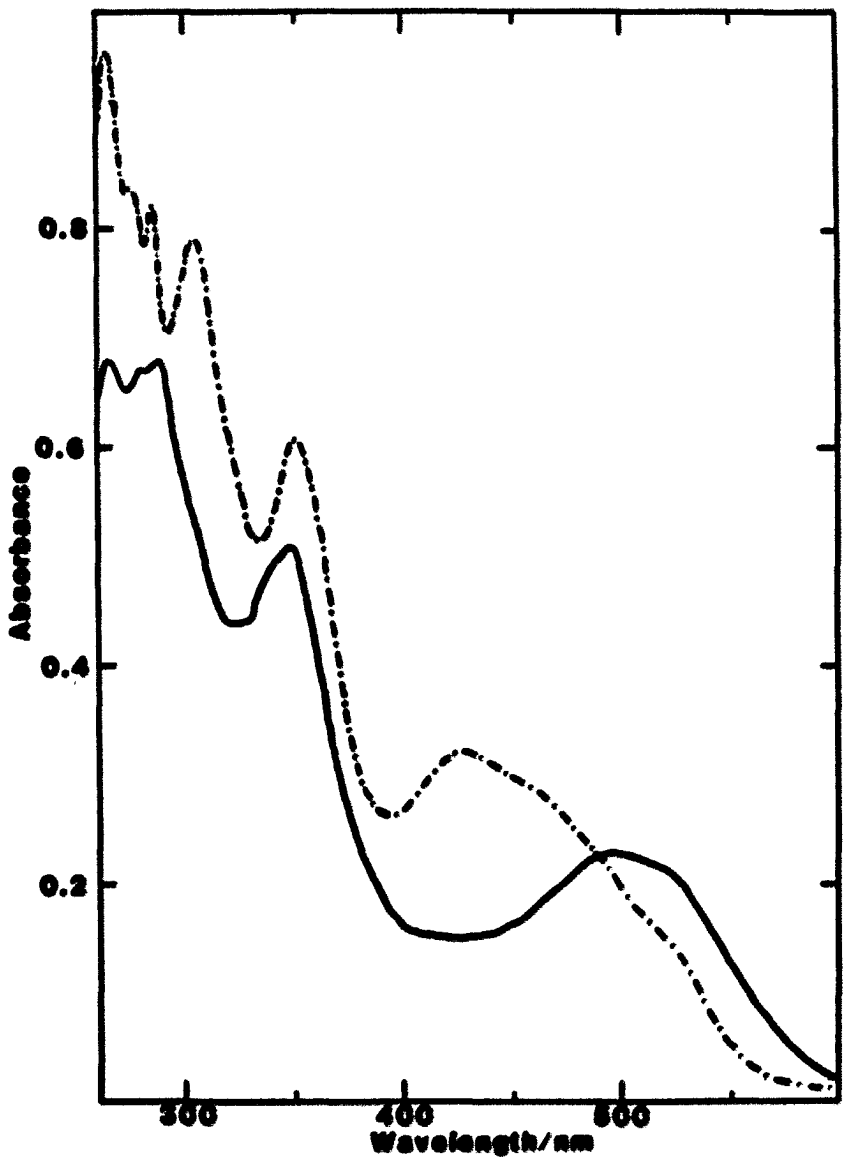

Figure III-1. UV-VIS spectra for benzylcobalamin (2 cm cell):
-·- 0.013 mM in 0.1 M $HClO_4$, for the ClO_4^- salt
ε_{428} = 9.52 x 10^3 M^{-1} cm^{-1}
—— 0.010 mM in 0.1 M acetate buffer (pH 5.5)
ε_{350} = 1.95 x 10^4 M^{-1} cm^{-1}

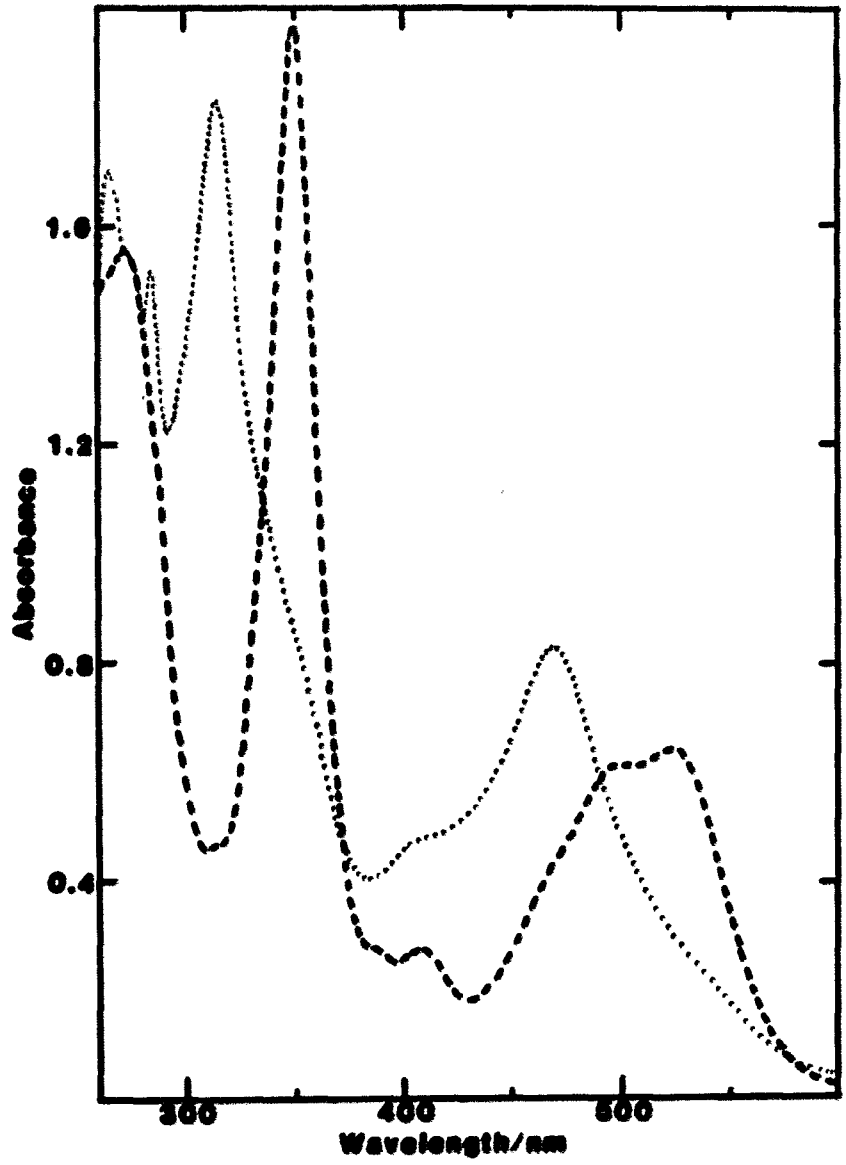

Figure III-2. UV-VIS spectra (2 cm cell) in 0.1 M $HClO_4$ for:
··· 0.033 mM Vitamin B_{12r} ε_{311} = 27500 M^{-1} s^{-1}
--- 0.037 mM Vitamin B_{12a} ε_{350} = 26200 M^{-1} s^{-1}

sufficiently slow to allow the presence of significant concentrations of [Co(II)] during the benzylcobalamin decomposition (see Figure III-3).

$$PhCH_2[Co] \underset{k_r}{\overset{k_h}{\rightleftharpoons}} [Co(II)] + PhCH_2^{\cdot} \qquad (12)$$

$$4\text{-HTMPO} + PhCH_2^{\cdot} \xrightarrow{k_s} \text{RNO (adduct)} \qquad (13)$$

$$4\text{-HTMPO} + [Co(II)] \longrightarrow [Co(III)] + \text{products} \qquad (14)$$

Rate Constants for Reactions of Benzyl Radicals

The following:

1. data derived from [Co(II)] inhibition of the 4-HTMPO reaction (eqs. 12-14),
2. the kinetically determined[2,4] equilibrium constant for the reversible homolysis of $PhCH_2Cr^{2+}$ ($K_{15} = 2.7 \times 10^{-11}$),
3. the equilibrium constant for benzyl transfer between benzylcobalamin and pentaaquo(benzyl)chromium(2+) ($K_{16} = (2.1 \pm 0.1) \times 10^{-3}$; see Figure III-4),

permit the evaluation (± 20 %) of k_r in equation 12 (3.5×10^8 M^{-1} s^{-1}), and and k_s in equation 13 (5.4×10^7 M^{-1} s^{-1}).

$$CrCH_2Ph^{2+} \underset{}{\overset{K_{15}}{\rightleftharpoons}} Cr^{2+} + PhCH_2^{\cdot} \qquad (15)$$

$$PhCH_2[Co]\cdot H^+ + Cr^{2+} \underset{}{\overset{K_{16}}{\rightleftharpoons}} [Co(II)]\cdot H^+ + CrCH_2Ph^{2+} \qquad (16)$$

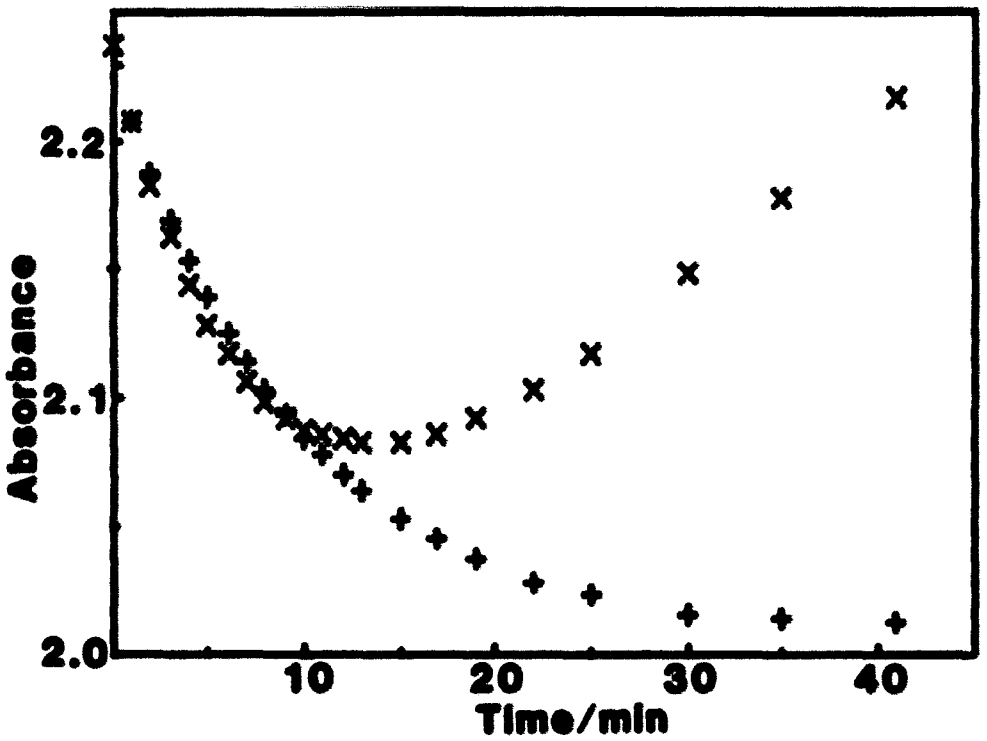

Figure III-3. Reaction after addition of 0.4 mM 4-HIMPO to a 0.1 M acetate buffer solution (pH 5.5, 25 °C, 2 cm cell) 0.023 mM each in Benzylcobalamin and [Co(II)] simultaneously monitored at (a) 336.2 nm (+), a [Co(II)]-[Co(III)] isosbestic, and (b) 341.7 nm (X), a $PhCH_2$[Co]-[CoIII] isosbestic; (a) shows the decrease in $PhCH_2$[Co] concentration with time, whereas (b) shows the increase (abs. decrease) followed by a decrease in [Co(II)] concentration with time

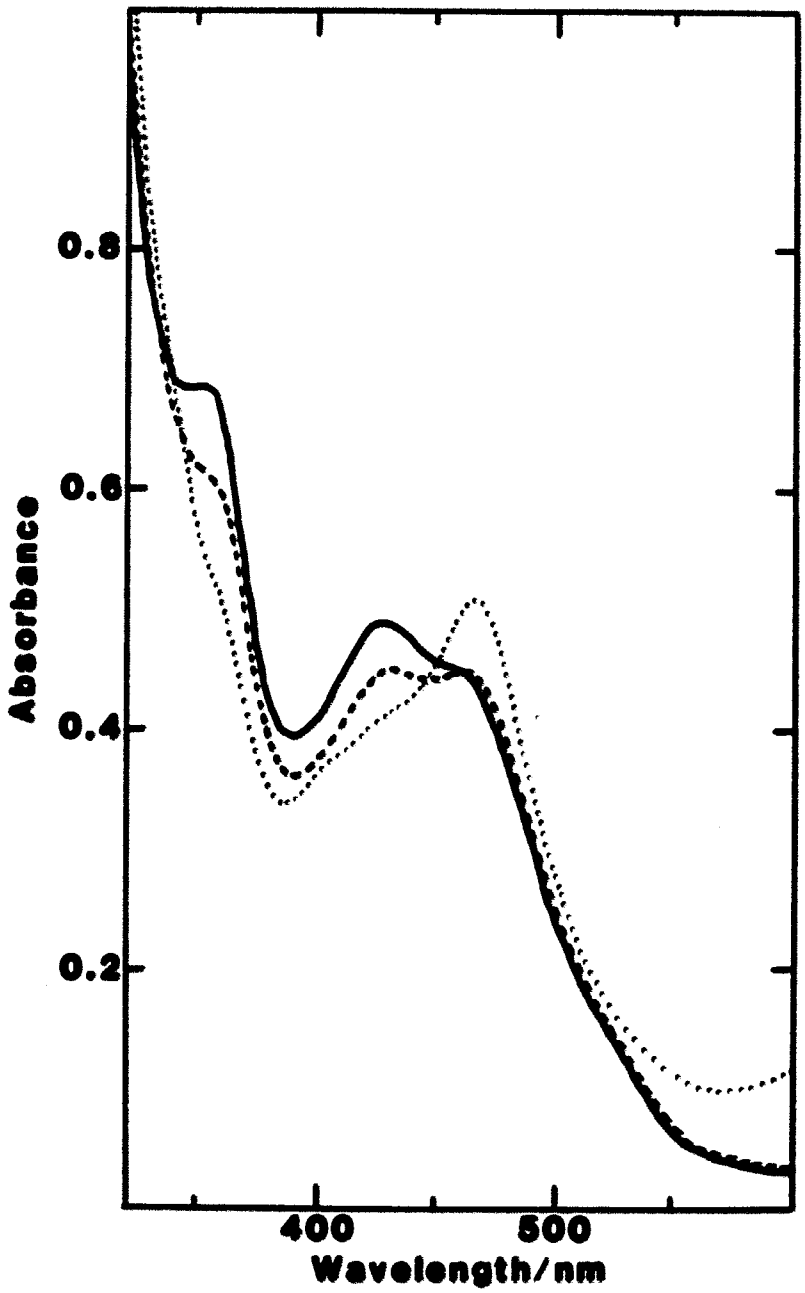

Figure III-4. Absorbtion spectra after the reaction of (0.023 ± 0.001) mM $PhCH_2[Co]^{\cdot}H^{+}$ (in 0.1 M $HClO_4$; 2 cm cell; μ = 1.0; 25 °C) with 0.60 mM (···), 0.99 mM (---), and 19.0 mM (——) Cr^{2+} illustrating equilibrium 16; abs maxima: 356 and 428 nm ($PhCH_2[Co]^{\cdot}H^{+}$); 470 nm ([Co(II)])

Oxidative Cleavage with Fe^{3+}

In addition to homolysis, there is a direct oxidative pathway for the reaction of $PhCH_2[Co]\cdot H^+$ with Fe^{3+}, which shows a dependence of rate upon $[Fe^{3+}]$ and $[H^+]$ consistent with rate-limiting internal electron transfer within a binuclear complex eq. 20:

$$\frac{-d[PhCH_2B_{12}]}{dt} = \left(k_h + \frac{k_{20}K_C[Fe(III)]}{1 + K_C[Fe(III)] + [H^+]/K_a}\right)[PhCH_2B_{12}] \quad (17)$$

Steps in the postulated mechanism are:

1. the known[8] acid ionization of the phosphodiester group of the nucleotide loop (see Figure III-5) to form a species symbolized as $PhCH_2[Co]^*$ (eq. 18);
2. rapid and reversible association of $PhCH_2[Co]^*$ with Fe^{3+} (eq. 19) (the deprotonated phosphoryl oxygen(s) may provide the binding site for iron);
3. rate-limiting electron transfer (eq. 20) forming a benzyl-Co(IV) intermediate (possibly more than a single step);
4. rapid nucleophilic displacement of [Co(II)] by Cl^- (if present) or H_2O forming organic products (eq. 21);
5. and rapid oxidation of [Co(II)] by a second Fe^{3+} (eq. 22).

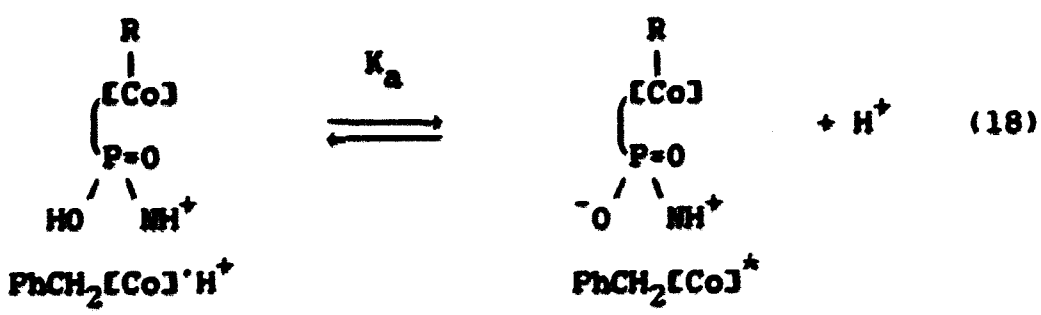

$PhCH_2[Co]\cdot H^+$ $\qquad$ $PhCH_2[Co]^*$ $\qquad$ (18)

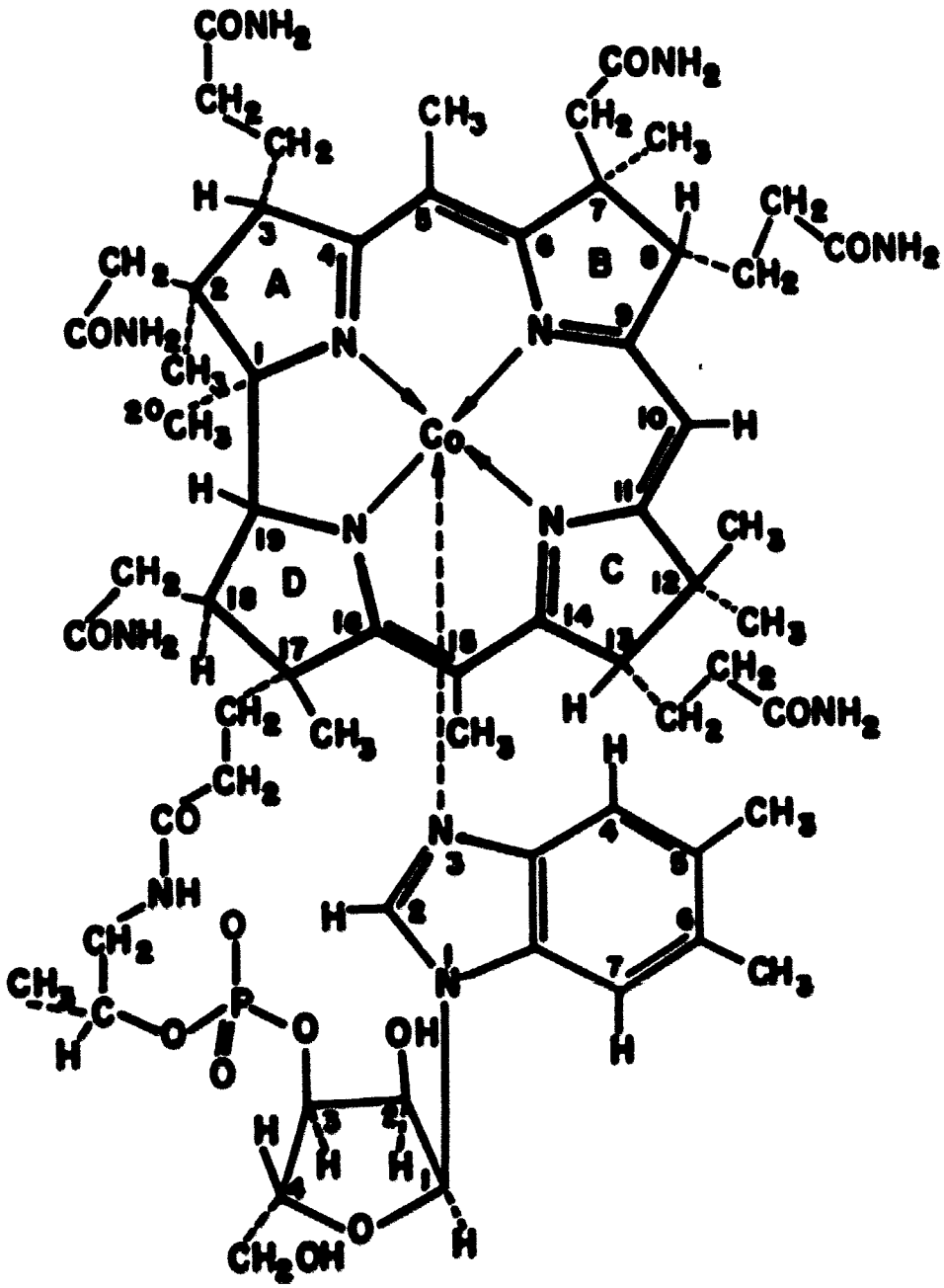

Figure III-5. "Base-on" Vitamin B_{12}

$$PhCH_2[Co]^{+} + Fe^{3+} \underset{}{\overset{K_{Fe}}{\rightleftharpoons}} PhCH_2[Co(III)]\cdots Fe^{3+} \qquad (19)$$

$$PhCH_2[Co(III)]\cdots Fe^{3+} \xrightarrow{k_{20}} PhCH_2[Co(IV)]^{+} + Fe^{2+} \qquad (20)$$

$$PhCH_2[Co(IV)]^{+} \begin{cases} \xrightarrow{H_2O} PhCH_2OH + [Co(II)] + Fe^{2+} + H^{+} \\ \xrightarrow{Cl^{-}} PhCH_2Cl + [Co(II)] + Fe^{2+} \end{cases} \qquad (21)$$

$$[Co(II)] + Fe^{3+} + H_2O \longrightarrow H_2O[Co(III)]^{+} + Fe^{2+} \qquad (22)$$

Accelerated Autoxidation of $PhCH_2[Co]$ by Mild Reducing Reagents

A three-component mixture of $PhCH_2[Co]\cdot H^{+}$, O_2, and ascorbic acid (H_2A) activates O_2 for oxidation of ascorbic acid (eq. 24) via binding of O_2 to the vacant "lower" coordination position of the base-off form of benzylcobalamin (eq. 23).

$$O_2 + \underset{\substack{\text{"Base-Off"} \\ PhCH_2[Co]\cdot H^{+}}}{\overset{R}{\underset{|}{[Co]}}} \underset{}{\overset{K_{Ad}}{\rightleftharpoons}} \underset{\text{Adduct}}{\overset{R}{\underset{|}{[Co]}}\underset{|}{O_2}} \qquad (23)$$

$$\text{Adduct} + H_2A \longrightarrow H_2O[Co(III)]^{+} + \text{other products} \qquad (24)$$

These reactions provide direct evidence for a mechanism in which an organocobalmin activates O_2 for further reaction.

Experimental observations describing the benzylcobalamin reactions and supporting their postulated mechanisms are discussed in greater detail in the article submitted for publication.[5]

Cu^{2+} Catalyzed Autoxidation of [Co(II)][9]

Autoxidation of [Co(II)] is normally sluggish ($t_{1/2}$ ≈ 4.5 min at 0 °C),[10] however, its rate increases almost 10 fold in the presence of Cu^{2+}.[10] Equilibrium 25 was observed at pH = 1-2 ($[B_{12}]_{tot}$ ≈ 0.02 mM; $[Cu^{2+}]$ = 0.08 - 4.1 mM) with K_{25} = 0.025 ± 0.005, this value is not too unreasonable considering the reduction potentials involved.[11] The production of $Cu^{+}(aq)$ by reaction 25 creates an efficient route for [Co(II)] autoxidation (eq. 26) since oxidation of Cu^{+} is very rapid.[12]

$$Cu^{2+} + [Co(II)] \underset{}{\overset{K_{25}}{\rightleftharpoons}} Cu^{+}(aq) + H_2O[Co(III)]^{+} \qquad (25)$$

$$Cu^{+}(aq) + O_2 \longrightarrow [Cu(O_2)]^{+} \qquad (26)$$

BIBLIOGRAPHY

1. Bakač, A.; Blau, R. J.; Espenson, J. H. Inorg. Chem. 1983, 22, 3789.

2. Blau, R. J.; Espenson, J. H.; Bakač, A. Inorg. Chem. 1984, 23, 3526.

3. Kochi, J. K.; Buchanan, D. J. Amer. Chem. Soc. 1965, 87, 853.

4. Mohr, R. S.; Espenson, J. H. J. Amer. Chem. Soc. 1975, 97, 3392.

5. Blau, R. J.; Espenson, J. H. submitted to J. Amer. Chem. Soc.

6. (a) Espenson, J. H.; Shveima, J. S. J. Amer. Chem. Soc. 1973, 95, 4468. (b) Bakač, A.; Espenson, J. H. J. Amer. Chem. Soc. 1984, 106, 5197.

7. References 11-14 in ref. 5.

8. Brown, K. L.; Hakima, J. M. Inorg. Chim. Acta 1982, 67, L29.

9. Blau, R. J.; Espenson, J. H. Department of Chemistry, Iowa State University, Ames; unpublished results.

10. Abel, E. W.; Pratt, J. M.; Whelan, R.; Wilkinson, P. J. S. Afr. J. Chem. 1977, 30, 1.

11. Lexa, D.; Saveant, J. M.; Zickler, J. J. Amer. Chem. Soc. 1977, 99, 2786.

12. (a) Basolo, F.; Pearson, R. G. "Mechanisms of Inorganic Reactions", 2nd ed.; Wiley: New York, 1967; pp. 500. (b) Stevanato, R.; Argese, P.; Viglino, P.; Rigo, A. Inorg. Chim. Acta 1984, 92, 177.

GENERAL SUMMARY

$[Pt_2(\mu\text{-dppm})_2Cl(PPh_3)]^+$ is formed from a rate-limiting bimolecular reaction of PPh_3 with $[Pt_2(\mu\text{-dppm})_2Cl_2]$ in CH_2Cl_2. Alternatively, it and its bromo and chloro derivatives can be formed from the reaction of halides with $[Pt_2(\mu\text{-dppm})_2(PPh_3)_2]^{2+}$ by (a) rate-limiting PPh_3 dissociation, or (b) rate-limiting $Pt_2(\mu\text{-dppm})$ ring opening at a Pt-P bond. Formation of product by (b) occurs after the formation of two observable intermediates, one of which, $[Pt_2(\eta^2\text{-dppm})(\mu\text{-dppm})X(PPh_3)]^+$, is readily characterized by $^{31}P\{^1H\}$ NMR. Rates of these ligand substitution reactions are very sensitive to the anions present in solution.

Atropisomers due to hindered rotation around the Pt-PPh_3 bond of $[Pt_2(\mu\text{-dppm})_2Cl(PPh_3)]^+$ are caused by phenyl-phenyl repulsions and can be distinguished by $^{31}P\{^1H\}$ NMR spectroscopy. Such repulsions also retard the rate of positional interchange of axial and equatorial substituents on its $Pt_2(\mu\text{-dppm})_2$ ring as observed by ^1H NMR spectroscopy.

Several correlations between ^{195}Pt-^{31}P coupling constants and Pt-P and Pt-Pt bond lengths were observed.

The synthesis, characterization, and reactivity of $[[Pt_2(\mu\text{-dppm})_2Cl]_2(di\text{-}\eta^2\text{-}P_4)]^{2+}$ is reported. This complex is a dimer of platinum dimers bridged by tetra-phosphorus. One platinum of each dimer is bound to two phosphorus atoms of P_4.

The formation and reactivity of the metal-carbon bonds in benzylcobalamin and chromium alkyls, $[(H_2O)_5CrR^{2+}$; R = CH_2Ph, $CH(CH_3)OC_2H_5$, $CH_2OCH_3]$, were also investigated.

ACKNOWLEDGEMENTS

I am very grateful to Dr. Espenson for his support and encouragement throughout my graduate career. His allowing of, and indeed, insistence of independent thought was very instrumental in my development as a scientist.

I would to like to thank Mr. Sangsoo Kim and Dr. Robert A. Jacobson for their assistance in solving the crystal structure for $[Pt_2(\mu\text{-dppm})_2Cl(PPh_3)](PF_6)*3(benzene)$. I would also like to acknowledge Dr. John G. Verkade, Dr. Walter S. Trahanovsky, Dr. Andreja Bakać, and Dr. S. Muralidharan for very useful discussions, and especially Murali for technical assistance.

I am indebted to Robyn's and my parents for their moral support and monetary assistance these past 4.5 years. I would not know what I would do without my wife, Robyn and three children, John, Charity, and Elizabeth. Their faith in me, love, and patient understanding have given me the impetus needed to successfully accomplish the tasks expected of me these past years.